



**WPI AIAA Research Rocket for the Investigation
and Observation of Recovery and Staging
(WARRIORS I)**

By

Michael Belliss

Thorsten Braun

Peter Brayshaw

George Matook

Kevin Moore

Amanda Otterman

Abel Sanchez-Torres

David Stechmann

Approved

Professor John Blandino
Project Advisor

April 27th, 2006

This project report is submitted in partial fulfillment of the degree requirements of Worcester Polytechnic Institute. The views and opinions expressed herein are those of the authors and do not necessarily reflect the positions or opinions of Worcester Polytechnic Institute.



Abstract

The WPI AIAA Research Rocket for the Investigation and Observation of Recovery and Staging (WARRIORS) is a two-stage, high-powered model rocket equipped with an onboard computer and a digital video camera. The goal of WARRIORS was to challenge students to develop innovative rocket staging and recovery techniques. The project was a joint effort between eight Worcester Polytechnic Institute senior undergraduates completing their Major Qualifying Project and American Institute of Aeronautics and Astronautics (AIAA), WPI chapter, student volunteers. This paper describes the design, testing, operation, and lessons learned from the creation and implementation of an innovative electromagnetic booster separation system, non-pyrotechnic parachute deployment mechanisms, a reliable ignition system that prevents asymmetric thrust, and a custom constructed durable airframe.

Acknowledgements

The WARRIORS MQP Group would like to thank:

Professor John J. Blandino

For his guidance, leadership, and encouragement on this project from the beginning of development until well after the rocket cleared the launch rail.

Eric Byrd-Krueger

For his work as Project Engineer, and for his work as a mentor to all of the group members.

Theodore McDonald & Ryan Caron

For their experience and assistance in all facets of the project development especially their design and construction of the avionics bay.

Alexander Hecht

For his work on the video camera payload and the design and construction of the mirror fairing.

Rachel Berg and Mathew Clark

For their comprehensive photography during launch day.

The Staff of the WPI Machine Shops

For their assistance in constructing airframe components, especially on short notice

All of the volunteers who lent us their assistance, however large or small, and those who were present to assist us in launching and recovering the vehicle.

The WPI AIAA Chapter.

Table of Contents

1. INTRODUCTION.....	1
1.1 GOALS AND OBJECTIVES.....	1
1.2 CONSTRAINTS.....	2
1.3 METHODOLOGY.....	2
1.4 DOCUMENTATION.....	2
2. OVERALL VEHICLE DESIGN.....	4
3. AIRFRAME AND MECHANICAL SUBSYSTEM.....	14
3.1.1 Nose.....	14
3.1.2 Body Tube.....	15
3.1.3 Motor Mount.....	15
3.1.4 Fins.....	16
3.1.5 Other Parts.....	16
3.1.6 Painting.....	17
3.2 METHODOLOGY.....	18
3.2.1 Testing and Simulations.....	18
3.2.2 Final Design.....	22
3.2.3 Construction.....	23
3.2.4 Integration of other Subsystems.....	28
3.3 RESULTS AND ANALYSIS.....	31
3.3.1 Tests and Simulations.....	31
3.3.2 Integration of other Subsystems.....	34
3.3.3 Flight.....	35
3.4 CONCLUSIONS.....	36
4. STAGING.....	37
4.1 STAGING BACKGROUND.....	38
4.1.1 Purposes of Staging.....	38
4.1.2 Types of Staging.....	40
4.1.3 Staging in Small Scale Rocket Vehicles.....	41
4.1.5 Magnetic Theory.....	46
4.1.6 Electromagnetic Theory.....	48
4.2 METHODOLOGY.....	56

4.2.1 Design Evaluation and Selection.....	56
4.3.3 Prototype Design.....	61
4.2.4 Prototype Fabrication.....	72
4.2.5 Interim Design Modifications.....	74
4.2.6 Final Design Fabrication.....	78
4.3.7 System Integration.....	82
4.3 RESULTS AND ANALYSIS.....	85
4.3.1 Prototype Testing and Evaluation.....	85
4.3.2 Integrated System Testing and Evaluation.....	91
4.3.3 Flight Performance.....	96
4.4 CONCLUSIONS.....	100
5. RECOVERY.....	101
5.1 RECOVERY BACKGROUND.....	101
5.1.1 Recovery System Function.....	101
5.1.2 Recovery Systems Overview.....	101
5.1.3 Other recovery methods.....	103
5.2 METHODOLOGY.....	104
5.2.1 Initial thoughts and Designs.....	104
5.2.2 Compressed Gas Recovery System.....	105
5.2.3 Spring Recovery Systems.....	106
5.2.4 Prototype.....	108
5.2.5 Flight Device.....	110
5.2.6 Booster Recovery System.....	122
5.3 RESULTS AND ANALYSIS.....	123
5.4 CONCLUSIONS.....	125
6. PROPULSION AND AERODYNAMICS.....	126
6.1 PROPULSION BACKGROUND.....	126
6.2 METHODOLOGY.....	130
6.2.1 Motor Selection.....	130
6.2.2 Hermes Rocket Design.....	131
6.2.3 Ignition.....	132
6.3 RESULTS AND ANALYSIS.....	135
6.3.1 Ignition Tests.....	135
6.3.3 Launch.....	137
6.4 CONCLUSIONS.....	139

6.4.1 Homemade vs. Commercial	139
6.4.2 Launch Analysis	139
6.5 AERODYNAMICS	143
6.5.1 Aerodynamic Background.....	143
6.5.2 Our Experiment	146
7. REFERENCES.....	149
APPENDIX A: INITIAL DESIGNS AND EVALUATION.....	151
APPENDIX B: ROCKET DESIGN DATA	152
APPENDIX C: LIST OF WIRES IN ROCKET	155
APPENDIX D: TEST SIMULATIONS POSSIBILITIES	157
APPENDIX D: TEST SIMULATIONS POSSIBILITIES	157
APPENDIX E: DESIGN DIMENSIONS.....	158
APPENDIX F: AIRFRAME TESTS.....	161
APPENDIX G: G-WIZ MC2 FLIGHT COMPUTER	170
APPENDIX H: PERMANENT MAGNET DESIGN SPREADSHEET	172
APPENDIX I: ELECTROMAGNET DESIGN SPREADSHEET	173
APPENDIX J: LAUNCH SHOCK TEST.....	174
APPENDIX K: RECOVERY TEST WITH COMPUTER SCREENSHOTS	176
APPENDIX L: PML IGNITER FAQ	177
APPENDIX M: PROPULSION SECOND STAGE IGNITER TEST	178
APPENDIX O: VIDEO STILLS FROM IGNITION TESTING	181
APPENDIX P: GUIDE TO MAKING IGNITERS.....	182
APPENDIX Q: IDEAS AND SUGGESTIONS FOR FUTURE WORK	183
APPENDIX R: FAILURE ANALYSIS.....	186

List of Figures

Figure 2.1: Rocket Design Process	4
Figure 2.2: CompuRoc Performance Analysis Software	5
Figure 2.3: RockSim Rocket Design and Analysis Software	5
Figure 2.4: Vulcan Rocket	6
Figure 2.5: Initial Rocket Configuration Ideas compared to a 5' 5" individual	7
Figure 2.6: Design Progression from Concept to Final Vehicle	9
Figure 2.7: Final Vehicle Subsystem Breakdown.....	9
Figure 2.8: Expected Flight Profile.....	10
Figure 2.9: WARRIORS on ascent	13
Figure 2.10: Post Flight Damage Analysis	13
Figure 3.1: Various shapes/ styles of noses	14
Figure 3.2: Centering ring and Retaining Clip Motor Mount Combination	15
Figure 3.3: Cross-sectional drawing of basic model rocket fin airfoils	16
Figure 3.4: Three fin shapes investigated for possible use on the rocket.....	18
Figure 3.5: Wet wood filler, Dry wood filler on body tube, and EASYGLAS sock from left to right.....	19
Figure 3.6: Compression stress and force diagram and Normal Stress force diagram	19
Figure 3.7: The fiberglass cloth during and after application	20
Figure 3.8: Shear test for testing the merit of the fin attachment method.....	21
Figure 3.9: Torque test for testing the structural merit of the fin material.....	21
Figure 3.10: Above- Pro-Engineer Model of the rocket, Below- Breakdown of the rocket	22
Figure 3.11: Actual Electronics Bay (diameter of the coupler tube is 2.56 inches).....	23
Figure 3.12: Cut Pieces of Phenolic (2.56 and 3.00 inch diameter tubing)	23
Figure 3.13: Centering Rings Test Fit to the Motor Mount Tube and Airframe.....	24
Figure 3.14: Balsa Transition (Prior to Fiberglassing) and PVC Transition.....	24
Figure 3.15: Fin Test Fit to the Motor Mount Tube and Centering Ring	25
Figure 3.16: Primed Airframe Pieces.....	25
Figure 3.17: Side View of the Fin Jig (left), and Back View of the Fin Jig (right)	25
Figure 3.18: The Heat Lamp Speeding Up the Curing Process	26
Figure 3.19: Fiberglass Fillets to Motor Mount Tube.....	26
Figure 3.20: Test Fitting Motor Mount/Fin Assembly in the Main Airframe Tube	27
Figure 3.21: Fiberglass Fillets from the Fins to the Airframe Tube	27
Figure 3.22: Final Cosmetic Scheme	28

Figure 3.23: Pro-Engineer rendering of staging integration section	29
Figure 3.24: Left- Final Pro-Engineer design of fin, Right- Actual fin	32
Figure 3.25: Setup for the actual compression resistance test	32
Figure 3.26: Tubes A and B after the completion of the repeated normal force stress test	33
Figure 4.1: Velocity Capability as a function of Mass Ratio and Number of Stages	39
Figure 4.2: Series Staging	40
Figure 4.3: Parallel Staging.....	40
Figure 4.4: Typical Black Powder Rocket Motors.....	42
Figure 4.5: Direct Staging with Black Powder Motors.....	42
Figure 4.6: The Public Missiles Inter-Stage 3000 System.....	45
Figure 4.7: Magnetic Flux Measurement.....	47
Figure 4.8: A typical Solenoid Coil	48
Figure 4.9: A Single Coil Electromagnet.....	50
Figure 4.10: Relative Magnetic Flux Density along the X-axis as a function of L/R Ratio	52
Figure 4.11: Magnetic Flux Density of a Solenoid versus a Permanent Magnet.....	52
Figure 4.12: Transient Response Analysis of an LC Circuit	53
Figure 4.13: Current Discharge Plot for the actuator circuit (computed in MicroSim).....	55
Figure 4.14: Capacitor Voltage during Discharge (computed in MicroSim).....	55
Figure 4.15: An Abstract Model of a Staging System	56
Figure 4.16: GWiz MC2 Flight Computer	57
Figure 4.17: Energy and Forces that can Create Mechanical Output	58
Figure 4.18: Actuator Classifications.....	59
Figure 4.19: Possible actuator design	62
Figure 4.20: Early Electromagnetic Staging Concept.....	63
Figure 4.21: Mount Angle Considerations.....	64
Figure 4.22: Aft Hook Mounting Concept.....	65
Figure 4.23: Separation Concept with Aft Hook	65
Figure 4.24: Electromagnetic Actuator	70
Figure 4.25: 0.33F Aerogel Capacito.....	70
Figure 4.26: Initial Power Circuit Design.....	71
Figure 4.27: Coil Assembly mounted in the Prototype.....	72
Figure 4.28: Aft Hook attached to the prototype booster.....	73
Figure 4.29: Completed Prototype	73
Figure 4.30: Redesigned Coil	74

Figure 4.31: Electrolytic Capacitor	75
Figure 4.32: Redesigned Capacitive Discharge Circuit	77
Figure 4.33: Redesigned Aft Booster Hook.....	77
Figure 4.34: Metal Retainers and Oversized Garolite Sheaths	78
Figure 4.35: Booster Airframes cut for Magnets	79
Figure 4.36: Final Wound Coil ready for Integration	79
Figure 4.37: Booster Hook fitted inside Main Airframe Slot	80
Figure 4.38: Location of the Staging Electronics	80
Figure 4.39: Lower Electronics Bulkhead (left) and Upper Electronics Bulkhead (right)	81
Figure 4.40: Assembled Staging Electronics Bay awaiting closure.....	81
Figure 4.41: Top Side of the Upper Staging Electronics Bulkhead	81
Figure 4.42: Complete Staging Electronics Bay	82
Figure 4.43: Extra Garolite for Alignment.....	82
Figure 4.44: Reinforced Coils.....	82
Figure 4.45: Boosters Installed and Aligned.....	83
Figure 4.46: Threaded Rod Installed at the Airframe Interface	83
Figure 4.47: Completed Staging Assembly	84
Figure 4.48: Magnet Tensile Testing	85
Figure 4.49: Magnet Discharge and Height Measurement Test Setup	88
Figure 4.50: Sub-Assemblies Link Together for Integrated Staging Systems Test	92
Figure 4.51: Revised Subassembly Test	94
Figure 4.52: Capacitor Voltage as a Function of Time	95
Figure 4.53: Leaf Blower Air Stream Separation Test	96
Figure 4.54: In-Flight separation with third booster firing	98
Figure 4.55: Post-separation flight trajectory	98
Figure 4.56: Forces on booster three at separation	99
Figure 5.1: Early Conceptual Drawing of Activation Device.....	107
Figure 5.2: Remains of Prototype after Testing.....	108
Figure 5.3: Section View of Operational Device without Lever	111
Figure 5.4: Photographs of Operational Device (2.5 inch diameter)	112
Figure 5.5: Piston	113
Figure 5.6: Springs (8 inch uncompressed length).....	113
Figure 5.7: Solenoid.....	114
Figure 5.8: Solenoid Mounting Bracket.....	114

Figure 5.9: Solenoid and Mounting Bracket.....	114
Figure 5.10: Solenoid, Mounting Bracket & Electronics Inside of the Airframe.	115
Figure 5.11: Shock Cord Mounting Brackets	115
Figure 5.12: Fully Assembled Device during Testing	116
Figure 5.13: Safety Pin	117
Figure 5.14: Shear Pins	118
Figure 5.15: Recovery Circuitry Diagram	119
Figure 5.16: Prototype Circuit	120
Figure 5.17: Prototype Circuit Next to Recovery Systems	120
Figure 5.18: Flight Circuitry with PSU Connectors.....	120
Figure 5.19: Initial plugs used for the circuit.....	121
Figure 5.20: Booster Recovery System (Post-Flight)	122
Figure 6.1: Components of a Solid-Propellant Rocket Motor	126
Figure 6.2: Components of a Reloadable Motor	128
Figure 6.3: Sample Motor Configurations	131
Figure 6.4: Ematch.....	132
Figure 6.5: Igniter with Pyrogen Coating	133
Figure 6.6: Progressive 1 st stage ignitiong	140
Figure 6.7: Rocket clearing the launch pad.....	141
Figure 6.8: Eight Degrees of Freedom.....	143
Figure 6.9: Three stability conditions with CG-CP relationships	144
Figure 6.10: Well-Damped and Under-Damped Model Rocket Design.....	145
Figure 6.11: Experimental Wind Tunnel Model Apparatus (not to scale).....	147

List of Tables

Table 2.1: Initial Specifications and Cost Estimates of Configurations A and B.....	8
Table 2.2: Expected Flight Sequence and Flight Events.....	10
Table 2.3: Subsystem Mass Breakdown.....	11
Table 2.4: Actual Measured Section Mass Breakdown.....	12
Table 3.1: Subsystem Integration Requirements	28
Table 3.2: Post-Flight Analysis of the Airframe.....	35
Table 4.1: Permanent Magnet Material Properties	46
Table 4.2: Electromechanical Actuators	59
Table 4.3: Fluidic Actuators	60
Table 4.4: Electromagnetic Actuators.....	61
Table 4.5: Coil and Circuit Properties	69
Table 4.6: Revised Coil and Circuit Properties.....	75
Table 4.7: Permanent Magnet Tensile Test Results.....	86
Table 4.8: Permanent Magnet Tensile Test Results for the Designed Geometry	86
Table 4.9: Discharge Energy Test.....	89
Table 4.10: Discharge Test Averages	89
Table 4.11: Testing Responses to Voltage and Capacitance Parameters.....	90
Table 4.12: Initial Booster Separation Tests.....	93
Table 4.13: Capacitor Leak Test Voltage Results.....	95
Table 5.1: Materials Ordered for Prototype Construction	107
Table 5.2: Spring Force Comparison	109
Table 5.3: Threshold Voltage Test.....	121
Table 6.1: Motor Classes	129
Table 6.2: Second Stage Ignition results.....	135

1. Introduction

1.1 Goals and Objectives

The WPI AIAA Research Rocket for the Investigation and Observation of Recovery and Staging (WARRIORS) is a two-stage, high-powered model rocket equipped with an onboard computer and a digital video camera. One goal of this project was to allow undergraduate students completing their Major Qualifying Project (MQP) and American Institute of Aeronautics and Astronautics (AIAA) student volunteers the opportunity to jointly design, build and test a complex aerospace system. The original concept of this project was conceived by the WPI AIAA chapter in an effort to allow all levels of undergraduate students to be involved with realistic engineering design, assembly, and test activities. A second goal was to achieve a minimum altitude of 1500 feet during a test flight.

The WARRIORS overall vehicle performance was fundamentally tied to the mass, construction, assembly, and integration of individual components. Additionally, this project provided the experience of working on a large team to build a complex device. A third goal was to design, test, operate, and evaluate the effectiveness of an innovative electromagnetic booster separation system and non-pyrotechnic dual parachute deployment mechanism. In order to achieve the three project goals, eight MQP students were divided into four subsystem teams in order to achieve the following objectives:

- Airframe and Mechanical: Design, Fabricate, assemble, and test the overall mechanical structure and integrate the other subsystems.
- Propulsion and Aerodynamics: Select commercially available solid motors for two stage rockets, fabricate, test and integrate igniters for the first and second stage motors, and investigate the aerodynamic stability of the completed vehicle.
- Recovery: Design, fabricate, assemble, and test an innovative parachute deployment system without use of pyrotechnic devices.
- Staging: Design, fabricate, assemble, and test an innovative stage separation system without use of pyrotechnic devices.

In conjunction with the four main subsystems listed above, two additional subsystems allowed volunteers to assist in the construction of the WARRIORS rocket. These subsystems allowed the rocket to carry enhanced capabilities including the following:

- Onboard Video Payload: Design and test a video capturing system to monitor flight events.

- Flight Computer: Purchase, assemble, program, and test a commercially available rocketry computer for control and monitoring of flight events.

1.2 Constraints

As in any real-world engineering project, WARRIORS was faced with design goals and constraints. One constraint was a monetary limit of approximately \$1200. A second constraint was the use of commercial solid fuel rocket motors no larger than “G” class (~120 Newton Seconds). Based on this limited motor size, in order to reach 1500 feet, the vehicle’s overall mass had to be minimized. For our final design it was limited to 3.4 kilograms, which will be explained in Chapter 6. The fourth constraint was having only one academic year to complete this project. Our final constraint was limiting the airframe to commercially available body tube diameters. Together, these goals and constraints provided a realistic and challenging engineering project, which would create a notable rocket system while providing a unique educational opportunity for all those involved.

1.3 Methodology

In order to keep this project on task, we followed an overall procedure to ensure the completion of all objectives in a timely manner. This consisted of different engineering and management tasks. The first of these were bi-weekly meetings in order to update subsystem teams on progress and to discuss any problems that had arisen. To organize these updates, a system engineer (Eric Byrd-Krueger) was designated. Due to the limitation of our budget, it was imperative that it be tracked throughout the entire project. This was done through updates to an Excel™ file. The same concept was applied in tracking the mass of the vehicle in order to ensure that it didn’t exceed the 3.4 kilogram constraint. In order to ensure all aforementioned processes to be completed on time, a Gantt chart was created. These three spreadsheets were continually updated by our system engineer.

1.4 Documentation

This report is organized as the following:

- Chapter 2: Overall Vehicle Design. This chapter provides an overview of the design process from the preliminary concepts to the final WARRIORS vehicle.
- Chapter 3: Airframe and Mechanics. This chapter provides the background, methodology, results, analysis, and conclusions of the airframe subsystem group.
- Chapter 4: Staging. This chapter provides the background, methodology, results, analysis, and conclusions of the staging subsystem group.

- Chapter 5: Recovery. This chapter provides the background, methodology, results, analysis, and conclusions of the recovery subsystem group.
- Chapter 6: Propulsion and Aerodynamics. This chapter provides the background, methodology, results, analysis, and conclusions of the propulsion subsystem group. Relevant aerodynamic issues are also presented.

2. Overall Vehicle Design

The most critical first step of in any engineering design project is to establish goals and constraints such as those listed in Sections 1.1 and 1.2. Following the establishment of these criteria, we investigated several possible design concepts in order to estimate the mass budget and vehicle power requirements. We created a flowchart of the design iteration process in order to assist us with this initial configuration (Figure 2.1).

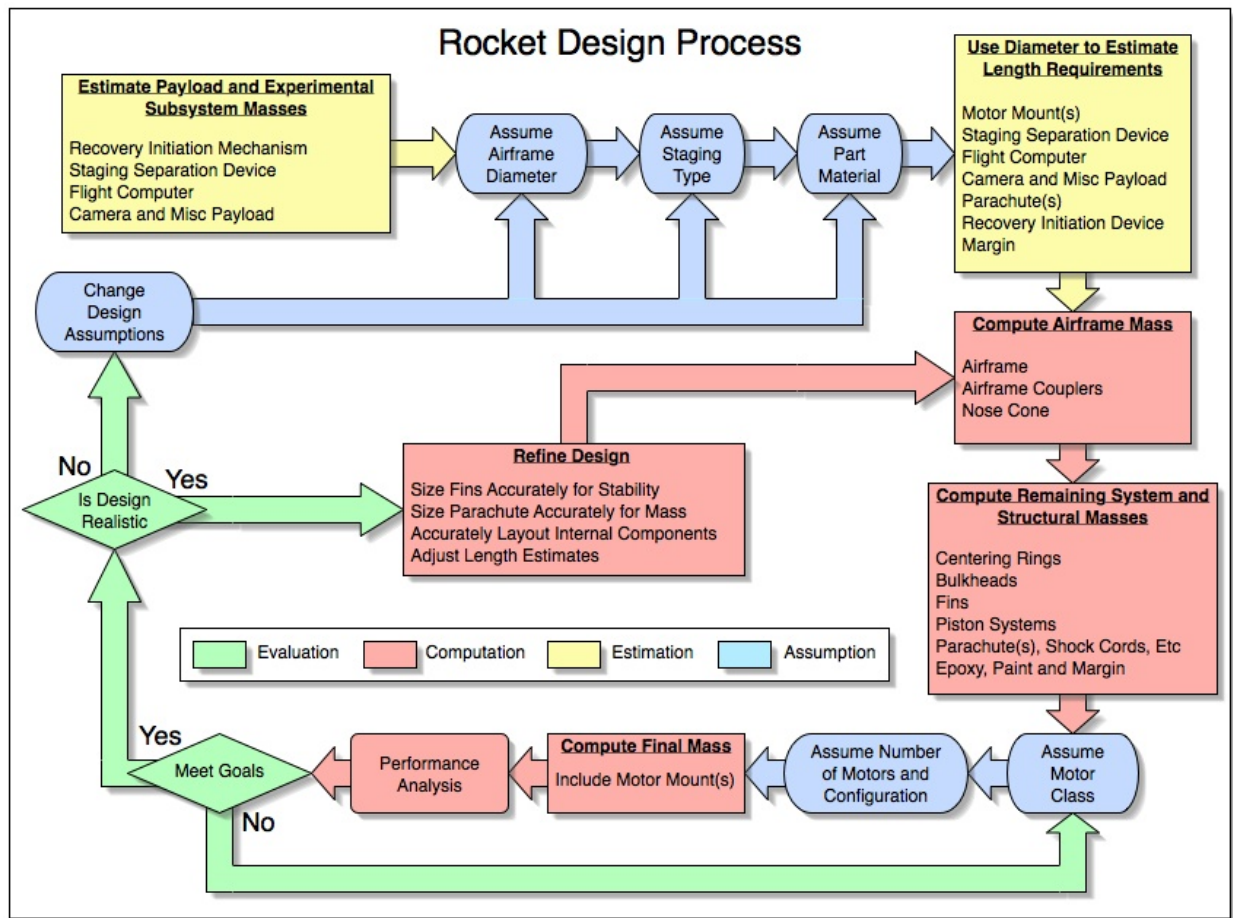


Figure 2.1: Rocket Design Process

In order to provide a more accurate configuration analysis, we utilized two commercial rocket simulation software packages to assist with the performance analysis portion of the design process. The first package, known as CompuRoc (produced by Greg Lyzenga and Doug Wade and shown in Figure 2.2), provided sufficiently accurate altitude approximations for a first order analysis based on inputs such as drag coefficient, rocket diameter, empty weight, and chosen motor configuration. The second software package, known as RockSim (produced by Apogee Rockets and shown in Figure 2.3), provided more

detailed performance analysis by allowing the user to construct a complete virtual model of the vehicle within the computer. RockSim was also capable of computing weight distribution and pressure distribution data, thus allowing determination of vehicle stability. While the significant simulation capability of RockSim was greatly beneficial in the design process, construction of a virtual model was a fairly time consuming process and was thus undertaken only after the approximate design was agreed upon.

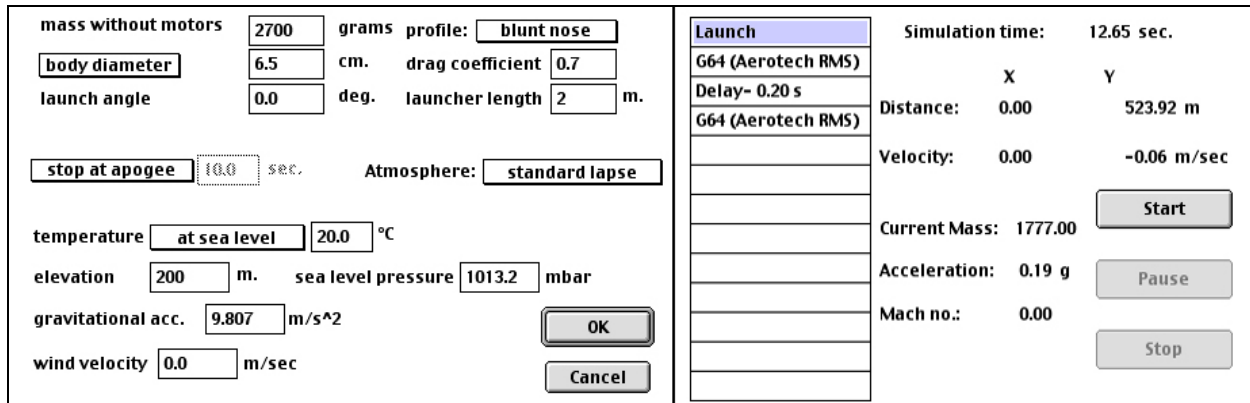


Figure 2.2: CompuRoc Performance Analysis Software

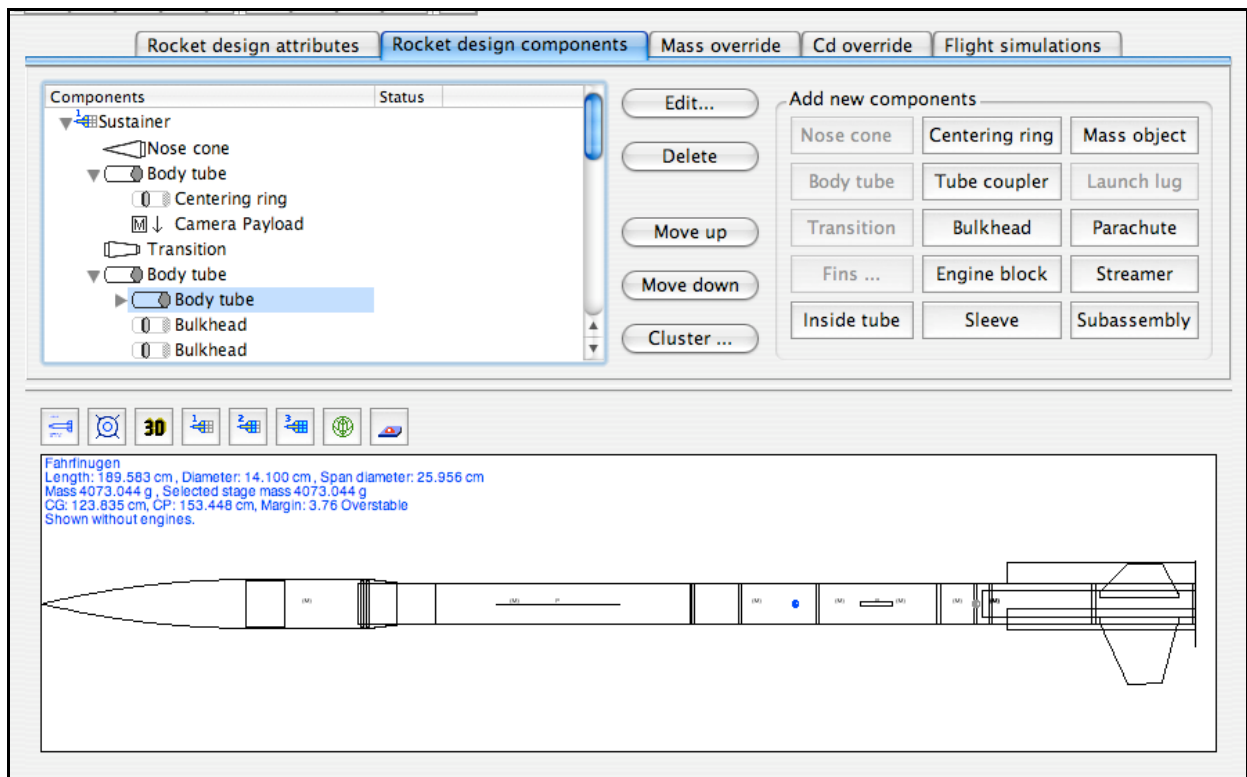
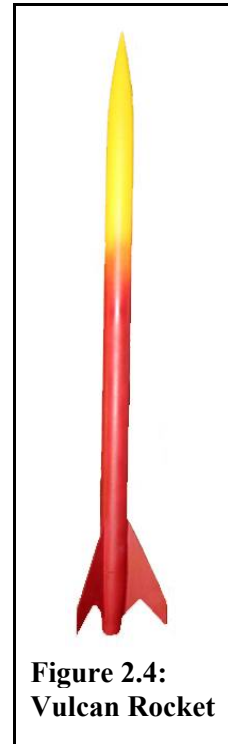


Figure 2.3: RockSim Rocket Design and Analysis Software

In addition to the computer assisted analysis, one existing vehicle known as Vulcan served as a specific design example. We used this rocket as a working example because the designer of Vulcan participated in the design of the WARRIORS vehicle (Figure 2.4). The Vulcan rocket consisted of a single "G" class rocket motor housed in a robust airframe 2.2" in diameter and 50.875" long. This structure utilized materials and construction techniques similar to those available for the WARRIORS project. Vulcan's structure along with internal systems (excluding the motor and motor casing) had a combined mass of approximately 900 grams. This mass was primarily due to the rocket's outer airframe, motor mounting hardware, and fins. Aside from a basic parachute recovery system, Vulcan contained no staging system, flight computer, or payload. The implementation of a staging system, flight computer and payload would represent increased capability compared with Vulcan, however they would also significantly increase the empty mass (mass excluding motor or motor casing). In order to determine quantitatively how much the additional subsystems would increase the mass of a vehicle this size, we obtained the following estimates from existing rocket designs (available from major rocket manufacturers):



- Flight Computer: ~100g
- Staging Electronics and Mechanism: ~150g
- Dual Chute Recovery System (excluding parachutes): ~250g
- Camera / Telemetry Payload: ~150g
- Additional Airframe Structure for subsystems and staging section: ~150g

It should be noted that some of these estimates might be optimistic as they are highly optimized in existing commercial rockets of this size. In any case, a WARRIORS vehicle with the same diameter as Vulcan and including the aforementioned additional subsystems would likely have an empty mass around 1400g to 1600g. The 2.2" diameter would allow one "G" motor to fit in the lower stage, and one "G" in the upper stage. Unfortunately given this empty mass, two G motors staged in series would barely be able to reach the 1500-foot altitude goal as determined from CompuRoc simulations. Consequently, this configuration would leave almost no performance margin unless all aforementioned subsystem mass estimates were conservative. The only way to obtain 1500 feet in a dual "G" configuration would be to shrink the diameter to the next available commercial airframe size of 1.4". Shrinking the diameter would reduce both structural mass and drag, however at the reasonably slow speeds the WARRIORS vehicle

will operate, weight would be more of a detriment to performance than drag. Nevertheless, a 1.4” diameter vehicle would have been capable of reaching about 1600 feet and thus the performance goal on two staged "G"s. Unfortunately, it would have resulted in a vehicle that would have been unreasonably long in order to fit in the necessary systems, and it would have left little or no payload volume.

From this initial configuration analysis, we concluded that two “G” motors would be inadequate to meet our project requirements. More performance and size margin was necessary. Given this, we investigated the performance capability of using three G motors- two clustered in the lower stage, and one in the upper stage. The required diameter of the vehicle would need to be increased when compared to Vulcan (either to hold the engine cluster or hold the parallel staging system for outboard boosters), since mass was more of a concern than drag as previously mentioned, larger airframes would not likely degrade performance significantly. Switching to a commercial 2.56" diameter airframe and adding an additional "G" in the lower stage would thus result in a vehicle with slightly more performance than the dual "G" 1.4" diameter vehicle, but with significant more payload volume in a more aesthetically pleasing rocket. This would thus be a more feasible design. Adding a fourth motor (making the second stage a dual cluster as well) would increase performance significantly as it would fit in the same size airframe and thus have little mass penalty. This fourth motor could also be added to the lower stage to form a tri-cluster if the diameter of either the whole rocket or just the first stage was increased to the next commercially available dimension of 3.” Using three outboard boosters in parallel would also generate similar performance.

In any case, the more general conclusion we reached from this initial analysis was that while it might be possible to achieve the 1500 foot goal with two staged "G" motors on the final WARRIORS vehicle utilizing commercial materials, we wouldn't have any room for error, the use of paint, or any form of a payload. A configuration with four "G" class motors would allow for a more capable vehicle with an excellent performance margin. Unfortunately, however, clustering motors in such a configuration would not be without risk. Asymmetric thrust due to slight differences in motor ignition timing could lead to an unstable flight in a vehicle this scale. Consequently, we would have to develop a reliable ignition system.

Assuming this could be done, however, we selected the four-“G” motor configuration as the best possible

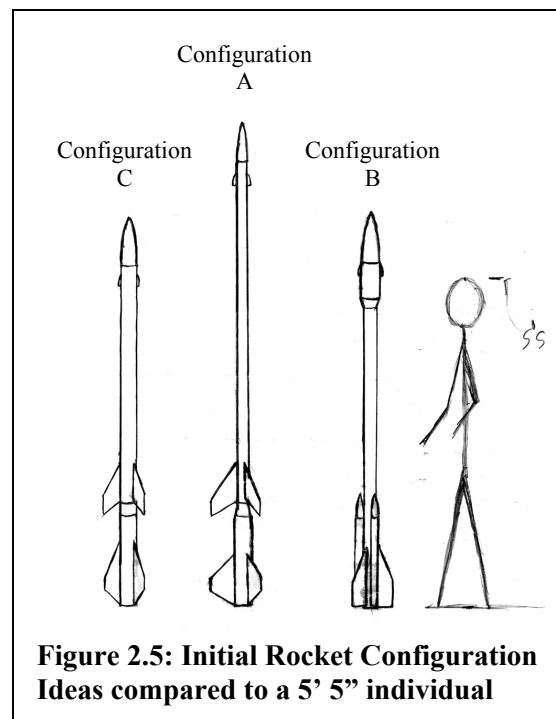


Figure 2.5: Initial Rocket Configuration Ideas compared to a 5' 5" individual

solution. Following this, we created three possible rocket configurations to match this motor configuration (Figure 2.5). All three would have somewhat different performance characteristics, but they would all be capable of achieving the required project goals.

After further discussion of the three vehicle configurations initially selected, we narrowed the possible options to two by way of a group vote (Configurations A and B in Figure 2.5). The first of the two remaining options (Configuration A in Figure 2.5) consisted of a 2.56” airframe transitioning to a 3” airframe for the lower stage. In this configuration, three internal G-class motors were housed in the booster stage, and a single G motor was housed in the second stage. The second configuration (Configuration B in Figure 2.5) was designed to have a single G engine within the lower portion of the rocket and three G engines mounted in attached boosters. The airframe diameter was the same as configuration A (2.56”), however it transitioned to a 3” airframe for the payload section. Initially we could not decide which of the two remaining options we should pursue, so we refined each design and evaluated the major airframe component costs. The initial cost estimates of these two options as well as general mass and size estimates (including 20% and 10% margin respectively) are shown in Table 2.1. More detailed performance analysis of these options (initially referred to as “Hickey” and “Fahrfinugen”) is shown in Appendix A and Appendix B. While Configuration A proved cheaper and had slightly higher performance, we decided to design our vehicle around Configuration B (later named “Hermes”) due to the technical merit of parallel staged boosters (not typically done in a rocket this size).

	Height (m)	Mass (kg)	Airframe Structure Cost
Configuration A	2.18	3.06	\$188.13
Configuration B	1.66	3.10	\$227.11

Table 2.1: Initial Specifications and Cost Estimates of Configurations A and B

Following the initial configuration analysis, we created computer models in RockSim and PTC Pro-Engineer to assist in more detailed performance analysis as well as vehicle construction. From this point, each project subsystem (Propulsion, Recovery, Staging, and Airframe) began design and testing of the individual systems and components. During this process, we continually refined the overall vehicle design specifications and computer models to reflect changes required by each of the individual systems. The results of these design refinements from the initial concept drawing to final vehicle are shown in Figure 2.6. Figure 2.7 shows the location of each major system in the vehicle. In addition to the vehicle design itself, we also defined the expected flight profile (Figure 2.8 and Table 2.2).

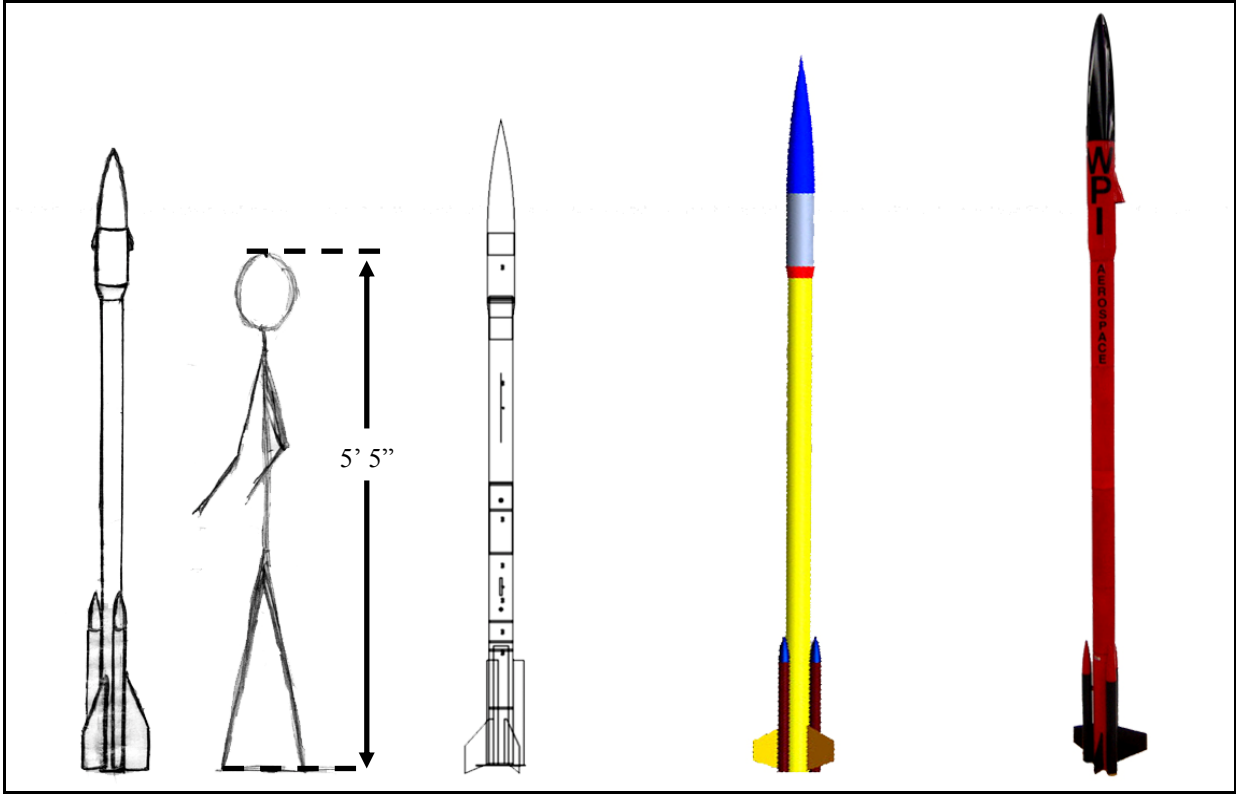


Figure 2.6: Design Progression from Concept to Final Vehicle

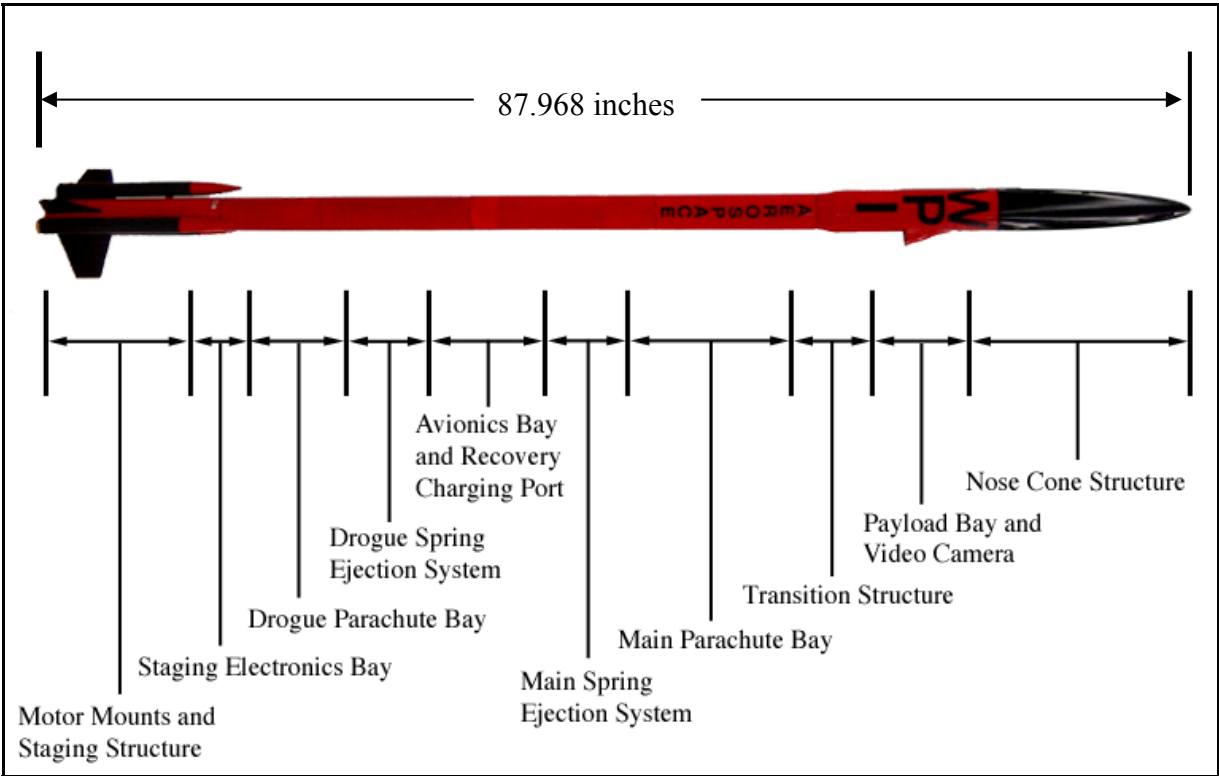


Figure 2.7: Final Vehicle Subsystem Breakdown

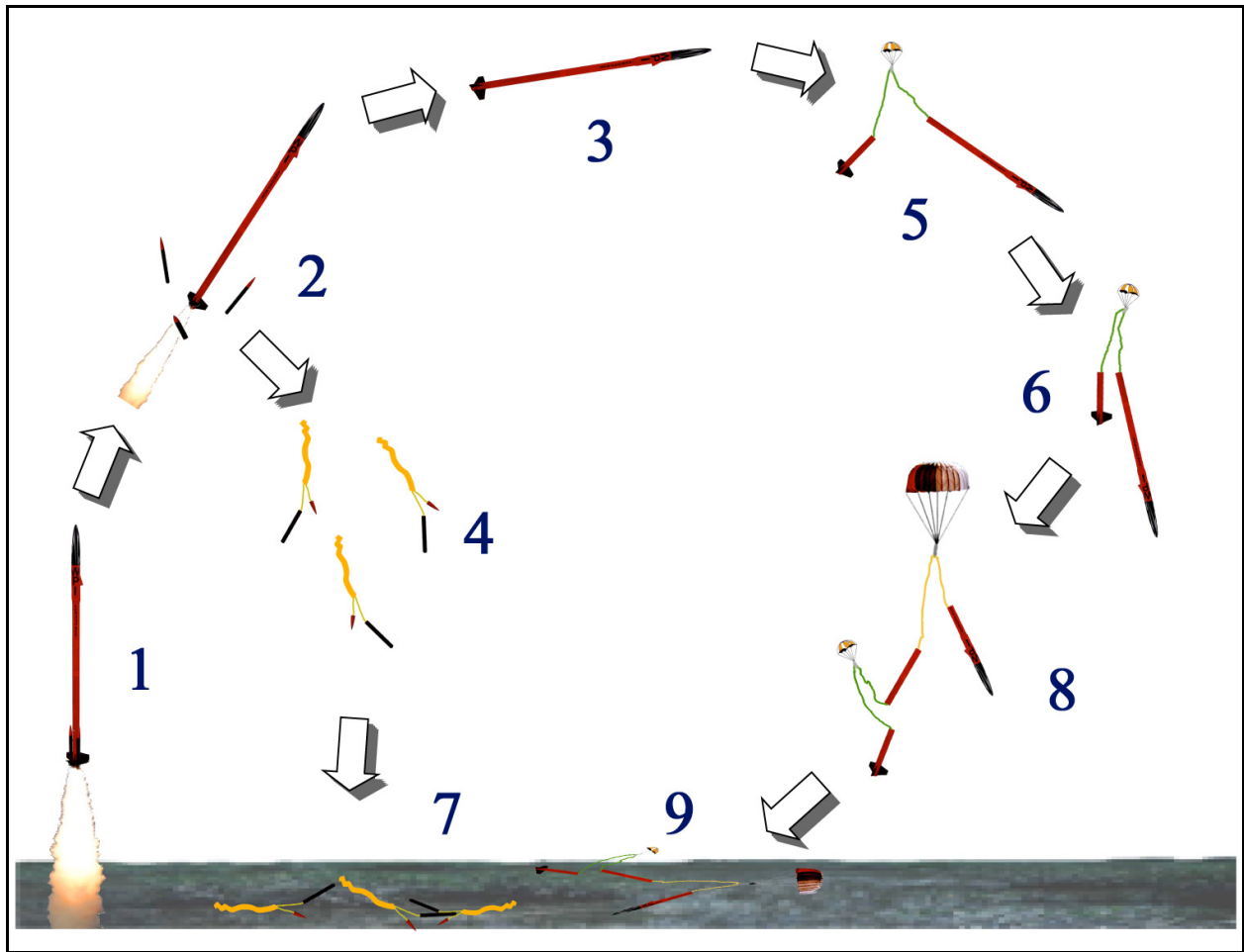


Figure 2.8: Expected Flight Profile

Sequence Number	Flight Event
1	The three first stage boosters ignite simultaneously and propel the vehicle off the launch pad.
2	The flight computer triggers the staging system and ignites the core motor after booster burnout.
3	The core motor burns out after another two seconds, and the rocket coasts upward.
4	The jettisoned boosters deploy their streamer recovery systems.
5	The main computer senses apogee and deploys the drogue parachute
6	The rocket descends under the drogue in order to minimize drift but remains under control.
7	The burnt boosters touch down gently under streamer control.
8	The flight computer senses 400 feet above ground level and deploys the main parachute.
9	The core sections of the vehicle touch down gently under the main parachute.

Table 2.2: Expected Flight Sequence and Flight Events

WARRIORS Mass Breakdown			
Subsystem or Component	Mass (g)	Subsystem or Component	Mass (g)
Airframe		Main Recovery	
Airframe Mass	650	Main Parachute	144
Airframe Coupler Mass	70	Piston Bulkhead	18
Nose Cone Mass	190	Phenolic Center Rods	5
Centering Ring Mass	26	Springs	50
Bulkhead Mass	91	Aluminum Lever	13
Fin Mass	120	Bulkhead & Lever Support	45
Epoxy, Paint, and Misc Mass	434	Solenoid	55
		Solenoid Coupler	7
Avionics		Shock Cord	75
Main and Backup Batteries	92.8	Electronics	40
Pyro Battery	47.7		
Main Computer (MC2)	40	Drogue Recovery	
Break-Wires	100	Drogue Parachute	35
Bay Structure	185	Piston Bulkhead	18
Avionics Mounting Sled	75	Phenolic Center Rod	5
Backup System	50	Springs	50
		Aluminum Lever	13
Staging		Bulkhead & Lever Support	45
Magnets	42	Solenoid	55
Wire Coils	4	Solenoid Coupler	7
Steel Retainers	21	Shock Cord	75
Garolite Sheath	2	Electronics	40
Staging Electronics	277		
		Propulsion	
Payload		Empty casing	58
Camera and foam	100	Empty casing	58
		Empty casing	58
		Empty casing	58
		Total Mass	3412.5

Table 2.3: Subsystem Mass Breakdown

In addition to the refined computer models, we also monitored component mass estimates and subsystem masses throughout the design and testing process to make sure the rocket remained light enough to achieve the specified altitude goals. The final mass breakdown of these systems is shown in Table 2.3. Note that the total computed does not reflect any propellant or propellant casings as all our calculation were based on empty mass. The initial total mass estimate of 3.1 kg shown in Table 2.1 did have a 10% margin included. Consequently, the rocket could increase to as mass of 3.4 kg before it would be unable to reach 1500 feet in altitude. In the final post-assembly subsystem mass breakdown, we appeared to be approximately at this limit. Unfortunately, when we measured the actual masses of each rocket section (usually containing combined subsystems), we found that the rocket was significantly over our design target of 3.4 kg as well as our final subsystem calculated mass breakdown estimate of 3.41 kg. The measured section mass breakdown is shown in Table 2.2.

Measured Section Mass	
Item	Mass (g)
Aft Body (without Boosters)	962
Booster One	70
Booster Two	67
Booster Three	68
Mid Body (Airframe Only)	240
Avionics and Spring System	1147
For Body (Airframe Only)	288
Camera Section (with Nose Cone)	780
Drogue Parachute	21
Main Parachute	143
Total	3786

Table 2.4: Actual Measured Section Mass Breakdown

We were initially uncertain as to why the mass values differed so greatly between the final breakdown by subsystem and the actual measured section values. Four possible sources of this extra mass were system wiring (not included in any specific subsystem), rail support structure, motor-mount adaptor, and miscellaneous epoxy used during general assembly that was not considered part of any specific subsystem. Of all these explanations, the wiring seemed the most likely culprit as this vehicle used much more wiring than originally conceived possible. In order to get an idea of how much additional mass the system wiring could contribute, we measured each electrical run in the vehicle and found over approximately 80 feet of wiring. This amount of wire would have contributed close to 200 grams of additional mass when connectors were factored in, and could help explain the unexplained mass.

A more detailed breakdown of the system wiring and mass values is shown in Appendix C. Given the system wiring, it is highly probably the other explanations listed above contributed the remaining additional mass observed.

The unfortunate outcome of such a significant mass increase was that we would no longer be able to achieve an altitude of 1500. This turned out to be a minor issue, however, because FAA regulations on the eventual launch date prevented us from entering controlled airspace at 1200 feet above ground (no waiver was obtained). In any case, such an altitude was deemed sufficient to test all subsystems and rocket performance characteristics. When all construction and individual testing was complete, we thus assembled the vehicle in its final configuration, added 250g of ballast (suggested by RockSim simulations to keep us

below 1200 feet), tested all systems together, and launched the WARRIORS vehicle. The vehicle is shown on ascent in Figure 2.9.



Figure 2.10: Post Flight Damage Analysis

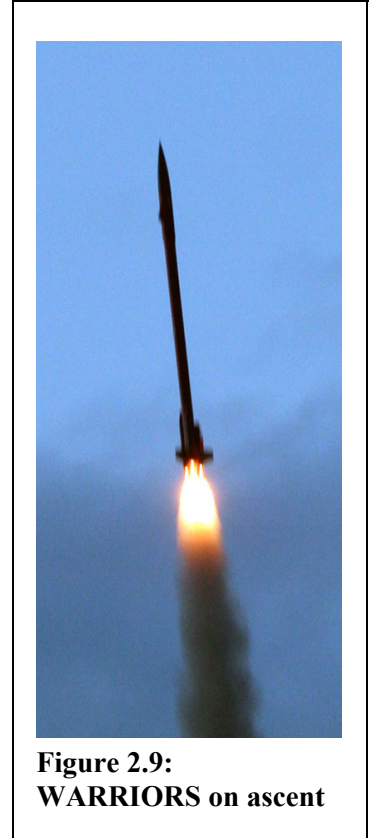


Figure 2.9: WARRIORS on ascent

The specific results of this launch are discussed further in each subsystem section, but in general the results were mixed. While the vehicle did not return to the ground such that it could be flown again without significant repair (Figure 2.10), many of the subsystems were tested as planned and flight data gathered from cameras on the ground proved the functionality of many of these systems. The launch was thus deemed partially successful with only a few elements failing or remaining untested.

3. Airframe and Mechanical Subsystem

Airframe and mechanical design for large-scale modern model rockets is largely based on the simple small-scale model rocketry that has existed since the early 1950s. The airframe is the main structural element and provides mechanical support for all subsystems.

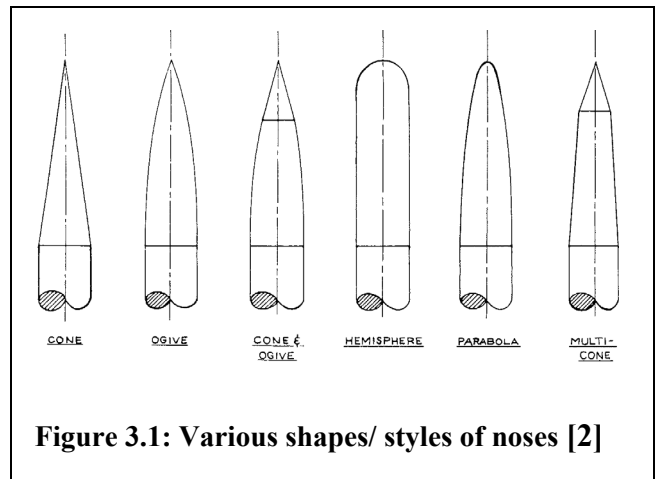
Model rockets, specifically airframe and mechanical subsystems, are composed of numerous parts and components. The major pieces include the nose cone, body tube (or airframes), motor mounts, fins, and recovery systems. In accordance with the National Association of Rocketry (NAR) standards, the aforementioned parts may only consist of lightweight, non-metallic materials. However, in some cases, limited amounts of ductile metal may be used. [1]

3.1 Airframe Background

For the WARRIORS project, the airframe was constructed largely from the parts described below. These parts were in compliance with all NAR standards and satisfied all pre-set flight specifications.

3.1.1 Nose

Nose cones (even though they are not always in a cone shape) are located at the top of the rocket. The nose has a few inches of a neck (a cylinder with a smaller diameter than the airframe), which slides into the airframe. It is important that the nose and body have a snug fit yet are not too tight since the nose on many rockets is removed during the deployment of the recovery device. The nose's outside diameter matches the body tube diameter to ensure that no gap exists to disrupt the airflow over the rocket. For examples of different shapes and sizes of noses that can be utilized, see Figure 3.1. All of the nose shapes have benefits and drawbacks which in the end directly affect the performance of the rocket. The ogive style has the lowest aerodynamic drag coefficient. This means it will slow the rocket down the least while in flight. [2]



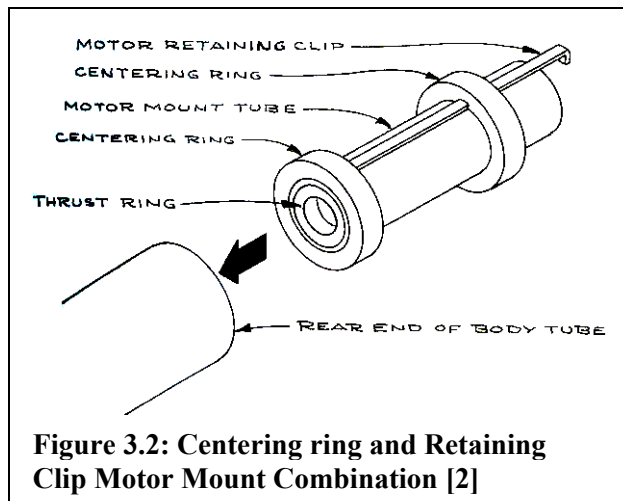
Again, to comply with NAR standards, no metal may be used in the construction of the nose because this can lead to greater damage of property if an impact were to occur for any reason.

3.1.2 Body Tube

The frame, which gives the rocket its recognizable cylindrical structure, is called the body tube or airframe. Body tubes are hollow cylinders that contain all the instrumentation and internal mechanical structures of the rocket, and they are constructed to withstand high levels of compressive, torsional, and flexural stress. [2] For smaller scale rockets, the body tube is usually a cardboard cylinder. However, for higher-powered rockets, the body tube composition is either Phenolic (compressed and cardboard impregnated with phenolic resin) or fiberglass. Both of these products have a higher level of structural integrity than simple cardboard. However, the price of fiberglass is approximately four times higher than phenolic. [3]

3.1.3 Motor Mount

Rockets are only able to fly if they have a motor that provides sufficient thrust to lift the rocket off the launch pad. In order for that to occur safely, the motor must be securely contained within the

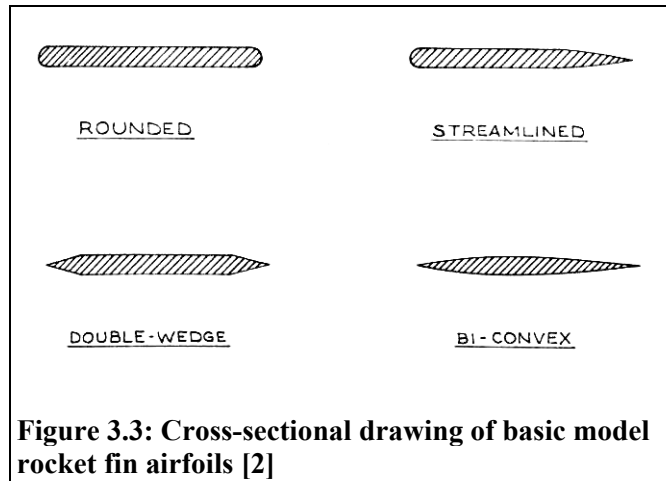


rocket. This is accomplished by using a motor mount. One typical method is to mount the motor with centering rings (a ring with an outer diameter equal to the body tube's inner diameter and a centered inner diameter equal to the motor's outer diameter). A retaining clip is often used to secure the motor (Figure 3.2). A second motor retention method is to apply masking tape to the exterior of the motor to create a "friction fit" to keep the motor in place. [2] Both methods are equally effective in terms of motor retention. However,

friction fitting is done for simplicity or when very small airframe diameters are used (since there is no room for a retaining clip). Additionally, either option remains valid regardless of the size of the rocket.

3.1.4 Fins

Fins are generally airfoils shaped like the wings of an airplane but, unlike wings, they are used to create stable flight and not lift. [2] Model rocket fins are typically constructed of balsa wood, plywood, plastic, fiberglass, or carbon fiber with balsa being the weakest material and carbon fiber being the strongest. Balsa and plastic are only used for small-scale rockets because they cannot withstand the forces experienced during higher-powered rocket flight. However, it is important to note that if wooden fins are used, the grain of the wood should follow the leading edge (the front of the fin) of the fin otherwise it will break easily during flight. When constructing the fins, it is important to reduce the effects of aerodynamic drag as much as possible. This can be done by shaping the fins in the form of an airfoil as shown in Figure 3.3. The ideal airfoil for a model rocket is a rounded leading edge and a tapered trailing edge, which is the streamlined airfoil pictured above.



It is necessary when placing the fins on to the body tube to ensure even spacing around the body tube in a triform (three fins placed 120 degrees apart) or cruciform (four fins placed 90 degrees apart) manner. Special attention should be paid to the vertical alignment with the body in order to minimize drag during flight. Fins are not always placed at the bottom of the rocket; rather their positioning is calculated to ensure the center of pressure, the point where the net pressure force can be considered to act, is behind the center of gravity. This is what creates stable flight. [2] When gluing the fins in place, it is important to create a fillet where the fins and the body tube intersect in order to guarantee a strong bond to the body tube. In addition, to further increase the bond strength of the fins to the body tube, fiberglass cloth can be filleted between the fins and body tube.

3.1.5 Other Parts

In addition to the parts already mentioned, model rockets contain other smaller parts such as bulkheads, centering rings, coupler tube, shock cords, u-bolts, payload, electronics, and staging systems. Details of these smaller airframe parts are as follows: [2]

- **Bulkheads** are wood or fiberglass disks with a diameter that matches the inner diameter of the body tube. They are used to separate sections within the body tube to keep rocket

components from shifting during flight. They are also used for mounting other internal systems.

- **Coupler tubes** are much like body tubes. The outer diameter of the coupler is the same as the inner diameter of the body tube; therefore, the coupler can be used to connect two separate pieces of body tube together and can act as an interface between the two pieces.
- **Shock Cords** are cords, usually made of nylon that is used to connect the body tubes, recovery devices, and the nose cones together. Shock cords are discussed in more detail in the recovery section.
- **U-Bolts** are U-shaped bolts that attach to bulkheads. They are used to fix where the shock cords connect to the overall airframe.
- **Shear Pins** are small nylon pins used to attach the body tubes and couplers.
- **Sleds** are platforms that can slide into the body or coupler tubes. They are used to safely secure important electronics and allow easy removal.
- **Launch Rails** are rods with U-brackets which guide the rocket in a vertical direction during the initial boost phase of its flight. A typical rail is between eight and twelve feet in length.
- **Rail Buttons** are small metal screws attached to a rocket's outer airframe. They guide the rocket up the launch rail by sliding vertically in the U-bracket.

The remaining assemblies: payload, electronics and staging, are all be discussed in complete detail in the following chapters.

3.1.6 Painting

Painting the rocket is not merely for aesthetic purposes, but it helps to protect the rocket and aid in recovery. It is usually better to use bright colors on the rocket, but due to New England's typically dull skies, maroon is also a useful option in order to assist in recovery. [2] Spray paints (i.e. Krylon[®]) or airbrushes provide the most efficient and effective method for painting the rocket.

3.2 Methodology

3.2.1 Testing and Simulations

In order to use the most effective and efficient materials for the airframe, it was essential to perform a series of tests and simulations. These included tests of body tube reinforcements, fin attachment methods, fin materials, epoxy type, and diameter transitions from 76mm to 65mm. In addition, a fin sizing/shape evaluation simulation was completed. These tests included qualitative and quantitative data collection. These data allowed us to make final determinations as to what materials and constructions methods would be the most efficient and effective. The standards of evaluation will be explained and detailed in each section.

Fin Sizing/ Shape Evaluation

To maximize the performance and stability of the rocket, we decided to test three different basic fin shapes using RockSim. These shapes were trapezoidal, swept, and clipped delta, see Figure 3.4.

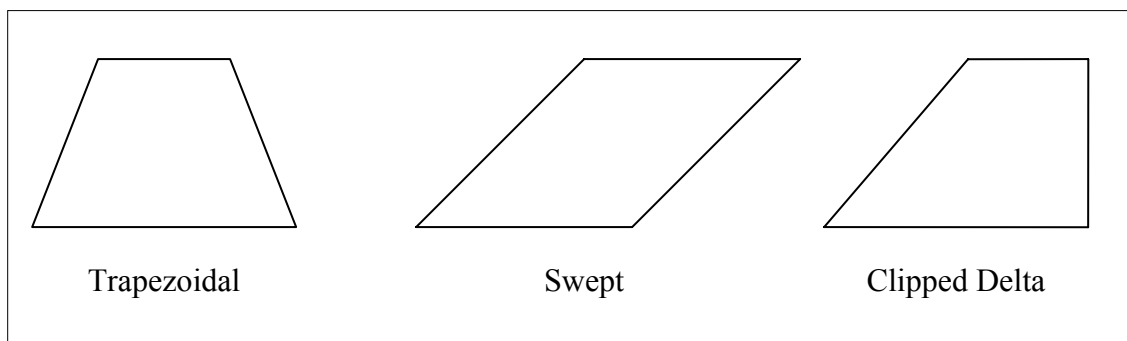
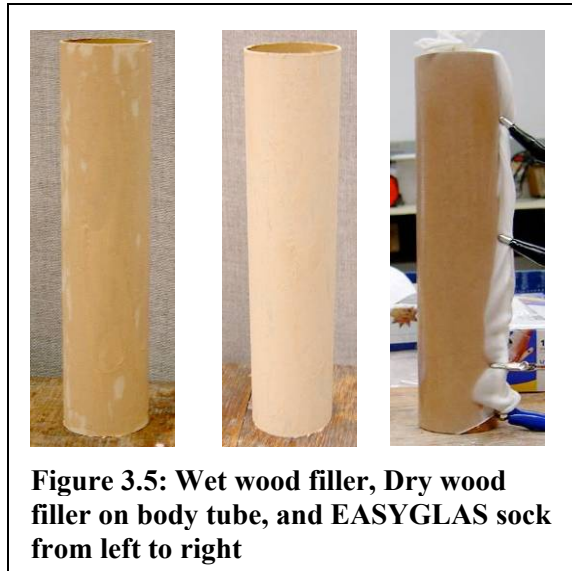


Figure 3.4: Three fin shapes investigated for possible use on the rocket.

Additionally, we assumed the “worst case scenario” of a single I-95 AeroTech[®] motor, 3 H-90 AeroTech[®] Motors, a one-gram payload, and a weight margin of 150%. We analyzed the three basic shapes through a series of iterations which compared the size of the fins, level of stability, and the altitude reached. For more details on the exact simulation process, see Appendix F.

Body Tube Reinforcement

Two tests were performed in order to investigate the effectiveness of certain types methods tube reinforcement, which allowed us to evaluate the strength and reliability of both methods. The two different types of reinforcement tested were as follows: Tube A was covered in wood filler to remove all seams and visible deformation within the tube, sanded down until smooth, and primed (Figure 3.5). Tube B had an EASYGLAS sock (fiberglass fabric) attached to the tube by thickly coating the tube and the EASYGLAS sock with epoxy. This was then primed as well (Figure 3.6). Following construction, both of these tubes were subjected to compression and repeated normal force stress tests.



The first test determined the material stability of both body tubes under compression. The compression resistance test was performed by placing loads with forces in the $-y$ direction and observing for any form of deformation (Figure 3.6). The second test was a repeated application of normal force. Both body tubes were placed in a vice and then subjected to quickly applied and released forces in the x -direction until failure occurred, (Figure 3.7). For more details on the body tube reinforcement test, see Appendix F.

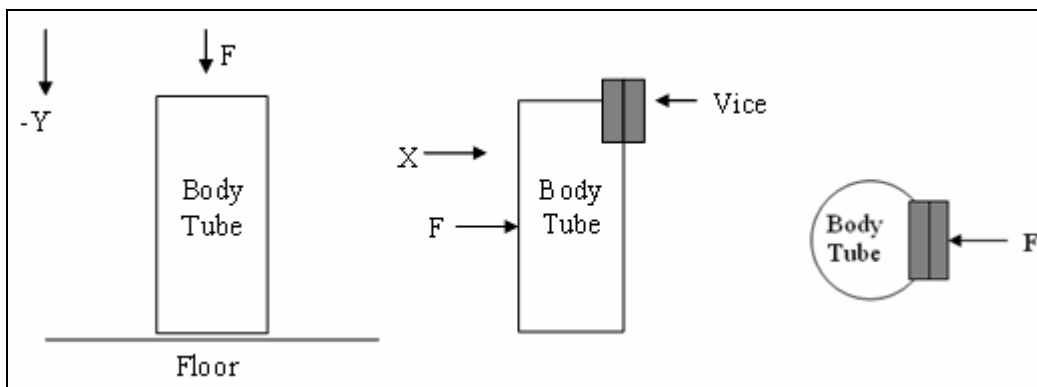


Figure 3.6: Compression stress and force diagram and Normal Stress force diagram

Fin Attachment Method

The purpose of the fin attachment method test was to determine if the use of fiberglass cloth fillets between the fin and body tube and through-the-wall fin attachment would be sufficiently strong for the fins in flight. In order to test the fin attachment, we attached the G10 fiberglass fins with through-the-wall construction. We then used epoxy to create a fillet between the fin and body tube. Once it was dry, we laid fiberglass laminating cloth and epoxy on the intersection of the fin and exterior surface of the airframe. We once again applied a fillet between the fin and body tube (Figure 3.7).



Figure 3.7: The fiberglass cloth during and after application

Following this, we tested the shear strength of the construction method. We placed the tube vertically on an elevated flat surface and draped a nylon cord over the top of the fin, where the fin and body tube join, then hung large metal weights off the edge of the fin starting with five pounds (Figure 3.8). The weights were added at five-pound intervals until the joint failed. For details and results from the fin attachment method test, see Appendix F.

Fin Material

Finding the most efficient fin material was the purpose of the next test. In this case, where efficiency was defined in terms of strength, mass, and cost of said fin materials. We utilized the same construction method as the fin attachment method, however, we attached both a G10 fiberglass and carbon fiber fin for this experiment. We subjected both fin materials to a torque test. This consisted of placing the body tube horizontally on an elevated flat surface with the first test fin overhanging and parallel to the flat surface. Then we hung the nylon cord on top of the fin where the fin and body tube joined. We then hung large metal weights on the nylon cord, starting with five pounds (Figure 3.9). The

weights were added at 2.5-pound intervals until the joint failed. For more information on the fin material test, see Appendix F.



Figure 3.8: Shear test for testing the merit of the fin attachment method



Figure 3.9: Torque test for testing the structural merit of the fin material

3.2.2 Final Design

Upon meeting with other project members, the Hermes design was refined to the point where final construction could begin. With all final dimensions set, Hermes stood six feet, five inches tall. Hermes contained six separate compartments; payload bay, main parachute and spring bay, computer and avionics bay, drogue parachute and spring bay, staging electronics bay, and the boost section (Figure 3.10). For more dimension details, see Appendix D.

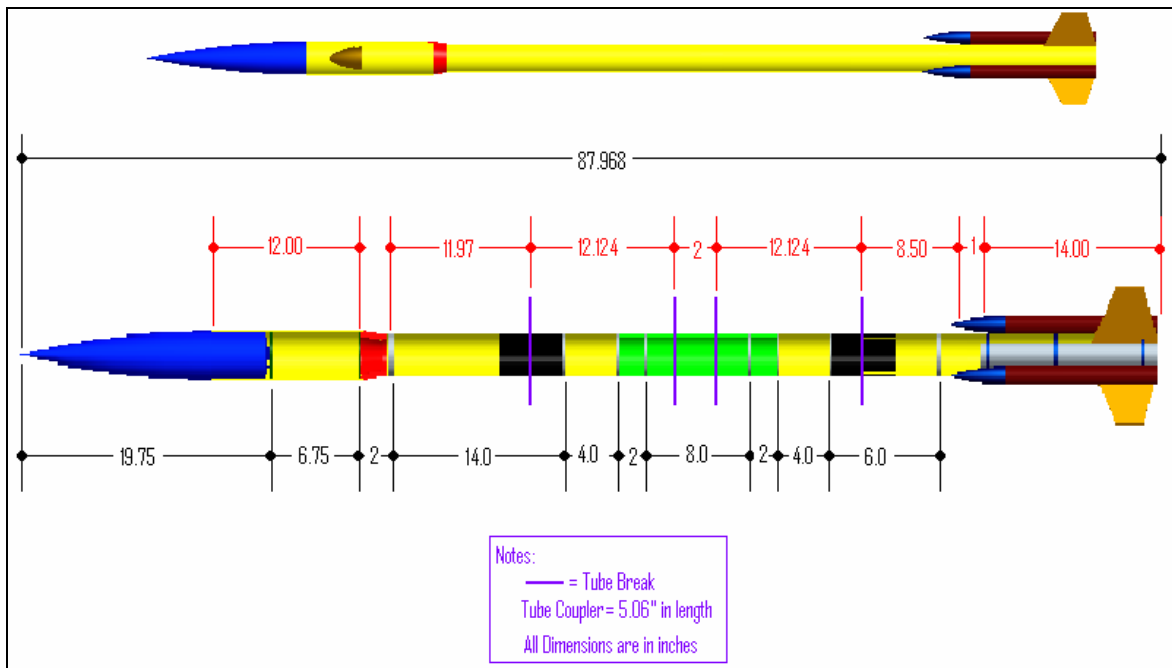


Figure 3.10: Above- Pro-Engineer Model of the rocket, Below- Breakdown of the rocket

The process of determining the dimensions was completed based on each subsystem's requirements. The payload bay contained the nose neck and carried a video camera for flight recording. It also had the ability to carry a CanSat for future competitions if necessary (the CanSat competition required that the payload bay be able to contain a soda-can sized electronics package). Both the main and drogue parachute compartments were made to fit the respective parachutes and spring deployment systems. The computer/recovery section contained the flight computer and backup timer. A very detailed layout was created in order to incorporate all the necessary components in this compartment. The electronics bay was flanked on both sides by a solenoid and piston assembly and was accessible through a removable bulkhead. Figure 3.11 shows the actual construction model of the electronics bay that was used in the final rocket.



Figure 3.11: Actual Electronics Bay (diameter of the coupler tube is 2.56 inches)

The staging electronics bay was sized according to the electrical needs of the staging system. For the booster section, the dimensions were based on the necessary length required to place an I-size motor in the motor mount as well as to allow the staging group to integrate their magnetic release system and the streamer recovery system (These are described in detail in Chapters Four and Six).

3.2.3 Construction

Construction began with the measuring and cutting of the main airframe and booster pieces of phenolic (pictured below in Figure 3.12) using the bandsaw in WPI's Washburn Shops. We proceeded to even out the cuts by using a combination of 60, 100, and 220 grit sandpaper as well as a dermal sander. Once the edges were level, a single coat of Pro Wood Filler was applied evenly over the outer surfaces (Figure 3.5). The wood filler was intended to fill in the grooves along the seams of the phenolic to create a smooth surface for painting. This coat was allowed to dry and was then sanded using the three grits of sand paper mentioned above. Typically, the first coat of wood filler was almost completely removed by this initial sanding. Another coat of wood filler was applied, allowed to dry, and sanded. This process was repeated once more and also included a final sanding using 600 grit paper. This produced a nearly shiny surface on the phenolic with an extremely smooth finish (Figure 3.5).



Figure 3.12: Cut Pieces of Phenolic (2.56 and 3.00 inch diameter tubing)

While the wood filling process continued, the WPI Shop Technician, Stephen Derosiers, cut multiple centering rings and bulkheads using sheets of plywood. This was accomplished with the use of rotary cutting tools in Washburn Shops. These bulkheads were then sanded and test fit into their respective airframe pieces (Figure 3.13).

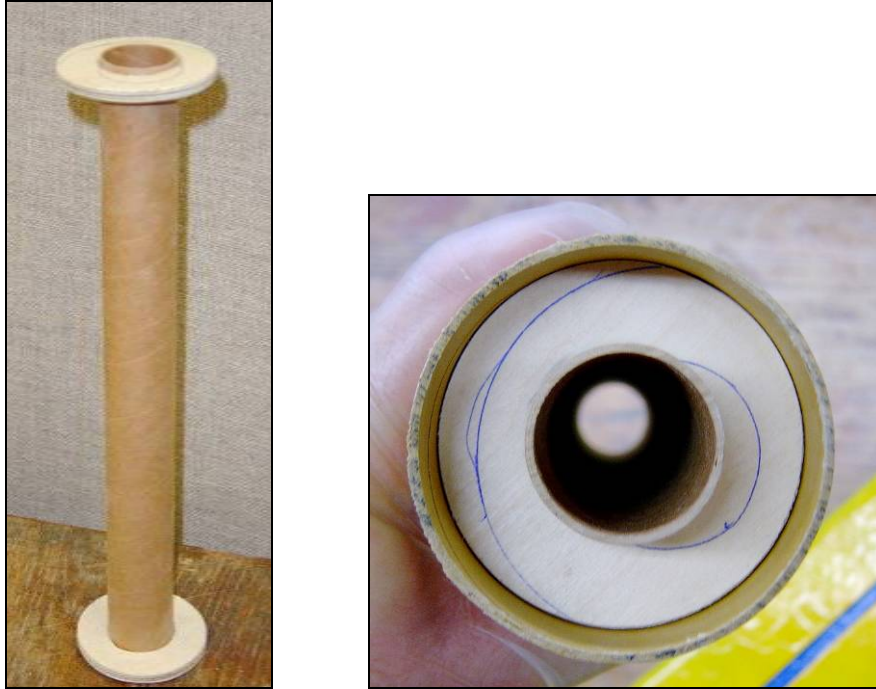


Figure 3.13: Centering Rings Test Fit to the Motor Mount Tube and Airframe

Mr. Derosier also machined a balsa transition piece for this project that we covered with fiberglass to strengthen it. It was decided, however, that this piece would still be too weak for the forces it would encounter, and a PVC transition Derosier had machined as a backup was sanded and test fit into the airframe (Figure 3.14).

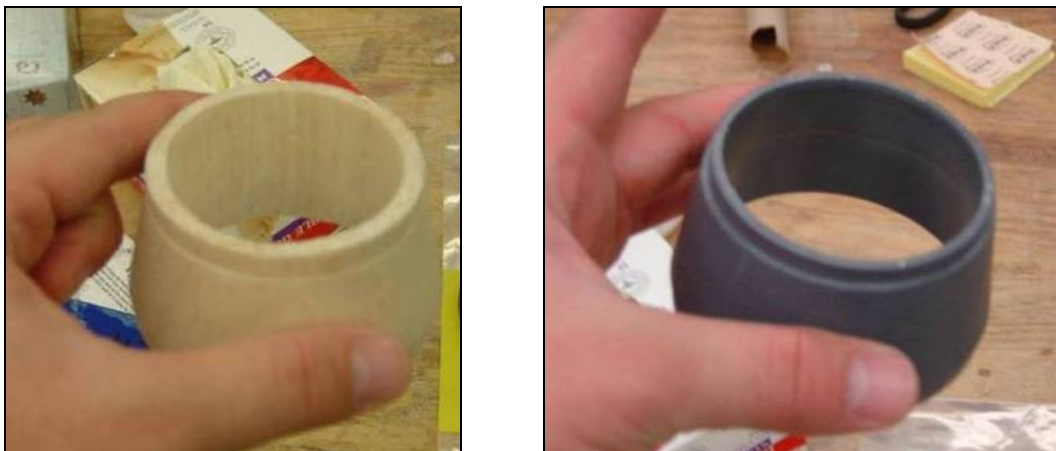


Figure 3.14: Balsa Transition (Prior to Fiberglassing) and PVC Transition

At this time, we also cut three fins out of G-10 fiberglass at the machine shop for use with this rocket. The fins were cut using the bandsaw previously used to cut the phenolic. These fins also had small narrow slots cut into the bottom edge that allowed us to use the “through-the-wall” construction method

(Figure 3.15). Through-the-wall construction involves the fin being epoxied directly to the motor mount tube, over the centering ring, and through the wall of the outer airframe. The epoxy process began by massing five parts resin to one part hardener and thoroughly mixing the two together. The epoxy was applied with a thin, balsa stick and was allowed to cure for twenty-four hours or until the texture felt smooth. For all epoxy needs, Gougeon® West System Brand® 105 Epoxy Resin and 206 Slow Epoxy Hardener were utilized.

Once the major components of construction were completed we chose to use Rust-Oleum® Painter's Touch® sandable primer and applied it to the outer surface of all airframe components. This usually required two-to-three coats (Figure 3.16).

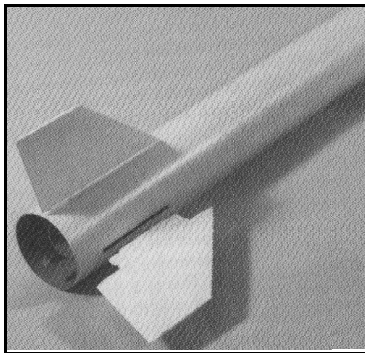


Figure 3.15: Fin Test Fit to the Motor Mount Tube and Centering Ring [2]

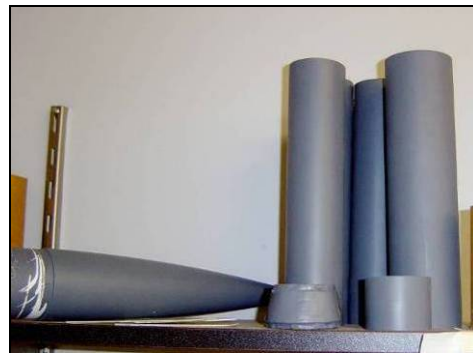


Figure 3.16: Primed Airframe Pieces

While we were priming these parts, Ryan Caron, one of the project volunteers, constructed a simple fin jig for aligning the fins (Figure 3.17).

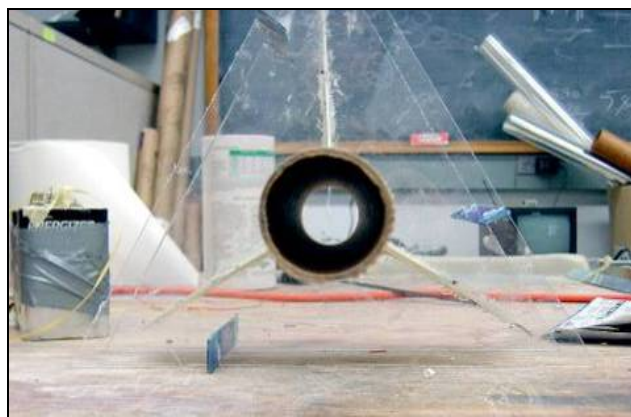
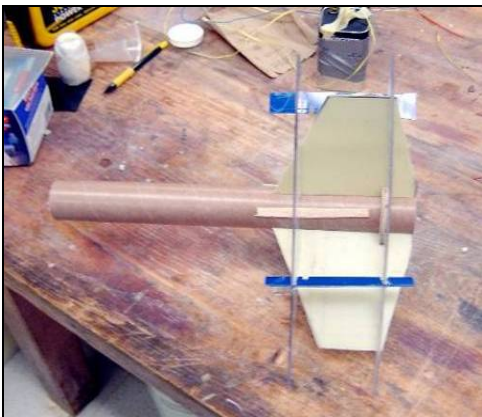


Figure 3.17: Side View of the Fin Jig (left), and Back View of the Fin Jig (right)

The lower centering ring was initially epoxied in place. After it dried, the fins were epoxied over it and the assembly was inserted into the jig. A heat lamp was moved nearby to help expedite the curing process (Figure 3.18).



Figure 3.18: The Heat Lamp Speeding Up the Curing Process

After the initial 30-minute epoxy had set, epoxy fillets were applied between the fin root and the motor mount tube. These fillets were applied one at a time in order to ensure proper curing and less runoff of the epoxy. Once this process was completed for the three fins, the fillets were overlaid with fiberglass. This was then epoxied down and sanded for a smooth transition between the fins and the motor mount tube (Figure 3.19).



Figure 3.19: Fiberglass Fillets to Motor Mount Tube

After the fiberglassing was completed, the tube and fin assembly was test fit into the airframe slots that had been previously cut (Figure 3.20).

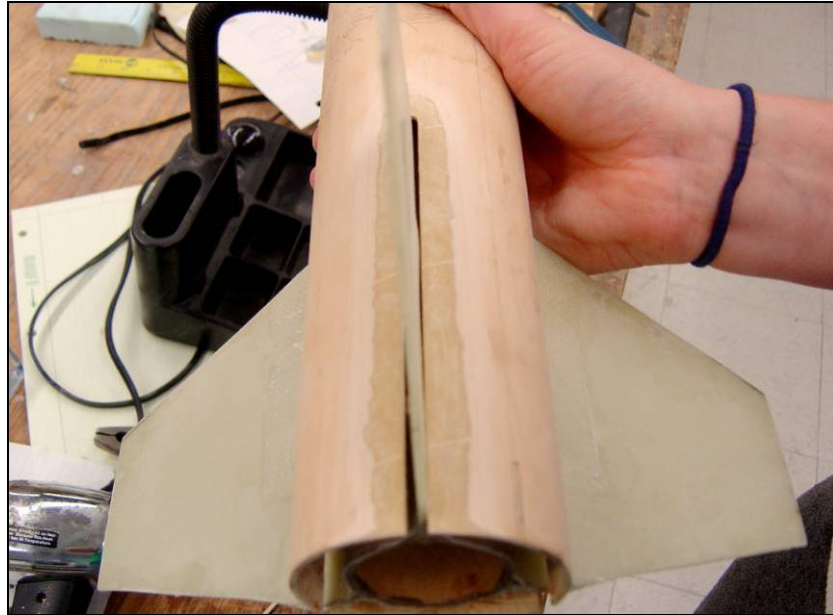


Figure 3.20: Test Fitting Motor Mount/Fin Assembly in the Main Airframe Tube

These slots were widened a little, and then the tube/fin assembly was epoxied inside of the airframe body. After this assembly was dry, we made more fiberglass fillets between the fin and the airframe tube using the same process that was mentioned above. Some of the wood filler was removed in order to assure that the fiberglass was attached to the phenolic and not the wood filler itself which would have been a much weaker anchoring surface (Figure 3.21).



Figure 3.21: Fiberglass Fillets from the Fins to the Airframe Tube

After all components had cured, we proceeded to airbrush each part according to the agreed upon color scheme. For this task, we utilized a Badger™ Professional Model 150 Airbrush, Createx™ opaque black, and transparent red paint. We applied three coats to each component. After the parts had dried sufficiently, we applied stick-on decal letters spelling out “WPI Aerospace” vertically on the main airframe. After this was accomplished, we applied a layer of Rust-Oleum® Crystal Clear Enamel to each piece to help seal in the paint and prevent environmental conditions from affecting the rocket. Each section of the airframe received three or more coats of clear enamel. The final product was left to dry in the laboratory on its stand (Figure 3.22).

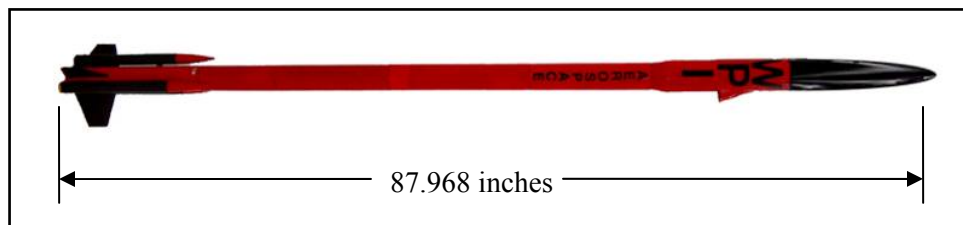


Figure 3.22: Final Cosmetic Scheme

3.2.4 Integration of other Subsystems

The process of integrating all subsystems required detailed planning prior to actual construction. The entire MQP group met and worked on a one-on-one basis to create a design that would meet the building specifications as well as allow ease of assembly after construction (see Table 3.1).

Subsystem	Total Length of Section(s)	Body Tube Diameter	Miscellaneous
Staging	15"	2.56"	Needed to be accessible via wires
Recovery	32"	2.56"	Required space 20" above and 12" below Electronics Bay
Propulsion	14" motor mount (main airframe) 3 x 12" boosters	.965" (motor mount) .74" (booster)	N/A
Avionics	8"	2.56"	Placed between Recovery sections
Payload	8"	3"	Small diameter hole and camera shroud were necessary

Table 3.1: Subsystem Integration Requirements

Staging

Before construction could begin, the final design of the airframe and staging hardware needed to be agreed upon. Certain constraints needed to be met for the entire system to work. The main motor mount needed to be, at minimum, fourteen inches long in order to accommodate the possible use of an I size motor. Additionally, it was necessary to place the small booster tubes tangent to the fins in order to have the needed space for the rail buttons and the launch rail (Figure 3.23). These constraints were met by the staging subsystem design for the booster deployment system.

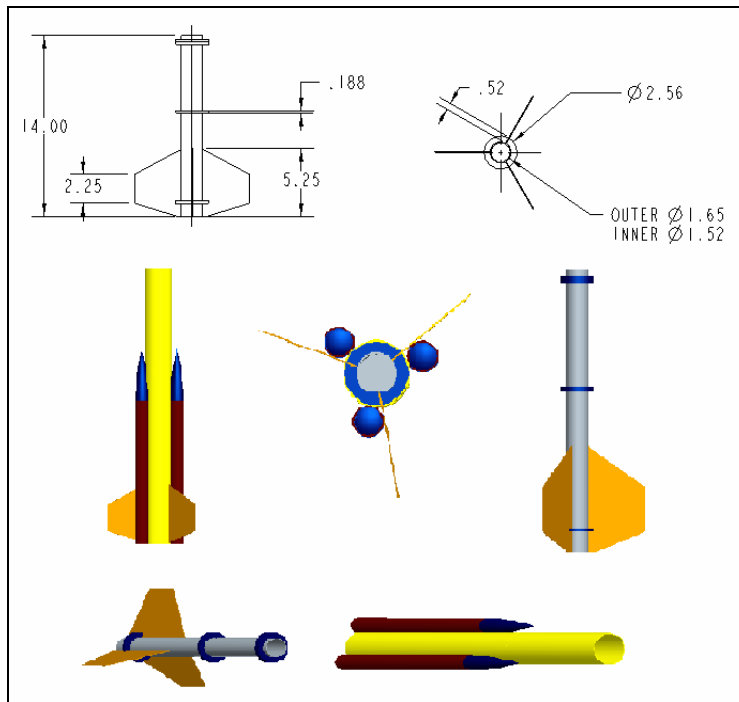


Figure 3.23: Pro-Engineer rendering of staging integration section

Incorporating the staging hardware was the most demanding integration process. The booster section body tubes were initially prepared by filling, sanding, and cutting the tubes to the specified lengths. The fins and motor mount were then attached allowing precise placement of the booster tubes. David Stechmann and Thorsten Braun, the staging group, then epoxied the magnets into each booster. In addition, the staging group's electronics and coils were placed within the main airframe. The staging group completed all of the physical integration, however the preplanning was completed by all group members. Details of this subsystem are presented in Chapter Four.

Recovery

Recovery system incorporation was of the utmost importance since it was necessary for a safe return and reuse of the rocket. This subsystem was largely self-contained in order to easily insert and

remove the parts for later modifications or repair. Initially, several problems arose with the recovery and avionics subsystems since they were attached to the same coupler tube. Both subsystems needed access to their components. In addition, there were wires for the avionics that needed to be passed through both sections. Consequently, the recovery section was connected to the electronics bay by rods and bolts, which could be removed when necessary.

Prior to integration of the recovery system, tests were performed using a body tube and the spring deployment system. A small level of damage was incurred on the body tube during these tests. We thus determined that the piston within the subsystem needed to have more constrained vertical motion. Once the entire adjustments were made, the recovery system (including couplers, parachutes, and shock cords) was ready to be placed within the airframe. A detailed discussion of the recovery systems is presented in Chapter Five.

Avionics

The avionics section contained the flight computer and back-up electronics which would control all of the rocket events during flight and collect altitude and acceleration data. Since this section was very critical to a successful flight, it was important that its integration be not only successful but that the electronics be placed in the most effective and safe location. Therefore, we determined that the electronics system would be placed within a coupler in between the recovery system (located approximately in the middle of the rocket). This allowed for access to the electronics system but more importantly, allowed the flight computer to easily control and power all electronic components of the rocket via wires strung within the airframe. Additionally, the location of this section helped move the center of mass forward in the rocket, and assured stable flight. Insertion of the avionics bay was completed at the same time as the recovery system since they were physically connected. The only difficult part of the integration was stringing the wires within the airframe to control and power the recovery and staging sections.

Payload

Placed at the top of the rocket was the payload section. This contained a video camera to record the entire flight. The major requirement when incorporating the payload bay was to have the video camera placed in the correct location so that, through the use of mirrors, the flight could be recorded.

3.3 Results and Analysis

3.3.1 Tests and Simulations

Upon further analysis of the material and fabrication options for the different components of the rocket, we further refined the five tests and one simulation displayed earlier. We concluded that any testing of the transition from 76mm down to 65mm would not be necessary. It was initially thought that two conceivable options for transitions were a balsa transition shaped by a Computer Numerical Control (CNC) lathe or one made from expandable foam. However, thanks to the help of Washburn Shops Machinist Stephen Derosier, two transitions were created. One as made from balsa as originally thought, but the other was made out of Polyvinyl Chloride (PVC). Both were perfectly shaped to our desired dimensions (Figure 3.14). Slow cure Epoxy would be used only for internal, non-load bearing parts. For all other needs, quick cure Epoxy would be employed.

The process for creating the balsa transition was not as simple as we had hoped. The balsa could not be machined in the CNC lathe due to the softness of the wood. However, Mr. Derosier converted a conventional metal lathe in the shop to a wood turning lathe in order to properly turn this piece. The transition turned out perfectly, weighing 28 grams less than the PVC transition. However, after fiberglassing the balsa wood to give it the proper structural strength, the balsa transition weighed only two grams less than the PVC transition and was no longer dimensionally accurate. Therefore, we determined that the PVC transition was the best to be used in the rocket.

Fin Sizing/ Shape Evaluation

Our criteria for the best fin shape and size were based on calculations of the highest attainable altitude during stable flight. We completed numerous iterations until finally deciding upon a trapezoidal shape that maximized both altitude and stability. This shape was found on iteration thirteen with measurements shown in Figure 3.24.

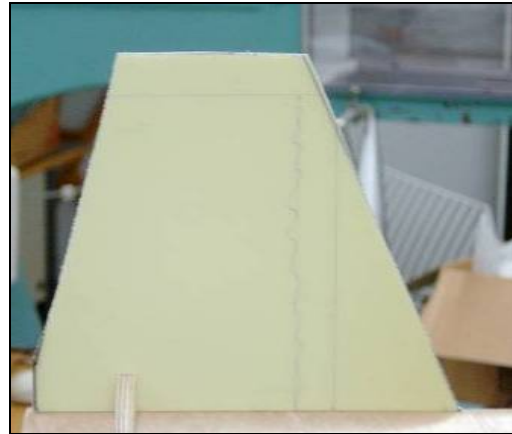
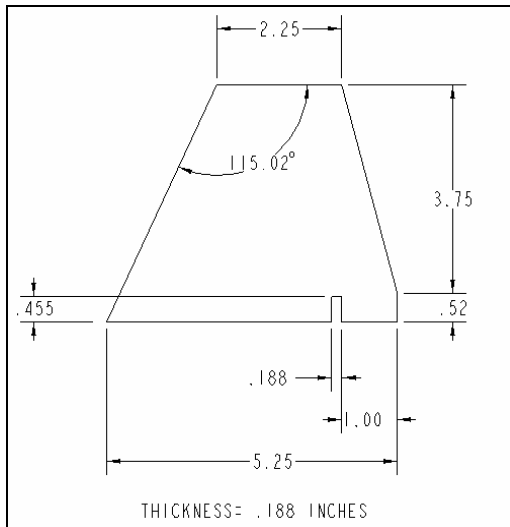


Figure 3.24: Left- Final Pro-Engineer design of fin, Right- Actual fin

This design was found to be stable and with a maximum altitude of 5,889 feet. For more details on the analyses, see Appendix E.

Body Tube Reinforcement

The compression tests of the body tube segments were performed at WPI's Fitness Center and used the free weights available. Tube A was tested first by placing individual 45-pound weights on top of the body tube. We were able to determine that the tube well exceeded the minimum strength requirement of 143 pounds, which was calculated in Appendix E. In fact, the body tube was able to hold 360 pounds without showing any sign of fracture, see Figure 3.25 for a picture of the test setup. The test was concluded at this weight because it exceeded a safety factor of 2.5 and, in addition, we felt that our own personal safety would be at risk if any further weight was added. After the testing of Tube A was completed, we followed the same procedure for Tube B and obtained the exact same results of reaching 360 pounds.



The repeated normal force stress test, despite the use of a simple testing method, allowed the structural integrity of the body tubes to be easily observed. Applying repeated instantaneous forces brought both tubes to failure. Tube A failed at a much faster rate and endured a higher level of

deformation than compared to Tube B which was able to (in general) retain its basic external shape because of the fiberglass sock (see Figure 3.26).

In making a final decision between Tube A and B, cost, mass, ease of construction, and test results were considered. The only difference in cost incurred was with Tube B and its use of the

EASYGLAS and epoxy. This was approximately \$2.00 more per foot than Tube A. Additionally, the mass of Tube B exceeded Tube A by 23 grams per foot, and Tube A's construction was far simpler than that of Tube B. Tube B took well over 10 additional hours to dry and required a higher level of precision during manufacturing. Tube A was more labor intensive with the sanding required to smooth out the tube, but it still was completed a day before Tube B.



Figure 3.26: Tubes A and B after the completion of the repeated normal force stress test

Using these two test results as well as the other aforementioned considerations, we concluded that though the fiberglass sock method was stronger and required less physical labor to create an ideal body tube, it was not worth the gains in weight, cost, or construction time. Therefore, we used Tube A for the rocket. For details on this decision process, see Appendix E.

Fin Attachment Method

The fin shear test began by using five pounds of weight. This produced no noticeable deformation or shift in the placement of the fin at this weight. No warping or fin displacement occurred while increasing the weight over five pound intervals until the weight rose to 55 pounds. At that point, we observed a slight $\frac{1}{4}$ " tear in the uppermost portion of the fiberglass where the fiberglass cloth met the G-10 fiberglass fin and phenolic. Another five pounds were added and the tear elongated another $\frac{1}{4}$ ". Finally, at a weight of 65 pounds, the fin joint failed and the fin tore away from the body. The through-the-wall construction coupled with the fiberglass fillets proved stronger than anticipated. Per our calculations, this weight of 65 pounds exceeded the requirements of the worst-case drag force of about 33 lbs. Therefore, we concluded the use of through-the-wall fin attachment with the fiberglass fillet would be sufficient to withstand the forces that would be encountered during flight. For more details on the fin attachment method test, see Appendix E.

Fin Material

We began the torque test by placing five pounds onto the G10 fiberglass fin which initially showed no visible signs of deformation. Weights were added at 2.5-pound intervals and no warping was present until 17.5 pounds was applied. At this point, the fin started to bend at the joint where it was attached to the body tube. At twenty pounds, the body tube just below the edge of the fiberglass cracked and the fins came loose even though the fiberglass cloth was still attached to the G-10 fiberglass fin and the body tube. The carbon fiber fin was then tested using the same forces and torques and the same results were found. Since in both cases the fin joints broke before the fins themselves, any possible strength differences between the two materials was negated. This test really became a measure of the torsional rigidity of the fin attachment method. The joints consistently failed at 16.25 ft-lbs. of applied torque. Because both materials withstood these in-flight forces with ease, the question of “fin efficiency” focused on price per volume rather than strength. G10 was simply cheaper to purchase than carbon fiber and therefore became the fin material used for this rocket. For more details on the fin material, see Appendix E.

3.3.2 Integration of other Subsystems

Upon complete integration of all subsystems, we were able to determine if the process was finished in a manner that was sufficient for flight requirements. Each subsystem was individually analyzed based on that particular subsystem’s requirements. However, in terms of the airframe, the main qualification was that all other subsystems be integrated within the airframe properly. The actual integration process was completed by the individual subsystems. Therefore, for a detailed explanation of the actual procedure and post integration tests, see the Staging and Recovery chapters.

3.3.3 Flight

The only post-flight analysis that we needed to consider was the overall physical state of the airframe upon landing. However, because the severity of damage was such a subjective judgment, we attempted to standardize the evaluation of the damage using a five point rating scale. These five points allowed us to clearly and accurately record the visual information that we observed upon inspection. For a detailed individual parts breakdown with post-flight conditions, see Table 3.2.

Launch Review of the Airframe & Mechanical Subsystem					
Date: 4.6.06					
Parts	Type of Inspection				Comments
	Fatigue	Cracking	Paint/Primer Condition	General Breakage	
Main Nose	1	1	1	1	2" Crack on top, Landed 10" into ground
3" Payload Section	1	4	4	1	Broke into ~20 pieces, Mirror Shroud- 1/2" crack, Foam dislodged, Mirror- 1/2" crack
12" Main Parachute Section	1	1	3	1	Broke into ~30 pieces, Completely destroyed
12" Spring Section (1)	1	1	3	1	Broke into ~10 pieces
2" Connector Tube	5	5	4	5	Small paint chipping at bottom
12" Spring Section (2)	1	4	4	2	Bottom half of section destroyed
8" Drogue Parachute Section	2	2	4	4	Top half of section destroyed
1" Spacer	5	5	5	5	Returned in perfect condition
14" Main Booster	5	5	4	5	1/2" patch of missing paint at Booster (3) connection point
Booster Tube (1)	5	5	5	5	
Booster Tube (2)	5	5	5	5	
Booster Tube (3)	5	5	4	5	Tiny Paint chipping along where it rests on the main airframe
Booster Nose (1)	4	5	4	5	1/2" paint cracking at base of the nose
Booster Nose (2)	Not found after release from the main airframe				
Booster Nose (3)	Not found after release from the main airframe				
Fin (1)	5	5	5	5	Returned in perfect condition
Fin (2)	5	5	5	5	Returned in perfect condition
Fin (3)	5	5	5	5	Returned in perfect condition
Epoxy Joints	5	5	5	5	Returned in perfect condition
Fiberglass Joints	5	5	5	5	Returned in perfect condition

<p>The chart is set-up so that each particular part will receive a number ranking as well as additional details as to what happened if the part does not receive that highest possible rank. The ranking scale is from 5 to 1, 5 being the best possible score:</p> <ul style="list-style-type: none"> 5- The part returned from flight with no visible damage 4- The part returned from flight with very little damage, only cosmetic issues to the paint, primer, and wood filler 3- The part returned from flight with crack(s) to the main part that are not just cosmetic issues but can be easily repaired 2- The part returned from flight with large scale damage however it can still be used after major repairs occur 1- The part returned from flight completely destroyed and need to be entirely reconstructed from new materials 					
--	--	--	--	--	--

Table 3.2: Post-Flight Analysis of the Airframe

3.4 Conclusions

The airframe retained its integrity and fulfilled its performance requirements throughout the flight failing only upon impact with the ground at high velocity. The only airframe issue during the flight was with regards to the early separation of a single booster nose cone due to unknown causes. After our post-crash analysis, we surmised that our construction and manufacturing methods were more than adequate for the requirements of this project. Due to the fact that the airframe performed in accordance with our design constraints, the only suggestion for future endeavors would be to tighten the fit of the booster nose cones. Prior to launch, we had checked the fit of the nose cones with three of the more experienced rocketeers on the team and they believed that the nose cones were actually too tight. They checked this by holding the booster horizontally and blowing in it; if the nose cone was too tight, the nose cone would not separate. We then adjusted the fit of the nose cone by removing some masking tape and ensuring a proper fit. Obviously, this “proper fit” was actually too loose. Overall, we believe that our construction methods were sound and should be repeated during the next iteration of the WARRIORS Project. Our only suggestion for next year’s group would be to precisely cut the airframe tube to guarantee that the outermost edges are perfectly flat to properly align with the adjoining airframe portion. Therefore, we deem the Airframe and Mechanical Subsystem’s work a success.

4. Staging

The primary goal of the staging subsystem was to design and fabricate a new and innovative staging system for small-scale rocket vehicles. Given the current state of staging systems in general, however, we felt this new staging system should be designed around the principles of low maintenance, reliability, consistency, and easy testing. These are the areas where current small scale-staging systems are lacking. In addition to these performance metrics, however, the staging system needed to be as light as possible in order to extract the greatest performance from the rocket vehicle. In spite of all their shortcomings, current staging methods are lightweight. It would therefore be a significant challenge to keep the mass of this staging system at or below existing systems.

In addition to the general performance goals, the overall vehicle design, size, and configuration would dictate many aspects of the staging system. In our case, the vehicle design called for three identical boosters attached to the aft end of the vehicle. These boosters would have very little internal volume, and in fact the majority of each would be completely filled by a rocket motor. The more detailed goal would thus be the design of the interfaces between the boosters and the main airframe. These interfaces would need to hold the boosters to the main airframe when desired, and would also need to push them away from the vehicle simultaneously during the first stage separation. Unfortunately, space constraints within the main airframe would also influence the size of these interfaces. In the aft portion of the vehicle, for instance, the distance between the core motor mount and the airframe surface was limited to 0.43” leaving very little room for staging hardware. If necessary, however, there would be more room for electronics or other auxiliary staging systems farther up the vehicle, along with a flight computer located in the avionics bay. This flight computer would deliver a signal to the staging electronics initiating the separation process. Consequently, our staging system design would need to accommodate a system to interface with the staging signal from the flight computer. All together, these requirements and limitations narrow the range of possible design options and provide a good starting point for a new staging concept.

4.1 Staging Background

Since the dawn of rocketry, aerospace engineers have continually attempted to increase the performance of their rocket designs. Countless methods have been developed, but the most frequently used and effective technique is known as “staging.” Staging essentially combines the thrust of several propulsion units into a sequence chosen by the designer. [2] This permits a great deal of hardware optimization for each portion of a rocket’s flight, and it allows used mass to be jettisoned from the vehicle when it is no longer needed. Both of these benefits combine to dramatically increase a rocket vehicle’s performance, and staging can be seen on almost all large-scale rocket vehicles.

Unfortunately, as is the case with most aerospace systems, staging involves trade-offs. The performance benefits come at the price of increased design and operational complexity. In fact, the complexities of most staging methods preclude their use in the majority of smaller rocket vehicles. Even when staging is used on smaller rockets, weight and size limitations drive designs that are often inconsistent, difficult to test on the ground, or mechanically crude in operation. Because of this, smaller scale rocket designers often sacrifice staging and its added performance benefits in order to ensure a reliable and inexpensive design.

While designers of smaller rockets tend to avoid staging due to reliability and complexity, larger staging systems must also address reliability issues. In fact, from 1980 to 1999, 8 out of the 20 launch failures in the United States were attributed to staging failure. [4] This was the second leading cause of failure following propulsion system malfunction.

Because of these failures and the problems with implementing staging in smaller rocket vehicles, our goal was to design and implement a new staging system that addresses the problems with current staging mechanisms. Operation of our system would be consistent, reliable, and easy to test. We accomplished this by evaluating several general staging ideas, selecting a design approach, and constructing a prototype. After testing this prototype, we made necessary design changes, constructed the final system, integrated it into the vehicle, and performed ground and flight tests. These tests demonstrated the validity of our approach, allowed us to draw design conclusions, and helped point the way toward future improved methods of staging.

4.1.1 Purposes of Staging

The primary reason for staging several propulsion units in a rocket vehicle is to increase the performance of the vehicle. This performance increase is achieved through two primary mechanisms. First, it reduces a rocket’s final burnout mass by discarding the used propulsion systems during ascent. [5] This allows a greater burnout velocity to be obtained with a given total energy expenditure. Second, it allows greater optimization of the propulsion units for their respective periods of flight. [6] This

optimization usually comes from designing the rocket nozzle for specific atmospheric conditions, but may come from changes to other vehicle systems as well.

In order to better understand the performance benefits of staging, a theoretical approximation can be found from the well-known rocket equation 4-1 where Δv = the velocity change capability, c = the propulsion system exhaust gas velocity, m_r = the stage mass ratio, and i = the number of stages. [5]

$$e^{\Delta v/c} = m_r^i \quad (4-1)$$

$$\Delta v = ci \ln m_r$$

In this case, each stage is assumed to have identical mass ratios (the ideal case). A graphical representation of the performance improvement in respect to velocity with a typical propulsion system exhaust gas velocity of 2.5 kilometers per second is shown in Figure 4.1.

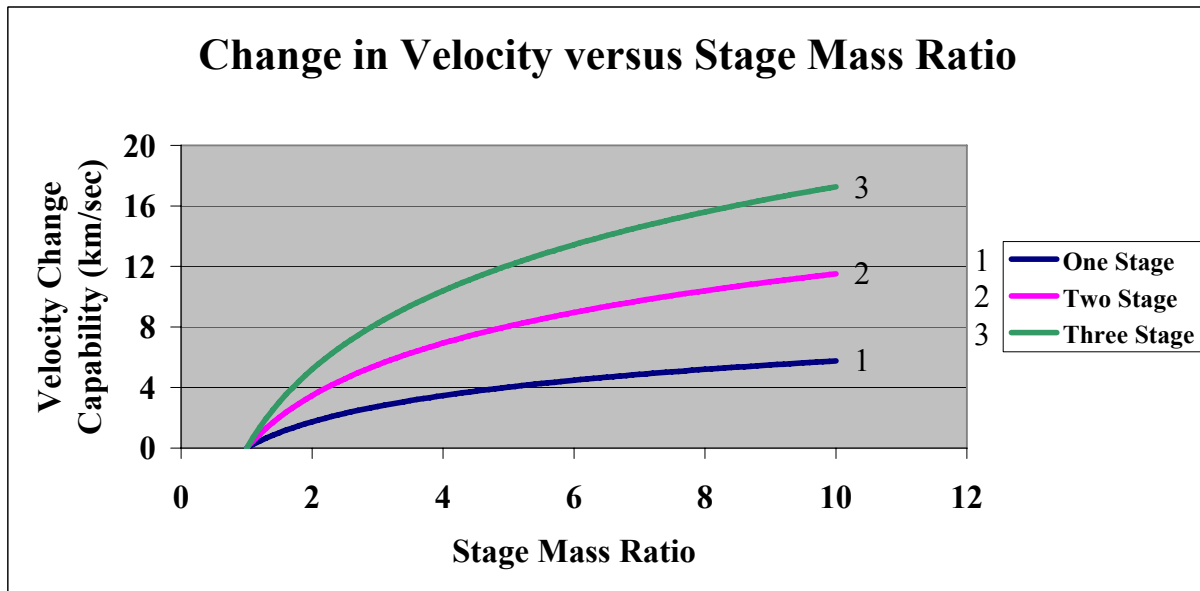


Figure 4.1: Velocity Capability as a function of Mass Ratio and Number of Stages

It should be noted that while the improvements of staging appear to be very significant in this graphical representation, the complexity and increase in required hardware tends to limit this benefit. Often when these other variables are factored in, little benefit can be obtained beyond three stages. [5]

Performance benefits aside, staging a rocket also allows the vehicle designer greater flexibility in propulsion system design. This is of particular interest to small-scale vehicle designers, because often times propulsion units of a given thrust or burn duration already exist. Thus it is often more efficient to design a staged rocket around existing propulsion units rather than attempt to design and construct completely new propulsion units in order to meet performance goals. In the field of model rocketry and

medium power rocketry (rockets with more than 40Ns total impulse), staging is not commonly used because extreme altitudes and speeds are not often paramount goals. Nevertheless, rockets of this scale designed for high altitude and high speeds integrate staging systems.

4.1.2 Types of Staging

There are two basic ways of classifying staging systems: Series and Parallel. Both have different performance advantages and design characteristics.

Series Staging

Rockets using series staging technology contain several motors stacked on top of each other inside the airframe Figure 4.2. The first stage is ignited on the launch pad and lifts the rocket off the ground. Upon burnout of the first rocket motor, the lower stage is jettisoned and the second motor is ignited. This leaves a smaller rocket with the second stage at the bottom delivering the thrust necessary for further acceleration.

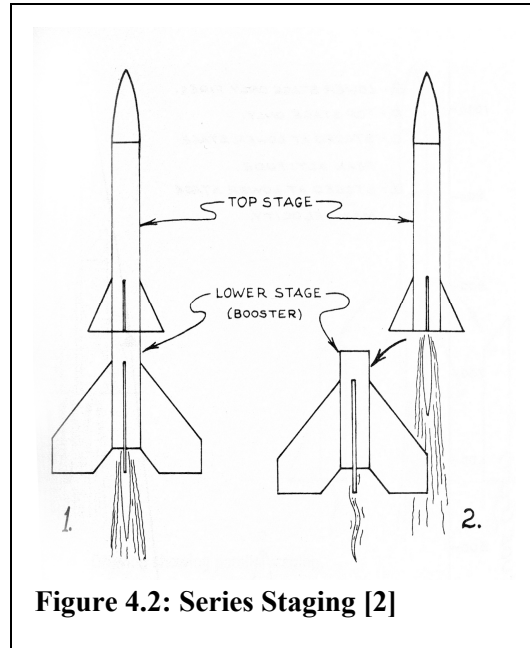


Figure 4.2: Series Staging [2]

This process is repeated until the motor of the final stage has burned out. While theoretically the number of stages may seem infinite, practically the number is restricted due to the weight of the structure required to connect and separate the stages. This tends to increase dry weight and defeats the purpose of staging. In addition, many stages increase the complexity of the rocket and therefore reduce overall reliability of the vehicle.

Parallel Staging

Another type of staging is called parallel staging, in which the rocket motors operate in parallel rather than in series. Such a configuration is shown in Figure 4.3, in which the boosters separate from the sustainer after burnout. Rockets using parallel staging technology leave the launch pad with several motors operating. Generally the booster motors are selected to have less duration than

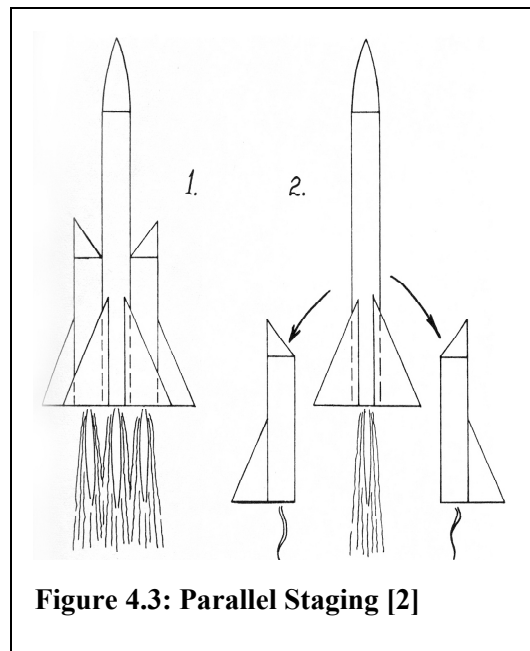


Figure 4.3: Parallel Staging [2]

the core motor, which is often referred to as the sustainer. This results in an earlier burnout of the boosters upon which they are separated from the main airframe to reduce the total mass and drag. The sustainer motor is still thrusting and accelerating the model's core vehicle. Examples for the use of this specific method of staging are numerous. The NASA Space Shuttle and the Atlas ICBM for instance are parallel-stage rocket vehicles.

In comparison to series staging, parallel staging can offer very high thrust and acceleration at lift-off (which is necessary for heavy payloads). In addition, traditional parallel staging does not require igniting one or more rocket motors during flight. However, the ignition of multiple or clustered motors on the ground is fraught with risk. Not all motors may ignite at the same time resulting in asymmetric thrust. An even worse scenario would be the total failure of one or more rocket motors.

Given the different performance characteristics of series and parallel staging techniques, we opted to use a hybrid scheme for this research vehicle. Such a system would combine the high thrust capabilities of parallel staging (necessary due to the rocket weight and motor limitations) with the longer burn capability of series staging. Generally, model rocket motors tend to burnout within two to five seconds, so igniting a second motor upon booster burnout would significantly increase overall thrust duration and therefore performance. On the other hand, we limited ourselves in this project to G-class motors, which would not have provided sufficient thrust for take-off given our vehicle design. Therefore a motor cluster resembling a parallel staging system was necessary for take-off. This led to a final design of three outboard boosters lit on the ground followed by a single core motor ignited after booster burnout. This design would be capable of delivering a desirable flight profile.

4.1.3 Staging in Small Scale Rocket Vehicles

Even though staging is a very common method of improving overall performance in large-scale rockets, it is not widely used in model rockets or smaller scale vehicles. This is unfortunate, because performance analysis conducted with help of RockSim™ and Compuroc™ software has shown that the overall performance (in terms of altitude) can be greatly enhanced with the addition of a second stage. In cases where staging has been adopted, an aerospace engineer can choose between series and parallel staging configurations. These two configurations are frequently used together in large-scale rocketry. In model rocketry however, staging tends to be restricted to series methods because commercial kits are available and can be easily integrated into existing rocket airframes. Traditional parallel staging has not entered the model rocket industry yet.

Over the years, two different series staging techniques have developed. They differ in complexity and application, so one may be more beneficial than the other depending on the specific rocket vehicle. The first method is called direct (passive) staging and is the easier one of the two. In direct staging, the

lower stage motor ignites the upper motor. As a result, there is no need for additional hardware to ignite the second stage. The second method, indirect (active) staging requires the use of a separate ignition system to light the upper stage motor upon burnout of the booster or boosters.

Direct staging

As mentioned above, direct (passive) staging is the simplest form of staging, in which the motor of the lower stage ignites the upper stage motor. No additional hardware such as a separate ignition system or a flight computer to trigger separation and ignition are necessary. Due to its simplicity, however, it is limited to black-powder motors only. It cannot be used in connection with high performance composite motors (which will be explained in more detail later in this section).

Direct staging works as follows. The lower stage is equipped with a special “booster” motor shown in Figure 4.4. Unlike a regular rocket motor, the booster does not possess a delay charge followed by an ejection

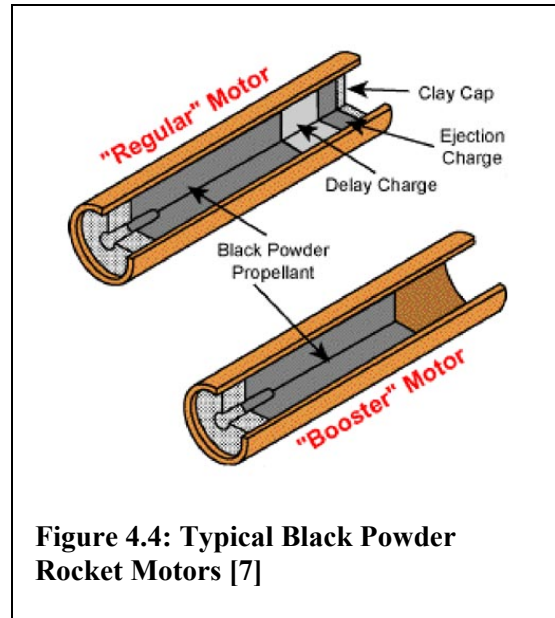


Figure 4.4: Typical Black Powder Rocket Motors [7]

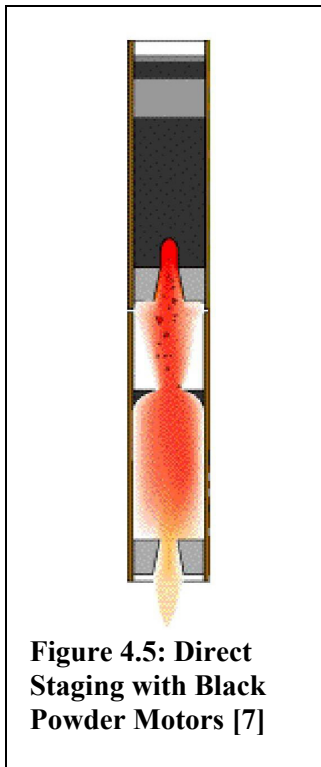


Figure 4.5: Direct Staging with Black Powder Motors [7]

charge (part of the recovery system in single stage rocket vehicle). The booster motor only contains the fast-burning black-powder propellant. Once the booster is ignited, the propellant burns upward towards the top of the motor and produces thrust. As the motor finishes its burn, it ejects a lot of heat and particles forward into the nozzle of the upper stage (Figure 4.5). The amount of heat supplied by the booster motor is sufficient to instantaneously ignite the upper stage.

In order for direct staging to work properly, several conditions have to be met. One of these conditions is the use of black-powder propellant, which imposes the biggest limitation on direct staging compared to indirect staging. Black powder motors burn linearly from the nozzle to the front end. This is important as the propellant serves the function of the bulkhead needed to hold the pressure inside the rocket engine. Without internal pressure, thrust would not be created. In a “booster” black powder motor, the unburned propellant becomes the bulkhead and holds the pressure inside the motor. As the propellant burns, the bulkhead becomes thinner

and thinner until the flame reaches the top. The bulkhead becomes so thin that it cannot withstand the pressure and bursts. Hot gasses and burning chunks of propellant from the lower stage motor reach the upper stage and ignite its black-powder.

This technique however is not applicable to composite motors. The propellant is soft and rubbery, and cannot serve as a bulkhead holding back built up internal pressure. In addition, composite motors operate at far higher combustion pressures. As a result, composite propellant motors always need to have a solid bulkhead made from another material to hold the internal pressure of the motor. This solid bulkhead prevents composite propellant motors from being used in the lower stage of multi-stage rocket vehicles if direct staging is desired.

This however does not explain why composite propellant motors cannot be used in as an upper stage motor. The reason for the top stage motor to contain a black powder propellant is because the flammable substance inside the upper stage must be near the nozzle. This is the case for black powder motors where the propellant is right inside the nozzle opening. But the internal setup of a composite motor is different. The propellant of a composite motor has a core through the middle of the propellant from the nozzle to the bulkhead. The big gap or open space increases the probability of ignition failure due to increased difficulty of the hot gases and burning propellant to reach the upper stage propellant. Composite propellant is also more difficult to ignite when compared to black powder and thus requires more heat flux than is likely available in black powder direct staging systems.

Indirect staging

Indirect staging is more complex than direct staging and involves at least three additional hardware components. These include a power source driving the ignition, igniters, and some type of control unit triggering the ignition. The advantage of indirect (active) staging methods is the possible use of high performance rocket motors with composite propellant. In addition, it enables the aerospace engineer to carefully select the timing of the ignition of the subsequent stage.

Power source

Batteries and capacitors are the main two main options currently used to power staging systems. Both are readily available but have different electrical properties. It is important that one chooses the optimal power source because it is critical to the performance of the ignition sequence. If the power source is too weak, in-flight ignition of the upper stage will not occur, leading to the failure of the flight. If instead the power source is oversized, the additional weight will decrease performance. Thus choosing the right type of power source highly depends on the type of electronic igniters used. In general, the duration and amplitude of the current pulse needed for proper ignition drive decisions about the proper power source.

Igniter

The second hardware component necessary for active ignition is the igniter itself. They must be carefully selected because their performance is highly dependant on the power source and the selected rocket motor. For further detail please refer to Chapter 6 on propulsion.

Control Unit

The last additional component needed for active staging is a control unit to trigger the ignition. There are a large number of different options including simple mercury switches (a type of deceleration switch device), acceleration switches, timers (both electronic and mechanical), complex radio controlled systems or sophisticated flight computers. Each system has different characteristics that may be more or less beneficial depending on the objectives of the project.

Due to the objectives of our overall project (which include gathering flight data such acceleration, velocity and altitude) a flight computer was mandatory. The flight computer chosen for this project was the GWiz MC2 (for details see Appendix G). The flight computer is capable of triggering ignition from a preset timer or by sensing deceleration. Therefore no system other than the flight computer was needed for control.

Existing Systems

In order to obtain first order approximations of mass and general requirements for staging systems, we investigated existing active staging mechanisms for small-scale rockets. One existing series staging system is the Interstage 3000™ by Public Missiles Ltd™ (PML) (Figure 4.6). [8] Interstage couplers are used to both house staging timers and control electronics, and they are used to connect the upper and lower stages together in a series staged vehicle together. The Interstage 3000™ is used in many commercial two-stage rocket kits, but it is also available for scratch builders designing their own staged rockets. Using an IS3000 system from PML is a quick and simple solution to the often-difficult design problem of staging, however their solutions are limited to series staging. They also require an airframe diameter greater than 54mm. Nevertheless, the system can be used as a design guideline providing reasonable weight and size estimates. The system as illustrated in Figure 4.6 requires approximately 3” of length and adds 150g of mass to the rocket. [8] Based on those numbers we can evaluate different design solutions and determine the best option.

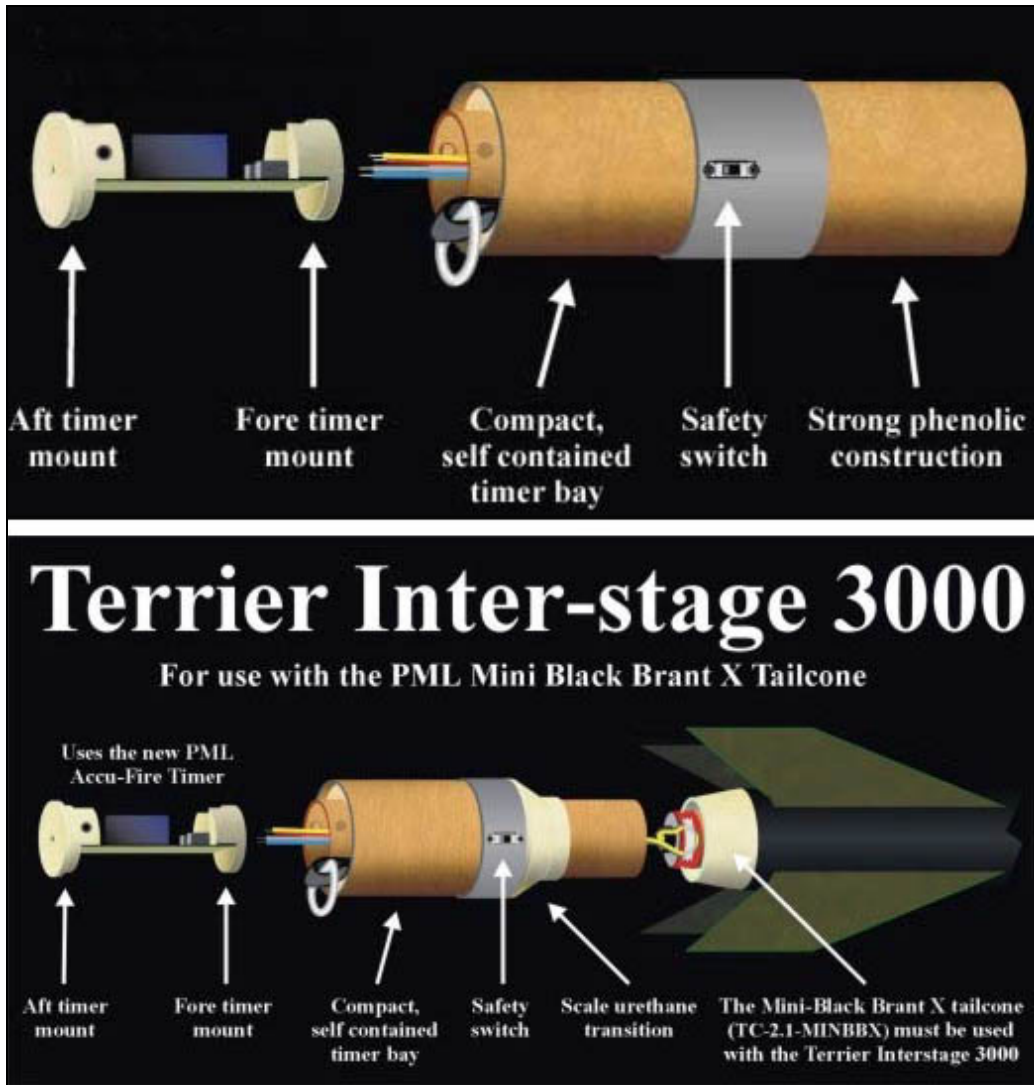


Figure 4.6: The Public Missiles Inter-Stage 3000 System [8]

4.1.4 New Staging System

Our research vehicle proposes the use of electromagnets, pneumatics or other non-pyrotechnic actuator designs in creating a reliable and low-maintenance staging system. Avoiding the use of pyrotechnics for the staging subsystem allows safe testing of the rocket while on the ground. Pyrotechnics are also dependent on many variables that are difficult to control in flight, and igniter failures are common enough to motivate us to seek a more reliable method. While the actuator design selection process will be discussed in the methodology chapter, we intend to provide the theoretical background for our selected electromagnetic system at this point. This information will be helpful in understanding the specific design characteristics of the actuator.

4.1.5 Magnetic Theory

One method of creating the force necessary for separating stages is through magnetic fields. Magnetic fields interact with all substances, however they create noticeable reactions with materials classified either as ferromagnetic or diamagnetic. [9] Ferromagnetic materials (such as iron) become magnetized in the presence of an externally applied magnetic field. [9] This magnetization has the same polarity as the applied field and will thus align opposite magnetic poles together and create an attractive force. Diamagnetic materials become magnetized with the opposite polarity of an applied field. [9] This aligns like magnetic poles together and thus produces a repulsive force.

Magnetic fields can be created either by electrical coils or permanent magnets. A Permanent magnet is essentially a block of ferromagnetic material that produces a magnetic field. Permanent magnets have the advantage that they can produce high field fluxes (and thus significant forces) without any applied power or control electronics. Permanent magnets have very different properties and performance characteristics however, so these must be considered in any design application. The properties relevant to the basic use of permanent magnets are shown in Table 4.1. [10]

Material	Residual Flux Density (Br) (Teslas)	Maximum Energy Product (MGOe)	Coercivity (KOe)	Maximum Working Temperature (C°)
Nd-Fe-B (sintered)	1.0 - 1.4	Up to 45	Up to 30	180
Nd-Fe-B (bonded)	0.2 - 0.6	Up to 10	Up to 11	150
Sm-Co (sintered)	0.8 - 1.1	Up to 30	Up to 25	350
Sm-Co (bonded)	0.4 - 0.8	Up to 12	Up to 10	150
Alnico	0.7 - 1.4	Up to 10	Up to 2	550
Hard Ferrite	0.2 - 0.4	Up to 4	Up to 3	300
Flexible	0.1 - 0.3	Up to 2	Up to 3	100

Table 4.1: Permanent Magnet Material Properties [10]

The Residual Magnetic Flux Density (measured in Teslas) refers to the field flux created by a single magnetic domain within the material (a group of molecules with aligned fields). [9] The Residual Flux Density can more easily be thought of as the inherent “strength” of a magnetic material, and it is used when computing the force created by a magnet. A magnet’s Maximum Energy Product is a general reference to the amount of energy required to permanently demagnetize the material. [9] This can be used to give a relative comparison between magnetic materials. A Magnet’s Coercivity represents the applied field required to reduce a magnet’s own field to zero temporarily. [9] The maximum working temperature represents the maximum temperature in which the magnet can be used before heat will temporarily affect its magnetic properties. Together these properties allow a basic comparison and selection of magnetic materials given usage and environmental requirements.

Once a magnetic material has been chosen, the force created between the magnet and a highly permeable ferromagnetic material (such as steel or iron) is a complex function of the magnet's geometry, the ferromagnetic material's geometry, the residual magnetic field flux density, and the distance between the two. Permeability refers to the degree a material will magnetize when subject to an applied field. [9] In many cases, it is difficult to calculate magnetic force without the aid of computer analysis, but for simple cylindrical magnets in direct contact with typical ferromagnetic materials, the force can be approximated by Equation 4-2: [11]

$$F \approx 4000CB_r^2L_m\sqrt{A_m} \quad (4-2)$$

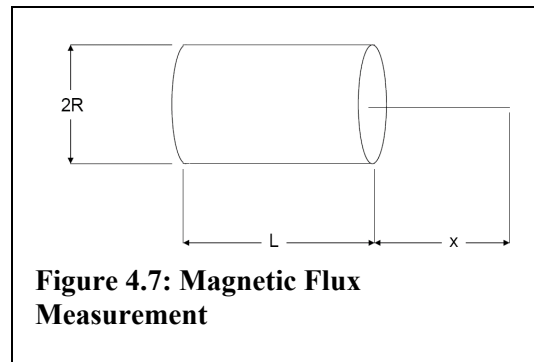
Where L_m represents the length of the magnet in meters, A_m represents the cylindrical cross sectional area in square meters, B_r represents the residual magnetic flux density of the material, F represents the force in Newton, and C represents the Empirical Force Coefficient. The Empirical Force Coefficient is essentially a correction factor inserted to account for non-ideal geometries of contact material. Thick flat plates have C near 1.0, however cylindrical disks or thin plates will have C less than 1.0. [11] If the relative geometry of the magnet and the attachment material remain the same over a range of sizes, C will remain constant. Thus it is possible to build a scale model of a magnet system and use the results to find C and therefore calculate the force for a different sized model.

Aside from the force, it is often useful to know the field flux density at a point some distance from the magnet's surface. While this is again a very complex function and often requires computer analysis, it can be approximated for cylindrical magnets using Equation 4-3: [11]

$$B_x \approx \frac{B_r}{2} \left[\frac{(L_m + X)}{\sqrt{R^2 + (L_m + X)^2}} - \frac{X}{\sqrt{R^2 + X^2}} \right] \quad (4-3)$$

In this case, R represents the magnet radius whereas X represents the distance as shown in Figure 4.7. All other variables are the same as before.

In cases where a ferromagnetic material is in direct contact with the surface of a cylindrical magnet, the flux density at the surface of the magnet (and thus the maximum flux present within the ferromagnetic material as well) can be computed by solving the above flux equation for $X = 0$. This results in Equation 4-4:



$$B_{surface} \approx \frac{B_r}{2} \left[\frac{L_m}{\sqrt{R^2 + L_m^2}} \right] \quad (4-4)$$

It should be noted that while cylindrical magnets are certainly not the only possible magnet geometry, they are the simplest geometry to design around due to the fact that one can easily and fairly accurately approximate how they will interact with other ferromagnetic materials (as demonstrated in the above equations). They also offer the most efficient field generation per unit mass. For these reasons, they are an attractive choice for any design involving permanent magnets.

4.1.6 Electromagnetic Theory

While permanent magnets offer great combinations of simplicity and performance, they are not controllable. Consequently, one cannot create or change a magnetic field originating from a permanent magnet without moving the magnet around. A solution to this problem lies with electrons. Electrons (and indeed all charged particles) create electromagnetic fields when they move, and they can thus have the same effect on materials that permanent magnets do. More specifically, coils of wire with electrons flowing through them can set up magnetic fields similar in geometry to permanent magnets. As a result, it is possible to use electromagnetic fields and switching power supplies to create different amounts of forces on objects in different directions without any moving parts. In the case of a staging system, such a capability could be capable of controlling permanent magnetic fields created by attached permanent magnets. Such a capability represents an ideal prospect for a highly reliable device.

In order to design a coil that creates a specific magnetic field flux density, we have to derive an equation that relates a solenoid's properties to its magnetic field strength. A typical solenoid is shown in Figure 4.8. For a first approximation we use Ampere's law and apply it to a cylindrical coil with N evenly distributed turns a radius R and an overall length of l_1 . If we assume the R

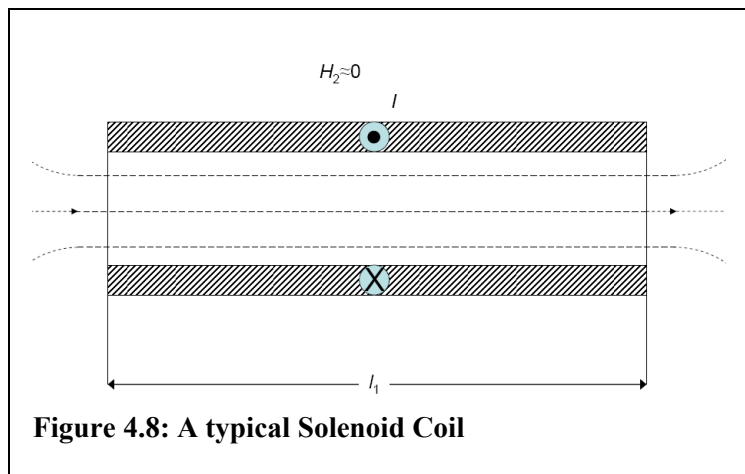


Figure 4.8: A typical Solenoid Coil

to be much smaller than l_1 the field is highly homogeneous inside the coil. This can be easily verified by experiments such as the iron filing experiment. This results in a very strong magnetic field strength inside

the solenoid whereas the magnetic field strength outside the coil (H_2) is highly non-uniform and of such low density, that we approximate H_2 to be 0. Thus we obtain using Ampere's Law:

$$\oint_L \vec{H} d\vec{s} = \sum_L I_k = \Theta = N \cdot I \quad (4-5)$$

$$H_1 \cdot l_1 + H_2 \cdot l_2 = N \cdot I \quad H_2 \approx 0$$

$$H_1 = \frac{N \cdot I}{l_1}$$

$$B_1 = \mu \cdot H_1 \quad , \quad \mu = \mu_r \cdot \mu_0$$

$$B_1 = \mu \frac{N \cdot I}{l_1} \quad (4-6)$$

This equation is a first approximation for the magnetic field strength that we can generate using a solenoid characterized by the length l and N turns. Further more, it depends on the relative-permeability μ_r initially assumed to be close to 1.0 (air).

Due to the small airframe diameter of the rocket, the coil is limited to 0.43". This in turn leads to a length/width ratio (L/R) of approximately one which is far from being infinite. This violates one of the assumptions made when deriving equation 4-6. Due to the small length/width ratio the magnetic flux density will be far from uniform resulting in a weaker field than calculated using equation 4-6. As a result, the magnetic field may be too weak for the coil's design objective.

In order to derive an equation that relates the magnetic field strength to the coil properties more precisely we apply BIOT-SAVART's Law [12]:

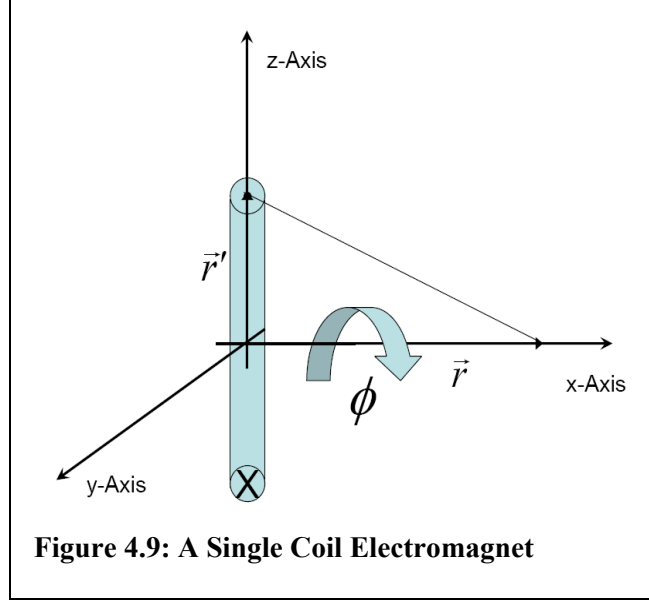
$$\vec{B}(\vec{r}) = \frac{\mu_0}{4\pi} \cdot I \cdot \int d\vec{r}' \times \frac{\vec{r} - \vec{r}'}{|\vec{r} - \vec{r}'|^3} \quad (4-7)$$

Before calculating the magnetic field strength along the x-Axis for a solenoid containing N turns, we apply BIOT-SAVART's law to a coil (one turn) with the radius R . We start by defining the different variables:

$\vec{r} = (x, 0, 0)$ (Coordinates of the point on the x-axis)

$\vec{r}' = (0, R \cos \phi, R \sin \phi)$ (Coordinates on the coil)

$d\vec{r}' = (0, -R \sin \phi, R \cos \phi) d\phi$



$$\vec{r} - \vec{r}' = \begin{pmatrix} x \\ -\cos \phi \\ -\sin \phi \end{pmatrix}$$

$$\begin{aligned} |\vec{r} - \vec{r}'|^3 &= |(x, -R \cos \phi, -R \sin \phi)|^3 \\ &= (x^2 + R^2(\cos^2 \phi + \sin^2 \phi))^{3/2} \\ &= (x^2 + R^2)^{3/2} \end{aligned}$$

$$d\vec{r}' \times (\vec{r} - \vec{r}') = R \begin{pmatrix} 0 \\ -\sin \phi \\ \cos \phi \end{pmatrix} d\phi \times R \begin{pmatrix} x \\ -\cos \phi \\ -\sin \phi \end{pmatrix} = R^2 \begin{pmatrix} \sin^2 \phi + \cos^2 \phi \\ x \cdot \cos \phi \\ x \cdot \sin \phi \end{pmatrix} d\phi$$

$$\vec{B}(\vec{r}) = \frac{\mu_0}{4\pi} \cdot I \cdot \int d\vec{r}' \times \frac{\vec{r} - \vec{r}'}{|\vec{r} - \vec{r}'|^3} = \frac{\mu_0}{4\pi} \cdot I \cdot \frac{1}{(x^2 + R^2)^{3/2}} \cdot \int_0^{2\pi} R^2 \begin{pmatrix} \sin^2 \phi + \cos^2 \phi \\ x \cdot \cos \phi \\ x \cdot \sin \phi \end{pmatrix} d\phi$$

$$\vec{B}(\vec{r}) = \frac{\mu_0}{2} \cdot \frac{I \cdot R^2}{(x^2 + R^2)^{3/2}} \quad (4-8)$$

Equation 4-8 gives the magnetic field strength B along the x-Axis produced by a coil with a single turn supplied with current of magnitude I . An example of a single turn coil is shown in Figure 4.9.

Next we considered a solenoid of length L containing N number of turns. By integrating over the entire length of the solenoid we obtain the magnetic field strength produced by the solenoid along the x-Axis:

$$\vec{B}_c = n \int_0^L \vec{B}(x-x') dx' \quad ; \quad n = N/L$$

$$n \cdot I \cdot \frac{\mu_0}{2} \cdot \vec{e}_x \cdot \left. \frac{x' - x}{\sqrt{R^2 - x^2 - 2xx' + x'^2}} \right|_{x'=0}^L \quad (4-9)$$

$$\vec{B}_c = n \cdot I \cdot \frac{\mu_0}{2} \cdot \left(\frac{L-x}{\sqrt{R^2 + (x-L)^2}} + \frac{x}{\sqrt{R^2 + x^2}} \right) \cdot \vec{e}_x \quad (4-10)$$

Using Equation 4-10, we could precisely calculate the magnetic field strength along the x-axis produced by the different coil designs.

To graphically show the affect of the L/R -ratio on the magnetic field strength inside the solenoid, we generated the following graphic (Figure 4.10) using MatLab. The y-axis represents the relative magnetic field strength for various L/R -ratios with respect to a very long solenoid ($L/R=\infty$) producing a magnetic field strength with a magnitude of 1.0 Tesla. For a ratio of approximately 1.0 as is the case for our coil design, the field strength is drastically weakened. It is approximately 45% (Equation 4-11) in magnitude compared to a solenoid which is has long length to width ratio. Figure 4.11 shows the field strength within the coil in comparison with a permanent magnet's field offset from the coil. This represents a good design setup for a combined permanent magnet and electromagnetic actuator.

$$\vec{B}_{\frac{L}{R}=1} / \vec{B}_{\frac{L}{R}=\infty} = \left(\frac{L-x}{\sqrt{R^2 + (x-L)^2}} + \frac{x}{\sqrt{R^2 + x^2}} \right) \cdot \vec{e}_x$$

$$\vec{B}_{\frac{L}{R}=1} / \vec{B}_{\frac{L}{R}=\infty} = \left(\frac{1}{\sqrt{5}} \right) \cdot \vec{e}_x \approx 0.447 \quad (4-11)$$

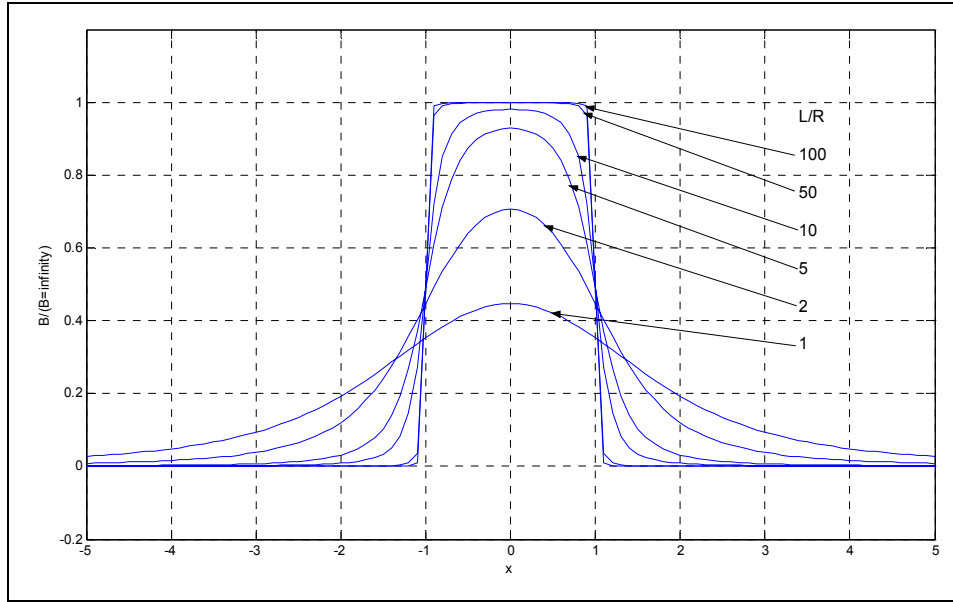


Figure 4.10: Relative Magnetic Flux Density along the X-axis as a function of L/R Ratio

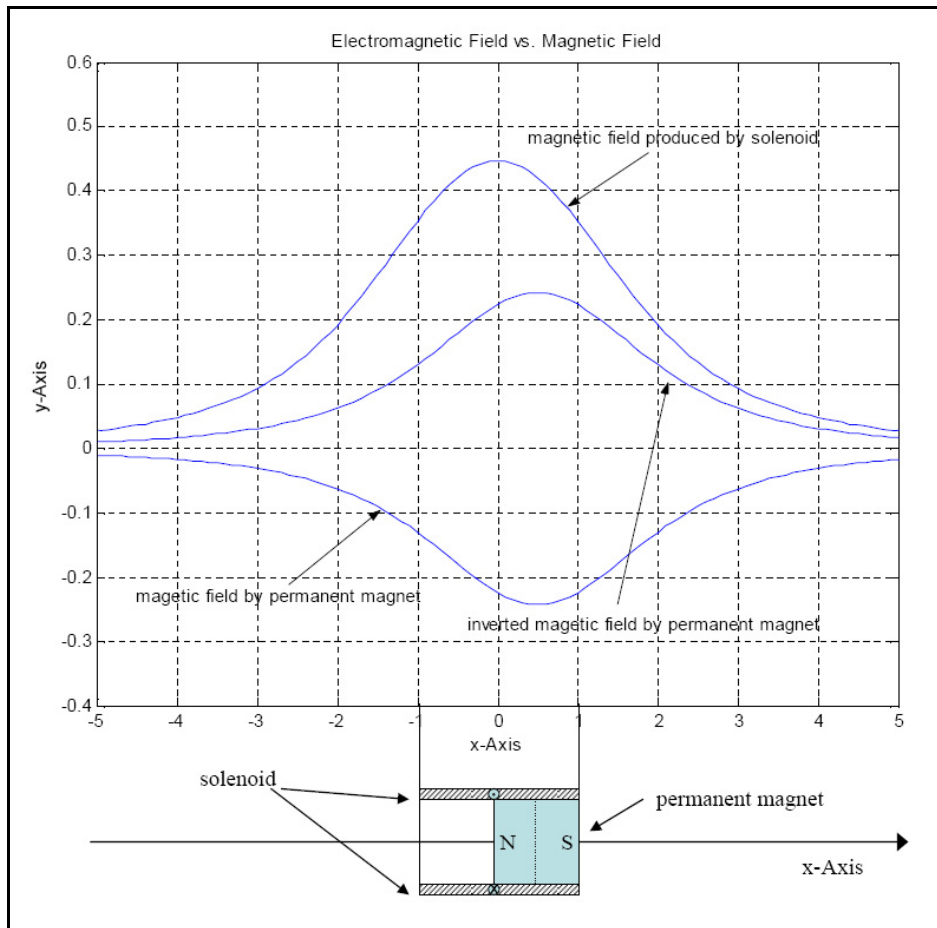


Figure 4.11: Magnetic Flux Density of a Solenoid versus a Permanent Magnet

Series LCR Circuit

In the previous chapter we talked about the fundamentals of electromagnetism and focused on how to calculate the magnetic field of a given solenoid using the BIOT-SAVART law. In doing so, we showed that the magnetic field produced by a coil is always proportional to the current. Consequently, the current flow is of great interest. The circuit diagram of the electromagnetic actuator is given in Figure 4.12 and represents the least complex circuit for use. The resistance R accounts for all the resistance within the circuit. The coil itself solely determines the net inductivity of the circuit, L . The same applies to the capacitance, C , which mainly depends on the capacitor. Prior to discharging the capacitor and measuring the transient response through the circuit, we charge the capacitor using four 12 Volt batteries hooked in series. This is also modeled in Figure 4.12 with Switch S_1 used for charging the capacitors. Once the capacitor is fully charged, switch S_1 is opened. To discharge the capacitor, S_2 is closed. It should be noted that U refers to the voltage drop across a circuit element.

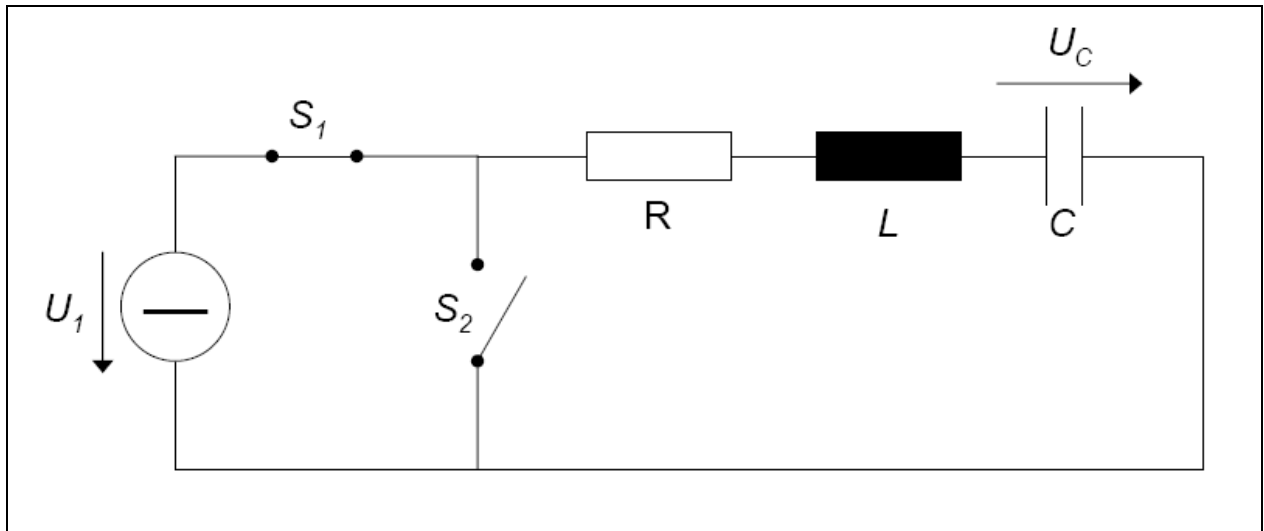


Figure 4.12: Transient Response Analysis of an LC Circuit

In order to calculate the precise current flow during discharge, we use Kirchoff's second equation [13]:

$$\sum U_v = 0 \quad (4-12)$$

$$Ri + L \frac{di}{dt} - \frac{1}{C} \int_{-\infty}^t i(\tau) d\tau = 0$$

or

$$Ri + L \frac{di}{dt} + \frac{1}{C} \int_{-\infty}^0 i(\tau) d\tau + \frac{1}{C} \int_0^t i(\tau) d\tau = 0 \quad (4-13)$$

Here, the first integral represents the charge Q_0 , to which the capacitor was charged until time $t = 0$. The relationship between this charge and the voltage across the capacitor is given by $Q_0 = CU_1$. Thus we obtain using Equation 4-14:

$$Ri + L \frac{di}{dt} + U_1 + \frac{1}{C} \int i(\tau) d\tau = 0 \quad (4-14)$$

In order to solve the differential equation, we used the Laplace transform to obtain the following:

$$RI(p) + L[pI(p) - i(0)] + \frac{U_1}{p} + \frac{1}{Cp} I(p) = 0 \quad (4-15)$$

The inductance prevents an immediate change of current: $i(0) = 0$. Thus we obtain:

$$I(p) = \frac{-U_1}{p(R + Lp + 1/Cp)} = -\frac{U_1}{L} \frac{1}{p^2 + \frac{R}{L}p + \frac{1}{CL}} \quad (4-16)$$

In order to transform the equation back into the time domain and to obtain the transient response of the current, we use Heaviside's Method based on the expansion into partial fractions. [13] First we calculate the zeros of the denominator of Equation 4-17 and obtain:

$$p_{1,2} = -\frac{R}{2L} \pm \sqrt{\left(\frac{R}{2L}\right)^2 - \frac{1}{CL}} \quad (4-17)$$

We denote the zeros $p_{1,2}$ and introduce Heaviside's Equation

$$f(t) = \sum_{k=1}^n \frac{Z(p_k)}{N'(p_k)} e^{p_k t} \quad (4-18)$$

And now we transform the current back from the frequency domain back into the time domain and obtain

$$i(t) = -\frac{U_1}{L} \left(\frac{1}{p_1 - p_2} e^{p_1 t} + \frac{1}{p_2 - p_1} e^{p_2 t} \right) \quad (4-19)$$

It should be noted that the transient response can be critically damped, over damped, or under damped. [17] In order to keep the electromagnet from reversing field during actuator separation, the capacitor size must be selected to produce an over-damped response. The following simulations shown in Figure 4.13 and Figure 4.14 represent a damped response.

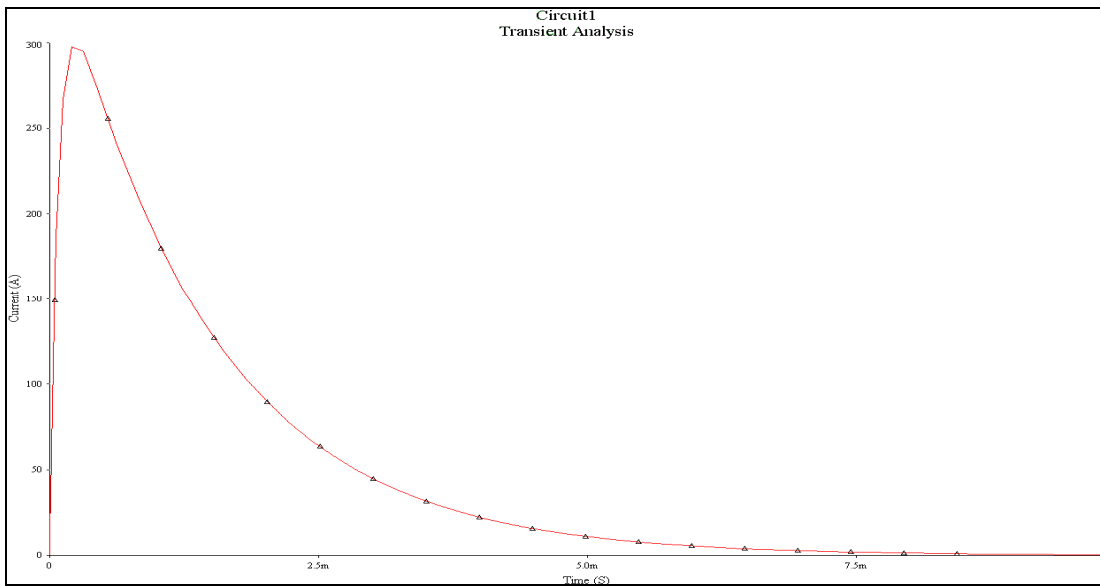


Figure 4.13: Current Discharge Plot for the actuator circuit (computed in MicroSim)

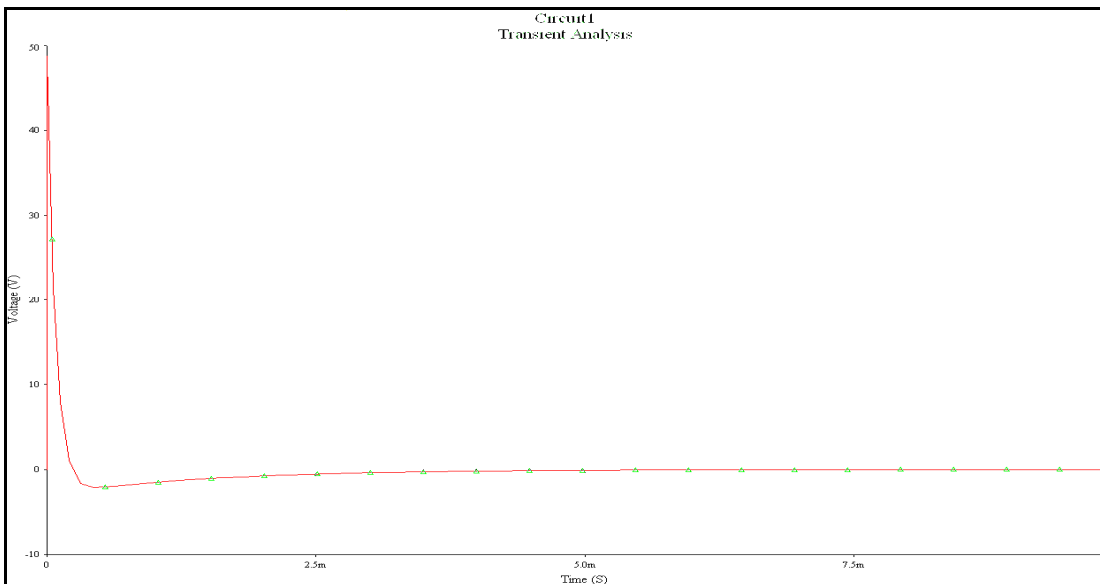


Figure 4.14: Capacitor Voltage during Discharge (computed in MicroSim)

4.2 Methodology

The primary goal of this project was to design a new and innovative staging system for small-scale rocket vehicles. The overall vehicle design dictated that the staging system be capable of separating three parallel boosters. In order to fulfill these goals, we broke the project down into the following sequential steps:

- Define project objectives and establish design requirements
- Select design approach and concept
- Design and fabricate a prototype staging system using the selected approach
- Make design changes based on prototype testing
- Fabricate a final staging system and integrate it into the vehicle airframe

Throughout the design and fabrication process, we tested individual aspects of the design in order to insure the final system functioned as intended. This also allowed us to draw conclusions about the design approach and fabrication techniques. This process culminated in flight-testing of the entire integrated staging system.

4.2.1 Design Evaluation and Selection

A successful staging system hinges on the generation of a force sufficient to keep the stages together when necessary and sufficient to separate the stages when triggered by an electrical pulse. There are many ways of expending energy to create a force. However before proceeding with any particular design approach, we investigated a number of different energy storage and transfer ideas.

We started by modelling the system and its individual components. This not only gave us a better understanding of the complexity of the process but let us break up the entire process into smaller subunits (shown in Figure 4.15).

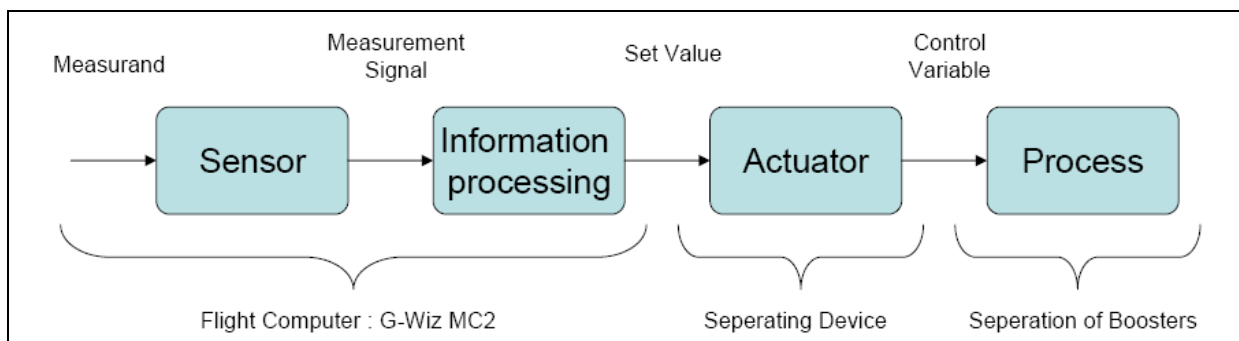


Figure 4.15: An Abstract Model of a Staging System

These subunits were modelled as black boxes each performing a specific task. The reason we used black boxes rather than assigning specific components was that we wanted to further investigate the design of those black boxes. We did not want to favor any possible solution up front.

Due to the complexity of our model rocket, it was clear from the beginning that a flight computer would be installed offering a certain set of functions. Rather than having a dedicated sensor and information-processing unit for the staging subsystem it, made sense to “outsource” these two subunits and integrate them into the flight computer shown in Figure 4.16 and Appendix G.

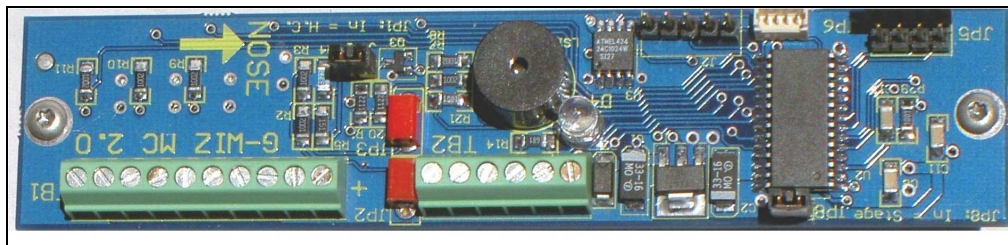


Figure 4.16: GWiz MC2 Flight Computer [14]

This decision placed the following requirements on the flight computer:

- 1) Must include a sensor or timer to detect correct timing for staging
- 2) Must be installed such that a signal can be delivered to the staging electronics.

With the decision to equip our rocket vehicle with the G-Wiz MC2, there was no further need to focus on sensors or information processing units. These two subunits were incorporated into the flight computer. Our task was now to develop an actuator that would (depending on the input signal) perform a designated function resulting in reliable and simultaneous separation of all three boosters. Before choosing a specific design for the actuator, we wanted to articulate the specific design goals we would use to evaluate the different options and compare them amongst each other in order to come up with our final design. The following list contains the major performance objectives:

- 1) High reliability (no operational failure in ground testing)
- 2) Low mass in respect to overall rocket ($\approx 150\text{g}$)
- 3) Impulsive dynamics (fast separation)
- 4) Reusable (several launches within a short period of time)

This list is not mutually exclusive as it only represents the objectives placed on the new actuator design. It does not include restrictions such as size and volume. Due to the airframe design, the actuator

length was limited to 0.43 inches. Another limiting factor was the type of energy used for actuator operation.

In order to obtain an overview of different actuator designs we focused on different types of energy and their exploitation in actuator design. Figure 4.17 shows this approach in which four different types of energy have been identified as possible sources for actuator operation. Due to the project constraints (no pyrotechnics), we limited ourselves to the first three energy sources including electrical, fluidic, and thermal energy. The use of chemical energy should be avoided and should only be considered as a last resort. This is mainly due to the fact that chemical energy in the form of black powder is currently used in series separation systems and we want overcome disadvantages associated with it.

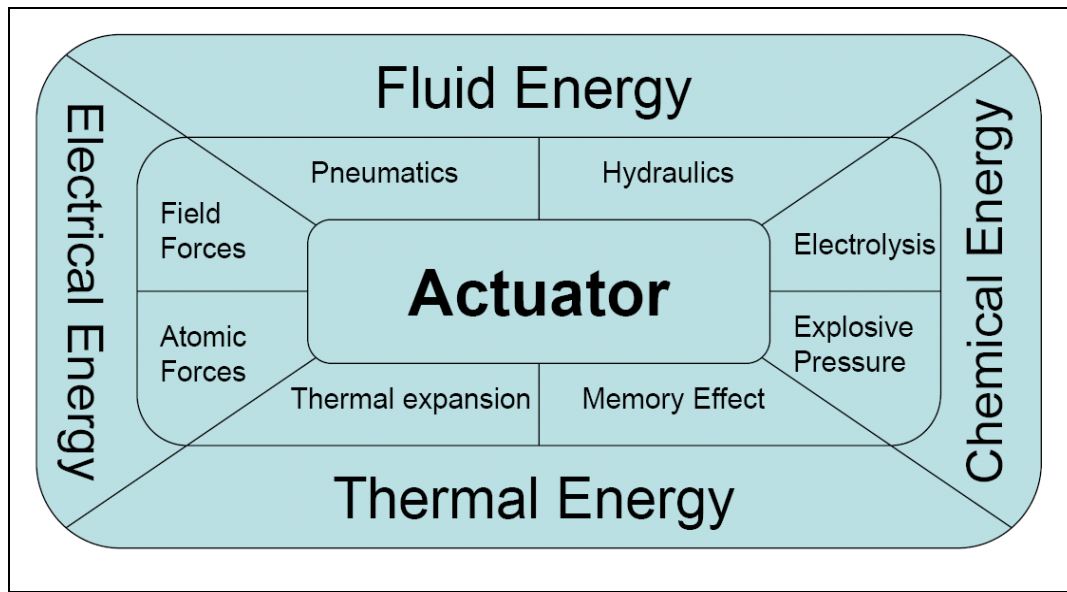


Figure 4.17: Energy and Forces that can Create Mechanical Output [15]

The next step was to develop as many possible actuator designs using one of the three energy sources. Through brainstorming as well as reviewing specific literature and journals, we generated several design ideas. Additional information was obtained from model aircraft designs that require frequent use of different actuator mechanisms. Selected findings are shown in Figure 4.18.

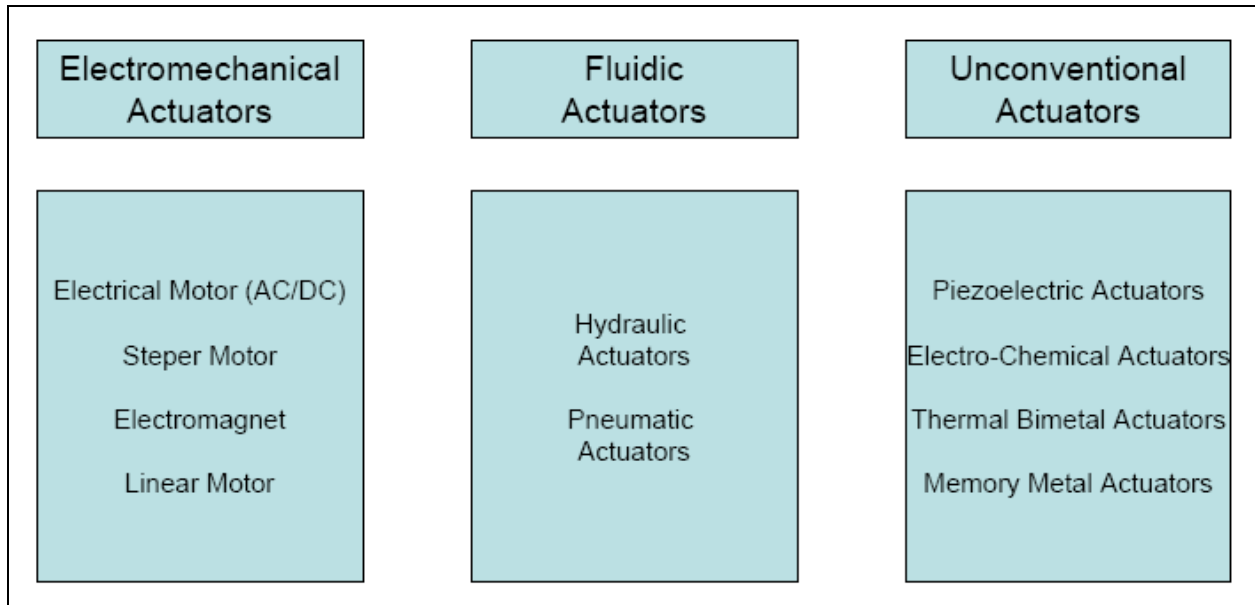


Figure 4.18: Actuator Classifications

Through this research we gained a deeper understanding of all possible options. We reviewed performance characteristics such as power density, dynamics, size and type of energy used in operation. We also evaluated the weight of each solution, the space required for implementation, the ease of ground testing, and the predicted reliability. General conclusions about these aspects were drawn from past experience with similar systems used in other fields of engineering.

Mechanical solutions in general such as springs could be lightweight, but the number of moving parts involved would add an unpredictable or high maintenance element given the dynamic forces, vibrations, and general flight conditions experienced by a rocket. The space limitation posed by the rocket design also made mechanical systems an unlikely solution. Consequently electromagnetic and fluidic actuators offered more promising solutions.

In the following two tables (Table 4.2 and Table 4.3), we provide general characteristics of electromagnetic and fluidic actuators. Unconventional actuators such as a piezoelectric design would prove difficult to implement due to their control requirements such as high voltage or temperature.

Advantages	Disadvantages
Reliable	Heavy
High dynamics	Low power density
Reusable	
Good control properties	
Low maintenance	
High overall efficiency	

Table 4.2: Electromechanical Actuators

Advantages	Disadvantages
Reliable	High maintenance
Impulsive dynamics	More difficult to control
High power density	Additional hardware required
High overall efficiency	Large Mass (Required for high pressure system)

Table 4.3: Fluidic Actuators

After reviewing the characteristics of many different fluidic actuators, we decided that only pneumatic actuators could possibly meet our design goals. The energy needed to operate all fluidic actuators must be stored in the fluid itself however. Since liquids are generally incompressible, pressure could not be stored in the liquid itself but would need to be created on board. This would require additional hardware and would not only increase the complexity, but would also add a lot of empty weight to the rocket and decrease its performance. This disadvantage only applied to liquid actuators, however, as pneumatic systems could store the energy in the fluid due to its compressibility. Several commercially available cartridges offered such pressure and could be used to operate micro-cylinders separating the boosters from the main rocket vehicle. The only additional hardware needed would be a valve to release the pressure when commanded by the flight computer. Many cartridges differing in volume and compressed gas were readily available and could provide energy to drive a pneumatic actuator.

While pneumatic systems represented a possible solution, electromagnets seemed even more promising. They feature the very same positive attributes as the pneumatic actuators such as reliability, impulsive dynamics (fast powerful discharge), and ability to produce linear motion. They have similar size constraints that allow installation between the motor mount and the main airframe. They are also easy to control, and they are consistent due to their solid-state nature. The energy required for operation could be supplied by lightweight capacitors as opposed to heavier pressure vessels that would be needed to store compressed gases. In addition, capacitors could easily be recharged at the field whereas restoring pressure would require more complex hardware not readily available. Electromagnetic staging methods would also be very innovative as no current or past staging systems have ever used this concept to our knowledge. Their attributes are listed in Table 4.4:

Advantages	Disadvantages
Compact	Non-linearity
Direct linear motion	Small to medium performance density
Impulsive dynamics	Magnetic Hysteresis
Good control properties	
Low maintenance	
High reliability	
Solid state (no moving parts)	

Table 4.4: Electromagnetic Actuators

4.3.3 Prototype Design

Due to the different advantages of permanent magnets and electromagnets, it was best to use each in roles that minimized their disadvantages. For this reason, we selected permanent magnets for use in attaching the staging components. These components had to be held together for a reasonable amount of time with a reasonable amount of force during launch preparation and ascent, and an electromagnet designed for this purpose would have required significantly more power than could be provided in a vehicle this size. Because electromagnets could be controlled, however, they represented a good solution for separation initiation. Consequently, we decided that permanent magnets on one part of the vehicle could attach to a ferromagnetic metal retainer or mount on the other part of the vehicle. The permanent magnet would thus hold the parts together until separated by a strong, short-duration pulse of an electromagnet in the opposite field direction. In the interest of structural rigidity, each booster would require more than one attachment point between it and the airframe. Many commercial, full-scale vehicles in service support external boosters at two primary locations, so it was logical to attempt a similar scheme on a smaller vehicle. Two mounts as far from the booster's center of gravity as possible would increase the stiffness of the mounting design (by increasing the moment of inertia about the booster's center of gravity) while minimizing the weight of each attachment point.

In addition to a dual mount design, we concluded early in the design process that the electromagnetic coils should reside within the main airframe. This was primarily due to the power requirements and the fact that the staging initiation signal would originate from the flight computer also located in the main airframe. While this design would add the control system weight to the more critical second stage (and thus reduce performance), it avoided complex signal transfer schemes to the boosters from the flight computer. In addition, we were uncertain early on if the booster airframe would provide enough volume for a coil, power storage, and control system.

The next step in the design process was to determine the specific shape and setup of the electromagnetic actuator. Different possible design solutions that could be used for our electromagnetic

actuator are shown in Figure 4.19. [15] In this figure, the force between the magnetic field source and magnetic field sink is shown for different possible geometries. In order to evaluate the different designs in respect to our staging system, we focused on the following two characteristics that were most important:

- a. Great force between permanent magnet and iron core upon contact
- b. Little energy dissipation during separation

The first objective focused on the launch and ascent during which all three boosters had to remain attached to the main airframe. A premature and uncontrolled separation could have been catastrophic not only for the flight mission itself but also in respect to safety. Consequently, the force upon contact had to be maximized.

The second objective was related to the actual separation process and focused on the energy dissipation. The amount of energy needed for proper actuator operation would determine the size and weight of the capacitors needed to store the energy. As pointed out earlier, weight was an extremely critical factor. Therefore, less energy dissipation during operation would result in a lighter staging system.

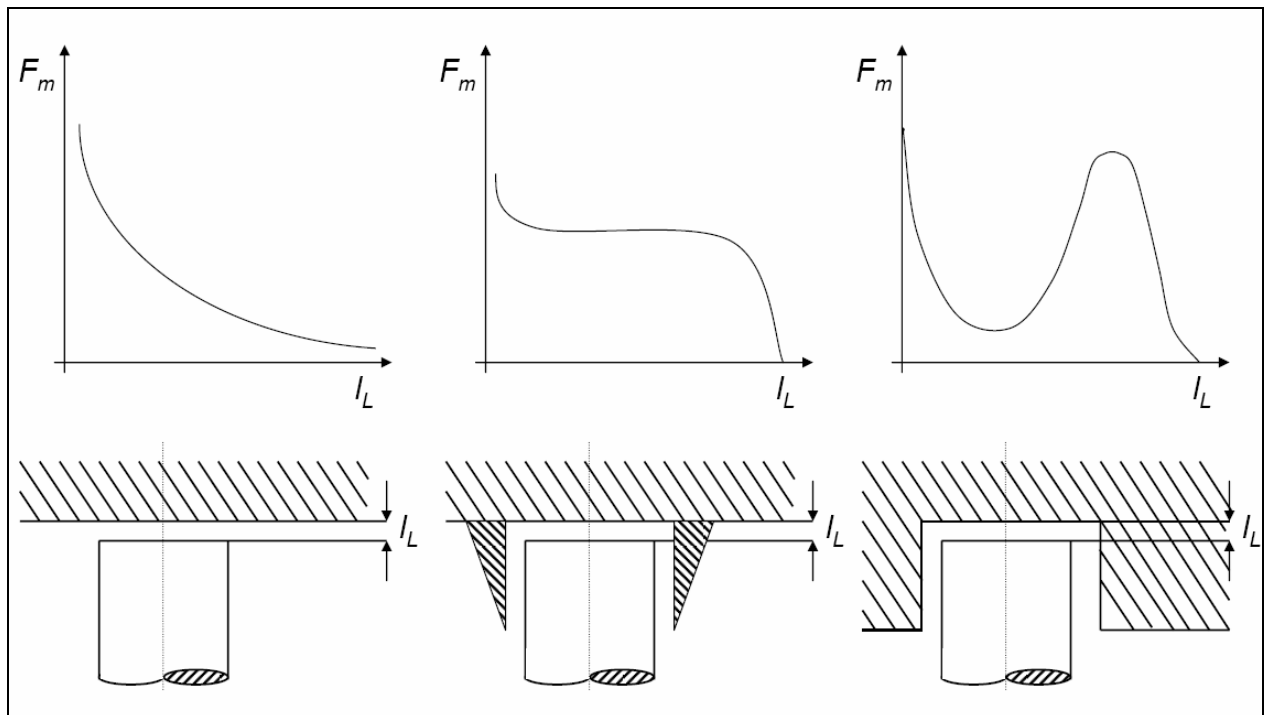


Figure 4.19: Possible actuator design [15]

The energy needed for separation could be obtained by using following equation:

$$E = \int \vec{F} d\vec{s} \quad (4-20)$$

$$E_1 < E_2 < E_3$$

Comparing the characteristics of all three different actuator setups in Figure 4.19, we concluded that a design resembling the first actuator setup would best suit our needs. It exerted maximum force upon contact between the magnet and the iron core and required the least amount of energy during separation.

Taken all together, these early design decisions and judgments led to an initial design sketch shown in Figure 4.20.

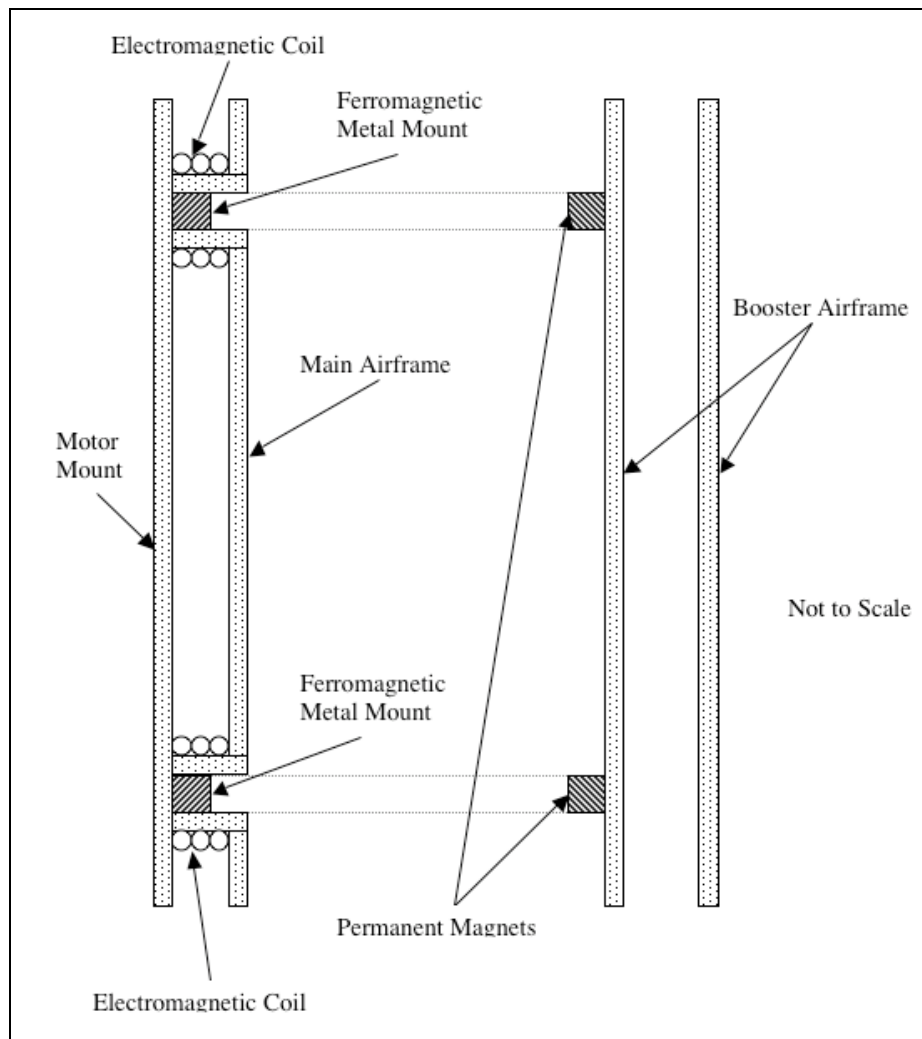


Figure 4.20: Early Electromagnetic Staging Concept

Once the initial concept was established, we turned our attention to specific aspects of the mounting mechanism. One particular consideration was the angle at which the mount was fixed relative to the vehicle axis. An example of possible mount angles is shown in Figure 4.21. Any angle would theoretically work, however the permanent magnets did not maintain a hard connection (like a locking mechanical system) so enough force could separate the magnetic mechanism prematurely. An upward mount angle would be less prone to separate during the thrusting stage (as it would be in compression), but it could be prone to accidental drag separation. A downward angle would avoid possible drag separation, but it would be prone to separate during periods of booster thrust. Because of these limitations, a mounting angle perpendicular to the vehicle's axis was selected. While this method would be more prone to separate from lateral or rotational forces, these forces were expected to be far less than the axial forces due to thrust and drag. In addition, a perpendicular mount allowed more room in the core stage for the necessary electromagnetic coil and metal retainer.

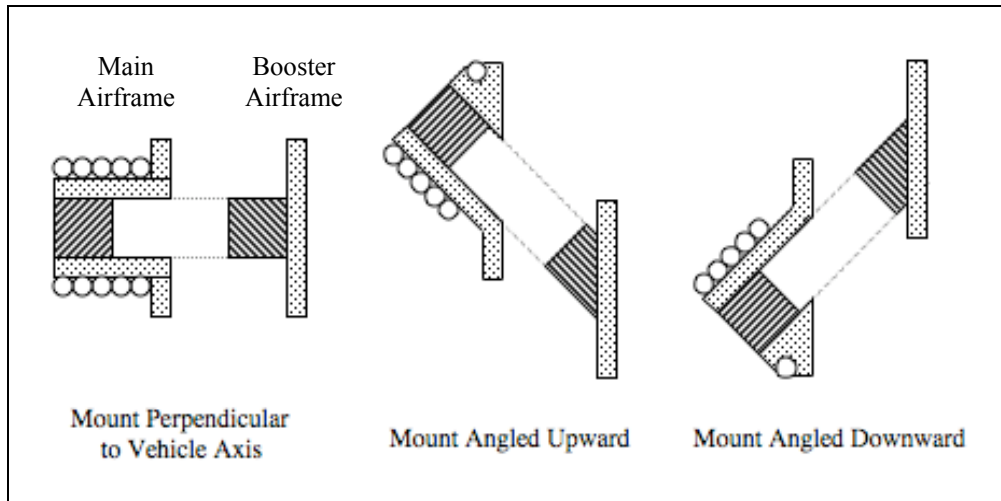


Figure 4.21: Mount Angle Considerations

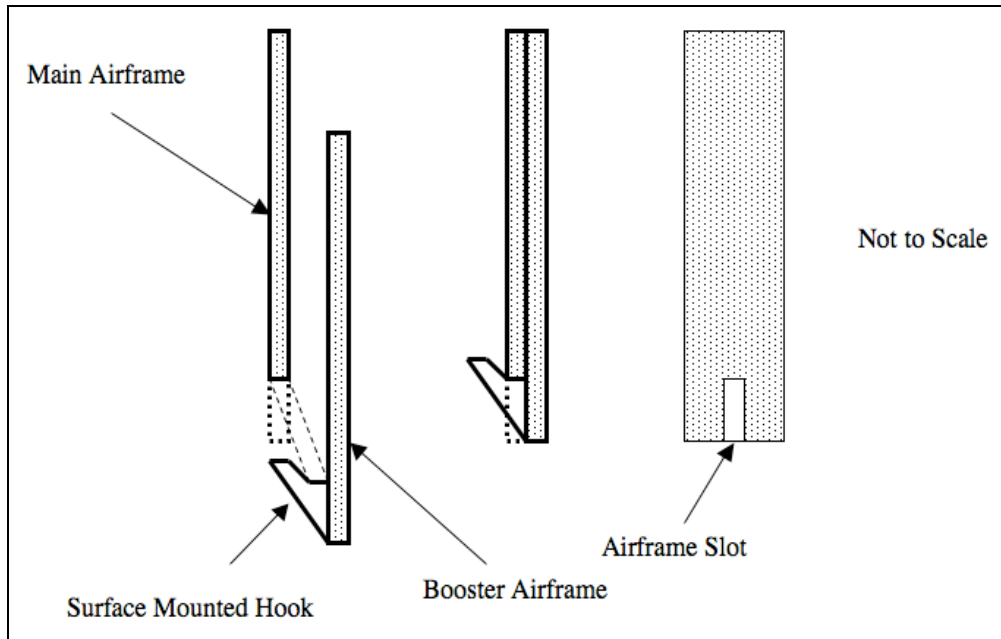


Figure 4.22: Aft Hook Mounting Concept

Following the mount angle selection, we concluded that only one magnetic system was actually required per booster. The forward mount would be a magnetic coupling perpendicular to the vehicle axis (as per the initial design sketch), but the aft mount could consist of a simple mechanical retaining hook on the booster coupled to an open-ended slot on the main airframe (shown in Figure 4.22). Eliminating the magnetic coupler in the lower

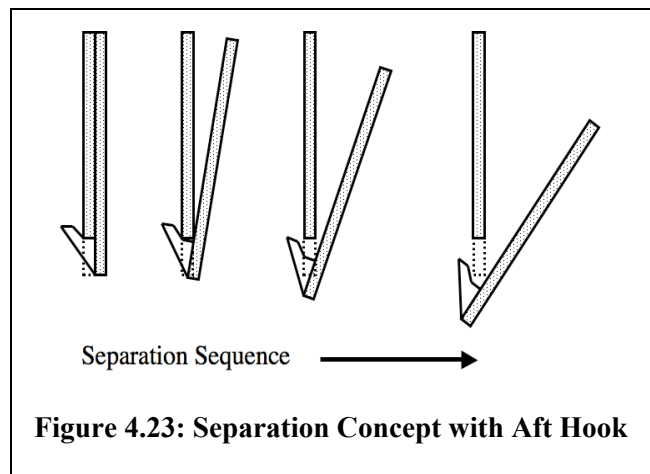


Figure 4.23: Separation Concept with Aft Hook

portion of the vehicle would also reduce the complexity and power requirements of the system. Additionally, if long magnets were required (and thus through-wall mounting in the booster), there would be no way to attach them on the booster at this location because the motor would be friction fit just inside the skin. Even surface mounting magnets at this location would prove a problem as the heat generated by the motor could affect the magnet's performance. We thus deemed the mechanical hook a better and simpler option. This hook would support motor thrust loads and lateral side loads during ascent just as the magnetic mount, but it would drop out and away when the forward magnetic actuator separated. Consequently, the separation event would appear more like a rotational separation than a straight lateral

separation. The boosters would rotate away from the core stage while falling off. An example of the separation profile this system could create is shown in Figure 4.23.

Once this design approach was selected, we needed to size the various components according to the loads they would experience. In the case of the magnet mount and hook, the lateral loads and accelerations would be the primary driver of size. Unfortunately, these lateral loads were difficult to predict. In theory, a perfect flight would not experience any lateral loading or spinning, but this never occurs in reality. In addition, rocket motor thrust and aerodynamic vortex shedding off the main airframe could create unpredictable accelerations or vibrations that would be difficult to quantify without testing. In light of these challenges and our limited testing capability, we decided to approximate loads created by worst case spin scenarios, worst case drag scenarios, and worst case asymmetric thrust conditions. We would then assume a large safety factor in order to compensate for the many unknown variables. In the case of vehicle spin, we assumed a spin scenario of 600 revolutions per minute (10 revolutions per second). This was a rather arbitrary value, but it was significantly higher than anything we had previously witnessed in small-scale rocket launches and was thus a good worst-case estimate. In order to calculate the force created by this rotation rate (ω), we employed equation 4-21:

$$F = \omega^2 r m \quad (4-21)$$

With a radius (r) of 5.08 centimeters and a maximum booster mass (m) of 300g, this resulted in a force of 1.5 Newtons. In order to estimate the next possible force – asymmetric drag – we first calculated the maximum axial drag on each booster by equation 4-21:

$$F = q_{\infty} C_d A = \frac{1}{2} \rho v^2 C_d A \quad (4-22)$$

With an air density (ρ) of 1.2 Kilograms per cubic meter, a maximum rocket velocity (v) of 275 meters per second, a frontal area (A) of 8.13 square centimeters, and an estimated drag coefficient (C_d) of 0.7 (typical values used as starting estimates in CompuRoc™ simulation software), this resulted in an axial drag force of 25.8 Newtons. Finding the actual amount of outward lateral force due to drag in odd flight attitudes would be extremely difficult without wind tunnel testing because of the complex geometry at the booster attachment points. Nevertheless, we thought this would likely be a small percentage of the axial drag. Consequently, we assumed 10 percent of the axial drag, (2.6 Newtons) for the worst-case lateral drag scenario.

Following the very rough estimation of worst-case spin and lateral drag loads, we calculated asymmetric thrust. Again, this estimate proved very rough because little data of this type exists for small-

scale rocket motors. Nevertheless, if a nozzle half angle of 15° is used (a typical value) and the flow was to become attached to one side and not the other (a rare but possible set of circumstances), the thrust would diverge 15° from center (λ). With the largest possible booster motor (an H90), the peak thrust (F_a) of 125N would thus create a side load of 32 Newtons by equation 4-22:

$$F = F_a \sin(\lambda) \quad (4-23)$$

All of these load cases taken together result in a lateral load around 36 Newtons. While this was for each entire booster and would thus be split between the two mount locations, a safety factor of 2.0 would give loads at each mount around 36N. Consequently, we knew each permanent magnet would need to be capable of supporting 36N or greater. It should be noted at this point, however, that the nature of the methods we used above to estimate this load value were based in many cases on speculation of flight dynamics. Very little data exists for vehicles at this scale, and the data that does exist are qualitative and vague in nature. Consequently, this load estimate may not represent actual flight loads very well, but it should be sufficiently large to allow reasonable sizing of components to avoid failures.

Once we established an estimate of the loads experienced at each support, we sized the permanent magnet and aft mounting hook accordingly. The permanent magnet size was calculated using equation 4-2 reprinted as follows:

$$F = 4000CB_r^2L_m\sqrt{A_m} \quad (4-24)$$

Early testing with smaller magnets against ferromagnetic mounts similar to those detailed in the diagram indicated a force coefficient (C) around 0.46. In addition, we estimated the residual magnetism (B_r) at 1.2 Teslas (the average for sintered Neodymium Boron Magnet Material). We selected Sintered Neodymium Boron magnets because of their high residual flux density and their resistance to permanent field reversal (necessary in an environment of changing magnetic fields). In order to select the proper geometry, we tried several combinations of magnet length (L_m) and contact area (A_m). In order to simplify the iterative design process, we employed Microsoft™ Excel™ software and created a spreadsheet with all the design parameters and equations. This spreadsheet is shown in Appendix H. With the help of this software, we quickly determined the optimum magnet necessary to create 36N of force would be about 1.25 centimeters long and 1.25 centimeters in diameter. These dimensions were almost identical to commercially available 1/2" by 1/2" Neodymium Boron magnets, so these commercial magnets were selected for integration into the magnetic actuator.

In addition to the force created by the magnet, we established the magnetic flux at the magnet's surface, by equation 4-4 reprinted here:

$$B_{surface} \approx \frac{B_r}{2} \left[\frac{L_m}{\sqrt{R^2 + L_m^2}} \right] \quad (4-25)$$

In this case, R represented the magnet radius (1/4" or 6.35mm), L_m the magnet length (1/2" or 12.7 mm), and B_r the residual flux density (1.2 Teslas). For this particular magnet geometry, the surface flux was thus computed to be 0.54 Teslas. It should be noted that this value would be identical to the greatest magnetic flux experienced by the ferromagnetic retainer in the main airframe when coupled directly to the surface of the magnet. Consequently, this value multiplied by a safety factor would set the required coil field. Since there were fewer unknowns in the calculation of field fluxes when compared to load estimation, we chose a safety factor of 1.5. Thus we computed the required coil field as 0.81 Teslas with the opposite polarity of the permanent magnet.

In order to accurately size a coil to match the specified field and size of the metal retainer, we created a second spreadsheet in Microsoft™ Excel™ with the equations necessary for calculating electromagnetic fields, coil inductance, and circuit properties using the same equations listed in the background section under Electromagnetic Theory. The spreadsheet also included standard wire reference data – information critical to relating electrical properties and physical size. This spreadsheet can be seen in Appendix I.

In addition to the field and diameter requirements, it was also necessary for the coil to fit within the confines of the main airframe. Specifically, the coil had to fit between the inner core motor mount and the outer airframe, a distance of only 0.43 inches. This was no easy challenge. After several iterations, we arrived at a set of coil and circuit parameters that would be capable of meeting field generation and size requirements. We also paid careful attention to the inductive time constant of the coils and the capacitive time constant of the power circuit as these values had to be sufficiently different in order to avoid resonance. The design parameters for the coil and circuit are listed in Table 4.5.

Coil and Circuit Properties		
Inner Diameter	0.5625	Inches
Number of Layers	2	-
Number of Turns per Layer	6.5	-
Wire Gauge	16	AWG
Total Extra Series Resistance	0.003	Ohms
Applied Voltage	12	Volts
Applied Capacitance	0.333	Farads
Relative Permeability of Core	100	
Outer Coil Diameter	.8	Inches
Coil Length	0.38	Inches
Total Wire Length	25.35	Inches
Total Resistance	0.01148	Ohms
Peak Current Flow	1045	Amps
Peak Power Dissipation	12542	Watts
Coil Inductance	0.003969	Mili-Henerys
2D Corrected Field	0.865	Tesla
Capacitive Time Constant	0.00382	Seconds
Inductive Time Constant	0.000345	Seconds
Time Constant Ratio	11	-

Table 4.5: Coil and Circuit Properties

When the coil parameters and magnet geometry were set, we investigated possible materials for the ferromagnetic metal retainer. Although many materials represented possible solutions (since any metal with iron in it will have ferromagnetic properties) we selected steel because it was cheap, easy to machine, and readily available. While Nickel-Iron alloys do exist with better magnetic properties, they are extremely expensive and difficult to machine. We also selected Garolite as the best material for the actuator sheath (Figure 4.24). Garolite is a cotton epoxy composite and was thus lightweight, strong, cheap, and easy to bond with other composite materials in the rocket. A third and final material we selected to use was G10 Fiberglass laminates for the aft mounting hook. G10 fiberglass was heavier and more expensive than many composites, but it was strong, easy to machine, and was already being used for the fins. G10 also had a long favorable history with many small-scale rocket manufacturers such as Public Missiles Ltd™, so it represented a logical choice. Unlike the permanent magnets, however, we did not size the fiberglass laminate used for the hook according to the estimated 36N load. In this case, the stiffness of the hook, the bonding area with the booster, and the load transfer area against the main airframe were all more important for sizing than the tensile strength. Consequently, a reasonably thick laminate (1/16") was chosen because it was already being used for the fins (thus reducing material costs).

The fin geometry was tested to far greater loads than the hook would experience, so even though we made no estimate of actual strength we knew the 1/16" would be more than sufficient. Following the selection of materials, we created a revised diagram of the magnetic actuator (shown in Figure 4.24).

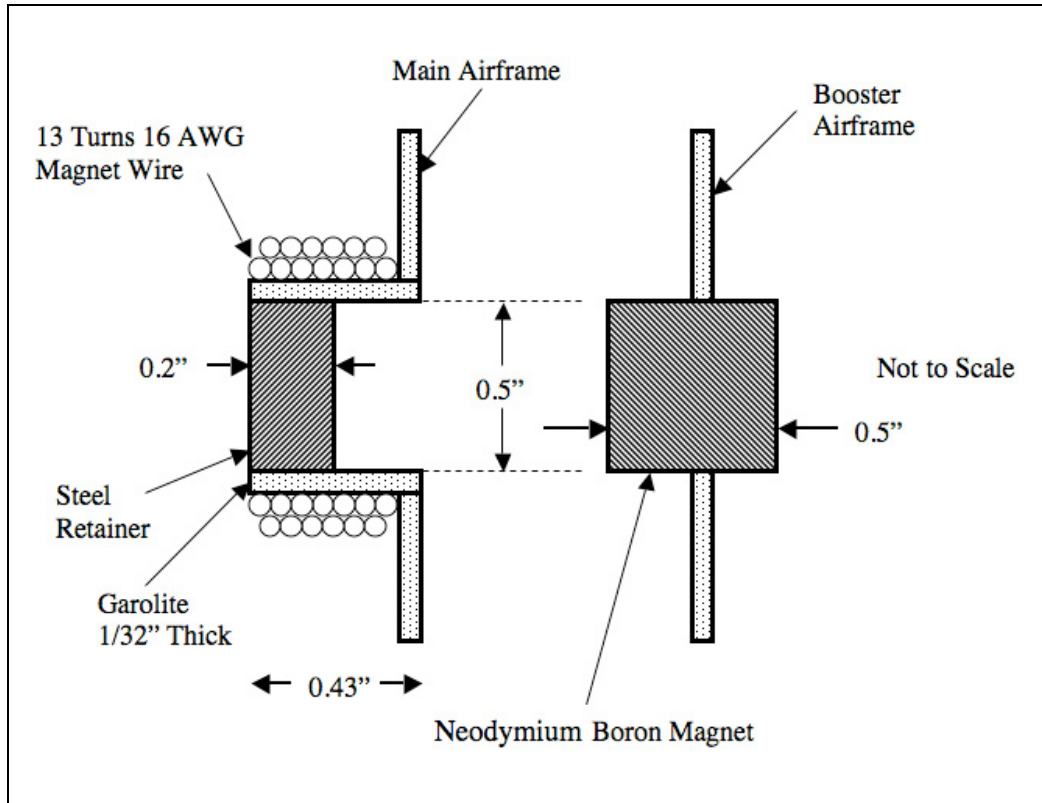


Figure 4.24: Electromagnetic Actuator

It should be noted that while the field produced by the electromagnet needed to be significant in order to overcome the permanent magnet's attraction, the duration of this field was minimal. Consequently, the electromagnetic coil was not designed for efficient heat dissipation. It was thus lighter and cheaper than possible in a situation where thermal effects would have been a factor. The short pulse also had the effect of minimizing power storage requirements to the point where small lightweight capacitors could discharge directly through the coils. Initially, Aerogel type capacitors were selected because of their superior power density relative to all other capacitors available. These capacitors (shown in Figure 4.25) would then be charged prior to launch through a 1 Watt, 150 Ohm resistor. We determined the resistance

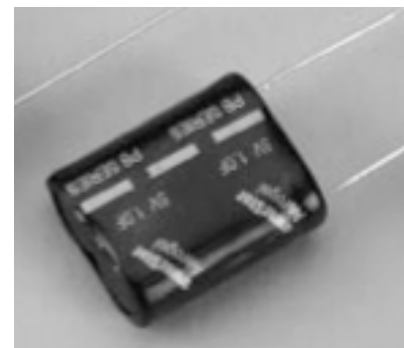


Figure 4.25: 0.33F Aerogel Capacitor [16]

and power dissipation requirements of this resistor based on Ohms Law with (P) as Power, (I) as current, and (R) as Resistance:

$$P = I^2 R \quad (4-25)$$

Aside from the power storage and charging requirements, a few other support components were needed to power and trigger the coils. Triacs were selected as the power-switching device in the power storage circuit because of their low resistance solid-state nature. Triacs function very similar to transistors but they are designed for more rugged applications. Once triggered, a Triac remains open until current no longer flows through. These Triacs would thus receive a trigger pulse from the main flight computer and allow current to flow from the capacitor through all three coils in parallel (in order to reduce the extra resistance from a series configuration). A diagram of this circuit is shown in Figure 4.26. In this diagram, R1 represents the charging resistance (150 Ohms), C1 represents the capacitor capacitance (0.33 Farads), and L1 – L3 represent the coil inductance shown in Table 4.5 above (0.003969 Mili-Henery's).

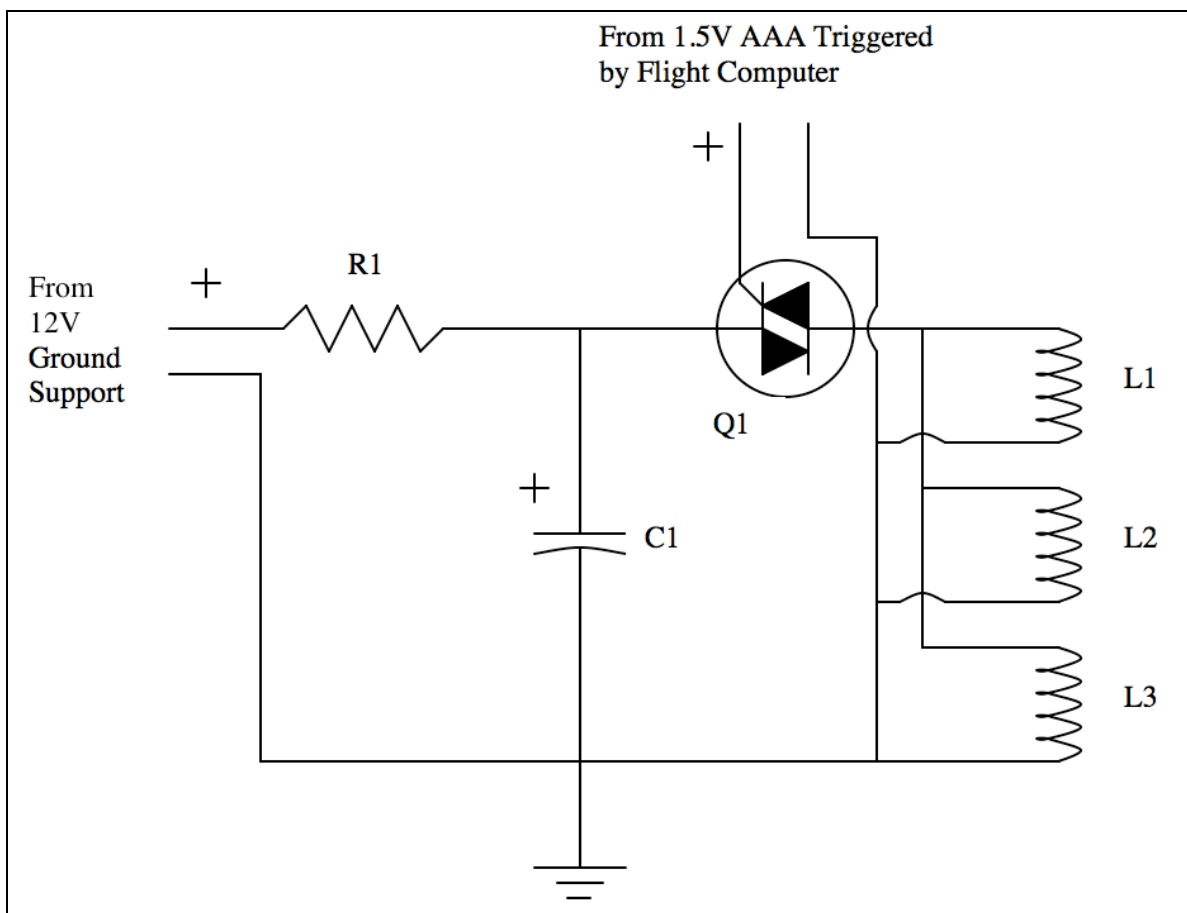


Figure 4.26: Initial Power Circuit Design

4.2.4 Prototype Fabrication

As discussed above, we designed the staging system design to the same specifications required in the final vehicle. Consequently, a prototype was fabricated identical in size and operation to the final vehicle system. Creating a prototype before the final construction allowed us to more easily determine any shortcomings in design or fabrication. Two exceptions to this design conformity, however, were the use of a single booster instead of three, and the use of cheaper paper laminate airframes instead of phenolic. We made these exceptions in order to save cost and construction time in an area that wouldn't have provided much more information. A triple coil test was considered useful, however it was possible to test the coils outside the assembly and still ascertain system performance. Thus we felt we didn't lose much by taking these shortcuts with the prototype.

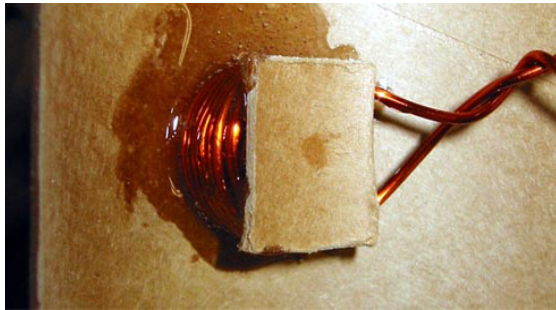


Figure 4.27: Coil Assembly mounted in the Prototype

Construction began with the sizing and cutting of parts. We cut the hole in the airframe for the actuator, the hole in the booster for the magnet, the slot in the airframe for the hook, and the steel retainer to size using standard machining tools. We also cut the Garolite and fiberglass, however they were cut larger than necessary in order to assist in aligning the actuator and trimming the hook at a later time. Following this, we assembled the components together. We epoxied the steel retainer into the garolite tube at one end while attached to the magnet. This would ensure proper alignment of the magnet/steel interface (a critical aspect of achieving the designed force). We then wrapped magnet wire for the coil around the garolite end with the steel and epoxied it in place before we mounted the whole assembly into the prototype airframe. This assembly can be seen in Figure 4.27 attached to a small cutout of paper laminate affixed over the steel end of the garolite. We installed this in order to assist with coil winding.

Construction began with the sizing and cutting of parts. We cut the hole in the airframe for the actuator, the hole in the booster for the magnet, the slot in the airframe for the hook, and the steel retainer to size using standard machining tools. We also cut the Garolite and fiberglass, however they were cut larger than necessary in order to assist in aligning the actuator and trimming the hook at a later time. Following this, we assembled the components together. We epoxied the steel retainer into the

Once the magnetic actuator was in place and aligned perpendicular to the airframe (by means of the remaining garolite protruding through the hole), we trimmed the garolite flush with the airframe surface. In the mean time, we epoxied the G10 fiberglass for the aft hook to the lower portion of the booster in a straight line with the magnet hole. Throughout this process, the magnet remained attached to the steel and was now protruding outward from the airframe. Using this as a guide, we trimmed the hook until the booster hole could be fitted around the magnet. An example of the trimmed hook is shown in Figure 4.28.



Figure 4.28: Aft Hook attached to the prototype booster

From this point, we epoxied the magnet to the booster from the inside in order to ensuring proper alignment. Once this was completed, the prototype was finished and ready for testing. While many tests were conducted, the most basic ensured proper coil orientation relative to the magnet. The completed prototype is shown in Figure 4.29.



Figure 4.29: Completed Prototype

4.2.5 Interim Design Modifications

In the process of testing the prototype staging actuator, a number of critical design deficiencies came to light. Because of these deficiencies, we redesigned several areas of the mechanism and circuit. One such area was the drive voltage. While the coil and circuit were initially designed around a drive voltage of 12V, we found this to be inadequate in practice. Such a low voltage created a circuit very sensitive to extra series resistance. Even a small amount of additional resistance due to the wire lengths and switching mechanisms (on the order of 0.01 Ohms) could reduce the magnetic field below that needed to activate the mechanism. Consequently, we redesigned the circuit and coil around 48V. This led to a coil with two layers of 24 AWG wire (17 turns and 16 turns respectively) shown in Figure 4.30. While the voltage required by this redesign would be more difficult to obtain at the launch site for charging (a special battery bank was required), it allowed some margin for extra resistance in the circuit and coil. The revised coil and circuit properties are shown in Table 4.6.

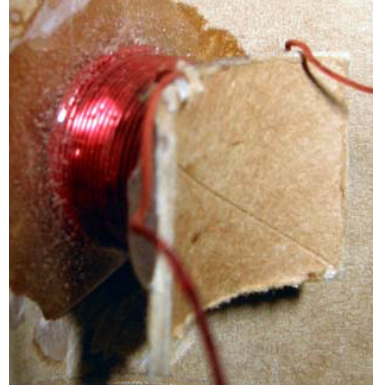


Figure 4.30: Redesigned Coil

Coil and Circuit Properties		
Inner Diameter	0.5625	Inches
Number of Layers	2	-
Number of Turns per Layer	16.5	-
Wire Gauge	24	AWG
Total Extra Series Resistance	0.01	Ohms
Applied Voltage	48	Volts
Applied Capacitance	0.01	Farads
Relative Permeability of Core	100	
Outer Coil Diameter	.66	Inches
Coil Length	.39	Inches
Total Wire Length	60.77	Inches
Total Resistance	0.140	Ohms
Peak Current Flow	343	Amps
Peak Power Dissipation	16458	Watts
Coil Inductance	0.011705	Mili-Henerys
2D Corrected Field	0.773	Tesla
Capacitive Time Constant	0.0014	Seconds
Inductive Time Constant	8.36E-05	Seconds
Time Constant Ratio	16.7	-

Table 4.6: Revised Coil and Circuit Properties

In addition to the voltage, the selected capacitors proved inadequate. As mentioned previously, we selected Aerogel capacitors initially because of their high energy density and low weight. Unfortunately, the Aerogel capacitors, while indeed light, contained too much internal resistance to provide the necessary current to drive the coil and separate the magnet. In fact, their discharge was so slow it created no detectible magnetic field through the coil. Their resistance was also too much for even the revised circuit voltage, so new higher voltage (50 volt) low resistance electrolytic capacitors were selected. These capacitors (shown in Figure 4.31) provided all the voltage, capacitance, and conductance necessary for good coil operation and were thus integrated into the design revision.

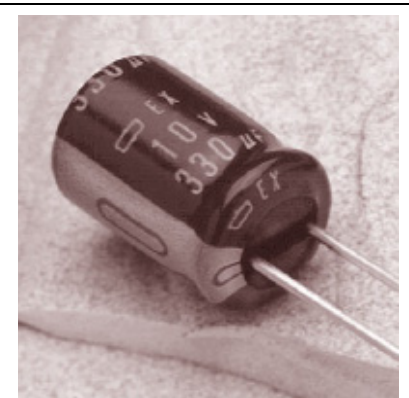


Figure 4.31: Electrolytic Capacitor [17]

While the drive voltage and capacitor change allowed successful coil operation, integration of three coils (for all three boosters) proved more challenging than expected. While the initial circuit design shown previously in Figure 4.26 would have worked for all three coils in theory, in practice, slight

manufacturing differences produced coils with slightly different impedance properties. Because of this, it appeared that one actuator would reach sufficient magnetic field for activation slightly before the others when discharging. This very slight timing difference would cause the impedance of the first discharged coil to drop. As a result, the voltage across the other coils would drop as well and would be insufficient to finish activating their mechanisms. In order to ensure the coils were supplied with the same amount of energy, each coil had to be driven by its own capacitive discharge circuit. In other words, each coil required its own capacitor switching mechanism. The circuit still required provisions for a single charging power source and a single activation power source however, so the modified circuit contained several additional resistors to assist with this function while maintaining relative isolation between each discharge path. These extra resistors were also needed because the flight computer signal voltage was revised to 12V. Without resistors, this would have created far more current than the Triacs were designed to handle. The revised circuit is shown in Figure 4.32. In this diagram, R1 through R3 were 1W, 2200 Ohm resistors for charging purposes. Resistors R4 through R9 were 1W, 62 Ohm resistors. These resistors shielded the three separate circuits from each other but still allowed sufficient current (~100mA) from the 12V flight computer signal to trigger the Triacs.

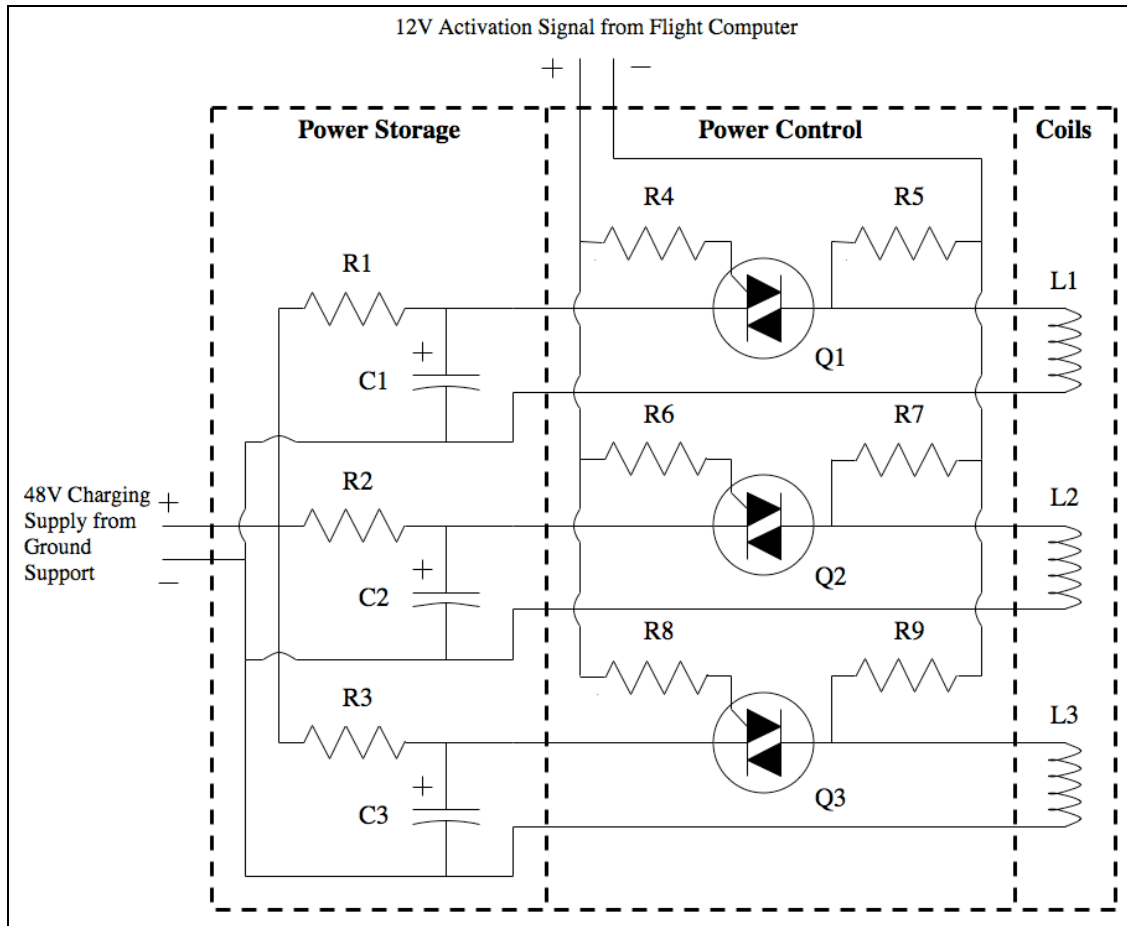


Figure 4.32: Redesigned Capacitive Discharge Circuit

In addition to the electrical changes, testing revealed several mechanical deficiencies as well. One such deficiency was the aft hook design. As mentioned previously, this hook was designed to support forward thrust loads as well as lateral loads while simultaneously allowing seamless separation of the booster when the forward support (the magnetic actuator) disengaged. The hook actually functioned as intended on the prototype, however the amount of rotational travel allowed during separation was



Figure 4.33: Redesigned Aft Booster Hook

somewhat limited. If the rotational travel was exceeded before the hook could fall away from its slot, testing revealed that it could jam. While this was considered an unlikely event under actual flight conditions (due to the extra wind resistance helping the booster to fall away), it was considered enough of a risk that a more reliable hook mechanism was designed. This new hook (shown in Figure 4.33) contained a G10 fiberglass laminate 0.125" thick

protruding away from the booster surface into the main airframe. This laminate was similar to the initial laminate but was twice as thick in order to provide better bonding area, increased load transfer area, and improved the stiffness. This laminate transmitted the forward thrust loads of the booster through its leading edge into the outer airframe structure at the top of the airframe slot just as the previous hook was designed to do. This laminate also supported a small steel cylinder long enough to grab the airframe structure around the slot and hold the booster against the airframe until separation. All together, this new hook provided similar functionality to the previous design but allowed the boosters to rotate almost 90° in the slot prior to departure from the vehicle in the unlikely event that much rotation were to occur in flight.

A second more qualitative mechanical deficiency found during testing was the structural integrity of all four load bearing areas of the staging mechanism: The magnet, the coil and steel support, the aft booster hook, and the aft airframe slot. While none of these areas were tested to destruction, weaknesses were apparent in the form of significant part flexing. Some of this was likely due to the thin laminated paper airframe material used in the prototype and would thus be significantly improved by the thicker and stiffer phenolic airframe material used in the final vehicle. Nevertheless, it was concluded that adding a single ply of fiberglass fabric reinforcement to the part and airframe interface would significantly improve the strength and stiffness of those critical areas. Adding fiberglass reinforcement to the airframe surrounding the staging components would also be prudent because it would greatly reduce any possible flexing that would occur in those high-stress regions. Unfortunately, the aft hook would pose a challenge to reinforce with fiberglass. The redesigned hook would have greater strength and stiffness in general, however, so adding fiberglass to the other three component interfaces was considered adequate. Single plies of fiberglass fabric are often used to reinforce critical areas in rocket vehicles this size, so this decision was in line with previous design experience.

4.2.6 Final Design Fabrication

Once we were satisfied the design modifications and testing had minimized the effects of any unwanted defects, we proceeded to fabricate the components necessary for the final rocket vehicle. Because our prototype was designed at the exact scale required for the final vehicle, the fabrication proceeded in exactly the same manner. We initially cut all components and mounting holes to the correct size with the exception of the Garolite and G10 Fiberglass (since these would be trimmed later). These manufactured components are shown in Figure 4.34 and Figure 4.35.



Figure 4.34: Metal Retainers and Oversized Garolite Sheaths



Figure 4.35: Booster Airframes cut for Magnets



Figure 4.36: Final Wound Coil ready for Integration

While the component placement on the prototype was good, we paid extra attention to dimensional accuracy and component alignment this time. This extra desire for precision led us to cut the steel on a lathe instead of a band saw as used previously. While a more lengthy process, the lathe ensured a better surface finish and a more accurate cut angle. Once the steel was cut, it was epoxied into the oversized garolite sheaths while attached to the magnet (as was done in the prototype) to ensure alignment.

Following assembly of the steel retainer, the coils were wound as per the revised design specifications. Two layers of 24 AWG wire (17 turns and 16 turns respectively) were wrapped around each Garolite sleeve on the end nearest the steel and coated with a thin layer of epoxy. Once the epoxy hardened, we checked to make sure the polarity of the magnets in the coil assemblies were identical. When we were certain this was the case, each coil assembly was set aside for later integration into the main airframe. One of these completed coil assemblies is shown in Figure 4.36.

Prior to installing the coils in the main airframe, we attached the G10 laminate to the boosters and drilled them for installation of the small short steel rods. We then mounted the steel rods and sanded the epoxy that had cured. This ensured smooth movement within the aft airframe slot. One such hook fitted within the aft airframe slot is shown in Figure 4.37.



The most challenging aspect of the final system construction was the required power circuitry. The initial circuit design called for relatively simple wiring and few required components. It was thus thought early on that this circuitry would easily fit within a coupler mounted just forward of the main motor mount (shown in Figure 4.38). This coupler was designed to attach the lower thrusting portion of the vehicle to the drogue chute bay and was thus not being used for anything else. Unfortunately, the revised circuit design required significantly more volume than the original circuit. The coupler still represented the best location for the power circuit, but several layout iterations were necessary to accommodate everything.

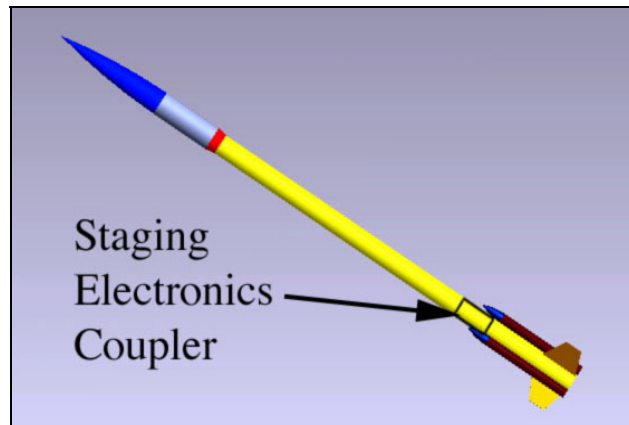


Figure 4.38: Location of the Staging Electronics

In order to simplify the integration of electrical components into this coupler (or “staging electronics bay”), we decided to divide the power storage and control areas into two separate locations. The power control circuitry would be mounted on the upper bulkhead, and the capacitors would be mounted on the lower bulkhead installed within the coupler. This configuration would allow easy access to the bay if necessary because the components wouldn’t be buried under one other. In order for everything to fit, however, components were laid out in many different orientations on each bulkhead until the most space efficient combination was found. The final component arrangement on these bulkheads is shown in Figure 4.39.

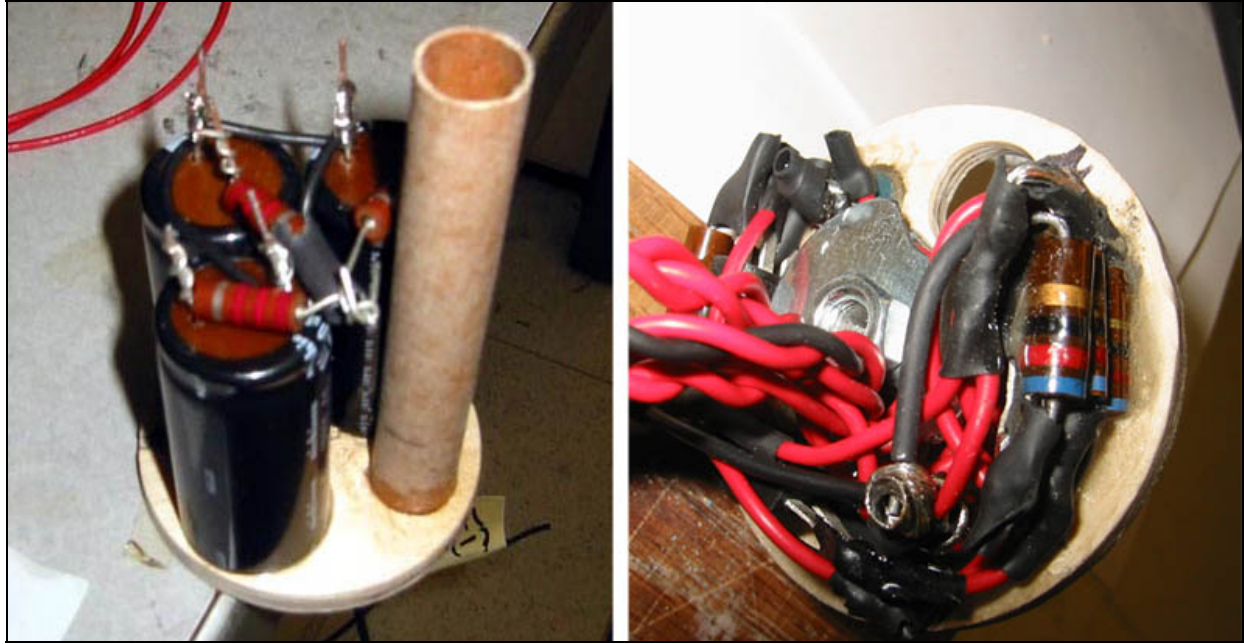


Figure 4.39: Lower Electronics Bulkhead (left) and Upper Electronics Bulkhead (right)

In addition to the basic electrical components, each bulkhead also required space for many components not associated with the staging electronics. One such component was a small pipe passing between the two bulkheads (also shown in Figure 4.39). This pipe was integrated into the staging electronics bay on the off chance the ejection charge gasses from the core motor were needed for drogue parachute deployment. If so, this pipe would act as a gas pass-through. Besides the ejection charge pass-through, the ignition wiring for the core motor

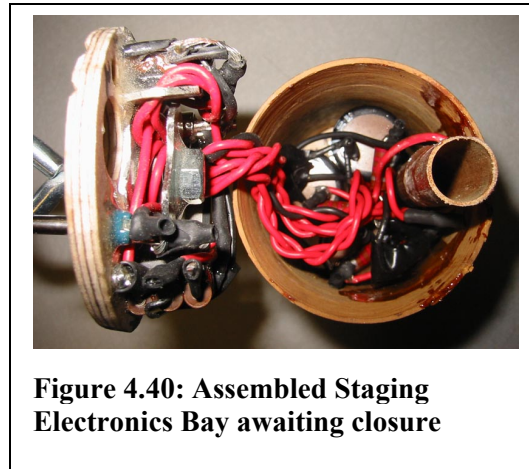


Figure 4.40: Assembled Staging Electronics Bay awaiting closure

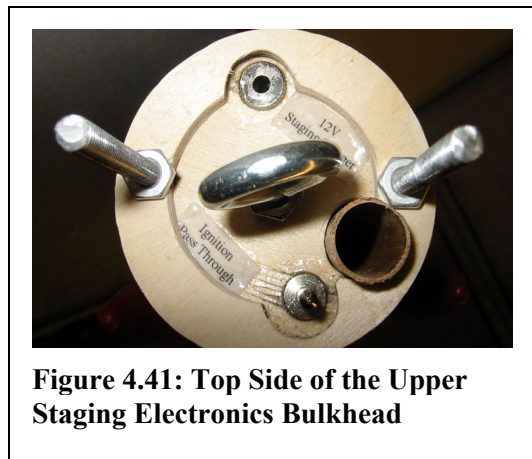


Figure 4.41: Top Side of the Upper Staging Electronics Bulkhead

also needed to pass between the upper and lower bulkheads on its way to the aft end of the vehicle. In light of this, we installed a plug on the upper bulkhead in much the same way as the jack for the staging trigger. We then routed the wiring for the ignition system along with the magnetic actuator wiring out the lower bulkhead where it could connect to wiring running farther down the rocket to the motor.

A final extra system we installed on the upper bulkhead was the structural support for the drogue parachute and nylon shock cord. This ring support along with ejection charge pass-through pipe, the ignition wiring pass-through plug, and the staging trigger jack can be seen in Figure 4.41. The staging electronics bay is shown in Figure 4.40 awaiting closure. Figure 4.42 shows the complete bay from the outside with a jack for charging the capacitors installed on the side.

4.3.7 System Integration

Once the various staging components were assembled as much as possible as a subsystem, we integrated them into the rest of the rocket. Just as was the case with the individual assembly, this process followed the prototype development closely. We began the final integration by inserting the individual coils through the holes cut in the main airframe. These coil assemblies were still attached to the magnets and the extra garolite, so the protruding material allowed easy alignment with the airframe surface prior to applying epoxy (shown in Figure 4.43). Once the initial epoxy hardened, we applied single layers of fiberglass cloth to the area surrounding each coil in order to reinforce these critical areas. We also applied one layer of fiberglass cloth around the inside of the airframe near each aft slot. The results of the internal reinforcement around the coils can be seen in Figure 4.44.



Figure 4.42: Complete Staging Electronics Bay



Figure 4.43: Extra Garolite for Alignment

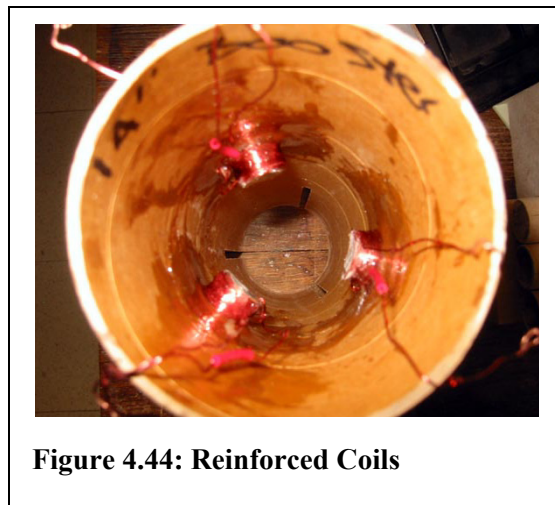


Figure 4.44: Reinforced Coils



Figure 4.45: Boosters Installed and Aligned

Once the coils were reinforced, we installed the motor mount assembly and applied epoxy to the areas surrounding the interface between the coils and the motor mount. In addition, we trimmed the excess garolite flush with the outer airframe. With the magnets now exposed, we were able to align the boosters and epoxy the magnets into each booster. In the process, we also reinforced each magnet interface and the surrounding booster airframe with one ply of fiberglass cloth. Following minor trimming and sanding of the aft slots and aft booster hooks, the airframe and booster integration was complete as shown in Figure 4.45.

The final step to integrating the entire staging system with the main airframe was the attachment of the staging electronics bay. While the staging electronics bay would fit into each section of the airframe and thus provide strength and load transfer like any other coupler, this was not a strong enough attachment method. There would be

no direct load transfer from the drogue shock cord (discussed in the recovery section) to the motor mount except through a friction fit. As a result, threaded rod was installed in the forward motor-mount centering ring (along with holes for the coil wires to pass through). This threaded rod can be seen in Figure 4.46 extending above the lower airframe interface. The threaded rod would then extend through the lower and upper bulkheads of the coupler and act as guide rails. Nuts installed on the threaded rod above the upper bulkhead could then lock the entire electronics assembly to the motor mount and lower airframe and provide a vastly improved load path. Before this could be assembled, however, the wires from the staging electronics bay were soldered to the coil wires and the ignition pass-through wires to the lower airframe ignition wires. We chose solder as the connection method because the



Figure 4.46: Threaded Rod Installed at the Airframe Interface

staging electronics bay, while not completely permanent, was also not likely to be removed. Soldering also provided a more reliable connection than many less permanent options.



Figure 4.47: Completed Staging Assembly

Once the solder cooled, we applied heat shrink tubing to the solder connections for insulation purposes. This step completed all the wiring necessary for staging integration. At this point, we slid the staging electronics bay together with the lower airframe and applied the nuts to the threaded rod in order to complete the assembly. This completed assembly is shown in Figure 4.47 (minus paint and finishing touches).

4.3 Results and Analysis

Throughout the course of this project, testing was a key element in affirming our approach, verifying our calculations, and optimizing our design. This testing and analysis was broken down into prototype testing (and testing of design revisions), integrated systems testing, and flight-testing. The prototype and integrated systems testing focused primarily on the performance of the electrical and mechanical circuit assemblies. In addition, we continually evaluated the more qualitative aspects of the different assemblies and compared these observations to our design objectives of reliability, consistency, and testing ease. This led to remarkable success and resulted in a final system that met our objectives well.

4.3.1 Prototype Testing and Evaluation

During the initial design phase, we knew we would need to correctly determine the force coefficient in the magnetic force equation (Equation 4-2) for the type of geometry we considered. With several small cylindrical Neodymium-Boron magnets already in hand, we conducted these tests by mechanically attaching a fish scale to each magnet and pulling it away from an attached metal cylinder with similar dimensions to the magnet. This test setup is shown in Figure 4.48.



Figure 4.48: Magnet Tensile Testing

While this was fairly simple test, the results were fairly consistent. By observing the force measured on the scale at the moment of separation, we were able to correlate the actual force with the predicted force (against a theoretical flat plate) and thus determine the force coefficient. Three trials were performed for each set of magnet and retainer geometries. The average force coefficient from all the trails was found to be 0.46. This value was subsequently used in calculating the necessary magnet size for the final design. The results of these tests and the calculated force coefficients are shown in Table 4.7.

Permanent Magnet Tensile Test Results				
Permanent Magnet Type	Magnet Geometry (in)	Predicted Flat-Plate Force (N)	Measured Force (N)	Calculated Force Coefficient
Nd-Fe-B	0.125 dia x 0.0625	2.6	1.3	0.5
Nd-Fe-B	0.125 dia x 0.0625	2.6	1.3	0.5
Nd-Fe-B	0.125 dia x 0.0625	2.6	1.1	0.42
Nd-Fe-B	0.25 dia x 0.25	21	10.2	0.49
Nd-Fe-B	0.25 dia x 0.25	21	9.8	0.47
Nd-Fe-B	0.25 dia x 0.25	21	9.3	0.44
Nd-Fe-B	0.375 dia x 0.25	31	14.2	0.46
Nd-Fe-B	0.375 dia x 0.25	31	13.8	0.45
Nd-Fe-B	0.375 dia x 0.25	31	13.8	0.45

Table 4.7: Permanent Magnet Tensile Test Results

Once the actuator design was finalized for the prototype and the parts obtained, we conducted identical tests on the final permanent magnets and metal retainer geometry. This was done in order to determine the tensile force our design would be capable of enduring as well as to verify that our force coefficient results obtained with the smaller magnets were accurate. As can be seen in Table 4.8, the results from these tests indicated that the magnets did not perform as well as calculated. Nevertheless, a 4 to 5 Newton loss did not represent a serious problem, so these magnets were still used in the design and construction of the prototype and final staging system.

Permanent Magnet Tensile Test Results					
Permanent Magnet Type	Magnet Geometry (in)	Predicted Flat-Plate Force (N)	Calculated Force (N)	Measured Force (N)	Error (%)
Nd-Fe-B	0.5 dia x 0.5	82	37.7	32.9	-14.59
Nd-Fe-B	0.5 dia x 0.5	82	37.7	31.6	-19.3
Nd-Fe-B	0.5 dia x 0.5	82	37.7	33.4	-12.87

Table 4.8: Permanent Magnet Tensile Test Results for the Designed Geometry

Following the magnet tensile testing, we constructed the prototype to the design specifications but did not attach the booster to the permanent magnet. This would be completed later. We began evaluating the prototype design by testing the coil separation system alone in the simulated airframe. These tests were conducted initially by charging the capacitor to the necessary voltage and then touching the capacitor across the coil leads. We hoped this would cause the permanent magnet to separate as per the design, or if not for some reason, at least visibly move. We started the tests with a low voltage, however

when nothing happened, so we increased the voltage to the 12V design point. Unfortunately, the magnetic actuator remained locked in its position, and nothing happened. We displaced the magnet from the metal retainer (in order to reduce the static force) and tried the same test. Again, nothing happened. The permanent magnet failed to show any effect from the capacitor discharging through the coil.

Upon further investigation with a digital voltmeter placed across the coil leads, we found that the voltage decay could actually be observed. This was not expected because the discharge time through such a low resistance coil should have been far too small to measure without much more sophisticated equipment. Since a capacitor should discharge through a resistor in a time period proportional to the resistance, we knew there was far too much resistance somewhere in the circuit. Measuring the resistance across the coil, however, proved that it was functioning properly: the resistance was too small to measure as expected. This left only the capacitor. In order to confirm our suspicions that the capacitor had too much internal resistance, we charged the capacitor and shorted it out while observing the voltage drop with a voltmeter. We observed the same long period voltage decay as when it was hooked to the coil. Thus we knew all the resistance was originating from within the capacitor.

Given the problems with our selected capacitor, we decided to use electrolytic capacitors on hand in order to see if we could get any response from the coil. Electrolytic capacitors do not have the energy density of Aerogel capacitors, but they are capable of discharging much quicker. While the capacitance and voltage of the capacitors on hand did not match the required specifications of the circuit, we hoped the much faster discharge would be capable of at least creating a noticeable magnetic response in the permanent magnet. We thus hooked two 50V, 10000 μ F capacitors in parallel to the coil (double the capacitance) and charged them to 24V (the limit of the power supply at the time). When discharged, the permanent magnet did not separate as before. This time, however, when the magnet was moved a few millimeters away to reduce the opposing force and tested again, a large enough magnetic force was generated to move the magnet a few inches. From this we knew the design would work, but we would need to use electrolytic capacitors and redesign the coil to optimize for this change.

Upon further testing of the same setup, we noticed that the length of the alligator test leads greatly affected coil performance. With short leads, the permanent magnet would move a very noticeable amount away from the coil (when displaced a few millimeters to begin with). When the test leads were long, however, the magnet hardly moved at all. These results made us realize that a very low voltage, high current coil such as this would be greatly affected by any additional series resistance. Thus the resistance of the test leads, while too small to measure with a basic ohmmeter, was enough to reduce the magnetic field of the coil. Consequently, we knew the coil would need to function at a higher voltage. Higher voltages would be capable of driving higher currents and thus magnetic fields, but a higher voltage would also allow the use of higher gauge wire. The increase number of turns the electromagnet could house

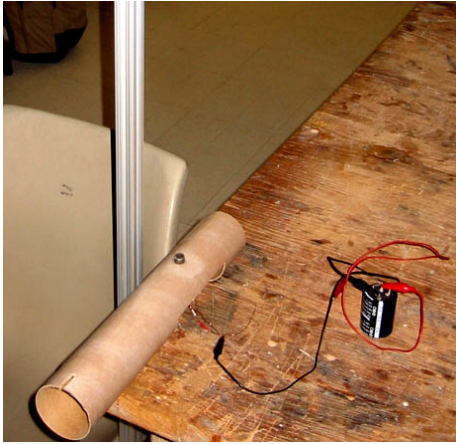


Figure 4.49: Magnet Discharge and Height Measurement Test Setup

within a given volume with this smaller wire would increase the magnetic field farther. Higher voltages would also be less affected by extra series resistance.

Once the coil was redesigned and rebuilt, testing commenced with the optimal capacitor and coil combination. We observed improved results immediately. Even when charged to the new design voltage of 48 volts, touching the leads of the capacitor across the coil would immediately eject the magnet from contact with the steel retainer. In order to better quantify the energy released during magnet discharge, we setup the prototype airframe and coil to discharge the permanent magnet itself straight

into the air. This setup is shown in Figure 4.49. From this we could measure the height the magnet would reach at different discharge voltages and calculate the energy. The energy imparted on the magnet, if completely converted to potential energy, would be (Equation 4-18):

$$E = mgh \quad (4-18)$$

Where E is the energy, m is the mass of the magnet (14 grams), g is the acceleration due to gravity (9.81 meters per second squared), and h represents the maximum height reached by the magnet. We tested at two voltages (~37V and ~50V) and conducted five trials in order to determine the test consistency. These results are shown in Table 4.9 with the Test averages and standard deviations shown in Table 4.10.

Discharge Energy Test			
Capacitor Voltage (V)	Capacitor Energy (J)	Magnet Launch Height (cm)	Magnet Energy (J)
38	7.22	58	0.0797
37	6.845	57	0.0783
36	6.48	56	0.0769
37	6.845	55	0.0755
37	6.845	56	0.0769
50	12.5	119	0.1634
50	12.5	123	0.1689
50	12.5	124	0.1703
50	12.5	122	0.1676
50	12.5	118	0.1621

Table 4.9: Discharge Energy Test

Test Averages		
	38V	50V
Height Average (cm)	56.4	121.2
Standard Deviation (cm)	1.14	2.58

Table 4.10: Discharge Test Averages

The discharge energy test results were somewhat unimportant from a design purposes, but it should be noted that the energy imparted on the magnet (a function of height) and the energy stored in the capacitor (a function of voltage squared) tended to follow one another. Thus doubling the energy in the capacitor more or less doubled the energy imparted to the magnet. It should also be noted from these results that the amount of energy actually transferred to the magnet from the capacitor was very low. A great deal of this energy was likely lost as resistance in the coil, as hysteresis in the steel retainer, or in overcoming the permanent field. While it was not clear if any one of these mechanisms dominated the energy loss, better results could likely be obtained in the future by minimizing these areas of loss. For this test, however, the separation mechanism performed as designed, and the consistency of the test results were a welcome observation.

Following the discharge energy tests, we further tested the actuator's response to differing voltages and capacitance levels. We performed these tests in much the same way as all the tests up until this point: by charging up a capacitor to the desired voltage (as read on the voltmeter) and then touching the capacitor across the coil leads. Different capacitance values were obtained by utilizing several different electrolytic capacitors on hand. This time, instead of measuring the height of magnet ejection,

we made more qualitative assessments of the discharge energy. The results of this test are shown in Table 4.11.

Parameter Testing				
Voltage (Volts)	Capacitance (Farads)	Predicted Field (Teslas)	Predicted Time Constant Ratio	Results
24	0.01	0.38	16.7	No Separation
36	0.0047	0.58	7.9	No Separation
36	0.01	0.58	16.7	Low Energy Separation
36	0.02	0.58	33.5	Low Energy Separation
48	0.0047	0.77	7.9	Low Energy Separation
48	0.01	0.77	16.7	High Energy Separation
48	0.02	0.77	33.5	High Energy Separation
48	0.027	0.77	45.2	High Energy Separation
60	0.0135	0.97	22.6	Very High Energy Separation
80	0.0135	1.29	22.6	Very High Energy Separation

Table 4.11: Testing Responses to Voltage and Capacitance Parameters

Changing the voltage and capacitance values altered coil performance as expected. Reducing the voltage lowered the apparent discharge energy (assessed by the apparent magnet launch height away from the coil) until the coil would no longer separate. Raising the voltage would increase the discharge energy until the test was no longer possible under a low ceiling. By the same token, lowering or increasing capacitance would similarly affect discharge energy, however the results were not as straightforward. Above a capacitance of 10000 μ F, no change in launch energy was apparent. Below 10000 μ F, however, a reduced energy discharge and even a total lack of separation were observed. From this we concluded that our selected capacitance value was exactly where we had hoped. Any more capacitance would serve little function, but reduced capacitance and the associated increased resonance between the capacitor and inductor (by virtue of their opposite electrical responses) did affect operation.

It should be noted from the results obtained in Table 4.11 that the coil failed to separate when less than 36 volts were available. In fact, in a further test this was found to be just slightly less than 36 volts (approximately 34 or 35 volts). In the design calculations, however, a 1.5 factor of safety was used to arrive at the design voltage of 48 volts. If this safety factor were removed, the minimum calculated voltage for separation would have been 32 volts. Thus the calculated separation voltage and observed separation voltage differed by only 9%. Observing such a close correlation between calculation and observation verified our design methods and improved our confidence in the design.

Before the permanent magnet was attached to the booster in order to observe actual booster separation performance, one final test was performed with the coil actuator alone. This test simply

compared the observed launch height of the magnet with and without the Triac in the circuit. As hoped, there was no discernable difference between each situation. From this, we concluded that the Triac was indeed a low resistance device and would thus work well as the triggering mechanism in the final design.

From this point, we attached the booster to the permanent magnet as per the construction method previously discussed. We set the simulated airframe on end with space left under the booster for it to fall when separated. We then hooked the coil to the capacitor and triac circuit as just tested and discharged the coil at various voltages. Just as we observed when testing the magnetic actuator alone, raising and lowering the discharge voltage had a visual impact on separation energy. In fact, in many cases even at the design voltage, the booster would rotate away from the airframe with so much energy that the lower hook would jam before gravity had a chance to pull it out of the lower airframe slot. This was both gratifying as well as alarming. On one hand, the booster rotated away from the airframe just as envisioned. Most of the time, the booster also dropped away as envisioned without jamming. Unfortunately, any possibility of a jam was unacceptable, so we redesigned the aft hook to allow greater rotation prior to the hook's departure from the airframe.

Aside from the potential jam, the static mounting scheme functioned as intended. Both the aft hook and the magnetic actuator kept the booster attached to the main airframe and helped carry lateral and axial loads imparted on the two by hand. Some minor part flexing was observed in all of these cases, however, so we considered reinforcement of the mounting locations a prudent step when constructing the final system. In general, however, the system functioned as intended when the coil, capacitor, and aft hook design revisions were implemented. More importantly, the staging mechanism prototype proved consistent, reliable, predictable, and easy to test. In fact, we tested the prototype on many occasions just to imagine what the final rocket would look like in flight. From past experience, there are few mechanical systems employed on commercial rockets this scale that can be tested in such a fashion.

4.3.2 Integrated System Testing and Evaluation

Following the single actuator testing in the prototype, we began testing all three final actuators together with the complete circuit design. The first test simply verified the operation and polarity of each of the three actuators built for the final vehicle. This test was accomplished in much the same way as the basic prototype testing: Charging a capacitor up to the specified voltage and then touching the leads of the actuator to the capacitor with the specified polarity. If the magnet were to fly away from the metal retainer and wire coil, we would thus know the polarity was correct and the actuator was functioning as intended. While this test could have been conducted at any time during the final assembly, we felt it would be best to test this prior to installing any components in the vehicle. As expected, this test successfully indicated that all three actuators were functioning well and with the intended polarity.

Following the individual testing of each final actuator, we hooked all three actuators in parallel to the specified set of capacitors through a Triac using alligator test wires. We then triggered this Triac using a bench power supply set to a low voltage (1.5V). This test setup thus mimicked the actual circuit configuration the actuators would be connected to when assembled into the vehicle. By charging the capacitors to the specified 48V, we were thus able to observe all three actuators and qualitatively determine their consistency and discharge energy (by observing how high the magnets would fly when discharged). Unfortunately, when this test was initiated, the actuators performed in an inconsistent manner. Several discharge tests confirmed these results. Only two of the actuators would even eject the magnet from the metal retainer, and they did, they would do so with different ejection energies. Occasionally all three actuators would separate when discharged, but the ejection energy appeared barely adequate to perform even this simple task. While the performance of each actuator differed from discharge to discharge, the same general system behavior was observed on every test. Altering the voltage and capacitance of the circuit did not change the behavior either.

Given the consistent and high-energy discharge performance observed when the actuators were tested individually, we considered these results inadequate. Since the individual behavior appeared to differ randomly during these integrated tests, however, we concluded that a problem specific to one circuit element was unlikely. The most likely explanation was interference between the actuators themselves when fired together. We further theorized that changes in coil inductance due to slight timing differences could potentially cause this interference. While these timing differences would be difficult to observe without more sophisticated equipment, a drop in one coil's inductance following slightly premature separation could create a current drain thus limiting the current available to fire the other actuators. Regardless of the exact failure mechanism, however, we concluded the best course of action would be to contain each actuator to its own capacitive discharge circuit. This would necessitate a circuit

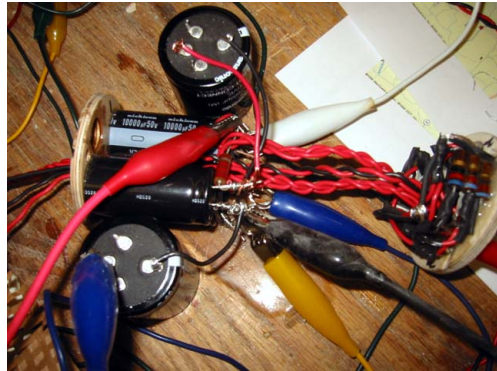


Figure 4.50: Sub-Assemblies Link Together for Integrated Staging Systems Test

redesign prior to final assembly, but it would prevent potential interference between coils and thus provide more reliable and consistent operation.

Following the circuit redesign, all components were assembled into the two main vehicle areas as previously discussed (actuators in the booster section and power circuit in the staging electronics bay). During this assembly, resistance measurements of the integrated circuit were taken intermittently to make sure all circuit elements were connected as intended. This testing revealed only one connection failure, but re-soldering the connection quickly rectified this. When assembly of the two individual areas was complete enough to allow performance evaluation, the two major sub assemblies were temporarily linked together using alligator wires and tested in much the same way the initial integrated testing was conducted. This test setup and the two major assemblies are shown in Figure 4.50.

Unfortunately, the initial results from the integrated subassembly test were less than stellar. In fact, we observed that the separation mechanism behaved exactly as it had done when testing the actuators together using the older circuit design. The separation was erratic, low energy, and inconsistent. Further testing with modified circuit properties (voltage and capacitance) did seem to have an effect, however, where as before it had not. The results of these modified circuit properties are shown in Table 4.12.

Initial Parallel Booster Separation Test			
Capacitance (μF)	Voltage (V)	Observed Separation Results	Notes
10000	50	No Separation	
10000	51	1/3	
10000	52	2/3	
10000	53	2/3	
10000	54	2/3	
10000	55	2/3	
10000	56	3/3	
13300	52	1/3	
13300	53	3/3	Marginal
13300	54	3/3	Adequate
13300	55	3/3	Strong
20000	50	3/3	Adequate
20000	52	3/3	Strong
37000	48	3/3	Adequate
37000	49	3/3	Strong

Table 4.12: Initial Booster Separation Tests



Figure 4.51: Revised Subassembly Test

It was initially unclear why each actuator required so much more power to separate when fired together than when fired individually. Magnetic field interference between the actuators was thought a possible explanation, however it soon became clear the test setup was invalid. The great lengths of alligator wire necessary to patch the two sub systems together created too much resistance and reduced the power that was able to reach the actuators from the capacitors. While ordinarily testing wire a few feet in length can be neglected from most resistance calculations, that was not the case in this setup due to the very high peak current flows. Since voltage drop is a function of current and resistance, the test leads were easily capable of dropping the voltage at the coils by ten to twenty volts – enough to cause the increased firing threshold we observed. Following this realization, the test setup was altered, and the two subassemblies were mounted together temporarily in order to reduce the length of wire necessary to link the two. This revised test setup is

shown in Figure 4.51. When testing was conducted with the improved setup, the system behaved as expected, and the boosters separated very quickly, consistently, and uniformly down to 38V. Since these tests confirmed everything behaved properly and thus no further modifications would be necessary, the assembly and integration of the vehicle was completed.

Once the staging components were assembled and integrated together, we charged and fired the entire system again to verify performance when fully assembled. As expected, the system behaved just as it had in the previous successful tests, and the boosters separated quickly and consistently. We also successfully conducted these tests using the flight computer as the triggering source to verify one additional aspect of integration prior to launch. While these tests all produced the same outstanding qualitative results, one particular aspect of operation became apparent during these tests: the power source had to be switched off prior to inserting or removing the charging plug. This was due to the charging plug design (a 1/8" audio jack) that would allow current to short from one terminal to the other if not inserted perfectly. Such a design aspect was not a concern with low voltage, low current audio applications, but high voltage operation required the addition of a resistor to keep current from accidentally shorting and damaging the system. One test in particular proved the importance of this operational requirement by shorting out the charging jack when the plug was inserted with the power on. While this did not damage the circuit, it required replacement of the charging jack and dictated an additional procedural item for the launch preparation checklist.

The above testing proved that the system worked as intended on the ground when fully charged, yet it did not guarantee the system would be capable of providing adequate flight performance. One parameter that could critically affect flight capability would be the amount of time between charging and firing. Because capacitors can only maintain charge for a short period of time (relative to batteries), it would be imperative that the time between charging and firing be kept short enough to maintain the capacitors above the firing threshold voltage (determined from earlier testing mentioned above to be 38V). Since the rocket could sit on the pad for an unknown amount of time after charging prior to launch, it was important

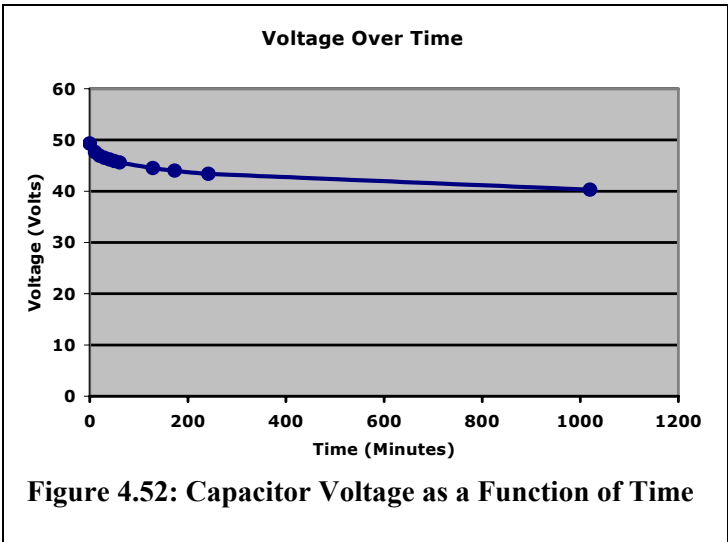


Figure 4.52: Capacitor Voltage as a Function of Time

to quantify how long could elapse before the system would no longer be capable of separating the boosters. To this end, we performed a leak test on the capacitors by charging the system to full voltage and then periodically taking voltage measurements over time. The results of this test are shown in Table 4.13 and Figure 4.52. As can be seen from these results, the capacitors were able to maintain sufficient voltage to separate the boosters through the point at which the test was discontinued (17 hours). Since there would be no reason the rocket would have to sit this long between charging and launch, we concluded the capacitor leakage would not be a factor in flight performance or hold time decision making.

Time (min)	Voltage (V)
0	49.3
11	47.6
20	46.9
30	46.5
40	46.2
50	45.9
61	45.6
129	44.5
173	44
242	43.4
1020	40.3

Table 4.13: Capacitor Leak Test Voltage Results

Aside from capacitor leakage, another factor that could affect flight performance would be the relative air stream. While we attempted to quantify the aerodynamic forces when designing the system, these forces are ultimately very difficult to predict on such a setup. Consequently, we qualitatively tested the booster separation system in an air stream simulated from by using a leaf blower (shown in Figure 4.53). While the test was not very accurate given the small size of the leaf blower and the peak airspeed velocity of approximately 85 mph (as measured by a mechanical anemometer), it nevertheless proved better than a simple ground test. Initially the leaf blower and aft rocket body were supported in a horizontal configuration while the booster was separated. This configuration represented the worst possible situation because the



Figure 4.53: Leaf Blower Air Stream Separation Test

actuator was pushing against both the attractive magnetic force as well as gravity. The leaf blower airflow also poorly represented the real airflow (which would normally help move the booster away from the rocket during separation), so it was no surprise the booster was unable to completely detach in this configuration (though it did move a significant distance away before falling back into place). A more realistic test was thus conducted with the airframe and leaf blower situated at approximately a 30° angle to the horizontal ground. While the actuator pushed against approximately 87% of the gravitational forces in this configuration (still more than it would experience in flight), some gravitation forces also acted in conjunction with the airflow to pull the booster aft and away from the vehicle. This test was conducted twice with successful and consistent separation observed both times. Given this, we discontinued further testing at any orientation with more performance margin. We concluded that the test was successful enough to indicate sufficient performance for in flight staging to occur.

4.3.3 Flight Performance

Flight Test Objectives

After all ground tests had been successfully conducted, it was time for in-flight performance testing. The main objective of the in-flight performance test was to verify the applicability of our design

solution to model rocket staging systems. The evaluation of the flight test was based on the following three critical objectives that drove the design process:

- Successful launch from the launch-pad with boosters attached
- Successful retention of the boosters until burnout
- Successful separation of the boosters after burnout

During lift-off from the launch pad, we expected increased stress on the boosters not only due to thrust but also due to vibrations resulting from interaction between the launch rail and the rocket. The peak thrust created by each booster during lift-off was approximately 100 Newtons according to the specifications of the rocket motor manufacturer. Anticipated stress caused by vibration could not be quantified as precisely, however, and therefore remained an unknown flight variable.

The same objective that all boosters remain attached to the main airframe applied to the accelerated flight following the launch. It should be noted that while thrust and vibration forces in this portion of flight might be lower than during lift-off, additional aerodynamic forces could potentially increase overall stress. During the design process we had approximated these aerodynamic forces to be 25.8 Newtons at maximum velocity.

The third and last objective focused on the separation process upon burnout of all three boosters. This would approximately occur two seconds after lift-off. Due the short time window between burnout and second stage ignition, separation needed to take place quickly and simultaneously. Based on successful ground tests as well as our load estimates and design criteria, we anticipated excellent in-flight performance. Nevertheless, flight-testing was necessary for final verification of our objectives.

To verify successful performance of our staging system during all segments of the flight, we recorded the launch from several different video cameras. These were also used to record the flight trajectory until separation of the boosters as staging was anticipated to take place at fairly low altitude. Additional data used to evaluate the performance of the staging system was obtained through photos taken during launch and flight. We also expected to obtain information on staging performance from the onboard flight computer and camera, but recovery failure prevented this.

Flight analysis

The flight test began with the simultaneous ignition of all three booster motors. The rocket then lifted off the guide rail and accelerated for approximately two seconds until two of the three booster motors burned out. Shortly after lift-off for unknown reasons, a nose cone detached from one of the boosters and was dragged along side the vehicle during its ascent. This likely produced significant aerodynamic stress on that particular booster. During ignition, lift-off, and acceleration, however, all three boosters including the one under additional stress remained attached to the airframe and showed no sign of structural failure. The magnetic actuator provided enough static force to keep all boosters attached to the main airframe during this time. As a result, the first two flight test objectives were met.

Following the burnout of two booster motors, the computer sensed deceleration and triggered the staging system. This resulted in fast, simultaneous separation of the two boosters. The third booster, however, remained attached to the vehicle and continued to burn. As can be seen in Figure 4.54 and Figure 4.55, two boosters separated from the main airframe while the third remained attached burning.

The extended burn time of booster number three was rather unusual given the near-simultaneous ignition of all three motors at lift-off. Therefore we suspect that inconsistencies within the purchased motors may have led to this problem. Because we had anticipated simultaneous burnout of

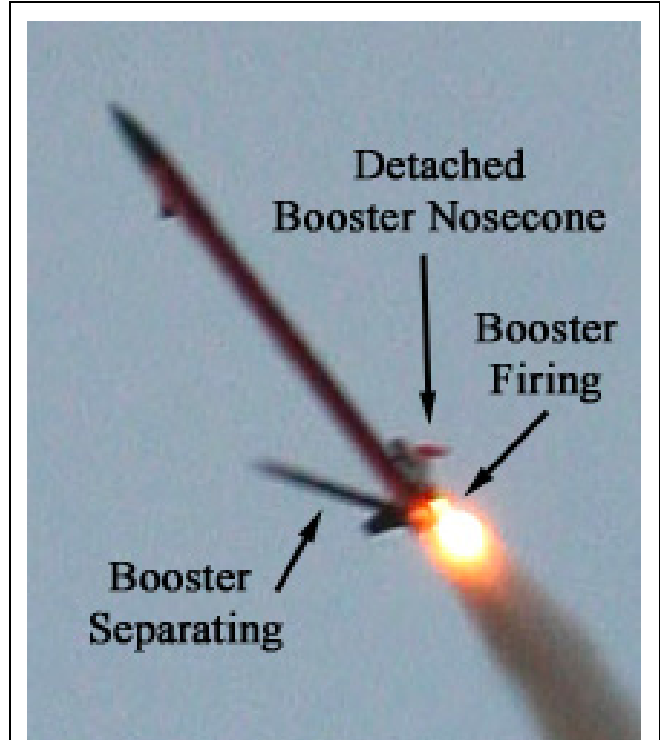
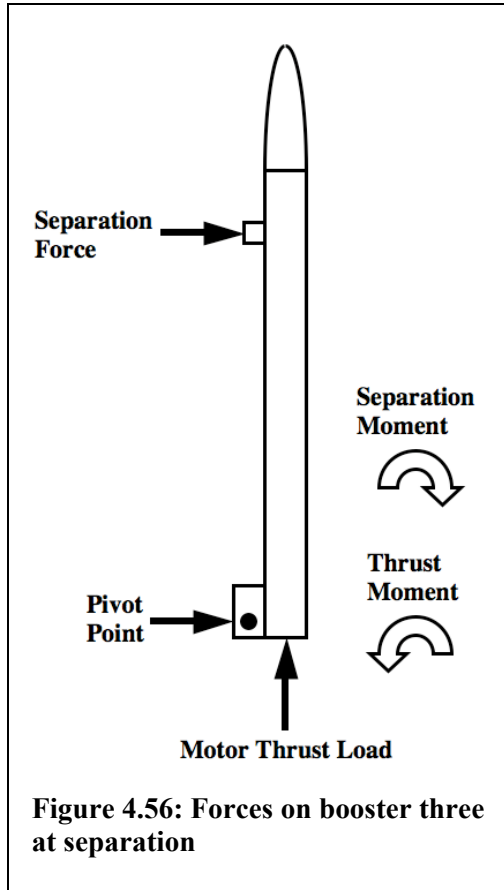


Figure 4.54: In-Flight separation with third booster firing



Figure 4.55: Post-separation flight trajectory



all three boosters, the flight computer was programmed to initiate staging upon detection of deceleration. The limited thrust created by the remaining booster was insufficient to maintain sufficient acceleration and thus led to staging activation before booster three burned out. Thorough post-flight analysis using video footage and still photos provided enough evidence to confirm that the thrust load produced by this extended burn caused the third booster to remain attached. This consistent with our design objective that the booster would not detach under forward load. As can be seen in Figure 4.56, the thrust created a moment that opposed the moment produced by the electromagnetic actuator during discharge. Furthermore, we assumed that even if the magnetic force was strong enough to partly separate the magnet from the steel core, the thrust load would have likely reattached the two.

This potential failure risk could be eliminated in the future by implementing a time delay between burn out detection and separation initiation. This time delay would

allow for differences in motor thrust profiles and ignition inconsistencies. This delay should not exceed one second, however, otherwise rocket performance would be degraded.

4.4 Conclusions

The primary goal of this project subsystem was to create a reliable, consistent, innovative, and easy-to-test rocket vehicle staging system. Once the design was complete, the vehicle constructed, and operational problems solved, ground testing proved successful. Every separation attempt in testing jettisoned the three boosters simultaneously and symmetrically. The system was also remarkably easy to setup and demonstrate. In flight, the staging system also demonstrated superb performance and confirmed the success of this system. While the flight profile was far different than expected, the staging actuators functioned as designed. They kept the boosters attached to the vehicle while thrusting (in spite of the excess drag created by a premature nose cone separation), and two separated cleanly after burnout when triggered by the flight computer. The third likely would have separated on command from the flight computer, but the continuing burn created enough force to hold the booster in place. While this asymmetric separation in flight was not desirable, it was in fact a positive aspect of the design; no booster was supposed to separate while burning. Since both the excess burn and timing of the flight computer's signal were outside the control of the staging system, we concluded that the system did in fact function successfully as designed.

While the operational objectives of the staging subsystem were achieved, the target mass was not. We originally expected a final staging mass of approximately 150 grams but in reality required over 346 grams to successfully implement the design. This was not surprising given the fact that the 150 gram estimate represented the mass for a single series staging system whereas this rocket required three separate staging actuators for the first stage. While this extra mass did not significantly degrade overall vehicle performance, it represented a very significant increase when compared to the original estimate. The increased weight was primarily due to much greater electrical complexity than anticipated. It was also due to the structural requirements of transferring shear loads into the main airframe as opposed to series staging in which thrust forces are transferred in compression. Consequently, future design improvements could thus focus on reducing staging system mass. Aside from this one potential area of improvement, however, the operational benefits exceeded expectations. We concluded that while further work could be done to improve certain aspects of the design, it was nevertheless highly successful.

5. Recovery

The recovery system, while an important consideration on any rocket, is often overlooked in model rocketry. Typically, recovery systems are simply a black powder pyrotechnic charge which separates the rocket body tube sections and deploys parachutes.

One of the goals of this project was to develop an innovative recovery system, preferably one which did not utilize pyrotechnics. To that end, the primary recovery devices for the WARRIORS rocket utilized the potential energy of springs, with pyrotechnic backup devices.

5.1 Recovery Background

Several months were devoted to investigating and acquiring a greater understanding of how recovery devices work, and learning about recovery methods other than pyrotechnics. This background research helped us develop the device that was eventually used in the final project.

5.1.1 Recovery System Function

The recovery system serves two important functions. It prevents damage to the rocket that would otherwise occur from descent. It also prevents the rocket from doing harm to people or property when falling. To help accomplish these goals, the NAR has established guidelines dealing with all aspects of model rocketry, including recovery. Part of the NAR rules state that *“The model rocket itself must be capable of more than a single flight and must return to the ground so that no hazard is created.”* While a rocket with no recovery device may not explode, it will come back to earth much like a missile, potentially causing damage or worse yet, injury. Also, *“The rules of the NAR do not permit the jettisoning and free fall of any part of a model rocket, such as motor casing, unless the falling part tumbles to slow its speed and uses a streamer or other readily visible surface that can be seen.”* This means any component of the rocket such as a staging section must be equipped with a recovery device or be light and small enough to qualify for tumble recovery. In the event of a recovery system failure, rocket design and the materials used in construction should be such that the rocket will sustain more damage than it causes. [2]

5.1.2 Recovery Systems Overview

In model rocketry, there are three common types of recovery systems commonly used for returning rockets safely. These three methods are designed to protect the model and people, and are subject to the guidelines set forth by the NAR. The three methods of recovery are: nose-blow recovery, streamer recovery, and parachute recovery.

Nose-Blow

Nose-Blow is the simplest of the three. The idea behind nose-blow recovery is to cause the rocket to become aerodynamically unstable, thereby lowering its terminal velocity and causing it to fall at a slower rate. This is done by causing the nose cone to come off of the rocket at apogee via an ejection charge. To prevent the nose cone from freefalling on its own, it is attached to the rocket via a shock cord. The rocket would then tumble to the ground at a much slower rate than if it were still aerodynamically stable. Even though nose-blow recovery reduces the rocket's velocity, it is not always enough to prevent damage to the rocket. For this reason NAR regulations state that nose-blow rockets are limited to weighing 2 ounces or less. This reduces the chance of injury to bystanders.

Streamer

The second recovery method is to use a streamer to increase drag on the descending rocket, and hence slow its descent. Streamer recovery, works in a similar fashion to nose-blow recovery; a streamer and the nose cone are ejected from the body tube of the rocket. The streamer is attached to either the shock-chord that keeps the nose cone attached to the fuselage. Streamers are often made of plastic, nylon or crepe paper. During flight the streamer sits inside the main body near the nose cone. Recovery wadding is placed between the streamer and the ejection charge. It is important to note that the recovery wadding must be flame proof to protect the streamer and shock cord from melting or catching fire. In addition to helping slow the descent of the rocket, the streamer also acts as a visual aid to help locate the rocket.

Parachute

The third type of recovery system is parachute recovery. Parachute recovery is used on rockets that are too large or heavy for streamer recovery. Parachute recovery has the slowest descent of the three common recovery methods. The general principle of this method is the same as streamer recover. An ejection charge fires at the rocket's apogee and ejects the nose cone and parachute, which is generally right behind the nose cone like a streamer would be. Like the streamer, it is protected by recovery wadding and is often made of similar materials.

The biggest advantage of parachute recovery is a slow descent which will keep the rocket from being damaged. Parachutes can be adapted to almost any size rocket - the bigger the rocket, the bigger the parachute. However, parachutes are much heavier than streamers and they take up more volume inside the rocket. They also drift in the wind more, requiring a larger field to ensure successful recovery of the rocket.

5.1.3 Other recovery methods

Besides the three methods previously described, there are three other less common methods of recovering model rockets. These are tumble recovery, glide recovery, and auto-rotation.

Tumble

Tumble recovery is seldom used because it can only be applied to very small, very lightweight rockets. In tumble recovery, the rocket ejects its engine casing, causing a change in the location of the center of mass. This makes the rocket unstable, and it “tumbles” to the ground, much slower than it would in a balanced, aerodynamic state.

Auto-rotation

Auto-rotation, works by using the ejection charge, or other release mechanism, to release three or four fins, either stored inside the rocket, or tucked against the main fuselage. Once released, they spring outward forming a blade arrangement much like on a helicopter. As the rocket falls, the blades create resistance and cause it to spin, slowing the descent. Some rockets use a combination of autorotation and other recovery techniques. For example, the main body may be recovered by parachute, but the nose cone may come down like a helicopter. Auto-rotation is not commonly used, as it has several drawbacks. It is heavier than a parachute and takes up more space. It also requires a more complicated mechanism, with more moving parts, which increases the chance of failure. That said, it can still be a fun and interesting way to recover a rocket if it is not designed for high performance. Auto rotation is most often seen on rockets that can be purchased at a local hobby store, and are manufactured by companies such as Estes.

Glide

Glide recovery works much like auto-rotation only instead of releasing blades, it releases wings. The wings are usually stored against the body, or folded up during ascent, and released at apogee. In order to glide like a plane, most rockets have one fin that is larger than the others. This fin acts as the vertical stabilizer would on an airplane and helps keep the rocket stable during its descent. Much like auto rotation, glide recovery has the drawback of being heavier and more complex. Another use for this technique is on rocket powered planes. They are launched like a rocket, only they have fixed wings, and some even have operational control surfaces (i.e. ailerons, etc). Many of these are RC equipped and the pilot can launch them to altitude, and then guide them as desired.

5.2 Methodology

5.2.1 Initial thoughts and Designs

When design began on the recovery system, decisions needed to be made regarding what goals this design needed to accomplish. The limiting factors were evaluated to determine if there were any options that could be eliminated right from the start. After some research and discussion, several goals were identified and general design decisions made.

First, because of the size and objectives of the rocket as a whole, it was quite clear that the recovery system needed to be a parachute, with the possibility of using streamers or small, drogue parachutes for smaller segments of the airframe. A streamer for the main body would have not been practical due to size and weight. Also, while glide and/or auto-rotation recovery could be very interesting and challenging, it was felt that because of the size these too should be considered impractical.

After choosing a parachute recovery system, it became possible to refine the specific goals of the recovery subsystem:

- To return the rocket safely with little or no damage. While this is an obvious goal, it would also allow for less time and money to be spent on repairs.
- Allow the rocket to descend fast enough that it will not have time to drift very far due to wind. This can be a problem in windy conditions; if the rocket descends too slowly it can drift far from the launch pad, possibly becoming lost. A quick yet safe descent rate is ideal.
- The deployment method should be safe, simple and reliable. Fewer working parts often mean fewer chances of something malfunctioning. Also, simplicity could save mass and cost, which could be an important issue.
- The primary recovery activation device should not incorporate pyrotechnics.
- The design must be innovative.
- The design must be consistent with NAR rules.

One initial idea was to make a maneuverable parachute. Many skydivers and members of the military use parachutes that can be maneuvered during descent. These parachutes often have different shapes than the standard circular parachutes used for dropping cargo, or for recovering model rockets. One idea was to rig the parachute so that it would be in a continuous left or right hand turn. This would force the rocket to drift in a circle, or spiral pattern as it came down. This could help reduce the distance it would drift from the launch pad. However, it was decided to focus upon the recovery deployment mechanism, rather than the parachute itself.

5.2.2 Compressed Gas Recovery System

Many high powered model rockets today use pyrotechnic ejection charges, either from the rocket motor, or from a separately placed charge, to deploy the parachute or other recovery device. This system works well for most model rocket enthusiasts; it is a fairly common and available ‘off the shelf’ method. However, the pyrotechnic charge system is less effective at higher altitude where the air becomes less dense. Pyrotechnic charges require the ignition of a highly flammable substance to create a small explosion which ejects the parachute. In order for this to occur sufficient levels of oxygen are needed. If the rocket reaches a high enough altitude, these oxygen levels may be too low and the system will fail.

The first conceptual design was to use a carbon dioxide system (CO₂) system to eject the parachute. The idea was to use 12 gram CO₂ cartridges that can be purchased at any sporting goods store. At apogee, they would be triggered to release into the parachute bay, causing an increase in pressure which would separate the bay and release the parachute. An interesting aspect of this system is it would actually work more efficiently at higher altitudes. As the rocket ascends, the outside air pressure drops, yielding a greater pressure differential between the pressure inside the parachute bay and outside the rocket.

CO₂ recovery systems already exist for model rockets in the commercial market. However, they are not commonly available, and typically incorporate a pyrotechnic charge to puncture the CO₂ cartridge. The pyrotechnic charge propels a metal dart into the top of the CO₂ cartridge, breaking the seal and allowing the compressed gas to escape. This was something we wanted to move away from in our design. We felt that using the using a pyrotechnic charge to actuate the CO₂ system defeated the point of using CO₂ in the first place. During our conceptual design phase, encountered issues with the design of a CO₂ release system. The first and most problematic issue had to do with the release of the CO₂.

At this point, we decided to use a valve and design the system so that the cartridge would be punctured before flight and the CO₂ released through the valve upon command from the flight computer. Again we encountered problems with this design. When researching valve manufactures, we had trouble finding one that could meet our requirements. Most commercial cartridges store CO₂ at 800-900 psi. The valves we found that could contain pressure that high were too large and heavy for what we wanted. They were also expensive.

We also considered using a piston that would be powered by the CO₂ or compressed air; however, the valve requirements would remain unchanged. At this point we started to consider designing our own cartridge that would hold the CO₂ at a lower pressure. Our “simple and reliable” design was quickly becoming more and more complicated as we ran into additional difficulties. We were having trouble determining how much pressure would be needed and if the parts we wanted to use could withstand 900

psi. It was finally decided during a group discussion that the CO₂ system was not going to work and we should try a different approach.

5.2.3 Spring Recovery Systems

Introduction

During the early stages of system design, we had discussed the possibility, should our other proposed designs fail, of constructing a mechanical system. However, in the early stages of the project, we saw promise in compressed gas systems, and the mechanical option was set aside.

After it became apparent that we did not have the capability of constructing a high pressure compressed gas recovery system, we revisited the idea of a mechanical system. Such a system would be required to store mechanical energy and release it upon command from the flight computer. The simple and relatively lightweight devices that were first discussed were compression springs.

Initial Design

Initial designs (shown in Figure 5.1) included a compression spring in between one fixed and one moveable bulkhead. The moveable bulkhead, referred to as the “piston bulkhead,” would be moved along the rocket’s central axis as the spring expanded, forcing the body tubes apart and deploying the parachute. The piston bulkhead had two components; the bulkhead itself, and a coupling ring epoxied to it, to prevent the bulkhead from twisting in the body tube.

The spring, when compressed, would be stored around a garolite tube, shown in the center of Figure 5.1. This tube would also serve as a way to center the piston bulkhead in the body tube. Initial conceptual design called for the tube to be a wooden dowel – the use of garolite was stumbled upon when we found it was also being used by the Staging subsystem.

Not only did this design benefit from conceptual simplicity, but it appeared (in the early stages) that it would not involve large amounts of custom fabrication or expensive parts. A push solenoid, triggered by an electrical signal from the flight computer, would actuate a lever retaining the piston bulkhead. A push solenoid is a solenoid whose functional mode is to open, rather than to close when electrical current is passed through it. Upon the bulkhead’s release, the spring would release its stored energy and deploy the parachutes.

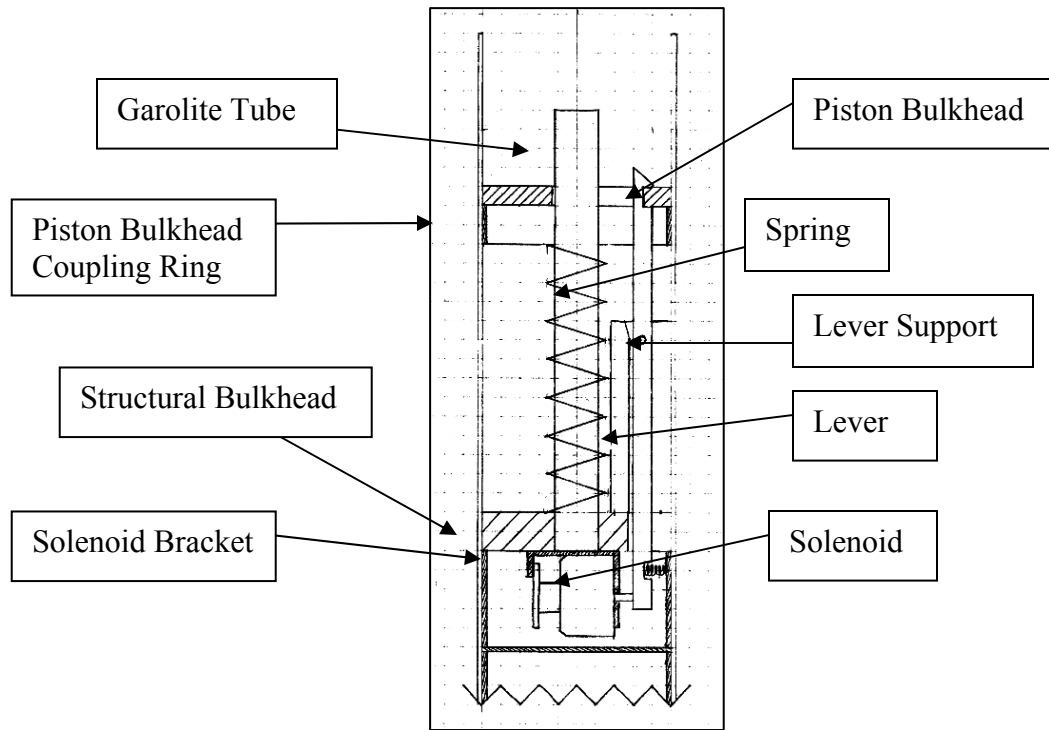


Figure 5.1: Early Conceptual Drawing of Activation Device

Internet research provided us with a short list of potential component suppliers. In an effort to expedite the development process, components were ordered early in the initial design phase to allow a prototype to be constructed soon after we arrived at an initial design. The components ordered are listed in Table 5.1; these same components would be recycled and used on the flight ready devices.

Supplier	Name	Serial Number
Magnetic Sensor Systems	Tubular Low Profile Clapper Solenoid 1" Dia by 0.66"	S-66-100
W.B. Jones Spring Company, Inc	Compression Spring	C24-062-256
McMaster-Carr	Square Aluminum Bar (1/4" x 1/4" by 6')	9008K17

Table 5.1: Materials Ordered for Prototype Construction

The spring system was designed to meet several simple requirements; it had to fit inside of the rocket and as light as possible as not to prevent its use during an actual flight. Since the flight computer could only output limited voltage and current (and at that point the flight computer choice was not known) it was decided to design a device to use 6 volts and 0.5 amperes, well within the limits of what known flight computers were capable of. Most importantly, the device would have to provide enough force to separate the two body tubes of the rocket.

5.2.4 Prototype

The construction and testing of a prototype activation device was important as it would address a number of concerns expressed about the system. The prototype was constructed out of a phenolic body and coupler tube, 3/16 inch plywood and epoxy. While crude, it provided the basis for developing an understanding of the spring system. During testing, the prototype was destroyed and reconstructed numerous times. The remains of the prototype device are shown in Figure 5.2.

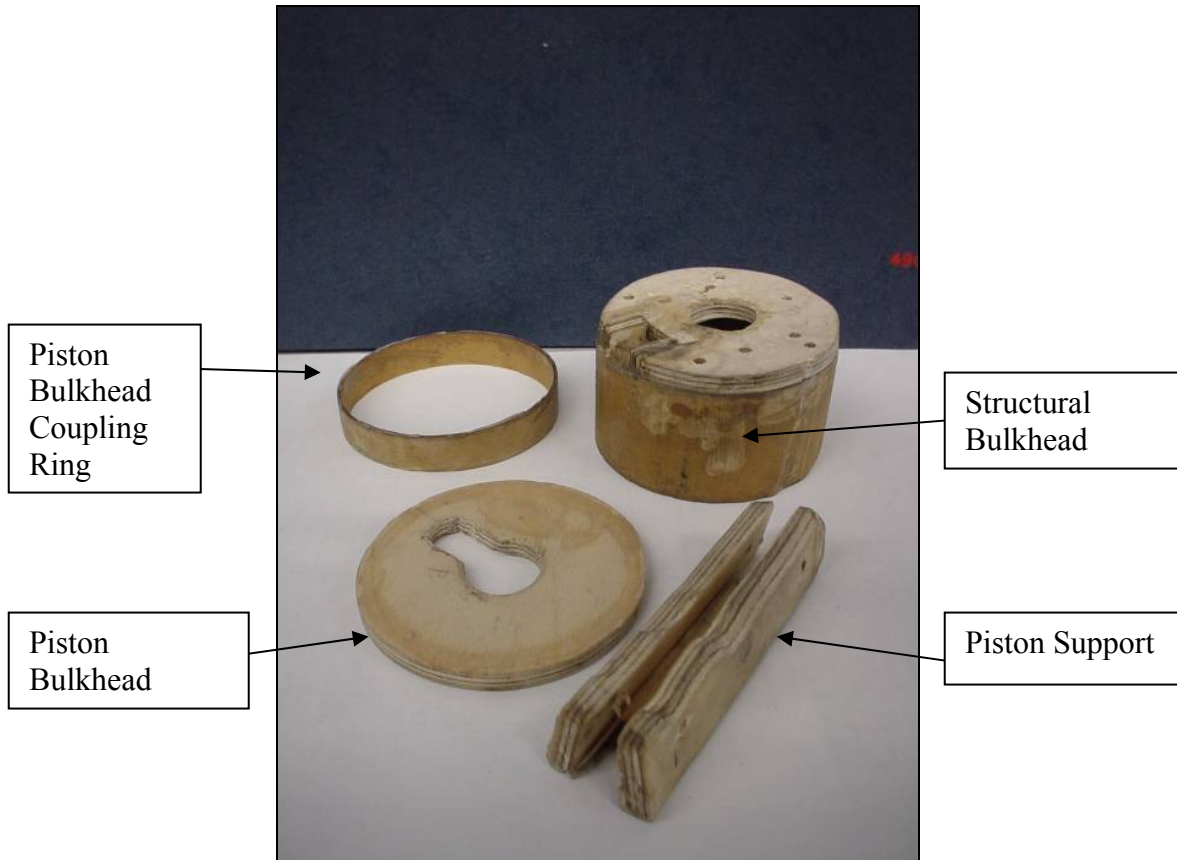


Figure 5.2: Remains of Prototype after Testing

Prototype Testing and Modifications

The tests performed on the prototype were not developed before or during the design process – many of them came about as the result of concerns of the other team members.

Premature Deployment

Initial assembly of the prototype device showed it was very sensitive to movement; it would often deploy with even the slightest force being applied to it. Obviously, this was a problem; during launch the

spring devices (as well as the rest of the rocket) would be subject to significant g-loading. A simple test was devised to subject the prototype device to approximately the same g-forces that rocket would experience upon launch (12 gs), allowing us to document the behavior. For photographs and the mathematical rationale behind the test, please see Appendix J.

Initially, the test confirmed what we already knew; the device would fire any time it was subjected to an impulsive force. However, upon careful inspection of the prototype, we noticed that the lever was not vertical. When subjected to a force, the lever would generate a moment, causing it to slip off of the piston. After correcting lever’s orientation and adding a rubber band to retain the lower portion of the lever, no further problems were observed. This test was performed numerous times to ensure that the system would not deploy upon takeoff.

Concern Over Spring Force

When the mass of the rocket segment is coupled with the aerodynamic drag force that it would be experiencing during its flight, the force that the spring must overcome to separate the rocket segments and deploy the parachute is substantial. After evaluation, it was determined that a single spring would not exert enough force to separate the fuselage segments, and it was decided to use two springs in series, and thus doubling the total force. The different spring options are outlined in Table 5.2. The third option, visible on Table 5.2, was to p on the table is a stiffer spring. We decided not to purchase stiffer springs was influenced by the fact that two springs in series would have a greater uncompressed length than a single spring, allowing them to conceivably push the airframe segments farther apart.

Quantity	Serial Number	Spring Constant (lbs/in)	Maximum Force (lbs)	Uncompressed Length (in)	Mass (g)
1	C24-062-256	2.6	14.7	8	25
2	C24-062-256	2.6	29.4	16	25
1	C24-091-256	11	42.6	8	66.6*
		*Calculated			

Table 5.2: Spring Force Comparison

System Failure

A disturbing issue experienced with the prototype was its structural failure. In Figure 5.2, the prototype is in pieces. During several of the tests, the plywood and epoxy structure failed, leading to the deployment of the spring system. For the actual devices, stronger materials and more durable construction techniques would need to be used.

Piston Twisting

The piston on the prototype (Figure 5.1) was only one half inch thick. Initially this seemed like enough thickness to prevent the piston from twisting. However, during tests, the piston often twisted in the body tube. In the flight devices, the piston would have to be thicker. As one half inch was not thick enough to ensure consistent deployment, it was decided that three times that length, or 1.5 inches, should provide enough surface area to prevent piston twisting. This was verified by using a piece of phenolic coupler as a new piece of the piston bulkhead during testing.

5.2.5 Flight Device

After completion of testing on the prototype device, construction of the flight devices began. While only two would actually fly, three were built to have a backup if necessary. It is worth noting that none of the flight devices are identical to one another. The manufacturing methods and techniques used, while effective, did not lend themselves to precision or perfect replication. Each device is a little different than the others, and its components were custom fit to work with only that singular device.

A section view of the flight device is shown in Figure 5.3. While it is very similar in overall design to the prototype, the precision and materials used in its construction were much more refined.

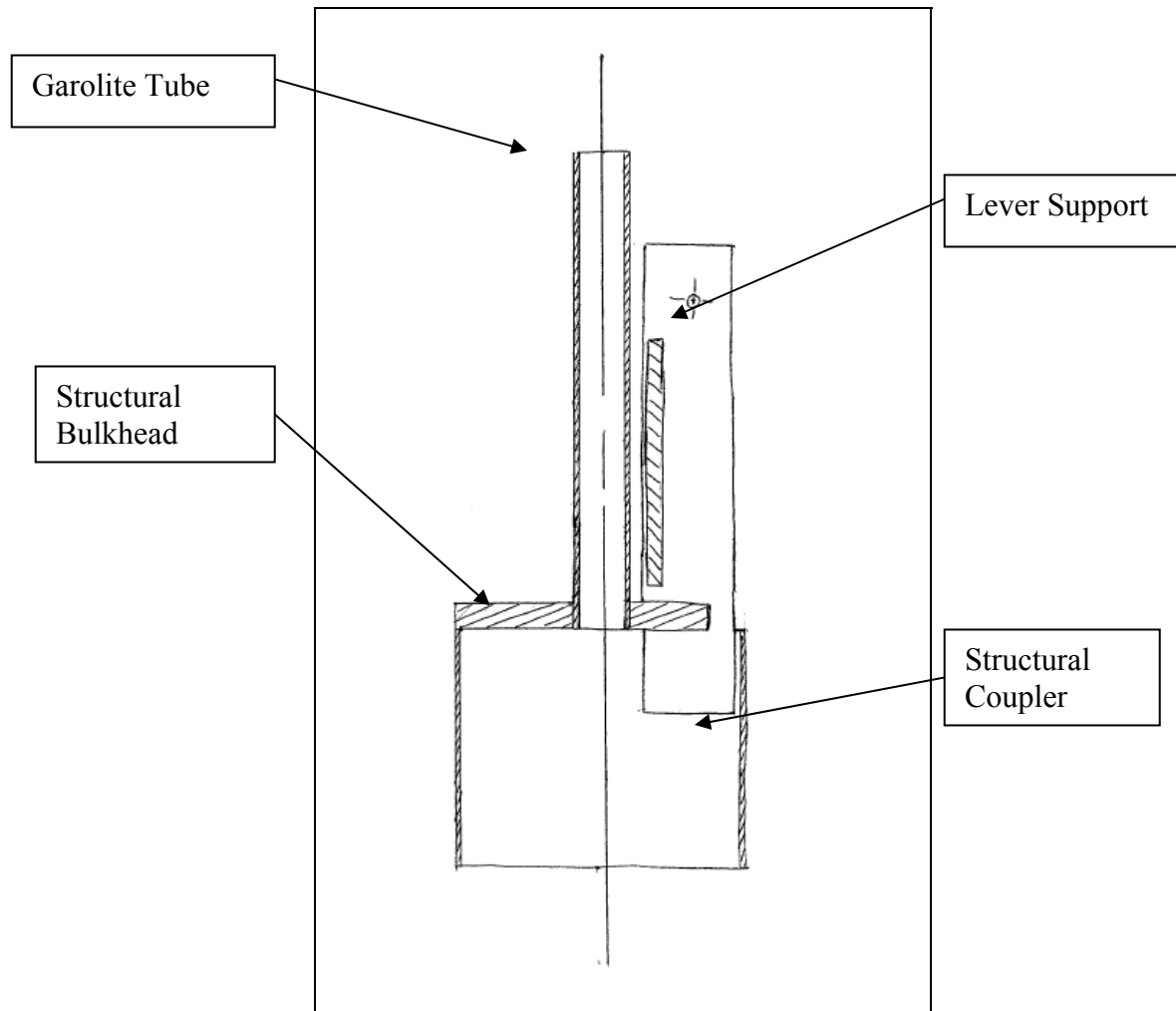


Figure 5.3: Section View of Operational Device without Lever

Having learned from the construction and testing of the prototype, the design and construction methods were modified to make the recovery devices stronger. While this did make them heavier, it was a necessary trade-off.

The primary modifications to the design were the use of G-10 fiberglass in place of, or to reinforce, the previously used plywood. Additionally, fiberglass was used to reinforce the interior corners of the device.

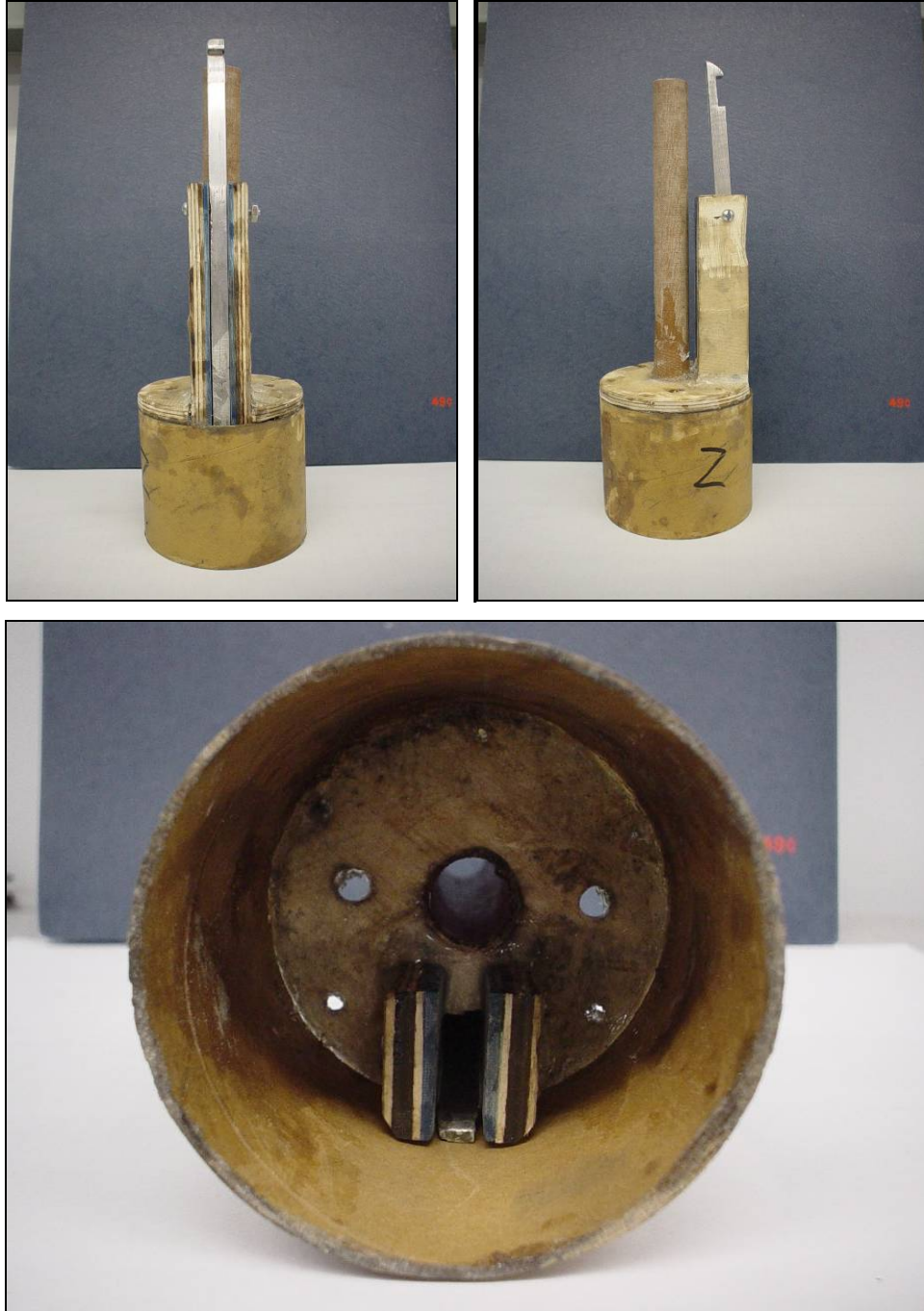


Figure 5.4: Photographs of Operational Device (2.5 inch diameter)

Figure 5.4 displays the materials and construction techniques used in the flight devices. The interior corners of both the lever support, spring support column, and the inside joint of the coupler and plywood base were reinforced with fiberglass cloth and epoxy. During construction, extra care was taken to ensure that the lever would be perfectly vertical with the solenoid installed, so that there would be no

moments upon it during takeoff. The plywood base of the system is identical to the bulkheads used throughout the vehicle.



Figure 5.5: Piston

The “piston bulkhead,” consisting of a coupler and a piece of G-10 fiberglass, had to be constructed with relative precision to ensure that the lever would release properly. Once again, the inside surface of this component is coated with fiberglass and epoxy. The Kevlar cord seen in the picture is used to retain the piston bulkhead and the springs after they deploy. The oval, off-center hole on the left in Figure 5.5 is to allow the shock cord and the wires for the pyrotechnic backup systems and/or the second stage ignition and booster separation to pass through.

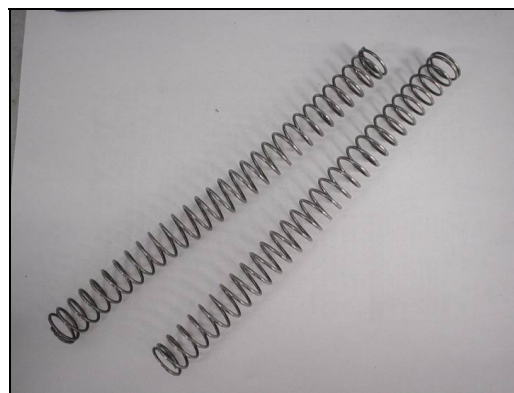


Figure 5.6: Springs (8 inch uncompressed length)

Each device would use two springs mounted in line with each other, for a combined, uncompressed length of 16 inches and a compressed length of four inches. The springs, shown in Figure 5.6, are eight inches long with an outside diameter of 0.720 inches.

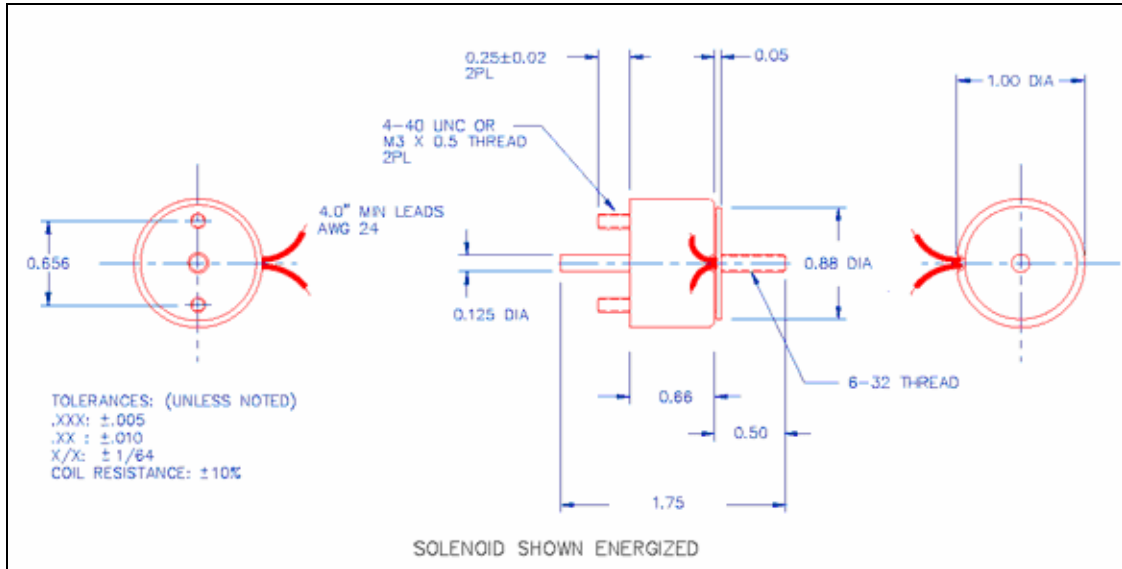


Figure 5.7: Solenoid [20]

The solenoids selected for use in the WARRIORS rocket were Magnetic Sensor Systems Low Profile Push Solenoids, shown in Figure 5.7. While the solenoid was designed to operate on six volts, we found it necessary to use 50V with it (see below for an explanation). The tip of the solenoid was threaded, and a small aluminum spacer mounted to it, to allow the throw of the solenoid to be adjusted to the specific length needed for the device to function correctly.

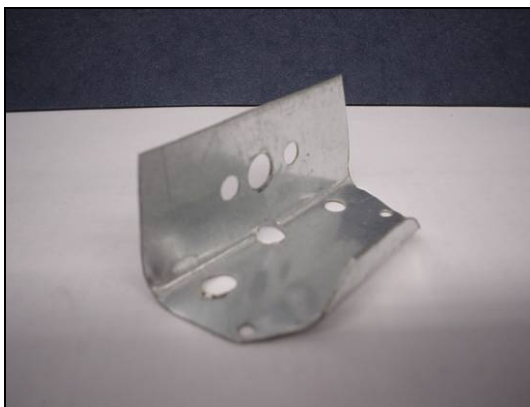


Figure 5.8: Solenoid Mounting Bracket

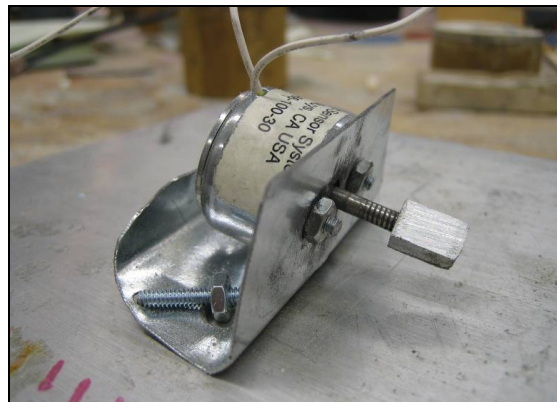


Figure 5.9: Solenoid and Mounting Bracket

The mounting bracket for the solenoids was constructed out of sheet aluminum. The tall vertical surface was used to mount the solenoid, while the shorter vertical surface is meant to retain the piston element of the solenoid. Figures 5.8 and 5.9 show both the bracket and the bracket with the solenoid mounted onto it. The solenoid was mounted using bolts that were part of the solenoid itself. A small aluminum block was threaded onto the end of the solenoid pushrod, both to assist in retaining the rod during flight and to allow the length of the solenoid's throw to be adjusted.

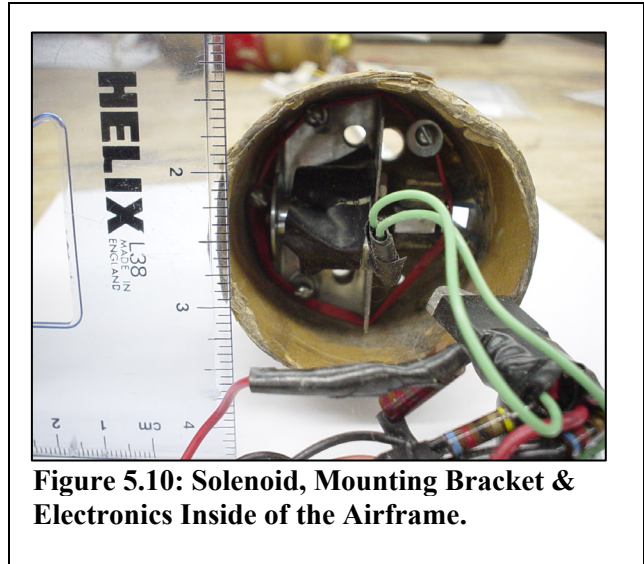


Figure 5.10: Solenoid, Mounting Bracket & Electronics Inside of the Airframe.



Figure 5.11: Shock Cord Mounting Brackets

The mounting brackets for the recovery bay side of the shock cord were machined out of aluminum, in order to allow for the eye-bolts to mate with the aluminum threaded rods. Figure 5.11 shows the entire recovery assembly, with the shock cord mounting brackets attached to the aluminum structural rods. This arrangement allowed for the forces exerted by the parachutes as they deployed to be passed through the electronics bay without stressing the airframe itself.

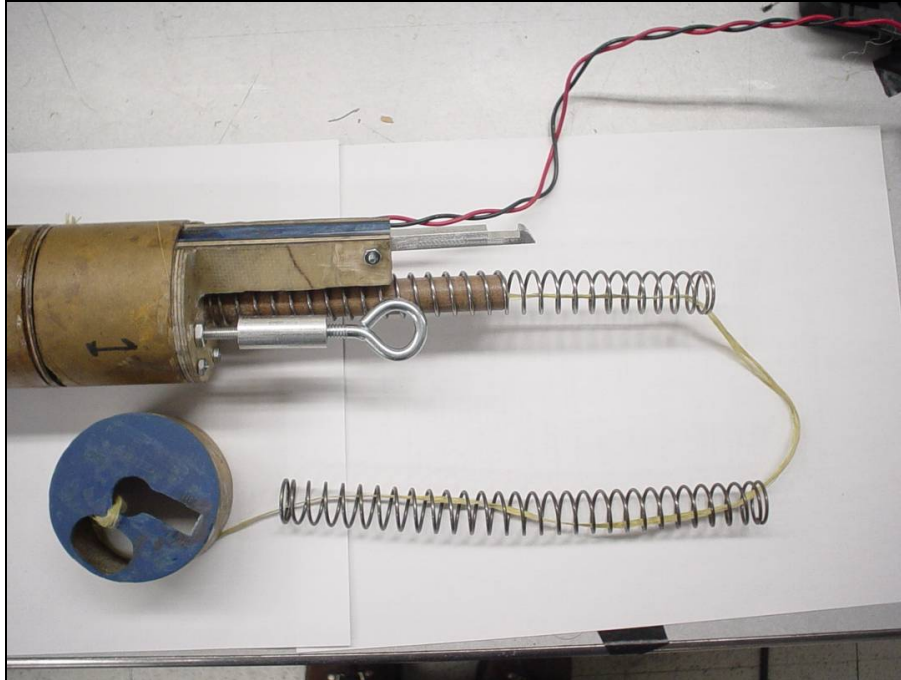


Figure 5.12: Fully Assembled Device during Testing

The fully-assembled activation device (uncompressed) demonstrates how the springs and piston bulkhead were retained and how the shock cord mount attaches. The wire in the upper section of the picture should be passing through the piston hole in the piston bulkhead.

Pre-Flight Testing and Modifications

The tests and modifications performed on the three flight devices were similar to the tests performed on the prototype device as they were designed to address concerns about the functionality and safety of the recovery devices.

Premature Deployment

The same premature deployment shock test was performed to the flight devices as to the prototype device. Unlike the prototype, the flight devices were constructed with enough precision and care that they did not experience the same problems. The flight devices never deployed by accident during testing.

Safety Pins

As the spring system produces a large amount of force, releasing the piston bulkhead at a high velocity, it was deemed necessary to develop a way to prevent the system from launching on the launch

pad. Therefore, two safety pins were constructed, one for each device. They pass through the airframe and do not allow the piston to move off of the piston bulkheads.

Shear Pins

Initial deployment tests of the recovery subsystem using the actual airframe led to concern among the team members as to whether if the springs could generate enough force to separate the two sections. As a rule, the airframe couplers are wrapped in masking tape to ensure a tight fit. The tape makes the joints tight enough so that the airframe can be held from the upper sections and shaken without the airframe sliding or separating. When pyrotechnic charges are used, they generate more than enough force to separate the tight-friction fitted airframe sections.



Figure 5.13: Safety Pin

However, using a spring system, much less force is generated than a pyrotechnic charge would generate. Initial tests confirmed that the airframe would not separate when wrapped in tape unless extreme care was taken to wrap the airframe in just enough tape to not allow separation.

To increase the consistency with which the spring system would fire, and to allow a greater degree of precision when coupling the airframe, shear pins were used.

The nylon pins typically shear at approximately 30 pounds of force, and for a 2.5 inch airframe, 2 pins are recommended. Therefore the pins were milled down from 0.08 inches (their original diameter) to a diameter of between 0.030 and 0.040 inches. At that diameter, the pins shear at approximately 10 pounds of force each.

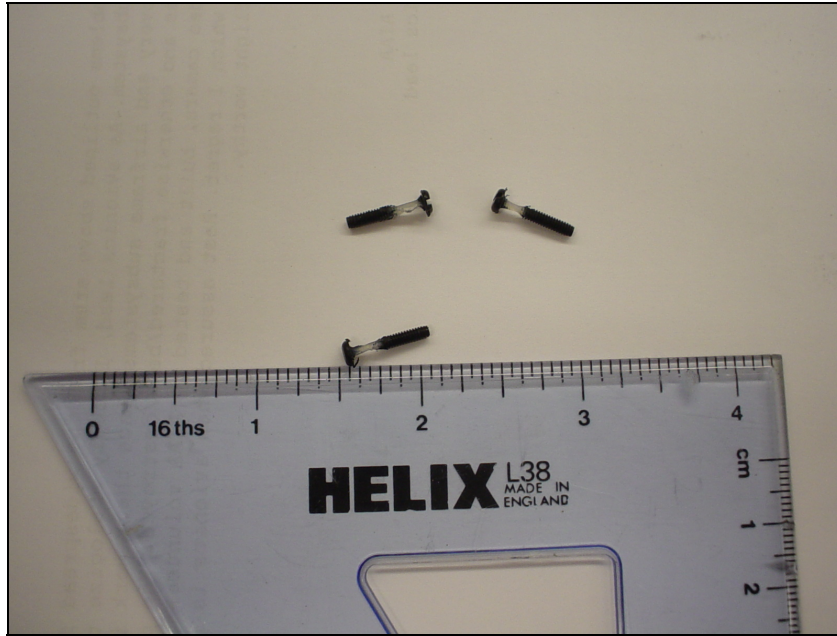


Figure 5.14: Shear Pins

Electronics

Our initial design for the recovery system called for two solenoids which would be triggered by the 12 volt signal from the flight computer. The solenoids used in the design were 18 volt long-duration solenoids. This means the circuit inside is meant to function on 18 volts for long periods of time, rather than just being turned on then off. However, it became clear that after a few test firings of the solenoid with a 12 volt power supply, 12 volts would not be enough for the performance we needed. While the solenoid would actuate at 12 volts, it was not strong enough to overcome the friction on the retaining lever holding the piston bulkhead in place.

When the rocket reaches its maximum altitude the computer will send a signal to the solenoid. The solenoid is in the ‘open’ position (the clapper is not touching the solenoid body) when the solenoid is off. When the signal reaches the solenoid, it closes and pushes on the retaining lever, releasing the parachute. As the solenoid closes, the magnetic force pulling on it increases until it reaches its maximum at the fully closed position. To make up for the lack of strength provided with the 12 volt source, we tried closing the solenoid slightly to increase its strength and allow it to activate the recovery device using only 12V. While the solenoid would actuate with greater force, it did not do so with a force sufficient to trip the devices.

Another way to strengthen a solenoid is to increase the voltage to it. Tests at higher voltages from the power supply showed that this would be a better option than using the solenoid partially closed. While this provided the solution we were looking for, it brought with it another problem; the maximum

voltage the computer can handle is 12 volts DC (VDC). This meant we had to come up with a circuit that could be triggered by the computer but had its own power source that could handle and provide the higher voltages we would need in order for the solenoid to properly function. We consulted the staging team about their circuitry. The staging team was using a circuit that worked very similar to the way we wanted ours to work. The staging team helped us design our circuit which is essentially a copy of their circuit with a slightly smaller capacitor.

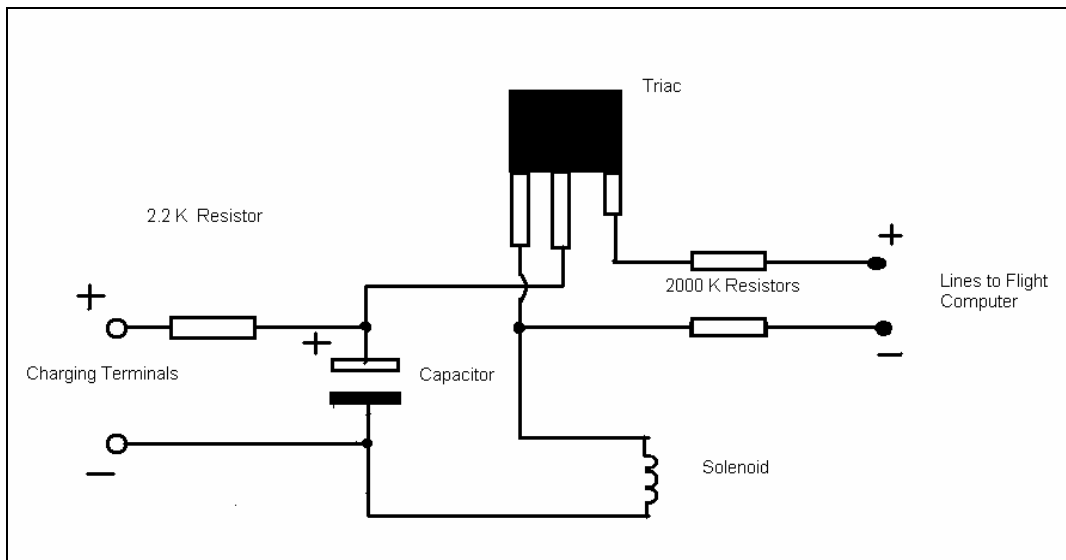


Figure 5.15: Recovery Circuitry Diagram

The above circuit is triggered by the flight computer signal and provides a 50 VDC pulse to the solenoid giving it enough strength to overcome the friction on the retaining lever.

The recovery circuit is designed specifically to meet the requirements of our subsystem. It charges from four 12V dry cell batteries providing a combined 48 VDC. Charging takes approximately 45 seconds to bring the capacitor to a charge of 48 to 50 VDC. Once charging is complete the batteries are disconnected from the circuit. The circuit can be charged while connected to the flight computer without shorting or overloading the computer's circuitry.

An important part in our circuit is the triac. A triac is essentially an electronic switch that stops current from flowing until it is triggered. It has three terminals; signal input, positive and negative. Once the system is ready, the computer sends a 12V signal to the input of the Triac. This triggers the system and it “releases” the electricity, which in this case comes from our capacitor. The current from the capacitor flows into the positive terminal, out the negative and to the solenoid. The positive lead from the computer has a 2000 K Ω resistor which drops the signal voltage from 12V to less than 2V, which is the maximum voltage the triac can handle on the signal input. The negative lead from the computer is also

run through a 2000 K Ω resistor. This is to prevent leakage from the system and to further help reduce the chance of damaging the triac.

Another important part of our circuit is the capacitor. This circuit uses a 3300 μ F capacitor which can be charged up to 50VDC. Once the circuit was built and ready to be tested, it was important to test how long these capacitors could hold their charge since there is a chance it could be several hours from the time the circuit is charged until the time the rocket is flown. Our basic method to test this was to try firing the solenoid and different voltages in order to see what the lowest operational voltage would be. This voltage was found to be 35V. The next step was to see how long it would take for the capacitor to drop to from a full charge to 35V. To test this we simply charged a capacitor in one of our circuits to 50V and let it sit for 12 hours. After 12 hours the charged had dropped to about 42V, which is enough for the circuit to operate properly. Also it should be noted that 12 hours is much longer then the rocket would ever be left on the launch pad.

Pictured in Figure 5.16 is the first iteration of the recovery subsystem circuit. A second circuit was later made, one to operate the main chute and the other to operate the drogue parachute or streamer. Both circuits were identical and fitted with small black plugs to make them easier to connect to the solenoid and computer. Later as the rocket was assembled it became clear that these circuits were too big to fit into their respective bays, along with the solenoid and other hardware. Both circuits were rebuilt to be smaller by shortening the wire length between each component. Also, after several testes it became apparent that small black plugs were not sturdy or reliable enough for our use. They were replaced with computer power supply unit (PSU) plugs.

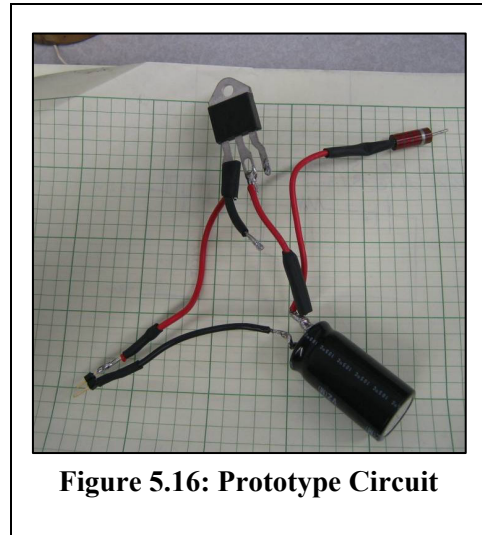


Figure 5.17: Prototype Circuit Next to Recovery Systems



Figure 5.18: Flight Circuitry with PSU Connectors

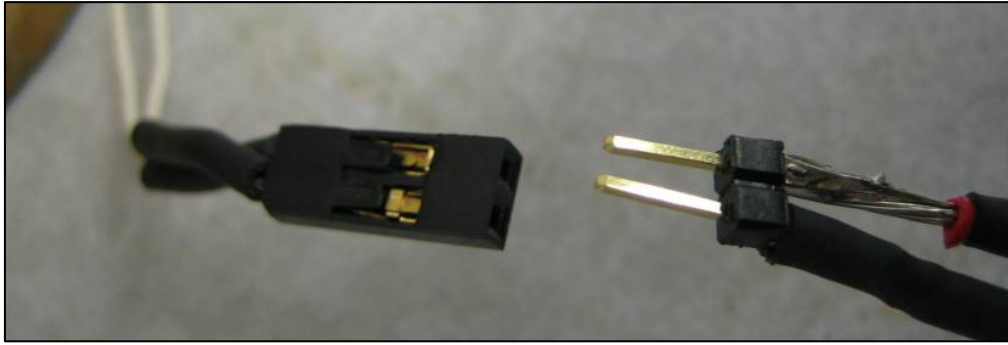


Figure 5.19: Initial plugs used for the circuit.

A pre-launch concern was the rate at which the capacitors would drain, and the threshold voltage at which the recovery system could successfully activate. To that end, a leak test on the circuit was performed to determine the length of time the circuit could sit, after having been charged and still be able to deploy the recovery devices. Table 5.3 shows the results of this test.

Time (minutes)	Voltage (V)
0	54
60	48.6
120	45.6
140	45

Table 5.3: Threshold Voltage Test

The threshold activation voltage, which is 35 volts, was never reached. However, in the improbable event that the rocket sits for over two hours on the launch pad, all electrical systems would certainly be re-charged prior to launch.

Deployment Tests with Flight Computer

The first big hurdle that the device had to pass was to successfully activate upon the reception of a signal from the flight computer. To that end, a low-friction track was procured along with small carts for it. The flight computer was placed in a dummy section of airframe, to which the deployment device was mounted. The springs were compressed, the piston locked in place, and a section of airframe placed upon the top of the spring section and locked in place with shear pins. The computer was then triggered to fire the system. For screen shots from the test video, please see Appendix K.

Full Pre-Flight Test

The last major pre-flight test before flight would be to test both devices with the airframe and the flight computer configured as they would be for an actual flight. This test was performed, successfully, the day before flight. However, due to time constraints, the test was not performed a second time.

The test was performed during a mock pre-flight of the rocket, during which all components and sections were loaded in the correct sequence. Unfortunately, no pictures video was taken of the test.

During the test, the main parachute deployment device deployed as designed. However, the drogue parachute deployment device did not function correctly. During preparations that day the drogue device had not functioned every time it was tested. However, since there would be pyrotechnic backup devices, it was determined that even if the drogue parachute did not deploy the rocket would be in no immediate danger.

5.2.6 Booster Recovery System

The recovery system for the three booster rockets was extremely simple. In essence, the boosters became overpowered model rockets; they were equipped with delay charges on each of the motors, and a streamer inside of the booster airframe.

The streamer was attached to the booster airframe and the booster nose cone by a short length (approximately 18 inches) of Kevlar cord. The booster recovery system, after flight and deployment, is shown in Figure 5.20.



Figure 5.20: Booster Recovery System (Post-Flight)

For an unknown reason, the nose cones of two of the boosters came off of their respective airframes shortly after leaving the launch rail – causing the booster streamers to deploy. However, the

nose cones became separated shortly thereafter. The shock cord on the boosters was probably both too short, and because of its constant winding and unwinding, frayed. In the future, greater care should be taken to prevent fraying, and the shock cords should be significantly longer than 18 inches. However, lengthening the shock cord could potentially cause the streamers and shock cord to be tightly crammed into the booster airframe, reducing effectiveness of the recovery system unless more volume was allotted for the recovery system.

Additionally, it is possible that the pyrotechnic charges in the boosters were oversized. The booster is essentially a small model rocket with a very large motor; the oversized ejection charges of the G-class motors could have ejected the nose cones much more violently than anticipated.

5.3 Results and Analysis

Post Flight Observations

During the rocket's first and only flight, the recovery systems, both primary and secondary, failed to function. While we will never know for certain what happened during the rocket's flight, from video and analysis of the wreckage there are several possibilities about what may have led to the failure of the recovery system.

No Signal

It is possible though unlikely that the primary recovery system, the spring device, never received a signal from the flight computer. As the analysis of the flight states (Appendix R), there was slim possibility that both the primary flight computer and the secondary flight computer became disconnected in flight. This could have caused the recovery system to fail.

Device Failure

In light of the issues experienced the day before the rocket's flight, it is more likely that the primary recovery systems were in fact triggered by the flight computer but failed to function as designed. Any number of factors could have contributed to this:

- The lever may have been unable to disengage from the "piston bulkhead" due to friction, or the shock cord near the spring and lever could have become jammed between the spring and the lever.
- The "piston bulkhead" may have been released, and could have become bound on the shock cord or wiring that passed through it. While care was taken to allow enough room for the piston to slide freely, it still could have bound up during flight, or the shock cord could have become twisted and snared the piston.

- The shear pins could have been too strong, either by themselves or when coupled with the friction of the shock cord. Only one full test was performed with the shear pins, shock cord, and parachutes installed in the airframe; in the future, more full system tests should be performed before flying the rocket.
- The pyrotechnic charges did not fire. Sadly, the charge for the drogue parachute was set on a time delay, and would fire approximately 12 seconds after liftoff. Because the core motor did not light, the rocket impacted the ground near the 12 second mark. In the future, neither the main and backup computers should be set to a timer.

For an unknown reason, the nose cones of two of the boosters came off of their respective airframes shortly after leaving the launch rail – causing the booster streamers to deploy. However, the nose cones became separated shortly thereafter. The shock cord on the boosters was probably both too short, and because of its constant winding and unwinding, frayed. In the future, greater care should be taken to prevent fraying, and the shock cords should be significantly longer than 18 inches.

5.4 Conclusions

The goal of the recovery subsystem was to develop an innovative and reliable recovery system which would not utilize pyrotechnics. The spring device that was developed proved to be reliable and robust during ground-based testing. However, in flight, the spring recovery systems did not function.

While conceptually simple in both design and construction, a spring system has many inherent difficulties that must be addressed. Construction techniques, tools, and the available materials did not lend themselves well to precision and tight tolerances between the individual devices. Additionally, the spring systems were designed around the vehicle airframe, rather than the other way around. This led to a cramped assembly of the devices and associated components, which probably affected flight performance.

Overall, it can be concluded that a spring device does hold promise as a recovery actuation system for high powered rocketry, due to its reliable performance during ground testing. However, should this system be pursued in the future, consideration should be given to designing the rocket vehicle around the tested subsystem(s), rather than trying to fit the devices into a predetermined volume of fuselage. If stronger materials were used, although the overall weight of the rocket would increase, it would allow for a more powerful and robust device to be utilized. We thus concluded that future work would be necessary to fully develop the potential of a spring recovery system.

6. Propulsion and Aerodynamics

The purpose of any propulsion system is to produce thrust. Rocket motors typically use liquid or solid propellant to produce and accelerate gas therefore creating thrust. The resources to create a propulsion system for our project were limited. We were restricted to the use of commercially available model rocket motors designed by experienced manufacturers. In order to meet our goals and comply with National Association of Rocketry (NAR) standards it was decided that the use of medium impulse, solid propellant motors would be more than sufficient. These types of motors are reliable, safe, and commercially available to non-professional consumers.

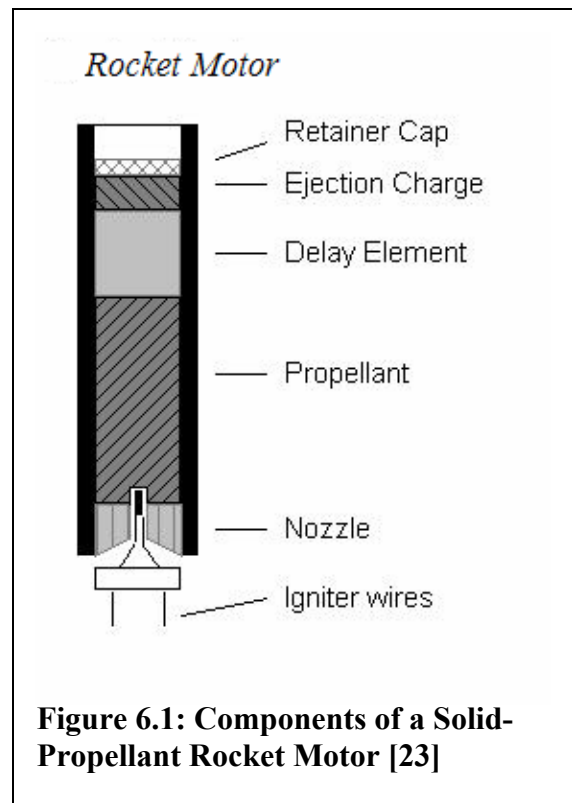
For the propulsion subsystem to it was important to specify project objectives to help organize the methods by which the objectives will be completed. The subsystem objectives were; stable flight pattern, to reach an altitude of 1500 feet, achieve simultaneous first stage ignition and achieve second stage ignition.

6.1 Propulsion Background

Motors

Most motors used today for model rocketry are made up of solid propellant. In solid propellants, both fuel and oxidizer are mixed and molded to a desired shape. Figure 6.1 shows the basic components of a solid-propellant model rocket motor.

Solid propellants are classified into one of two categories- homogeneous or composite. Homogeneous propellants come in either single based or double based propellants. Single based propellants only consist of one compound, usually Nitrocellulose that has both oxidation and reduction properties. Double based propellants consist of two compounds, typically nitrocellulose and nitroglycerine, along with a plasticizer to impart flexibility. The advantages of this type of propellant are that it reduces smoke, while increasing energy and burn time. [24]



Composite propellants are heterogeneous powders which use a crystallized or finely ground mineral salt as an oxidizer, which makes up between 60 to 90 percent of the propellant mass. The fuel is generally aluminum. A polymeric binder holds the propellant together, usually polyurethane or polybutadienes which is also consumed as fuel. Other compounds are sometimes added such as a catalyst to help increase the burn rate. [24]

Above the propellant is the time delay charge. The time delay charge is a slow burning solid-propellant that produces little gas and practically no thrust. The time delay allows the rocket to coast to apogee before deploying its recovery system. The time delay charge automatically activates the ejection charge, which pressurizes the inside of the airframe, expelling the nose cone and recovery system from the rocket. The nozzle is usually ceramic in order to withstand high temperatures. The smallest change in dimension to the nozzle can affect the performance of the motor.

Reloadable Motors

A reloadable motor is a motor designed to be used multiple times by inserting new propellant and replacing other expendable parts. The major reason reloadable motors were introduced to Model Rocketry was the low cost. Reloadable motors have a high initial cost, but are more cost effective in the long run. Most reloadable motors used today are in the high powered motor ranges. Large single use motors get to be expensive. [2]

Figure 6.2 shows all the components in a reloadable motor. A reloadable motor consists of an aluminum tube, forward closure and aft closure. The purpose of the aft closure is to hold the nozzle. The forward closure seals the other end and seals the time delay grain and ejection charge used for the recovery system. [25]

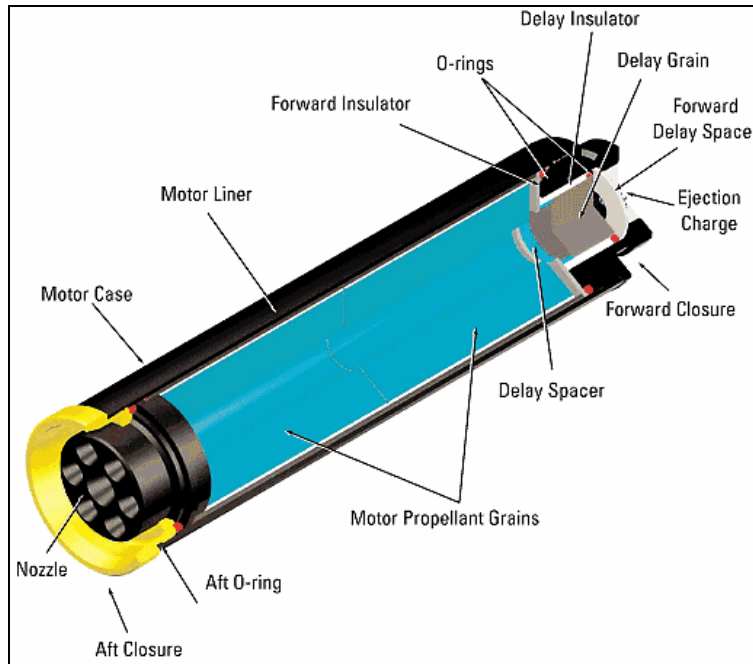


Figure 6.2: Components of a Reloadable Motor [25]

Reloadable motors only use composite solid-propellants. Each module of propellant comes incased in a cardboard tube. A cardboard or plastic insulator is inserted into the tube first, to keep the propellant from raising the external temperature of the casing beyond 200° C. This is also the same external temperature limit imposed on single use model rocket motors. [2]

Motor Code

The NAR has set up a code system to classify model rocket motors. A motor code consists of a letter and two numbers for example “B6-4”. The letter represents the total impulse in Newtons-second (N-s), which is average thrust multiplied by the total firing time. Table 6.1 shows the different motor classes and their total impulse ranges. Note that total impulse doubles each time the motors size goes up a class. Motors with higher total impulse then 160 Newton-seconds such as I and J type motors are referred to as high power motors. Certifications are required to purchase high powered motors. [2]

Type	Newton-Seconds
1/4 A	0.00 to 0.625
1/2 A	0.626 to 1.25
A	1.26 to 2.50
B	2.51 to 5.00
C	5.01 to 10.00
D	10.01 to 20.00
E	20.01 to 40.00
F	40.01 to 80.00
G	80.01 to 160.00
H	160.0 to 320.0
I	320.0 to 640.0
J	640.0 to 1280.0

Table 6.1: Motor Classes [2]

The first number in the code represents the average thrust in Newtons. Motors do not deliver a constant thrust over time, so the average thrust is measured. Lower average thrust motors have slow burning propellant. Additionally, the burn time of a motor can be estimated by dividing the total impulse in that class by the average thrust. [2]

The last number in the code is the time delay. It represents the number of seconds between the motor burn out and the activation of the ejection charge to deploy the recovery system. Since it is unsafe to release the recovery system while in mid-flight, the time delay allows the rocket to reach apogee before deploying its recovery system. [2]

6.2 Methodology

Our main project objective was to reach an altitude of 1500 ft. Through research and testing we were able to make an educated selection of motors to be used and construct a reliable ignition system.

6.2.1 Motor Selection

Limitations

Rocket motors can be dangerous and because this was the first time WPI has offered a project such as this and the need to guarantee safety, the project had some rigid motor size constraints. We were limited to G class motors. Higher powered motors require certifications from the NAR and unfortunately, not everyone in the MQP group was certified.

The total budget of approximately \$1200 gave our project another limitation. Therefore, motors and ignition system parts had to be cost effective. We also had to improvise for unexpected dilemmas such as commercially available parts not always being obtainable. The use of a G-80 reloadable motor would have given the rocket a higher average thrust. Unfortunately G-80 reloadable motors were not commercially available, only G-80 single use motors were.

Available Motors

The higher the total impulse of a motor, the easier it would be for us to reach our desired goal of 1500 feet. Limited to a total impulse maximum of 160 N-s per motor (G class motor), there was not much choice but to use type G motors.

The size of a rocket alters the flight performance for a given average thrust. The heavier the rocket the higher the average thrust should be. Looking at commercially available motors, an unexpected constraint arose; a G-64 was the highest average thrust reloadable motor available. Since the rocket was going to be launched more than once, using reloadable motors was more cost efficient. These considerations drove us to use a motor with an average thrust of 64 Newtons.

Clustering

To reach an altitude of 1500 feet, it was obvious that we would need more than a single G-64 motor. With the help of RockSim™, several vehicle-motor options were evaluated with different types of motor configurations. With an estimated maximum mass of 3400g, the simulations concluded that four G-64 motors would provide enough thrust to reach our desired altitude. Figure 6.3 shows different types of motor configurations for different numbers of motors.

Since the rocket was going to have a second stage, three different configurations were tested on RockSim consisting of series and parallel staging. The first configuration was set up in series that consisted of two motors on the first stage and two motors on the second stage. These stages would be set similar to the “2” (side by side) arrangement in Figure

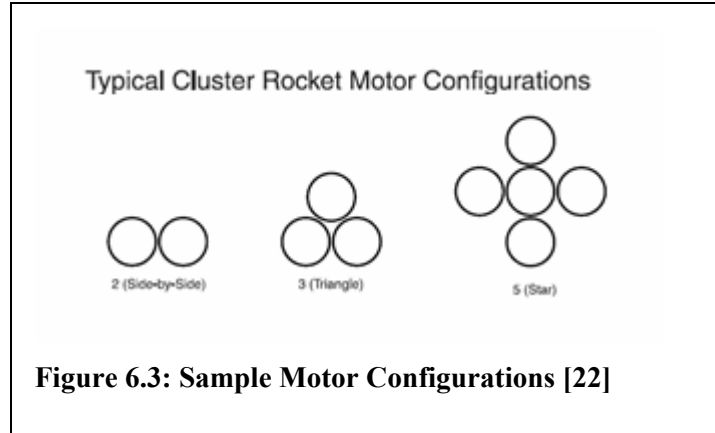


Figure 6.3: Sample Motor Configurations [22]

6.3. The second configuration was in series and consisted of three motors for the first stage and one motor for the second stage. The first stage of the second configuration would resemble the “3” (triangle) arrangement (Figure 6.3) and the second stage would just be a single mounted motor. The third configuration was in a parallel booster arrangement with three motors in the first stage and one in the second stage. The parallel configuration resembles the “5” (star) figure, with the exception of one less motor, and the motors being spaced equally (120 degree separation) around the airframe. With small differences, all three of the main configurations were suitable for reaching our desired altitude. See Appendix B for computer software simulations.

6.2.2 Hermes Rocket Design

Although we were limited to G-64 motors it was important for this project to be expandable. Future teams will certainly want to take this rocket higher and faster than the previous year. The foundations for expansion are laid out within this project, which will allow for forthcoming innovations and improvement. With this taken into consideration the propulsion team decided to use the booster staging configuration.

Boosters make the upgrading of motors more simple; instead of changing the dimensions of the airframe to fit bigger and higher class motors, booster airframes can easily be replaced to house a higher class motor. The main airframe limits how many motors one can fit inside, and also how the electronics, staging equipment, and recovery apparatus are configured. At this point in time, the use higher class motors are the most efficient way to increase the maximum altitude of the rocket. Therefore boosters provide a less expensive replacement solution, with easily mountable tubing and simpler recovery systems. Boosters will not need a dual-chute deployment system which can be costly. For the unique staging system that the WARRIORS rocket houses, boosters need to only replace one magnet, to refit to the main airframe. While an airframe change would require rework of the entire staging system that is housed within the main airframe.

6.2.3 Ignition

The Propulsion team was responsible for the ignition of the rocket motors. This included the first stage, consisting of three boosters, as well as a second stage ignition of a single motor. It was up to the Propulsion team to ensure that these ignitions were successful. Though ignition materials are by no means as expensive as other components of the rocket, it was important for the team to consider costs along with reliability of the ignition system. This section discusses the differences between commercially available and homemade igniters, the processes to select one, and the testing needed to ensure reliable ignition.

Commercially Available Igniters

The devices commonly used for ignition are an Electric Match (Ematch), shown in Figure 6.4, or an igniter. Electric Matches are intended for black powder motors and black powder charges within the rocket, such as ejection charges. Because black powder is very easy to light, Ematches utilize a quick electric charge sent through a highly conductive material. This burn will only last for a fraction of a

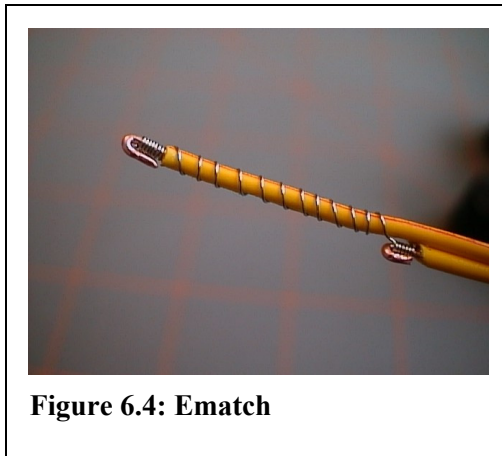


Figure 6.4: Ematch

second. Igniters however, utilize a different type of combustion. They are intended to burn at a higher temperature and for a longer duration (often up to 1 full second). These igniters will contain a type of accelerant such as pyrogen, which will be discussed in the following sections. Igniters are intended to light the composite propellant grain that commercially available motors are produced with. In comparison to one another, Ematches require less current than igniters do, which was an important factor for the propulsion team when determining

power sources. [Appendix L]

Igniters are readily available to the public. Many companies that offer motors, also supply igniters that either they produce themselves, or are supplied by a different manufacturer. The popular motors producer, *Aerotech*, often provides their *Copperhead* igniter with every motor purchase. [21] Igniter's such as these will vary in size just as motors do. They are made so that they fit within the nozzle of specific classes of motors. Commercially available igniters have been tested extensively by model rocket hobbyists.

In general, igniters will come pre-dipped with a pyrogen or equivalent compound already on their igniter. Pyrogen will be discussed in more detail in the next section, as it is more essential to understand

the use of pyrogen when making one's own igniters. The use of this compound does enhance the performance substantially.

Finally commercial igniters will cost on average one dollar per igniter. They are often sold in packs of 5, 10, and 20. Refer to Appendix L for cost comparisons of commercially available igniters that were considered during the early design phase.

Homemade Igniters

Another option for the propulsion team, with respect to igniters, was to produce our own igniters. Homemade igniters are created at a lower cost per igniter than purchasing pre-made igniters. Homemade igniters allow for the igniter to be augmented to better suit the application that the igniter is intended for.

Several standard procedures have been developed for non-professional construction of igniters. The first procedure is the solderless wrapped wire approach. This does not require the use of any soldering equipment. It requires wrapping a bridge wire between 2-lead copper wires. This bridge wire is often nichrome or tungsten. The resistance of the bridge will be determined on how much is used for each igniter and which material is used. A detailed guide for this process can be found in Appendix O.

The next procedure requires soldering equipment. Though it will still require a 2-lead copper ignition wire, the bridge is a solid plate. This plate would have one lead soldered to each side connecting the bridge. This process creates a smaller more pin-point heat source, but is just as effective as the wrapped method as long as the soldering was done correctly.

Both methods require the use of pyrogen. Commercially available igniters may come pre-dipped in pyrogen but this compound can also be purchased separately. It is highly recommended that one should purchase the compound or its components from a retailer unless they have adequate experience working with flammable materials.

Another method for ignition is the use of lower impulse propellant grain to ignite higher impulse propellant grain. The propellant grain from a smaller impulse motors, such as an A or B class motor, would be used to ignite the propellant grain from a higher impulse motor such as a J or K. Since it is much easier to ignite a lower impulse grain, the resultant combustion can be used as the match for a higher grain. These grains can be purchased from single use or reloadable kits (if available) and cut into



Figure 6.5: Igniter with Pyrogen Coating

strips. The cuts would be taken lengthwise along the propellant grain and into small but useable widths. These strips are then attached to the igniter. This process is not recommended for staging ignition, as igniting more layers of propellant will decrease the efficiency of the process (especially when one is looking for one motor ignition in the second stage). As mentioned before, safety precautions must be taken when augmenting any such propellant, additionally reading all safety and manufacturing warnings is quite necessary.

This section has covered the basics of assembling igniters. Though there are more advanced methods, or certainly more unique approaches, the propulsion team only considered the methods mentioned above. These techniques may seem quite simplistic by first glance, but have been proven reliable by the rocket community. It was important to explore these options to ensure a successful launch.

Tests of Homemade Igniters

Since the propulsion team decided to produce homemade igniters for the WARRIORS rocket, it was necessary to perform adequate testing of the igniters to ensure that they would indeed successfully launch the rocket. The task was to construct an experimental model, which can be used as a template for future tests, and to record appropriate data, which may or may not alter construction methods for the homemade igniters. Please refer to Appendix K for the experimental record document used.

Listed in Appendix K is the igniter test record sheet that the propulsion team used. It was written in easily readable and replicable format to allow for future experiments. The first experiment was conducted under the observation of Mr. Dave Messier, the WPI Safety Coordinator, and met the safety guidelines established by the WARRIORS team.

While the ignition setup is different between the two stages, the testing procedure was made to produce results for both stages. For the first stage, the ground stage, the team had to determine whether or not all igniters would light within a sufficient relative time (within in one second) of each other. This is to ensure that the rocket will be leaving the launch pad without asymmetric thrust. Asymmetric thrust in this case is produced when the thrusting force of the rocket motors forces the rocket towards a horizontal angle of attack. Since the power supply used for first stage ignition is not limited to a confined area within the rocket, this will not be a factor in determining the adequacy of the igniters for the first stage. The consistency of the construction methods is a key factor that was looked at.

For the second stage the propulsion team had to determine the voltage and current needed to light the second stage motor. This power is to be supplied by the flight computer, which is limited to a confined area. This constrained the power source to a smaller size. These igniters must have the smallest amount of resistance possible, while dissipating enough thermal energy to ignite the motor grain.

6.3 Results and Analysis

6.3.1 Ignition Tests

Initial Igniter Testing

The first test run by the team was to determine the voltage and current needed to fire the homemade igniters for second stage ignition. The results are presented in Table 6.2 for each voltage tested.

Current (mA)	Voltage Actual (w/ R_{ig}) V	Voltage Required (w/ R_{ig} and R_c) V	Test 1	Test 2	Test 3	
400	1.72	1.8	Fail	-	-	
750	3.23	3.375	Fail	-	-	
1000	4.3	4.5	Fail	-	-	
1500	6.45	6.75	Fail	Fail	Fail	
2000	8.6	9	Pass	Pass	Pass	≈ 1 sec
2667	11.5	12	Pass	Pass	Pass	< 1 sec

$R_{ig} = 4.3$
$R_c = 0.02$

Table 6.2: Second Stage Ignition results

From these results we concluded that 9 V would be adequate to produce enough current for reliable ignition within one second. A 12 V supply resulted in almost instantaneous firing. This gave the flight computer and avionics team an accurate range to decide the type of power supply to be fitted into the rocket.

The next test conducted to help ensure a reliable second stage ignition was lighting the igniters with the flight computer and recommend power source. A second round of igniters were made for this test, utilizing the same method of igniter construction. From this we were able to determine that the power source was adequate to produce a reliable ignition, characterized by maximum of one second ignition from the time the flight computer applied the voltage. From this test, we also determined that the igniters could use less nichrome wire, reducing resistance and decreasing the time to combustion to much less than one second.

The remaining test conducted was for first stage ignition. The power supply used was a car battery pack. With a fully charged pack, this produces an almost instantaneous ignition for a single igniter. However in this test, three igniters are wired in parallel. This results in approximately 6 A of

current draw, 2 A per igniter. The main purpose of this test was to evaluate the consistency of igniter construction so that each igniter would fire within one second relative to one another. The one second time to ignition was established as the largest allowable ignition mismatch for the rocket to have the an acceptable amount of asymmetric thrust leaving the launch pad. Data from this series of tests conducted are presented in Appendix O.

Continued First Stage Testing

More conclusive testing was necessary to assess the reliability of the first stage ignition. The launch control system is able to produce 24 V or 12 V with essentially no current limit. This is unlike the initial first stage ignition test that used a current controlled power supply. The construction resulted in a resistance of 2 Ohms for igniters. It was brought to our attention that this resistance is actually for the 6 A of current drawn from a 12 V and far below what the nichrome can handle from 24 V. Nichrome wire has a resistance of only 17.01 Ohms per foot according to factory information.

The launch system was used in this test to represent its use on launch day. Utilizing the 24 V power source, three igniters were connected in parallel to simulate booster ignition. These igniters have 2 Ohms of resistance per igniter. The launch system audibly signals continuity through the circuit indicating a good connection. When the controller was activated to send the charge, the nichrome erupted almost instantaneously. However, the nichrome discharged so fast, and lost continuity as a result, that it failed to ignite the pyrogen dip. This test was repeated three times at 24 V and three more times at 12 V. Each time, even at the lower voltage, the igniter failed to light the pyrogen and in two cases discharged the pyrogen off the tip of the igniter unlit.

The results of this testing changed our thought process. The second stage ignition requires a lower resistance, as only a maximum of 9 V is available from the power source. This provided the desired results of one second ignition for the second stage. However, we have concluded that nichrome is overloaded when 12 V is passed through it. As a result another set of igniters were produced. These igniters had 4 Ohms of resistance. To double the resistance required that each first stage igniter be wrapped twice as many times as the second stage igniters. These igniters were then tested with the same setup as mentioned above. The tests confirmed that the pyrogen dip was ignited within the one second time frame. The three igniters were also lit within one second of each other, fulfilling the other requirement set by the Propulsion team. Therefore it was concluded that the igniters for the launch day would be produced to have a resistance of 4 Ohms.

6.3.3 Launch

Performance Evaluation

For the first launch of the WARRIORS Rocket, the rocket itself was subject to scrutiny by the entire team. During this flight there were factors that determined whether or not the flight was considered a success from the propulsion subsystem team. The performance of the rocket was highly dependent on the motors used and the ignition methods used for launch. There were two main areas that the propulsion team monitored for success: first stage ignition and second stage ignition.

First stage ignition was perhaps the first and most important phase of the launch that needed to be monitored. For most rockets success and failure are easily determined. Did the motor light or did it not? However in the first stage of this rocket, three boosters were fired simultaneously. This means that more questions than just “Did the motors light?” needed to be answered for the ground stage to be considered a success. These questions are listed below:

- Did all motors light?
- Did all motors light at the same time or within the 1 second between first and last to light?
- Did the rocket leave the launch rod with little to no degree of asymmetrical thrust?

If any of these questions were answered “No” the first stage ignition would be considered a failure. The reasoning behind this was: all motors must ignite at the same time during liftoff. Asymmetric thrust could, and more than likely would, cause the rest of the flight to be catastrophic. During the launch, video was taken from multiple angles and throughout the complete flight. We were able to focus on the video playback of the first stage ignition, slowed the video feed down to a frame by frame view in order to find the answers to the above questions provided.

The second area of evaluate was the second stage ignition, which consisted of the single motor main motor. There are not as many factors in determining success or failure but they were just as important as for the first stage. The questions to be answered here were:

- Did the second stage motor fire within a reasonable time (one second) of the charge being sent by the flight computer?
- If question 1 was answered “no”, did the rocket reach its minimum altitude?

If the answer was “No” for the second question, then this area was considered a failure. This quick transition was necessary for the rocket to be able to achieve one of its goals: to reach an altitude minimum of 1500 feet. A long delay would drastically slow down the rocket in which case the second

stage will not provide the necessary power to reach the height of 1500 feet. Data from the flight computer and altimeter was to be downloaded to determine the final altitude. Video playback was to be analyzed for visual confirmation that the second stage did indeed light and frame by frame analysis was to be used to determine the time factor mentioned in the second set of questions.

From these success and failure criteria the propulsion subsystem was to analyze the rocket's performance since there was a very small margin for error. The construction procedures, power supply, assembly of motors, and ignition units all needed to be reevaluated if a failure occurred. Should a failure occur in either the first or second area, or both, the launch for the propulsion for subsystem would be considered a failure. The answers to these questions are presented in Section 6.4.2.

6.4 Conclusions

6.4.1 Homemade vs. Commercial

Homemade and commercial igniters were discussed in Section 6.2.3. The propulsion subsystem team weighed the advantages and disadvantages to decide which approach we wanted to take for ignition. It was decided that the team would make its own igniters from purchased materials.

This decision was based on a couple of points. First was that it would save the team money. While most pre-made commercial igniters go for about one dollar per igniter, the team has been able to purchase the supplies and construct igniters to roughly ten cents per igniter. Though these costs are minor in comparison to other sections of the rocket construction, the management of the costs was certainly a desired outcome. Furthermore, when homemade igniters are produced correctly, they provide effectiveness equivalent to that of a commercial products.

The decision to produce the homemade igniters defined the testing to be done by the propulsion team. This was to ensure that these igniters would be adequate for the launch, as well as determining the requirements needed for ignition. The commercial recommendations can be used to evaluate how our igniters would perform in comparison to commercially produced igniter, but the igniters produced would be tailored to our specific power, size, and performance needs.

6.4.2 Launch Analysis

Flight Analysis

The WARRIORS rocket was able to liftoff on Thursday April 7th at dusk. The launch was completely recorded on video to ensure an accurate analysis of the flight performance questions that were proposed in section 6.3.3. The playbacks of the recordings were adequate in determining the success or failure of the ignition and propulsion systems. These analyses were for both first and second stage of the rocket flight. The first stage of flight, the ground ignition stage, was considered a success by the propulsion team by meeting the following requirements:

- All three of the first stage motors lit
- All three motors lit within the 1 second time limit, relative to one another
- The rocket did not leave the rail at an angle denoting asymmetric thrust

The second stage of flight, however, was deemed a failure by the propulsion team, because the second stage single motor did not light.

These results answered the questions listed in the previous section, 6.3.3. In the following section a more in-depth analysis is given with regards to the success and failure, along with recommendations.

Post-Flight Analysis

Though the first stage of the rocket flight was considered a success, it was not 100 percent perfect. As seen in Figure 6.6 from the camera positioned to record the first stage ignition, all the motors did indeed light, but not exactly at the same time. Two of the three motors did light simultaneously. The third motor, seen in the foreground did not light until momentarily after the first two. It did indeed light before the aft end of the rocket left the view frame of the camera. This is conclusive that the third motor did indeed light within the 1 second ignition margin that the propulsion team allowed. This 1 second was the time from when the first motor lit, to the time the last motor was lit.

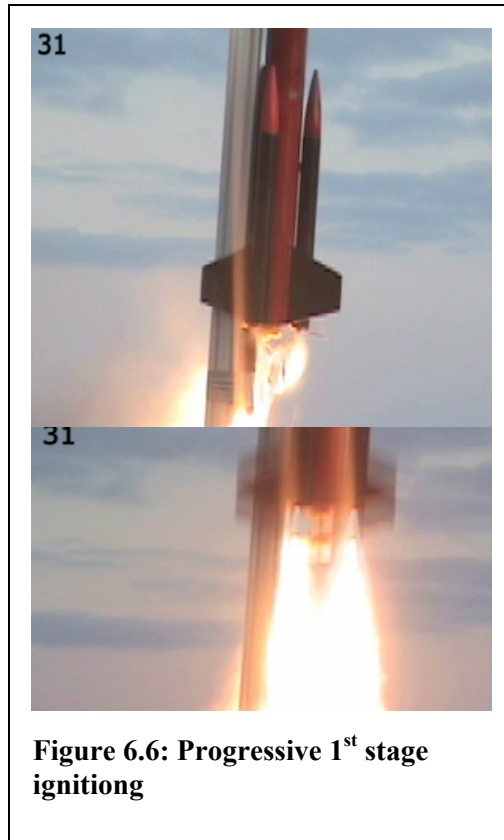


Figure 6.6: Progressive 1st stage ignition

The rocket accelerated rather quickly with just two motors igniting. The delay was minimal; however it was taken into consideration that if the third motor did not light until after 1 second delay, the rocket leaving the rail would indeed have asymmetric thrust. This has a great potential to be a catastrophic event. It is our recommendation, that the maximum allowable delay time for multiple motor ignitions be lowered from 1 second. A more appropriate time delay of 0.5 second as the maximum time delay would substantially decrease the chance of failure if that requirement was met.

The rocket then accelerated off the launch rail without incident. It left the rail without any indication of asymmetric thrust produced by the rocket as confirmed in Fig 6.8.



Figure 6.7: Rocket clearing the launch pad

After the rocket reached burnout of the first stage the second stage was suppose to light. After a several second delay it did not light however. During the flight and even after reviewing the flight recordings there was no indication that the ignition of the second stage occurred. This brought about further discussion of why this had happened. As at the time of this writing the exact cause of the failure of the second stage ignition is unknown but a few plausible reasons have been considered:

- The flight computer lost power during the booster stage of the flight resulting in zero voltage being applied to the igniter.
- The connection located at the aft end of the rocket, that connected the igniter to the power source, was faulty, or possibly disconnected during the initial liftoff.
- The voltage was applied the igniter, however the added resistance of the wiring located between the avionics bay and the aft end of the rocket, was too high for the igniter to light.
- The battery voltage was too low to activate the igniter and light the core motor.

Any of these reasons would prevent the second stage from igniting. It is also possible that it could have been a combination of failures that occurred.

One final analysis of the rocket flight with respect to the propulsion system was the separation of boosters at their burnout. Two out of the three boosters were jettisoned from the rocket. However the third booster remained attached to the aft end of the rocket in its original position. This was the same booster that was ignited slightly after the other two boosters. Though this may not have affected the end result, this booster continued to thrust after the other boosters were separated. This thrust is believed the cause of the booster remaining attached to the airframe. The design of the booster connection to the

airframe was intended to keep a thrusting booster from separating. Plausible reasons behind the additional thrust of the attached booster were:

- Small leakage between O-ring seals, which would cause a small amount of pressure leakage and a longer burn.
- The propellant grain was manufactured with a difference in grain size, in this case more grain, than the other grains that were used in the other boosters.
- The fractional difference in the third booster ignition, provided an offset time for burnout. The third booster burnout would occur after the staging separation was triggered.

These are possible explanations for why the booster remained thrusting after separation was triggered. There is not enough evidence however, to support which of these was the cause, and the end result was in no way detrimental to the remainder of the flight.

In conclusion of the flight analysis, the first stage of the flight was a success. The second stage of flight was not a success as the center motor did not fire. This failure, as the case with the non-separating booster, was inconsequential and unattached to subsequent failures.

6.5 Aerodynamics

Aerodynamic forces exerted on the rocket needed to be understood for this rocket to have a successful flight. Aerodynamics is a branch of fluid dynamics concerned with gas flows. The study of this gas flow over various bodies and the forces and moments created during the process is called aerodynamics [2]

6.5.1 Aerodynamic Background

Static Stability

After leaving the launch rod a rocket becomes a free body in space. Aerodynamics forces acting on the rocket can cause it to move in eight different ways. Figure 6.8 shows the eight different movements or degrees of freedom. Any motion during flight can be reduced to a combination of one or more of the basic motions shown in Figure 6.8 [2]

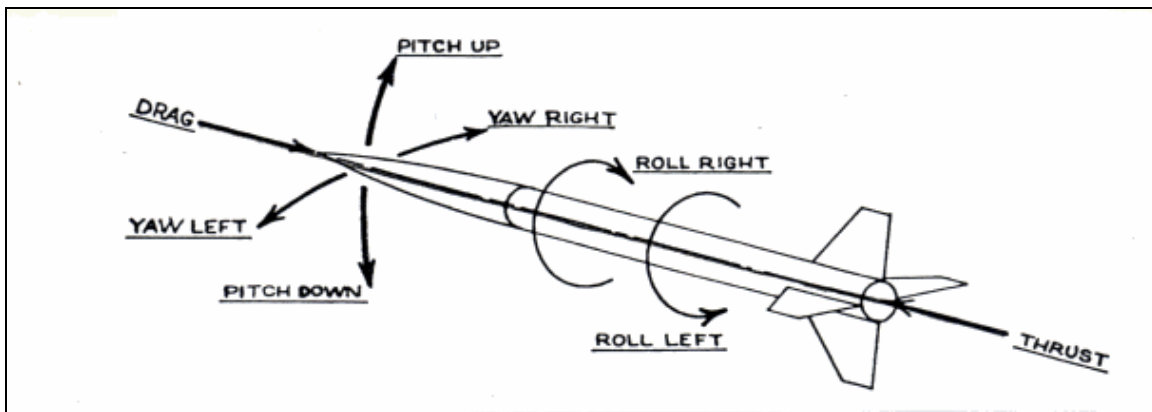


Figure 6.8: Eight Degrees of Freedom [2]

Thrust is meant to overcome the weight of the rocket, moving it upward. This force comes from the rocket's motors. Drag is the aerodynamic force of the air acting on the rocket. The direction of the drag force is always opposes the thrust force, attempting to slow down the rocket. Drag and thrust are linear forces; producing motions in a straight line called translational motion. [2]

Pitch is the up or down motion of the nose. Yaw is the left or right motion of the nose. Roll is the left or right rotational motion of the rocket along its long axis. A rotational axis is an imaginary line from which a body spins around. Figure 6.8 shows the rotational axis of a model rocket; starting at the tip of the nose to the nozzle of the motor. Yaw, pitch and roll all describe rotational motion. [2]

A body rotates around an imaginary point, where all the weight of the object can be considered to be concentrated. This is a balanced point called the center of gravity or CG. A rocket in flight will rotate around its CG in the pitch, yaw and roll axes. [2]

As a rocket flies through the air, aerodynamics forces act on all parts of the rocket. The aerodynamic forces are a result of pressure variations around the surface of the rocket. In the same way that the weight of the rocket can be considered to be concentrated at the CG, the air pressure forces act through a single point called the center of pressure or CP. [2]

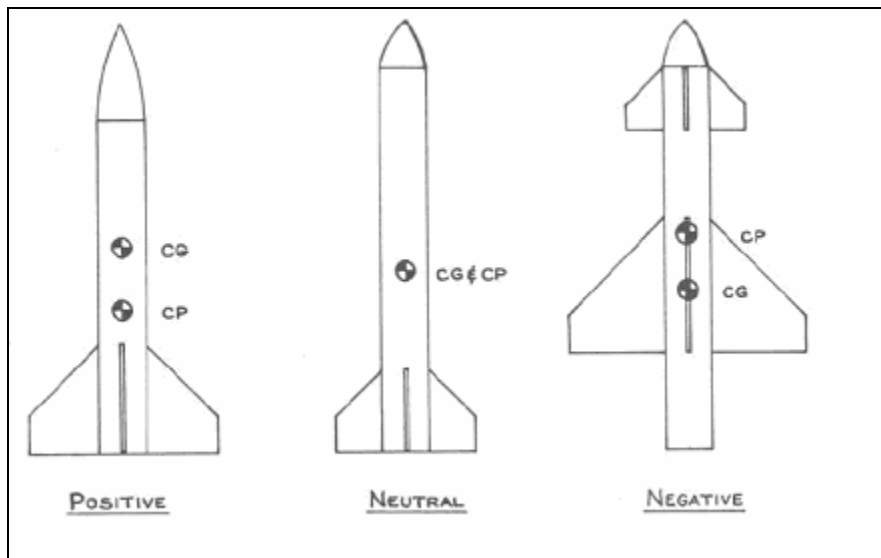


Figure 6.9: Three stability conditions with CG-CP relationships [2]

The location of the CP and the CG are important in determining a model rocket's stability. There are basically three stability conditions for a model rocket. Figure 6.9 shows the three different stability conditions. As defined in "Handbook of Model Rocketry" [2] they are

1. *Positive stability*, where in a model rocket the CG is ahead of the CP. It has large fins set far back on the body tube. It will fly straight when launched and will weathercock into the wind at launch.
2. *Neutral stability*, where the CP and CG lie at the same location on the model. This might be caused by lightweight nose or by fins that are too small, or both. There are no stabilizing and restoring forces present in the model during flight. It's free to wander anywhere in the sky, and some of its wanderings may be wild and certainly unpredictable. It may become stable or unstable at any moment because of the burnoff of the propellant, then it might keep right on going in the direction it happens to be pointed at that instant.
3. *Negative stability*, where the CG lies behind the CP. In this case, the aerodynamics forces on the fins try to make the model fly tail-first, pitch or yaw after leaving the launch rod, a force exists to

keep it swinging. The unstable model usually pinwheels end over end and winds up going nowhere except to flop to the ground.

Dynamic Stability

A stable rocket that is disturbed from its flight path normally swings back and forth returning to its original flight path. This oscillation occurs about its center of gravity. The damping ratio is a measurement of how well and how fast it returns to its original flight path. Figure 6.10 shows a well-damped design and an under-damped design.

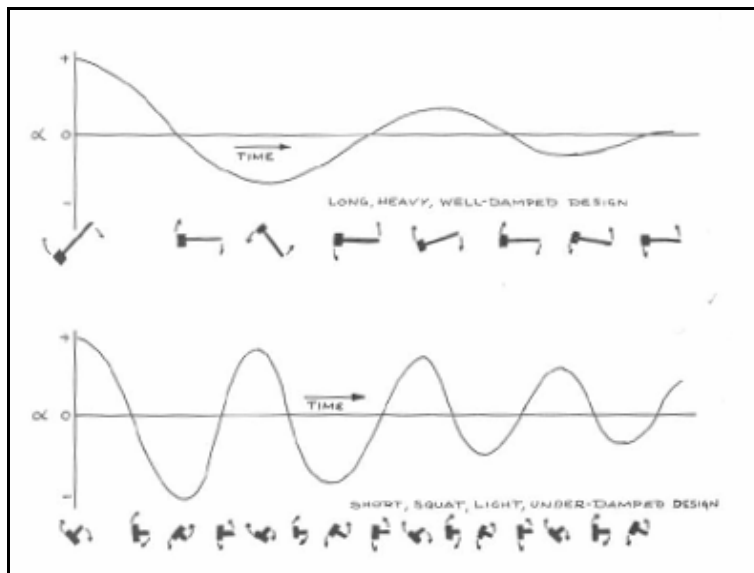


Figure 6.10: Well-Damped and Under-Damped Model Rocket Design [2]

Dynamic stability of a rocket is related to how it reacts to wind disturbances. The difference between static stability and dynamic stability is that of balancing a nonmoving device versus a moving one. A rocket might be statically stable with its CP and CG in the proper location but dynamically unstable during flight. As stated in “Hand Book of Model Rocketry” [2], several kinds of dynamic stability problems are:

1. A *statically stable but dynamically undamped model*. This is represented by the short, squat, fat little rocket model that wobbles excessively as it flies.
2. A *statically stable but dynamically unstable model*. In this model, the CP and the CG may be properly located with respect to one another, but the model is too heavy and has fins that are too small. These small fins, while creating a statically stable model with a CP behind the CG, are too small to produce enough restoring force to return the model quickly to zero angle of attack. They

aren't large enough to overcome the turning momentum of the model. By the time the small fins can create sufficient restoring force, the model is doing something else.

3. *A statically stable but dynamically overdamped model.* In this condition, the model might have a long, skinny body with fins that are far too large. When the model weathercocks or rotates in the pitch-yaw axes, the fins produce too much restoring force and stabilize the model too quickly, causing it to fly as if it were almost neutrally stable.
4. *A model with pitch-roll coupling.* This is a weird form of instability that can really frustrate you if you don't know about it. In this situation, the model has some roll that's induced by the fin, nose, or motor misalignments. At some point in the flight, the frequency of the roll becomes the same as the frequency of the motion back and forth in the pitch-yaw axes. The model will start to exhibit a coning motion where it spins about the roll axis at the same time that it begins to rotate in both pitch and yaw about the CG. The model can become completely unstable as it rolls madly around its long axis and spins horizontally end over end, going nowhere. The problem of pitch-roll coupling occurs in full-scale fin-stabilized rockets.

6.5.2 Our Experiment

The aerodynamic stability of the WARRIORS rocket is an important factor of the flight performance. Simulation of the rocket in flight is a helpful asset, so that the team has an opportunity to visualize the flight as well as correct possible errors before the launch. A scale model of the rocket was constructed. The actual rocket was too large to fit within the test section of a wind tunnel. This model is downsized by a scale of 2.01574. The mass distribution has also been scaled down by the same factor and placed within the appropriate sections of the model. The model will need to be very accurate to simulate the behavior of the full size rocket in flight.

The intent was for the model to experience atmospheric flight conditions within the wind tunnel. The main concern was that the rocket will be diverted by a strong cross wind. This cross wind may occur at the key points during the rocket's ascent. As the rocket leaves the rail and approaches its maximum velocity it is quite susceptible to being diverted from its course by a heavy wind. The WARRIORS rocket was deemed overstable by preliminary calculations. From these calculations, if a strong wind occurred, the rocket would face into the wind, like a weathervane. The test in the wind tunnel was to evaluate whether the rocket was overstable and to also assess possible flight characteristics.

In the proposed test, a stand would be fitted into the test section of the wind tunnel. This stand would be fashioned so that the rocket can pitch up or pitch down. This is to test the simplest of disturbances in the confined area within the test section. A rod, fitted to two frictionless bearings, one at

either end, would be used to allow the model to pitch. This rod would be attached to support legs on either side of the test section that are strong enough to withstand the force produced by the tunnels wind speed but small enough to not disrupt the flow on the model.

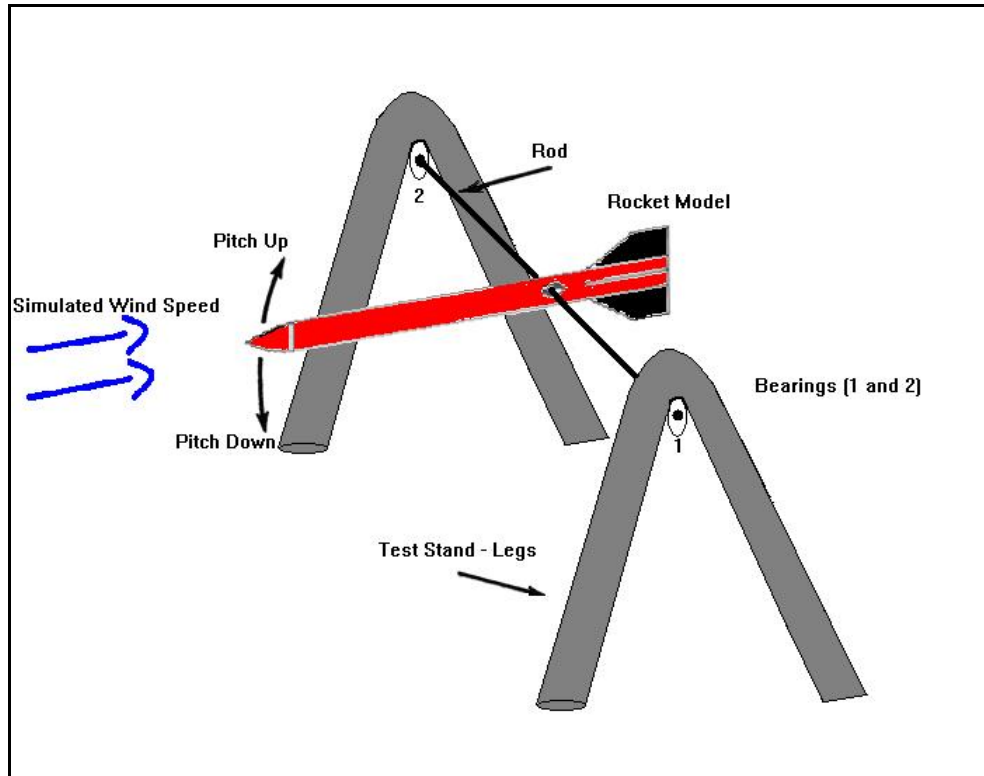


Figure 6.11: Experimental Wind Tunnel Model Apparatus (not to scale)

Ideally, the speed in the wind tunnel simulates the velocity of the rocket. The theoretical launch velocities calculated in RockSim, at different altitudes during the flight, will be used to set the speed of the wind tunnel. As the wind tunnel velocity approaches the designated value, the rocket position will be disturbed by an “arm” (a thin rod). This arm is the representation of the crosswind. The rocket will pitch upwards. The geometry of the fins and the moment of the rocket should cause the rocket to correct itself.

This motion would be recorded by a digital camera along with the readout from a potentiometer attached to the rotating bar of the test stand. The potentiometer will be calibrated to associate a given voltage value to an angle of attack. The pitching motion will be recorded for the length of time until the vehicle stabilizes, i.e. returns to zero angle of attack, or fails by not returning. The desired data would be a plot of angle-of-attack versus time. This type of perturbing force experiment best simulates a “gust” of wind.

From these recordings the team would need to interpret the data to assess stability. The maximum and minimum deflection angles before stabilizing at zero angle of attack will be recorded.

Specifically the maximum angle will be observed. In each of these tests, what happens after the maximum angle is reached will be observed. It may be that the rocket does not correct itself at all. This would imply that for the given flight velocity, the perturbing force was too great for the rocket to stabilize. These are preliminary ideas as to what could happen to the model. These types of tests, performed multiple times, would help the team estimate flight characteristics of the full-sized vehicle. Unfortunately these ideas and tests were unable to be completed. Due to time constraints and the completion of the school year, only theoretical and experimental designs were produced.

7. References

1. National Association of Rocketry [homepage on Internet]. Marion (IA): Model Rocket Safety Code; c2002- [updated 2005 Dec 1; cited 2005 5 Dec]. Available from: <http://nar.org/NARmrsc.html>
2. Stine GH, Stine B. Handbook of Model Rocketry. 7th ed. Hoboken (NJ): John Wiley & Sons, Inc.; 2004.
3. Giant Leap Rocketry [homepage on the Internet]. Baton Rouge (LA): Giant Leap Rocketry High Power Rocketry Materials; c1998-2005 [cited 2005 Oct 15]. Available from: <http://www.giantleaprocketry.com/hpdefault.asp>
4. Chang, SI. Space Launch Vehicle Reliability. The Aerospace Corporation. 2005. Online. Available: <http://www.aero.org/publications/crosslink/winter2001/03.html>
5. Sutton GP. Rocket Propulsion Elements. 7th ed. New York. John Wiley and Sons, Inc. 2000.
6. Simmons, FS. Rocket Exhaust Plume Phenomenology. The Aerospace Corporation. 2005. Online. Available: <http://www.aero.org/publications/simmons/simmons-1.html>
7. How Multi-Stage Model Rockets Work. Apogee Rockets, Inc. Colorado Springs. 2006. Available from: http://www.apogeerockets.com/education/how_to_multi-stage.asp
8. Staging Systems. Public Missiles Ltd. 2003. Online. Available: <https://secure.consumersinterest.com/pml/components.asp?groupid=6180110241450>
9. Graham GD. Magnet and Magnetism. Encyclopedia Americana. 2006. Online. Available: <http://go.grolier.com/>
10. Permanent Magnet Products. Stanford Magnets Company. 2005. Online. Available: <http://www.stanfordmagnets.com/magnet.html>
11. Permanent Magnet Design Guidelines. Magnet Sales and Manufacturing Company, Inc. 2000. Online. Available: http://www.magnetsales.com/Design/DesignG_frames/frame_dgbod2.htm
12. Clausert H, Wiesemann G. Grundgebiete der Elektrotechnik 1. 7. Auflage. Munich: Oldenburg Wissenschaftsverlag GmbH; 1999.
13. Clausert H, Wiesemann G. Grundlagen der Elektrotechnik 2. 7. Auflage. Munich: Oldenburg Wissenschaftsverlag GmbH; 2000.
14. GWiz Partners. Inc. Los Gatos. 2006. Available from: <http://www.gwiz-partners.com/>
15. Isermann R. Mechatronische Systeme. 1. korrigierter Nachdruck. Berlin: Springer Verlag; 1999.
16. P Series Aerogel Supercapacitors: PowerStor. Cooper Bussmann through Digikey. Theif River Falls. 2006. Available from: <http://www.digikey.com/>

17. EX Series Electrolytic Capacitors. Solen Online. St-Hubert. 2006. Available from:
<http://www.solen.ca/caps/ex.htm>
18. Pfeiffer W. Simulation von Meßschaltungen. Berlin: Springer Verlag; 1994.
19. Moskowitz LR. Permanent Magnet Design and Application Handbook. 2nd ed. Florida: Krieger Publishing Company; 1995.
20. Magnetic Sensor Systems Low Profile Push Solenoid, Van Nuys, (CA) c:2002: Available from: <http://www.magneticsensorsystems.com/solenoid/lowprofile/S-66-100.asp>
21. Aerotech Rocketry [Homepage on Internet]. Aerotech Rocketry; Las Vegas (NV) c:1982-2005 [cited 2006 Jan 29] Available from: <http://www.aerotech-rocketry.com/>
22. ROCstock.org [homepage on the Internet], Sosnow, Hyam R: c: 1995-2006 [cited 2005 Sept Available from: <http://www.rocstock.org/wizards/clusterwizard.pdf>
23. Space Exploration [homepage on Internet]. New Berlin (WI): Space Exploration Merit Badge; c2005- [updated 2005 Oct 16; cited 2006 Nov 05]. Available from:
<http://www.rocketcentral.org/motortech.htm>
24. The Encyclopedia of Astrobiology, Astronomy, and Spaceflight [homepage on Internet]. The Worlds of David Darling; c 2003 [cited 2006 Jan 16]. Available from:
http://www.daviddarling.info/encyclopedia/S/solid_propellant.html
25. Rocket central.org [homepage on Internet]. Cedar City (UT): Rocket Central.org; c 2003 [cited 2006 Feb 23]. Available from: <http://www.rocketcentral.org/motortech.htm>
26. Mandell GK, Caporaso GJ, Bengen WP. Topics in Advanced Model Rocketry. Cambridge (MA): The MIT Press; 1973.

Appendix A: Initial Designs and Evaluation

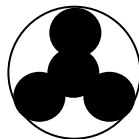
Configuration Comparison

Configuration A



Part	Phenolic		Phenolic w/ FG		Price	Misc.
	Dimension	Unit	Dimension	Unit		
Body Tube Dia.	65	mm	2.559	in		
BT Length	2.835	mm	2.835	mm		
BT Weight	583.846	g	906.389	g		
# of G- Motors	3	qty	3	qty	\$ 44.97	G20-7, Ellis
G Motor Weight	340.194	g	340.194	g		
Recovery	250	g	250	g		
Staging	150	g	150	g		
Computer	100	g	100	g		
Payload	100	g	100	g		
Nose	132.517	g	132.517	g	\$ 15.70	Intelli-cone
Fins Front	109.236	g	109.236	g	\$ 18.00	FIN-B-06
Fins Back	258.86	g	258.86	g	\$ 32.52	FIN-C-06
Bulkhead	40.722	g	40.722	g	\$ 3.90	BA2.14- LOC
Center Rings	7.229	g	7.229	g	\$ 2.26	CR-2.1-1.5
Rail Lugs	15.688	g	15.688	g	\$ 4.95	LRL-10-2-2
Motor Mounts	45.153	g	45.153	g	\$ 19.75	MMA3 Adapter/ MMT1.14 (3)
Epoxy	25.75	g	25.75	g	\$ 21.98	Slow and Quick Cure
Total	2159.195	g	2481.738	g	\$164.03	(Phenolic only)

Configuration B



Part	Phenolic		Phenolic w/ FG		Price	Misc.
	Dimension	Unit	Dimension	Unit		
Body Tube Dia.	65	mm	2.559	in		
BT Length	2.835	mm	2.835	mm		
BT Weight	493.282	g	793.787	g		
# of G- Motors	5	qty	5	qty	\$ 74.95	G20-7, Ellis
G Motor Weight	566.99	g	566.99	g		
Recovery	250	g	250	g		
Staging	150	g	150	g		
Computer	100	g	100	g		
Payload	100	g	100	g		
Nose	132.517	g	132.517	g	\$ 15.70	Intelli-cone
Fins Front	109.236	g	109.236	g	\$ 18.00	FIN-B-06
Fins Back	258.86	g	258.86	g	\$ 32.52	FIN-C-06
Bulkhead	13.574	g	13.574	g	\$ 3.90	BA2.14- LOC
Center Rings	7.229	g	7.229	g	\$ 2.26	CR-2.1-1.5
Rail Lugs	15.688	g	15.688	g	\$ 4.95	LRL-10-2-2
Motor Mounts	75.255	g	75.255	g	\$ 28.75	MMA3 Adapter/ MMT1.14 (5)
Epoxy	25.75	g	25.75	g	\$ 21.98	Slow and Quick Cure
Total	2298.381	g	2598.886	g	\$203.01	(Phenolic only)

APPENDIX B: Rocket Design Data

Vehicle Name: Fahrfinugen	Date:9.17.05	Version: Two
----------------------------------	---------------------	---------------------

Vehicle Design Parameters		
Subsystem/ Payload Mass		
Recovery Initiation Device Mass Estimate	0.25	kg
Staging Separation Device Mass Estimate	0.15	kg
Flight Computer Mass Estimate	0.09	kg
Camera/ Misc Payload Mass Estimate	0.2	kg
Total Subsystem/ Payload Mass Estimate	0.69	kg
Airframe Diameter	65-76	mm
Staging Type	Parallel	
Part Materials and/or Manufacturers	PML	
Length		
Motor Mount(s) Length	0.35	m
Staging Separation Device Length	0.06	m
Recovery Initiation Device Length	0.076	m
Flight Computer Length	0.127	m
Camera/ Misc Payload Length	0.203	m
Parachute(s)/ Recovery Hardware Length	0.7	m
Margin (%)	10	
Total Airframe Length Estimate	1.668	m
Empty Mass		
Computed Airframe Mass	0.813	kg
Computed Airframe Coupler Mass	0.11	kg
Computed Nose Cone Mass	0.16	kg
Computed Centering Ring Mass	0.026	kg
Computed Bulkhead Mass	0.091	kg
Computed Fin Mass	0.26	kg
Computed Parachute Mass	0.127	kg
Computed Piston System Mass	0	kg
Computed Recovery Hardware Mass	0.1	kg
Computed Epoxy/ Paint Mass	0.15	kg
Margin (%)	5	
Motor Type/ Configuration	3xG40, 1xG40	
Computed Motor Mount Mass	0.06	kg
Total Empty Mass Estimate	2.682	kg

Performance and Flight Analysis		
Maximum Altitude	2098	ft
Maximum Velocity	261	ft/s
Maximum Acceleration	5.43	Gs
Time to Apogee	13.11	s
Launch Rail Exit Velocity	46.3	ft/s
Static Drag Coefficient (1 Stage)	0.85	
Static Drag Coefficient (2 Stage)	0.55	
Stability Margin (1 Stage)	N/A	
Stability Margin (2 Stage)	N/A	

Notes or Additional Performance Metrics
1. Static Drag Coefficients were assumed
2. Simulation was done with CompuRoc.
3. Effective Diameter was assumed to be 9.4cm on the first stage.

Vehicle Name: Not Too Shabby	Date:9.18.05	Version: One
-------------------------------------	---------------------	---------------------

Vehicle Design Parameters		
Subsystem/ Payload Mass		
Recovery Initiation Device Mass Estimate	0.25	kg
Staging Separation Device Mass Estimate	0.15	kg
Flight Computer Mass Estimate	0.09	kg
Camera/ Misc Payload Mass Estimate	0.2	kg
Total Subsystem/ Payload Mass Estimate	0.69	kg
Airframe Diameter	76	mm
Staging Type	Series	
Part Materials and/or Manufacturers	PML	
Length		
Motor Mount(s) Length	0.7	m
Staging Separation Device Length	0.05	m
Recovery Initiation Device Length	0.06	m
Flight Computer Length	0.127	m
Camera/ Misc Payload Length	0.127	m
Parachute(s)/ Recovery Hardware Length	0.51	m
Margin (%)	10	
Total Airframe Length Estimate	1.731	m
Empty Mass		
Computed Airframe Mass	0.65	kg
Computed Airframe Coupler Mass	0.135	kg
Computed Nose Cone Mass	0.16	kg
Computed Centering Ring Mass	0.052	kg
Computed Bulkhead Mass	0.12	kg
Computed Fin Mass	0.3	kg
Computed Parachute Mass	0.127	kg
Computed Piston System Mass	0	kg
Computed Recovery Hardware Mass	0.1	kg
Computed Epoxy/ Paint Mass	0.2	kg
Margin (%)	5	
Motor Type/ Configuration	3xG40, 1xG40	
Computed Motor Mount Mass	0.06	kg
Total Empty Mass Estimate	2.689	kg

Performance and Flight Analysis		
Maximum Altitude	2145	ft
Maximum Velocity	270	ft/s
Maximum Acceleration	5.42	Gs
Time to Apogee	13.09	s
Launch Rail Exit Velocity	46	ft/s
Static Drag Coefficient (1 Stage)	0.65	
Static Drag Coefficient (2 Stage)	0.6	
Stability Margin (1 Stage)	N/A	
Stability Margin (2 Stage)	N/A	

Notes or Additional Performance Metrics
1. Static Drag Coefficients were assumed
2. Simulation was done with CompuRoc.

Vehicle Name: Hickey	Date:9.18.05	Version: One
-----------------------------	---------------------	---------------------

Vehicle Design Parameters		
Subsystem/ Payload Mass		
Recovery Initiation Device Mass Estimate	0.25	kg
Staging Separation Device Mass Estimate	0.15	kg
Flight Computer Mass Estimate	0.09	kg
Camera/ Misc Payload Mass Estimate	0.2	kg
Total Subsystem/ Payload Mass Estimate	0.69	kg
Airframe Diameter	76	mm
Staging Type	Series	
Part Materials and/or Manufacturers	PML	
Length		
Motor Mount(s) Length	0.7	m
Staging Separation Device Length	0.05	m
Recovery Initiation Device Length	0.076	m
Flight Computer Length	0.127	m
Camera/ Misc Payload Length	0.127	m
Parachute(s)/ Recovery Hardware Length	0.9	m
Margin (%)	10	
Total Airframe Length Estimate	2.178	m
Empty Mass		
Computed Airframe Mass	0.692	kg
Computed Airframe Coupler Mass	0.11	kg
Computed Nose Cone Mass	0.13	kg
Computed Centering Ring Mass	0.039	kg
Computed Bulkhead Mass	0.091	kg
Computed Fin Mass	0.3	kg
Computed Parachute Mass	0.127	kg
Computed Piston System Mass	0	kg
Computed Recovery Hardware Mass	0.1	kg
Computed Epoxy/ Paint Mass	0.2	kg
Margin (%)	5	
Motor Type/ Configuration	3xG40, 1xG40	
Computed Motor Mount Mass	0.06	kg
Total Empty Mass Estimate	2.631	kg

Performance and Flight Analysis		
Maximum Altitude	2325	ft
Maximum Velocity	283	ft/s
Maximum Acceleration	5.54	Gs
Time to Apogee	13.63	s
Launch Rail Exit Velocity	47.21	ft/s
Static Drag Coefficient (1 Stage)	0.65	
Static Drag Coefficient (2 Stage)	0.6	
Stability Margin (1 Stage)	N/A	
Stability Margin (2 Stage)	N/A	

Notes or Additional Performance Metrics
1. Static Drag Coefficients were assumed

Appendix C: List of Wires in Rocket

Wire Purpose	Polarity	Length (in)	Weight (g)
Core Motor Ignition from Staging Bay	+	24	4.44
Core Motor Ignition from Staging Bay	-	24	4.44
Core Motor Ignition from Avionics to Staging Bay	+	72	13.32
Core Motor Ignition from Avionics to Staging Bay	-	72	13.32
Staging Coil One Wire	+	12	2.22
Staging Coil One Wire	-	12	2.22
Staging Coil Two Wire	+	12	2.22
Staging Coil Two Wire	-	12	2.22
Staging Coil Three Wire	+	12	2.22
Staging Coil Three Wire	-	12	2.22
Staging Charging Wire	+	2	0.37
Staging Charging Wire	-	2	0.37
Staging Power Transfer to Triac	+	6	1.11
Staging Power Transfer to Triac	+	6	1.11
Staging Power Transfer to Triac	+	6	1.11
Staging Initiation Wire from Avionics	+	72	13.32
Staging Initiation Wire from Avionics	-	72	13.32
Backup Drogue Pyro from Avionics	+	70	12.95
Backup Drogue Pyro from Avionics	-	70	12.95
Backup Main Pryo from Avionics	+	60	11.1
Backup Main Pryo from Avionics	-	60	11.1
Main Computer Power	+	10	1.85
Main Computer Power	-	18	3.33
Pyro Power Supply to Main Computer	+	8	1.48
Pyro Power Supply to Main Computer	-	8	1.48
Backup Computer Power	+	10	1.85
Backup Computer Power	-	18	3.33
Drogue Spring Circuit Charging	+	16	2.96
Drogue Spring Circuit Charging	-	14	2.59
Main Spring Circuit Charging	+	14	2.59
Main Spring Circuit Charging	-	12	2.22
Drogue Spring Power Transfer to Triac	+	2	0.37
Drogue Spring Power Transfer to Solenoid	+	3	0.555

Drogue Spring Power Return from Solenoid	-	3	0.555
Drogue Spring Initiation from Avionics Bay	+	12	2.22
Drogue Spring Initiation return from Avionics Bay	-	12	2.22
Main Spring Power Transfer to Triac	+	2	0.37
Main Spring Power Transfer to Solenoid	+	3	0.555
Main Spring Power Return from Solenoid	-	3	0.555
Main Spring Initiation from Avionics Bay	+	12	2.22
Main Spring Initiation return from Avionics Bay	-	12	2.22
5% Margin for Wire Twist Effects		44.1	8.1585
Total Length and Weight		926.1	171.3285

Appendix D: Test Simulations Possibilities

Name	Engine	Series/Parallel	Diameter (mm)	Length (ft)	Altitude (ft)
Knitting Needle Version 1	2 by 1	Parallel	54	6.36	1308
Knitting Needle Version 2	3 by 1	Parallel	54	6.36	2256
Barely Adequate Version 1	2 by 1	Series	65	7.15	1504
Barely Adequate Version 2	2 by 2	Series	65	7.15	2370
Barely Adequate Version 3	2 by 1 by 1	Series	65	8.5	1654
Fahrfinugen Version 1	3 by 1	Parallel	65	5.18	2317
Fahrfinugen Version 2	3 by 1	Parallel	65-> Payload 76	5.45	2098
Not to Shabby Version 1	3 by 1	Series	76	5.68	2145
Not to Shabby Version 2	2 by 2	Series	76	5.68	2002
Not to Shabby Version 3	4 by 1	Series	76	5.68	2890
Not to Shabby Version 4	4 by 2	Series	76	5.68	3600
The Hickey Version 1	3 by 1	Series	76-> 65	7.15	2325
The Hickey Version 2	3 by 2	Series	76-> 65	7.15	3189
Hellfire	3 by 1	Parallel	76	4.46	1915

Notes:

- = Investigated further in terms of cost
- Length= Airframe Only

Name	Final Price
Fahrfinugen V2	\$202.12
Not Too Shabby 1	\$176.15
The Hickey 1	\$196.50

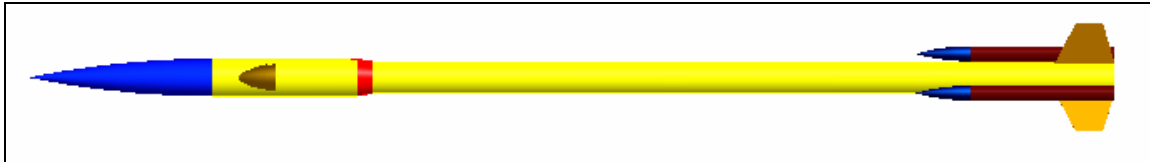
Notes:

- = Chosen Design

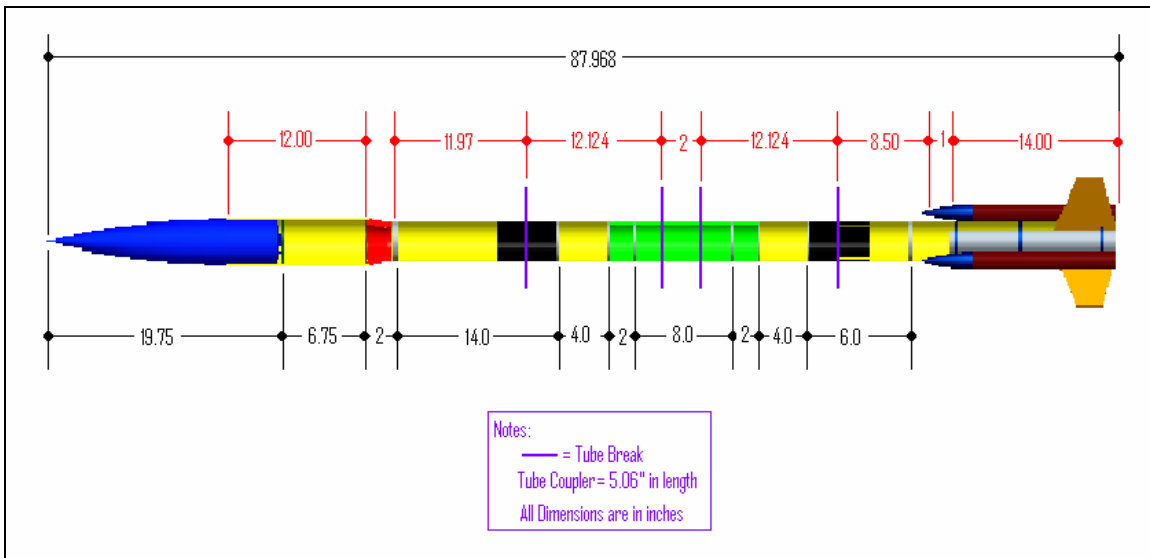
Appendix E: Design Dimensions

Hermes Dimensions (inches)

Overall Length= 87.968



Full Hermes Scale Model (Exterior)

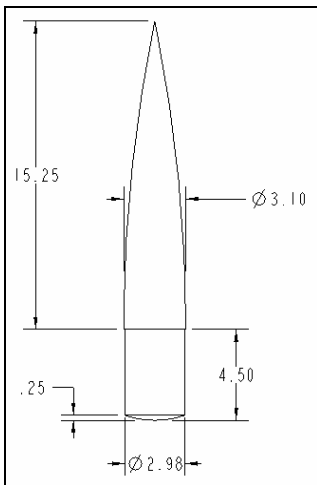


Full Hermes Scale Model (Interior)

Main Nose (diagram below)

Height= 15.25

Quantity= 1



Payload Bay (3")

Length= 12.00

Inner Diameter= 3.002

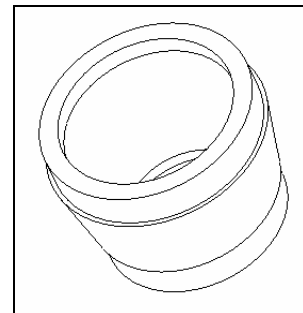
Outer Diameter= 3.126

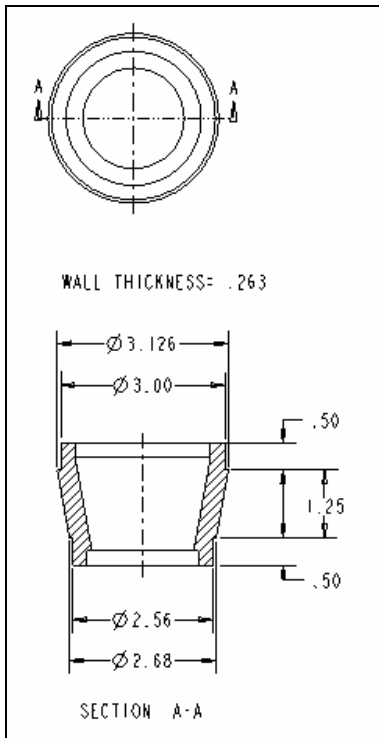
Quantity= 1

Transition (diagram below)

Total Length= 1.25

Quantity= 1





Main Parachute Body Tube (2.56")

Length= 11.97
 Inner Diameter= 2.56
 Outer Diameter= 2.684
 Quantity= 1

Spring Recovery Body Tube (2.56")

Length= 12.124
 Inner Diameter= 2.56
 Outer Diameter= 2.684
 Quantity= 2

Computer Body Tube (2.56")

Length= 2.00
 Inner Diameter= 2.56
 Outer Diameter= 2.684
 Quantity= 1

Drogu Parachute Body Tube (2.56")

Length= 8.25
 Inner Diameter= 2.56
 Outer Diameter= 2.684
 Quantity= 1

Staging Add-On Body Tube (2.56")

Length= 1.00
 Inner Diameter= 2.56

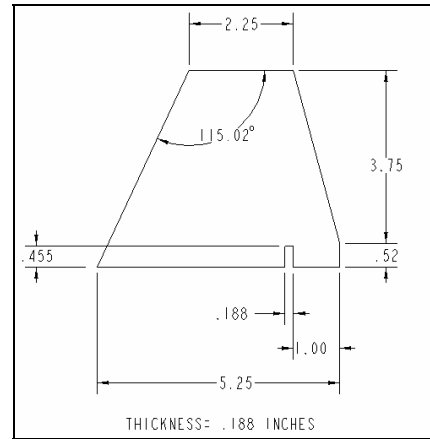
Outer Diameter= 2.684
 Quantity= 1

Main Booster Body Tube (2.56")

Length= 14.00
 Inner Diameter= 2.56
 Outer Diameter= 2.684
 Quantity= 1

Fin (diagram below)

Thickness= .063
 Quantity= 3

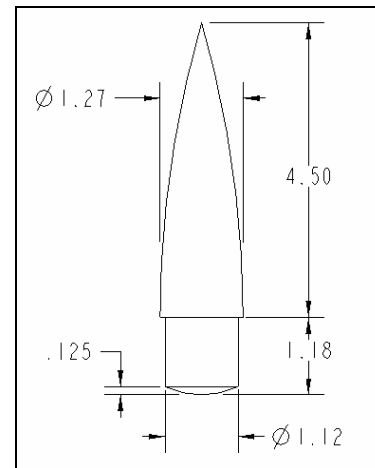


Booster Body Tube

Length= 12.00
 Inner Diameter= 1.15
 Outer Diameter= 1.27
 Quantity= 3

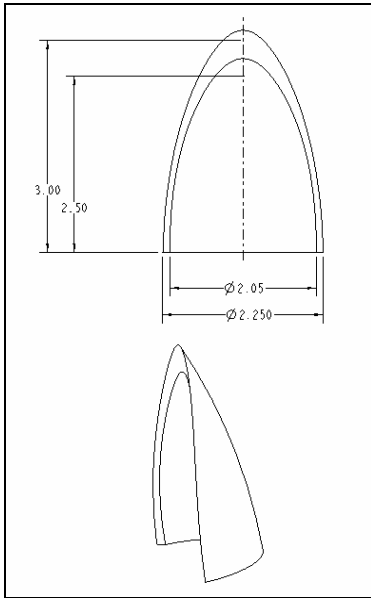
Booster Nose Cone (diagram below)

Quantity= 3



Camera Cover (diagram below)

Quantity= 1



Bulkhead (3")

Thickness= .188

Inner Diameter= 0.00

Outer Diameter= 3.002

Quantity= 2

Bulkhead (2.56")

Thickness= .188

Inner Diameter= 0.00

Outer Diameter= 2.56

Quantity= 10

Recovery Solenoid Coupler (2.56")

Length= 2.00

Inner Diameter= 2.44

Outer Diameter= 2.56

Quantity= 2

Computer Coupler (2.56")

Length= 8.00

Inner Diameter= 2.44

Outer Diameter= 2.56

Quantity= 1

Transition Coupler (2.56")

Length= 5.12

Inner Diameter= 2.44

Outer Diameter= 2.56

Quantity= 2

Motor Mount (1.52")

Length= 14.00

Inner Diameter= 1.52

Outer Diameter= 1.65

Quantity= 1

Centering Ring (1.52")

Thickness= .188

Inner Diameter= 1.65

Outer Diameter= 2.56

Quantity= 4

Appendix F: Airframe Tests

Airframe & Mechanics- Simulation 1: Fin Sizing/ Shape Evaluation

Purpose

The purpose of this test is to determine the most effective size and shape fin for the rocket.

Equipment needed for Fin Sizing/ Shape Evaluation Simulation

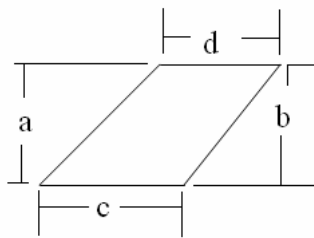
- RockSim v8.0

Test Procedure

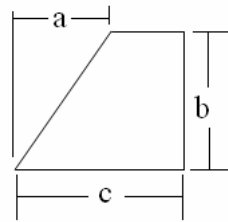
1. Use the Swept, Clipped Delta, and Trapezoidal shaped fin
2. Use worse scenario for rocket loading, single I-95 AeroTech[®] motor, 3 H-90 AeroTech[®] Motors, a one gram payload, and a weight margin of 150%
3. Plug in numbers into RockSim for the fin sizes to calculate the stability and altitude
4. Repeat Step #3 until the most effective shape fin is determined, which is when the achievement of the highest altitude among the stable configurations occurs

Observations/ Data

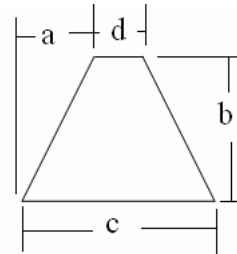
The three basic shapes, which were analyzed:



Swept



Clipped Delta



Trapezoidal

Each feature of the fin is labeled with a letter. The chart below matches the numerical data within the chart to each letter above to determine the size of each fin.

Note: All measurements are in inches unless otherwise noted.

Iteration	Configuration	A	B	C	D	Stability	Altitude (Ft.)
1	Swept	3.15	2.75	5.11	3.15	Unstable	5922.26
2	Clipped Delta	3.25	2.75	5.25	-	Unstable	5937.42
3	Clipped Delta	4.25	2.75	5.25	-	Unstable	5955.32
4	Trapezoidal	2	2.75	5.25	2	Unstable	5938
5	Clipped Delta	4	2.75	6.25	-	Unstable	5906.32
6	Trapezoidal	2.25	2.75	6.25	2.5	Unstable	5901.79
7	Swept	4	2.75	6.25	3.75	Unstable	5880
8	Swept	3.5	4.5	6.25	-	Stable	5748
9	Trapezoidal	2.25	4.5	6	2.5	Stable	5799.55
10	Swept	3	4.5	5	3	Stable	5827.16
11	Trapezoidal	2.5	4	5.5	1.5	Stable	5857.91
12	Trapezoidal	2.5	3.75	5	1.5	Marginally Stable	5906
13	Trapezoidal	1.75	3.75	5	2.25	Stable	5889
14	Trapezoidal	1.75	3.25	5	2.25	Marginally Stable	5914
15	Trapezoidal	1.75	3.5	5	2.25	Stable	5901

Conclusions

Iteration 13 was determined to be the final fin design. It is a trapezoidal shaped fin, with the measurements of a=1.75", b=3.75", c=5", and d=2.25" and was the most stable (based on RockSim) with a maximum altitude (simulation altitude not actual altitude) of 5,889 feet. Iteration 15 was not chosen because it was considered to be too close to marginally stable for use on the rocket.

Additionally, the clipped delta and swept were quickly deemed to insufficient for use because of the large size requirement needed to achieve stable flight. The altitude reached was also relatively less then the trapezoidal shape.

Airframe & Mechanics- Test 1: Body Tube Reinforcement

Purpose

The purpose of this test was to determine the ease of finishing, overall strength, and visual appeal of the body tubes.

Equipment needed for Body Tube Reinforcement Test

- Phenolic Body Tube
- Epoxy Resin
- Sandpaper
- Primer
- EASYGLAS sock
- Wood Filler
- Kevlar String

Test Preparation

1. Cut two identical pieces of phenolic tube, label one Tube A and the other Tube B
2. Wood fill Tube A by thinly covering the phenolic body tube with wood filler. Be sure that no seams can be seen.
3. Wait for Tube A to dry (when dry the wood filler is lighter color) then sand the tube until perfectly smooth
4. If any seams or deformations appear in the body tube, repeat step 2 and 3 until the tube has no visual imperfections
5. Slide fiberglass sock over Tube B
6. Prepare a large quantity of 12 hour Epoxy
7. Completely cover the fiberglass sock on Tube B with Epoxy
8. Leave to dry until no longer tacky, be sure to rotate the tube so it dries evenly
9. Sand Tube B down until smooth
10. Spray primer both Tube A and B, approximately two coats should be sufficient cover

Pre-Test Calculations

In order to evaluate the structural integrity of the body tubes, determination of the force that it must withstand first needed to be calculated. This force was calculated by using data from the RockSim simulation. The rocket's maximum acceleration is estimated to be 684.15 ft/s^2 and the mass of the rocket is approximated at 6.73 pounds. This information allows the drag force to be calculated.

$$F_{\max} = m \cdot a$$

$$F_{\max} = 6.73 \cdot 684.15$$

$$F_{\max} = 4604.3295 \text{ ft} \cdot \text{lb} / \text{s}^2$$

$$F_{\max} = \text{weight} \cdot \text{gravity}$$

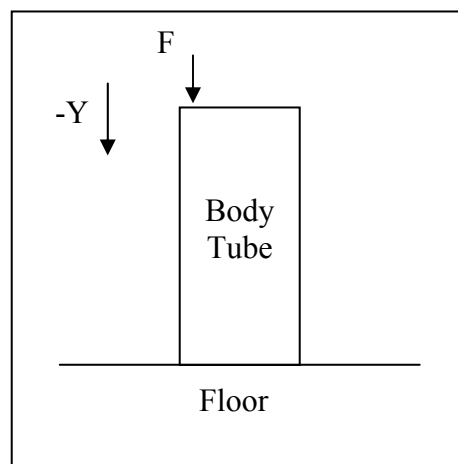
$$4604.3295 = \text{weight} \cdot 32.2$$

$$\text{Weight} = 142.992 \text{ lb} \approx 143 \text{ lb}$$

The total weight is the amount of weight in pounds that body tube must be able to hold to prevent a failure during flight.

Compression Resistance Test Procedure

1. Place Tube A on the floor, sitting so the tube is vertical, see Figure F.1.
2. Sit 45 pound weight on top of the body tube
3. Repeat Step #2 until the required weight (~143 lbs.) that the body tube must withstand is met
4. Repeat Steps #1-3 for Tube B



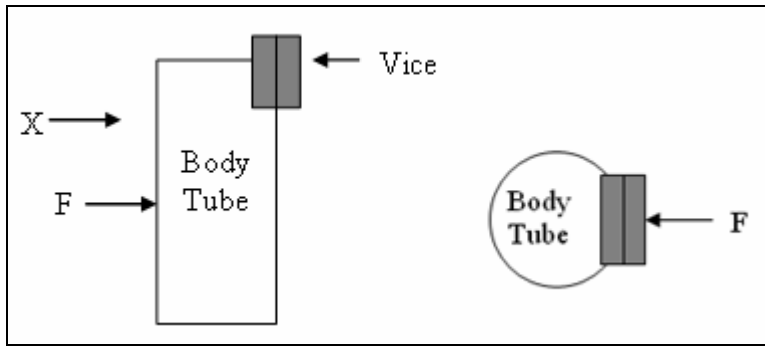
Set-up for compression resistance test

Observations/ Data

Tube A was tested first and it was determined that the tube well exceeded the minimum strength requirement of 143 pounds. In fact, the body tube was able to hold 360 pounds without showing any sign of fracture. The test was concluded at this weight because it exceeded a safety factor of 2.5. In addition, we felt that our own personal safety would be at risk if any further weight was added. After the testing of Tube A was completed, we followed the same procedure for Tube B and obtained the exact same results of reaching 360 pounds.

Repeated Normal Force Stress Test Procedure

1. Place Tube A in a vice
2. Subject it to repeated instantaneous forces in the x-direction until failure occurs, see Figure F.2.
3. Repeat Steps #1-2 for Tube B



Set-up for repeated normal force stress test

Observations/ Data

The repeated normal force stress test, despite the use of a simple testing method, allowed the structural integrity of the body tubes to be easily observed. Applying the repeated instantaneous forces brought both tubes to failure. Tube A failed at a much faster rate and endured a higher level of deformation than compared to Tube B, which was able to (in general) retain its basic external shape because of the fiberglass sock.

Conclusions

In making a final decision between body tube A and B, incurred cost, mass, and ease of construction must also be considered. Since both tubes used phenolic and primers, these costs do not need to be accounted for. However Tube B is approximately \$2.00 more per foot than Tube A due to cost of the EASYGLAS sock and epoxy. In addition, the mass of Tube B exceeds Tube A by 23 grams per foot, see Table F.1.

Mass, Per Foot			
Body Tubes	Before	After	Difference
Tube A	92 G	121 G	29 G
Tube B	92 G	144 G	52 G
Overall			-23 G

Mass breakdown of Tube A and Tube B

Tube A was far more simple to construct than Tube B. Tube B took well over 10 additional hours to dry and required a higher level of precision during construction. In addition, the sock was too large for the body tube, which meant there was a seam that had to be fixed in order for the tube to be smooth. Tube A was more labor intensive with the sanding required to smooth out the tube, but it still was completed a day before Tube B.

The final evaluation will be based on how much force both tubes can handle before the tube breaks and the abovementioned considerations. Using these two test results, it was concluded that though the fiberglass sock method is stronger and does require less physical labor to create an ideal body tube, it is not worth the gains in weight, cost, nor time to use Tube B in the final rocket construction. Therefore, Tube A was used for the rocket's construction.

Airframe & Mechanics- Test 2: Fin Attachment Method

Purpose

The purpose of this test is to determine if the use of fiberglass cloth fillets between the fin and body tube and through-the-wall fin attachment is sufficient strength for the fins in flight.

Equipment needed for Final Attachment Test

- Fiberglass laminating cloth
- G10
- 12" of a Body Tube
- 29mm Motor Mount
- Centering Rings for 65mm diameter with 29mm hole (2)
- Nylon Rip Cord

Test Preparation

- o Cut a 3.125" in the bottom of body tube
- o Cut a 3" by 5" rectangle fin out the G10
- o Epoxy a centering ring to each end of the motor mount
- o Epoxy the G10 fin to the motor mount
- o Before the epoxy on the center rings and fin dry slide the motor mount into the body tube and epoxy into position
- o Fillet with 12 minute epoxy between the fin and motor mount
- o Once all epoxy is dry, use fiberglass laminating cloth and epoxy (12 hour) to cover both the fin and the exterior part body tube, which should be filleted between the fin and motor mount
- o Allow everything to cure overnight or until no long tacky

Pre-Test Calculations

Worst-Case Scenario anticipated drag force:

$$D = \frac{1}{2} \rho V^2 C_D A_f$$

$$C_D = \text{DragCoefficient} \approx 0.75$$

$$A_f = \text{FrontalArea}$$

$$V = \text{max Velocity} = 885.83 \frac{\text{ft}}{\text{s}}$$

$$\text{Total Rocket Drag} = D \approx 31 \text{ lbs.}$$

$$\text{Axial Fin Drag} = D_f$$

$$D_f = \frac{1}{2} \rho V^2 C_D A_{f\bar{c}}$$

$$C_D \approx C_f \approx \frac{0.455}{(\log_{10} \text{Re})^{2.58} (1 + 0.144 M^2)^{0.65}}$$

$$\text{Re} = \frac{\rho V \bar{c}}{\mu}$$

$$\bar{c} = \text{mean fin chord} = \frac{5.25 + 2.25}{2} = 3.75" = .3125 \text{ ft}$$

$$Re = \frac{(.00237 \frac{slugs}{ft^3})(885.83 \frac{ft}{s})(.3125 ft)}{3.62 * 10^{-7} \frac{lb * s}{ft^2}} = 1.81234 * 10^6$$

$$M = \frac{V}{c} = \frac{885.83 \frac{ft}{s}}{1087.6 \frac{ft}{s}} = .814$$

$$C_D \approx C_f \approx \frac{0.455}{(\log_{10} 1.812 * 10^6)^{2.58} (1 + 0.144 (.814)^2)^{0.65}} \approx .00378$$

$$D_f = .5(.00237)(885.83)^2(.00378)(.188) = 0.6608 lb$$

$$\text{For 3 fins} = 3 * D_f = 1.98 lb$$

$$\text{Overall Total Drag} \approx 33 lb.$$

Test Procedures

1. Place body tube vertically on the edge of a table so that the fins are at the top of the tube
2. Lay nylon cord top of the fin/body tube joint
3. Attach weight to the rip cord, start with five pounds
4. Repeat Step #3 adding five pounds each time, be sure to note any deformation or changes in the fin joint, continue until complete joint failure

Observations/ Data

Weight (lbs)	Observations
5	No Visible Deformation Or Shift In The Placement Of The Fin
10	No Visible Deformation Or Shift In The Placement Of The Fin
15	No Visible Deformation Or Shift In The Placement Of The Fin
20	No Visible Deformation Or Shift In The Placement Of The Fin
25	No Visible Deformation Or Shift In The Placement Of The Fin
30	No Visible Deformation Or Shift In The Placement Of The Fin
35	No Visible Deformation Or Shift In The Placement Of The Fin
40	No Visible Deformation Or Shift In The Placement Of The Fin
45	No Visible Deformation Or Shift In The Placement Of The Fin
50	No Visible Deformation Or Shift In The Placement Of The Fin
Beyond Worst-Case Scenario	
55	Slight ¼” Tear In The Uppermost Portion Of The Fiberglass, Where The Fiberglass Met The Fin And Phenolic
60	Tear Elongated About Another ¼”
65	Fin Joint Failed And The Fin Tore Away From The Body

Conclusions

The through-the-wall construction coupled with the fiberglass fillets proved to be stronger than anticipated. Per our calculations, the weight of 65 pounds, at which the joint failed, exceeds the requirements of resisting the worst-case anticipated drag force of 14.45 lbs. Therefore, the use of through-the-wall fin attachment with the fiberglass fillet will be sufficient for flight.

Airframe & Mechanics- Test 3: Fin Material

Purpose

The purpose of this test is to determine the most efficient fin material.

Equipment needed for Final Attachment Test

- Fiberglass laminating cloth
- G10
- Carbon Fiber
- 12" of a Body Tube
- 29mm Motor Mount
- Centering Rings for 65mm diameter with 29mm hole (2)
- Nylon Rip Cord

Test Preparation

- o Cut two 3.125" in the bottom of body tube, 180 degrees apart
- o Cut a 3" by 5" rectangle fin out both the G10 and the carbon fiber
- o Epoxy a centering ring to each end of the motor mount
- o Epoxy both fins to the motor mount, 180 degrees apart
- o Before the epoxy on the center rings and fins cure, slide the motor mount into the body tube and epoxy into position
- o Fillet with 12 minute epoxy between the fin and motor mount
- o Once all epoxy has cured, use fiberglass laminating cloth and epoxy (12 hour) and cover both fins and the body tube
- o Allow everything to cure overnight or until no long tacky

Test Procedures

1. Place body tube on the edge of a table horizontally so that the G10 fin is hanging over the table edge and parallel to the table
2. Lay nylon cord top of the G10 fin/body tube joint
3. Attach weight to the rip cord, start with five pounds
4. Repeat Step #3 adding 2.5 pounds each time, be sure to note any deformation or changes in the fin joint, continue until complete joint failure
5. Repeat Step #1-4 for carbon fiber

Observations/ Data

G10		Carbon Fiber	
Weight (Lbs)	Observations	Weight (Lbs)	Observations
5	No Visible Deformation	5	No Visible Deformation
7.5	No Visible Deformation	7.5	No Visible Deformation
10	No Visible Deformation	10	No Visible Deformation
12.5	No Visible Deformation	12.5	No Visible Deformation
15	No Visible Deformation	15	No Visible Deformation
17.5	Fin Started To Bend At The Joint Where It Was Attached To The Body Tube	17.5	Fin Started To Bend At The Joint Where It Was Attached To The Body Tube
20	The Body Tube Just Below The Edge Of The Fiberglass Cracked Causing The Fin To Come Loose Fiberglass Was Still Attached To The Fin And The Body Tube	20	The Body Tube Just Below The Edge Of The Fiberglass Cracked Causing The Fin To Come Loose Fiberglass Was Still Attached To The Fin And The Body Tube

Conclusions

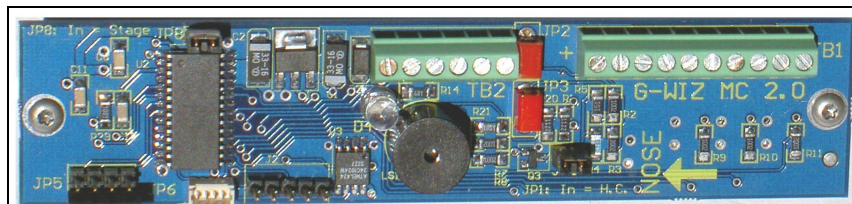
In both cases, the fin joints broke before the fins themselves thus negating any possible strength differences between the two materials. Because both materials will withstand these in-flight forces with ease, the question of “fin efficiency” now focused on price per volume rather than strength. G10 was simply cheaper to purchase than carbon fiber and therefore became the fin material that was used for this rocket.

Appendix G: G-wiz MC2 Flight Computer

The flight computer purchased for use in this rocket was the G-wiz MC2 unit. This computer was responsible for controlling all flight events including staging, core motor ignition, drogue parachute deployment and main parachute deployment. The MC2 (shown below) had the following specifications, features, and control functions [14]:

- Pyro output 1 - Jumper select between Launch detect (for clusters) and Burnout detect (for staging). When Staging, 1st, 2nd, or 3rd stage selectable. Optional timer as well.
- Pyro output 2 - Fires at Apogee detect. Apogee detection is generally based on Accelerometer data, but Barometric Apogee can be selected, and is not subject to problems with Mach transition. Also with optional timer.
- Pyro output 3 - Fires at a programmable low altitude, settable in 10 (foot or meter) increments. Also, may be configured to fire a given number of seconds after Apogee instead. Also with optional timer.
- Pyro output 4 - User programmable. May be turned on with one event, and off with another. Or with an event plus a time delay in both cases.
- Status LED / Speaker shows and beeps readiness at launch, and maximum altitude plus optional maximum speed upon landing. Readiness consists of Continuity checks, and both CPU and Pyro battery voltage levels.
- Arming jack provided on board, and via terminal block for external placement. Not vibration sensitive, and continuity checks work even when disarmed.
- Analog to Digital converter reads accelerometer and barometric sensors to 12 bit precision. Equivalent to about 7 ft/count barometric, or .03 G per count acceleration.
- Acceleration and Barometric data sampled and recorded 33 times per second along with all detected events. Enough memory on board for up to 18 min of flight (128k), and can record multiple flights. More memory available as an option.
- Barometric altitude up to 70k+ feet
- Altitude selection, and readout in English (feet) or Metric (meters) units.
- USB or RS-232 connection.
- High performance processor uses proprietary techniques to calculate altitude properly. It does not rely on linear simplifications, but follows atmospheric pressure to altitude models very closely.
- High current FET driven pyro outputs are capable of delivering up to 15 amps for a full second, each. Outputs capable of delivering up to 50 amps are available on request.

- Can use 2 batteries to ensure that the battery driving the pyro output does not interfere with the computer.
- Optional low current mode (jumper selected) allows use of one battery by limiting current draw. Works with DaveyFire 28B and Pratt Hobbies WEC-1A. May work with other low-current matches as well.
- Reverse voltage protection on all connections.
- Positive retention header as standard.
- Complete with mounting standoffs and battery clips.
- Unit dimensions: 4.9" x 0.9"



G-wiz MC2 Flight Computer Front



G-wiz MC2 Flight Computer Back

Appendix H: Permanent Magnet Design Spreadsheet

Inputs		
Residual Magnetism	1.2	Teslas
Length	1.25	Centemeters
Diameter	1.25	Centemeters
Emperical Force Correction Factor	0.46	-
Magnet Density	7.5	g/cm ³
Magnet Properties		
Surface Flux Density	0.536656315	Teslas
Surface Area	0.000122718	Meters ²
Max Pull on Permeable Material	36.68977922	Newtons
Max Field at Magnet Surface	0.536656315	Teslas
Magnet Mass	0.011504846	Kg

Appendix I: Electromagnet Design Spreadsheet

Inputs			Wire Data					
Field	Quantity	Unit	awg	dia	nom dia	turns / in	Ohms / 1000'	
Inner Diameter	0.5625	Inches	4	0.2043	0.2062	4.413	0.2484	
Number of Layers	2	-	5	0.1819	0.1837	4.954	0.3133	
Number of Turns per Layer	6.5	-	6	0.1620	0.1638	5.556	0.3950	
Wire Gauge	16	AWG	7	0.1443	0.1460	6.233	0.4981	
Total Extra Series Resistance	0.003	Ohms	8	0.1285	0.1302	6.989	0.6281	
Applied Voltage	12	Volts	9	0.1144	0.1160	7.845	0.7920	
Applied Capacitance	0.333	Farads	10	0.1019	0.1039	8.662	0.9988	
Number of Coils in Parallel	1	-	11	0.090740	0.0927	9.709	1.295	
Relative Permiability of Core	100	-	12	0.080810	0.0827	10.88	1.588	
Single Coil Properties			13	0.071960	0.0738	12.19	2.003	
			14	0.064080	0.0658	13.68	2.525	
			15	0.057070	0.0587	15.33	3.184	
			16	0.050820	0.0524	17.18	4.015	
			17	0.045260	0.0468	19.23	5.063	
			18	0.040300	0.0418	21.53	6.384	
Field	Quantity	Unit	19	0.035890	0.0373	24.13	8.051	
Wire Diameter	0.05082	Inches	20	0.031960	0.0334	26.95	10.15	
Turns Per Inch	17.18	-	21	0.028460	0.0298	30.20	12.80	
Ohms per 1000'	4.015	Ohms	22	0.025350	0.0266	33.83	16.14	
Outer Coil Diameter	0.795328871	Inches	23	0.022570	0.0238	37.82	20.36	
Coil Length	0.378346915	Inches	24	0.020100	0.0213	42.25	25.67	
Total Wire Length	25.35009864	Inches	25	0.017900	0.0190	47.37	32.36	
Wire Resistance	0.008481721	Ohms	26	0.015940	0.0170	52.35	40.81	
Total Resistance	0.011481721	Ohms	27	0.014200	0.0152	58.55	51.46	
Peak Current Flow	1045.139532	Amps	28	0.012640	0.0136	65.44	64.89	
Peak Power Dissipation	12541.67439	Watts	29	0.011260	0.0122	72.95	81.83	
S value	4.74232E-06	-	30	0.010020	0.0109	81.65	103.2	
Coil Inductance	0.003969303	Mili-Henrys	31	0.008928	0.0097	90.72	130.1	
2D Field Calculation	0.888585037	Tesla	32	0.007950	0.0088	100.0	164.1	
2D Correction Angle	1.06237939	Radians	33	0.007080	0.0078	112.8	206.9	
2D Correction Function	0.973590053	-	34	0.006305	0.0070	125.7	260.9	
2D Corrected Field	0.865117553	Tesla	35	0.005615	0.0062	141.9	329	
			36	0.005000	0.0056	155.4	414.8	
			37	0.004453	0.0050	174.0	523.1	
System Properties			38	0.003965	0.0045	193.3	659.6	
			39	0.003531	0.0039	220.5	831.7	
Field	Quantity	Unit	40	0.003144	0.0035	245.7	1049	
Total Wire Length	25.35009864	Inches	41	0.002800	0.0031	274.2	1322	
Total Resistance	0.011481721	Ohms	42	0.002494	0.0026	326.9	1668	
Peak Current Flow	1045.139532	Amps	43	0.002221	0.0023	369.6	2103	
Peak Power Dissipation	12541.67439	Watts	44	0.001978	0.0020	425.0	2652	
Total Inductance	0.003969303	Mili-Henrys	45	0.001761	0.0018	466.7	3344	
Capacitive Time Constant	0.003823413	Seconds	46	0.001568	0.0017	494.1	4216	
Inductive Time Constant	0.000345706	Seconds	47	0.001397	0.0015	553.3	5317	
Time Constant Ratio	11.05971476	-	48	0.001244	0.0013	638.5	6704	

Appendix J: Launch Shock Test

From preliminary computer simulation, we knew that upon liftoff, the rocket g-loading changes from one to twelve times the gravitational force of the earth in one sixteenth of a second. First, the velocity after one-sixteenth of a second was calculated.

$$v = v_0 + at$$

$$\text{Where: } a = 12g \quad g = 9.81 \text{ m/s}^2 \quad t = \frac{1}{16} \text{ s} \quad v_0 = 0$$

Therefore, the velocity of the rocket after one-sixteenth of a second is 7.36 m/s. The shock test is one in which the spring activation device is accelerated to approximately that speed and then stopped abruptly. While crude, this will approximately simulate the stresses the device would be placed under upon motor ignition.

The force that the device could be accelerated to using a single spring of the same type used within the device itself is as follows:

$$F = kx$$

$$\text{Where: } k = 455 \text{ N/m (Spring Constant)}$$

$$x = 0.15 \text{ m (Distance of spring compression)}$$

Therefore, the force exerted by the spring system is 70 Newtons. Since force is equal to mass multiplied by acceleration:

$$F = ma$$

$$\text{Where: } m = 200 \text{ g (Test Device Mass)}$$

Therefore, using a single spring, the device is accelerated at 350 m/s². The velocity after this acceleration is calculated using Equation 1 once again, where:

$$a = 350 \text{ m/s}^2 - g, \quad g = 9.81 \text{ m/s}^2, \quad v_0 = 0 \text{ (Initial Velocity - the system was at rest)}$$

The use of a single spring during this test would accelerate the recovery activation device to a velocity of 21.26 m/s. This velocity is well in excess of the required 7.36 m/s, so this test would be conservative in certifying the devices are flight ready.

The test was set up as shown in the picture below. The spring recovery device was erected around a dowel, and placed on top of another spring. Between the recovery device and the second spring

section, a spacer was used to ensure that the force would be evenly transferred between the two segments, and to minimize the chance of the lower spring binding on some of the internals of the activation device.

As shown in the Figures 1 and 2, an airframe section was placed over the test section, and the springs compressed and locked into place by the lever. The whole setup was then compressed and released. At the upper end of the dowel is the underside of a table, to bring the whole setup to a sudden stop.



Test Setup Without Airframe

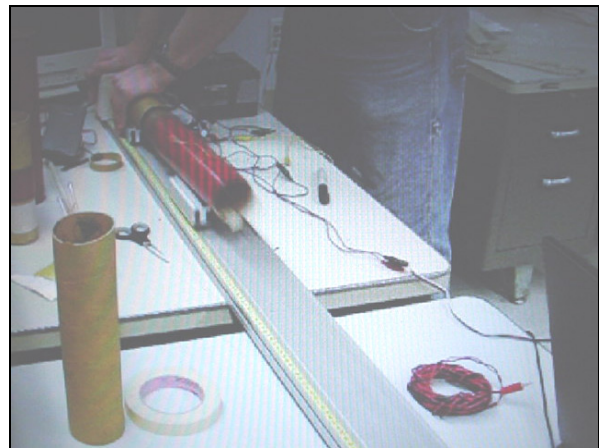


Test Setup With Airframe

Appendix K: Recovery Test with Computer Screenshots

Below are screenshots of the recovery deployment tests performed upon each spring device upon a frictionless track. The recovery systems were set up inside of a segment of the body tube modified to allow the access to the flight computer. The springs were loaded, and the airframe segments were fitted together and pinned in place with the shear pins. Upon a signal from the flight computer (controlled by a laptop for ground testing) the solenoid would activate the device.

During pre-flight testing the devices functioned as designed roughly half the time. However, on the day prior to the actual flight of the rocket, the devices began to not function as well, for unknown reasons.



Appendix L: PML Igniter FAQ

PMLIgnitersFAQ.doc3/02/02 1/1

2/15/02

Igniter manufacturers will specify the electrical usability (ohms and volts) range for their devices; contact the igniter manufacturer for their specifications.

Igniters

PML offers two different igniters

1. The PML Rapidfire \Leftrightarrow , which is included with each of our Thrusters \Leftrightarrow motors, and also available separately.
2. Magnelite igniter kits, which allow you to make your own igniters, ranging from A size BP motors all the way up to M and larger motors, depending upon the igniter wiring size purchased.

See the Igniters page in our webstore for more information.

Ematches vs. Igniters

The difference between Ematches and igniters is that Ematches are intended to ignite an easy-to-burn substance quickly, such as the Black Powder used in rocket ejection charges. However, an igniter is intended and constructed to produce a large, hot ball of flame for an extended period (say, 0.5-0.75 seconds) to ignite a rocket motor. Ematches typically will not ignite motors unaided, as they do not produce a hot enough flame for long enough, whereas igniters certainly could ignite BP. Another significant difference between them, which is critically important for onboard rocket electronic use, is their current requirements. Igniters typically require much more current than an Ematch; the current requirements are usually more than altimeters can provide. Therefore, for onboard altimeters, which need to ignite deployment charges, Ematches are needed. For staging timers, which need to ignite motors, igniters are needed. Be sure to always check to be sure an Ematch or igniter will work with your onboard electronic device.

Appendix M: Propulsion Second Stage Igniter Test

Purpose

The purpose of this test is to determine the most reliable ignition with the least amount of current. This is useful in determining the size and types of power source needed in the second stage.

Equipment needed for Ignition test

- Igniters
- Pyrogen Compound
- Power Supply (Battery for igniters)
- Extension Cables (alligator clipped/banana plug)
- Video Recorder
- Extension cords if needed
- Safe Area to conduct testing
- Metal Rod
- Clamp
- multimeter

Test Procedure

1. Measure the Resistance across a non-dipped igniter. (Non-dipped means there is no pyrogen coating). This resistance is R_{ig} .
2. Measure resistance across our extension cables while they are clipped together and not connected to the power supply. This resistance is R_c .
3. Using $V = IR$, compute the required voltage, V_{req} , for the predetermined set of currents that we are testing for. These currents were 400mA, 750mA, 1A, 1.5A, and 2A for the igniters tested.
4. In testing area, connect extension cables to the igniter with the alligator clips. Do not connect them to the power supply yet.
5. Plug in power supply.
6. Set voltage to the first V_{req} and using a voltmeter, test to see if the proper voltage is being applied.
7. Turn off power supply.
8. Start video recorder

9. Plug in extension cables (banana plug end) to the power supply.
10. Make sure everyone is clear from igniters and a safe distance away (10ft)
11. Countdown to turn on power supply, 3...2...1. Turn on power supply.
12. Record if igniter fires within 1 second. This will be a visible ignition and can be concluded by either counting to 1 or using a stopwatch.
13. **Safety rule** – if the igniter does not ignite for the given voltage. Turn off power supply. Increase voltage on the power supply to a max level, and then turn on power supply to ensure that igniter burns off.
14. Turn off power supply and disconnect extension cable from power supply.
15. Give igniter a minute to cool off, and then proceed to disconnect the igniter from the alligator clips. Do not touch near the tip of the igniter. Dispose of igniter and replace with new igniter.
16. Repeat steps 4-16 for the given currents in step 3. Repeat multiple times for each current.

Appendix N: Propulsion Cost Iterations

Component listings

Component	Size	Quantity	Price(per unit in \$)	Manufacturer	Vendor
Motor Casing	RMS 29mm/40-120	4	47.99	Aerotech	www.redarrow.com
Motor Casing	RMS 29mm/40-120	4	46.99	Aerotech	ehobbies.com
Reload Kit	G64W	4	9.95	Aerotech	www.redarrow.com
Reload Kit	G64W	4	9.99	Aerotech	ehobbies.com
Motor Mount	38mm	4	5.50	LOC	www.locprecision.com
Motor Mount A dapter	38mm-29mm	4	4.25	LOC	www.locprecision.com

Adjusted Component Listings

Component	Size	Quantity	Price(per unit in \$)	Manufacturer	Vendor
Motor Mount	38mm	1	5.50	LOC	www.locprecision.com
Motor Mount(booster)	29mm	3	4.50	LOC	www.locprecision.com
Motor Mount A dapter	38mm-29mm	1	4.25	LOC	www.locprecision.com

Price Summary (hardware only)

	Quantity	Total Price (US dollars)
*contains 4 x 29mm casings, 1 x 38mm motor mount, 3 x 29mm motor mount, 1 x 38-29mm motor adapter	9	211.21

Test Pricing for Commercial Test

Reload Kit	G64W	6	9.95	Aerotech	
*Twiggy Igniter	F and G class	1(pack of 10)	10	Quick Burst	http://www.quickburst.net/
*Pryogen(firestar) Compound	Bottle A and B		18.95	Firestar	http://www.craftershome.net/

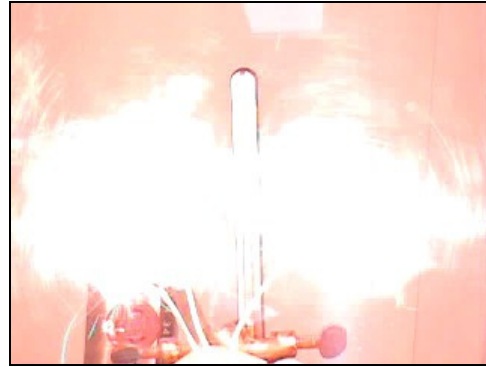
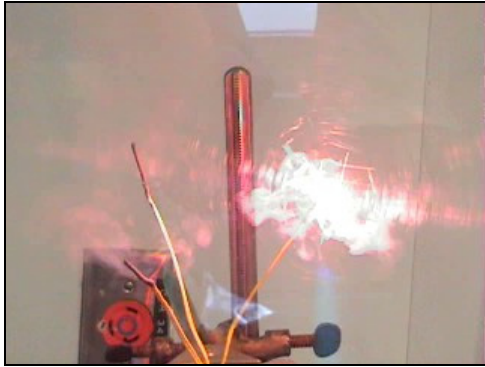
Estimate Commercial Cost for :

* 6 x Reload G64W, 1 Pack Twiggy Ignitors, 1x Bottle of Pryogen Compound		Total (US dollars)	88.65
--	--	--------------------	-------

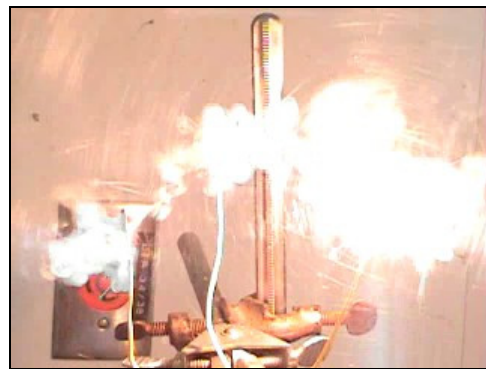
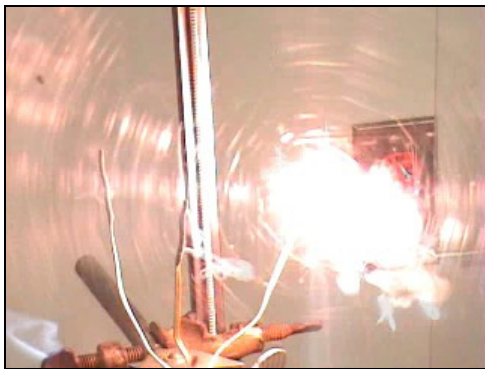
Summary Cost Totals

			Price (US Dollars)
Hardware Only			211.21
Flight Cost	<i># of flights</i>	<i>cost per flight</i>	
*this includes cost of 4 x G64W reload kits per single flight	1	39.8	39.8
Test Cost			88.65
Propulsion Cost to date			339.66

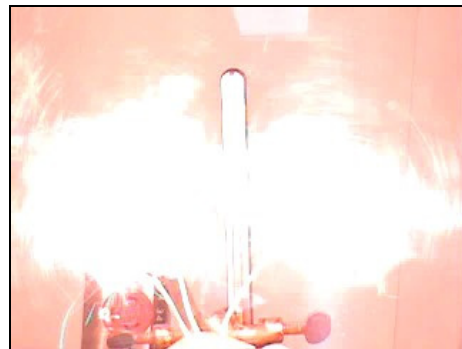
Appendix O: Video Stills from Ignition Testing



[Frame 1] Successful time between lighting < 1 sec [Frame 2]



[Frame 1] Non successful igniter test > 1 sec [Frame 2]



[Frame 1] Successful igniter test simultaneous ignition < 1sec [Frame 2]

Appendix P: Guide to making Igniters

GROUND SUPPORT

[Launch Pads](#)
[Firing Consoles](#)
[Clip Whips](#)
[Build a Launcher](#)
[Build a Launch Pad](#)
[Multi-Pad Launcher](#)
[Solderless Igniters](#)
[Copperheads](#)
[Cluster Wires](#)

The thumbnail images below are clickable links to the photos referenced in the article. Click on the thumbnail of the photo you wish to view. Use your browser "back" button to return to this page.

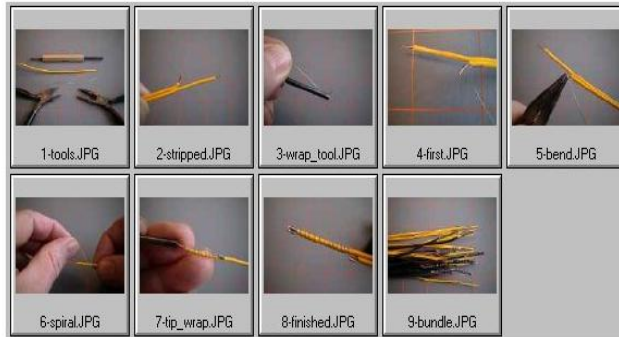


Photo 1:

Get a wire wrap tool. Radio Shack has cheap ones. Electronics suppliers have better quality ones. Either will work. You will also need a small pair of needle nose pliers and a small pair of wire cutters.

Cut your nichrome about 1/2"-1" longer than normal. How much extra length depends on how much manual dexterity you have. The author can get by with 1/2" extra, but an extra inch is easier to work with, and the cost difference is about 0.25 cents--1/4th of one cent--per igniter.

Photo 2:

Trim and strip the lead wire as shown.

Photo 3:

Thread the nichrome through the side hole in the wire-wrap tool with about 1/4" sticking out the end.

Place the center hole of the wire-wrap tool over the shorter lead conductor as if that lead were a wire-wrap post on a pc board.

hold the 1/4" nichrome (sticking out the end of the tool) against the igniter leads and give the wire-wrap tool about 6-7 turns.

Photo 4:

Carefully pull the wire wrap tool off the lead wire. You should now have a very neatly wire-wrapped piece of nichrome secured to the copper lead.

Photo 5:

Either trim off the extra copper wire beyond the end of the nichrome, or bend it over in a U against the nichrome coil. (I prefer to bend it and crimp it against the nichrome) Trim away the 1/4" of nichrome you held against the leads in the previous step.

Photo 6:

Spiral the nichrome up the longer lead to the tip the required number of turns for your application. You should have about 1/2"-3/4" of nichrome left.

Photo 7:

Thread this short length back up the side hole in the wire wrap tool. Thread it in from the end of the tool, not the side slot as you did the first time. Carefully place the copper lead wire in the "post" hole of the wrap tool, being careful not to pull the nichrome out of the "wrap" hole. Be careful, it's easy to get both wires in the same hole on the tool--that won't work and will probably break your remaining nichrome off too short!

Give the wire-wrap tool 6-7 more turns until all the remaining nichrome is wrapped around the end conductor.

Trim or bend as in the first one.

Photo 8:

Voilà! a solderless lead.

Check your continuity & resistance to make certain that you have not changed the nominal resistance of the lead compared to your soldered leads.

It actually takes longer to describe this process than it does to do it. With a little practice, you should be able to produce them as fast or faster than by the solder method without all the hassle and mess of setting up the solder station, etc.

Submitted by Jim Ball

Appendix Q: Ideas and Suggestions for Future Work

1. During the design process, subsystems should be kept as independent and modular as possible. This will keep integration efforts to a minimum, and it will allow for more easy maintenance and inspection of each subsystem once the vehicle is constructed.
2. While dual parachute style recovery is required for high altitude rockets, it is not a practical addition to a high impulse rocket going below a few thousand feet. This is because the motor impulse will dictate site dimensions large enough to recover most single parachute deployment systems in all but the most extreme winds.
3. Use a larger airframe diameter if weight allows. While the 2.56" Airframe used with this project was adequate, the final design of the different systems required a great deal of length to have sufficient volume for everything. This resulted in a very long and slender rocket for its diameter. In addition, integrating all systems proved more difficult with such a small airframe because we could not fit our hands inside the vehicle to adjust or install components.
4. Avoid airframe diameter transitions if necessary. While these transitions can improve rocket appearance or fill specific system needs, they tend to be fairly heavy, and the volume of the airframe they occupy is not readily usable because of the extra structure required in around the transition.
5. Use caution when approaching mechanical designs with moving parts. While such designs can be very reliable, they are more likely affected by the extreme acoustic, vibration, and acceleration loads experienced in a rocket vehicle. These forces are difficult to test on the ground, so systems with moving parts may be more difficult to fully test prior to flight.
6. Possibly design the airframe around an internal support frame with a removable outer skin. While fully tubular structures are the most mass efficient in compression or bending applications, it is difficult to integrate, test, repair, or demonstrate the internal systems of a vehicle when the outer surface cannot be removed. If such a structure was created, it could also be made more modular as systems could be bolted instead of epoxied.
7. Investigate the use of more advanced composite materials such as to construct major airframe components. Such construction could significantly save weight.
8. Separate the vehicle structure in as few places as possible. Most current model rockets and high power rockets separate their primary structure (the outer tubular structure) in many places. This is done primarily to allow system access on the ground or deploy parachutes during flight. Every additional separation introduces extra airframe and recovery structure to transfer launch and/or recovery loads through the separation point. Avoiding separation may dictate more innovative

recovery systems such as rear deployment parachutes, however such a system, while innovative, might also prove more structurally efficient as the parachute recovery loads would be transferred through the strongest section of the airframe: the motor mount.

9. If electromagnetic booster staging is implemented in the future, find a method of transferring the electronics and power systems from the main airframe to the boosters. Great care will need to be taken to ensure symmetrical separation in this case, however this method would allow the boosters to provide more benefit as the staging system mass would be jettisoned after it was needed.
10. Power and electrical distribution must be factored into the design process from the beginning. While these systems may not take up significant room, they are critical elements of vehicle integration and thus require consistent design and implementation across all subsystems.
11. Investigate the use of a combined battery and capacitor power system. Rockets of this scale need consistent but low current requirements for some systems, however they also require intermittent but high current outputs for motor igniters or system actuators. Such a combined power system may be more weight efficient than a simple battery or set of batteries sized to meet the highest peak current loads.
12. Investigate the use of a remote-controlled backup recovery system. If such a system could be obtained or created for minimal cost, it would eliminate the effect flight profile changes would have on timer-based backup circuitry.
13. Possibly create a cheap and easily constructed working model of the entire vehicle during the overall design process. The purpose of this model would be to eliminate the difficulty in visualizing how parts and subsystems would later integrate. It would not need to be to scale necessarily, and it could make use of simple materials such as foam board, paper, and wooden dowels. It would nevertheless serve as a working model and allow integration issues to be addressed more easily from the very beginning.
14. Each subsystem should be constructed with enough time to allow for redesign if problems are discovered during integration. While a design may work well by itself, issues often come up during vehicle integration that cannot be easily fixed with minor changes. If redesign is deemed unnecessary, the remaining time can be used to more thoroughly check and test systems on the ground prior to launch.
15. All electrical connections or circuitry onboard the vehicle must take into account the acceleration and vibration loads they will experience. Robust terminal blocks or anchored solder joints should be used as much as possible.

16. Precision machining and manufacturing of parts should be used as much as possible, and the ability to manufacture the parts should be considered during the design process. While it often appears easy to simply cut a part with a Dremel™ tool and then use sandpaper to make it fit as would be done on a model rocket, such a process can lead to poor and inconsistent tolerances in large parts. In many cases it also leaves a part not fitting for display or demonstration.

Appendix R: Failure Analysis

(This analysis was performed by Ryan Caron, AIAA volunteer, based on discussions with the entire team)
 (Photo documentation courtesy of AIAA volunteers Matthew Clark and Alexander Hecht)

Anomaly #1: One booster nosecone separated in flight

Evidence:

	<p>PICT0700</p> <ul style="list-style-type: none"> - Shortly after liftoff - High velocity relative to camera position; significant motion blur - Reddish streak visible to right of rocket - Streak either nosecone or streamer
	<p>Picture 20210</p> <ul style="list-style-type: none"> - near booster burnout - right booster shorter than left booster - red object, probably nosecone, is visible in front of booster

Flight Impact:

- Increased drag

Probable cause:

- Attachment to booster airframe too loose

Analysis:

Nosecones were loosely fitted to ensure a clean separation. As such, they were prone to misalignment relative to the airflow. Any such misalignment would create a force on the nosecone perpendicular to the booster's axis of symmetry. Provided the misalignment was large enough, aerodynamic loads would force the nosecone to separate from the booster. This would leave only the Kevlar shock cord connecting the nosecone to the rest of the vehicle.

A contributing cause to asymmetric aerodynamic loads is if the nosecone itself was an asymmetric nosecone. Such asymmetry was caused due to heating during the manufacturing

process. Heating was necessary for disassembly of the components after painting, which had created a significant bonding seal. The plastic that the booster nosecones are not used anywhere else on the vehicle, and their sensitivity to even modest heating was not anticipated.

Unresolved issues:

- None

Resolution:

- Increase structural connection between nosecone & booster
- Ensure alignment and symmetry of nosecone

Turnaround impact:

- New nosecone
- New shock cord (frayed due to loads)

Anomaly #2: One booster remained attached after separation of the other two

Evidence:

- Photo documentation

	<ul style="list-style-type: none">- Picture 20213- Jettisoned boosters visible in motor exhaust- Attached booster still producing flame and dense exhaust
	<ul style="list-style-type: none">- Picture 180- Third booster depleted- Jettisoned boosters still visible- Third booster never separated

Flight impact:

- Increased drag, higher second stage mass

Probable cause:

- Booster still thrusting at time of separation

Analysis:

In this case the staging system functioned as designed. Since the boosters are not aerodynamically stable when independent from the rest of the vehicle, the system was

designed not to jettison a booster that was thrusting. This was easily performed by having the magnetic system at a mechanical disadvantage with respect to the motor, since the booster had to pivot about its aft hook to separate.

The flight computer detected the deceleration of two boosters. With a majority of the thrust absent it triggered staging. Future flights will have a small delay programmed into the flight computer to provide additional time for burnout. Future efforts will also need to work on developing ground hardware that will ignite the boosters more quickly and symmetrically.

Unresolved issues:

- Motors did not ignite simultaneously
 - Stills taken from miniDV ground video camera
 - Number in upper left of each still is the frame #
 - Each frame is $\sim 1/30^{\text{th}}$ of a second
 - Camera angle placed forward booster in front of rear booster
 - difficult to assess individual performance of forward & rear boosters

 <p>4613</p>	 <p>4618</p>
<ul style="list-style-type: none"> - Right booster ignition started - Smoke from forward booster 	<ul style="list-style-type: none"> - Rear booster (not visible) ignition started - Other boosters emitting smoke

<p>4619</p> 	<p>4620</p> 
<ul style="list-style-type: none"> - Rear booster begins to produce thrust - No thrust plume from other boosters 	<ul style="list-style-type: none"> - Rear booster at max thrust - Right booster begins to produce thrust
<p>4626</p> 	<p>4627</p> 
<ul style="list-style-type: none"> - Right booster near max thrust - Only single plume origin visible at left 	<ul style="list-style-type: none"> - Forward booster at max thrust - two plume origins visible at left

- ~200ms elapsed between max thrust between rear booster and forward booster
- Right booster showed earliest signs of ignition, yet took the longest to build up thrust

- Forward booster (with different color nosecone), was last to get to achieve max thrust. This is same booster that remained with vehicle

Unresolved issue analysis:

Video footage was invaluable in the analysis of the booster ignitions. However, the placed camera angle left some ambiguity since the plumes of the front and rear boosters overlapped. In this specific case, had the camera been placed approximately 45 degrees to the right, the booster plumes would not have overlapped. Yet even in that case not all information will be available. As such, multiple cameras from varying angles should focus solely on motor ignition. To synchronize footage from various sources a high-intensity LED should be wired in parallel to the ignition circuitry so it is apparent in the video footage when the system is armed and will provide a convenient reference point.

Resolution:

- Ensure booster separation is triggered after all boosters are depleted
- Start upper stage ignition process before booster separation
 - Allows for more time for boosters to burnout
 - Minimizes velocity lost via staging process
- Reconfigure ground ignition system so that booster ignition occurs closer together
 - Separate power sources & relays for each booster
 - Prevents current drain to only one igniter
 - analogous to early difficulties with power system for electromagnetic staging

Turnaround impact:

- Booster damaged upon impact
- Primary airframe damaged at booster attachment points

Anomaly #3: Upper stage did not fire

Evidence:

- Igniter intact & unlit upon recovery

Flight impact:

- Reduced apogee
- Resulting flight profile exceeded timer settings of backup flight computer

Probable cause:

- Insufficient power to light igniter

Analysis:

Earlier designs of the power system included two 9v batteries since it was feared one was insufficient. Two batteries required a voltage regulator to prevent the batteries from exceeding tolerances of the flight computer. Unfortunately, the regulator would drain the batteries regardless of actual loading. Time on the pad prior to ignition was limited to 15 minutes in this configuration.

As such, the regulator was abandoned and replaced with a lithium-polymer battery. Initial tests were successful, and a net mass savings was seen. However, for reasons still unknown the lithium-polymer had discharged while in the lab. Due to the specifics of the battery's chemical reaction, care needs to be taken to avoid such a discharge since the battery will then be useless.

With minimum time remaining, and the mass & volume savings of the power system being consumed by the charging circuitry for recovery, it was not possible to revert to the dual battery & regulator configuration even if we could accept the limited time on the pad. Ignition tests were performed with a single, unregulated battery, and this is the configuration that was flown. Those tests were successful and disposed our earlier concerns about using a single battery configuration.

All the hardware and wiring associated with upper stage ignition survived the crash and additional tests were performed. Despite successful ignition tests prior to launch, the flight battery could not ignite an igniter of the same batch used for the second stage. Ignition was successful when using flight hardware and performed with a fresh battery. Apparently, only a very small window exists in which such a battery would be successful.

Unresolved issues:

- Why did the lithium-polymer discharge?
- Does the flight computer drain the ignition battery when not in use?

Resolution:

- More robust power system for ignition
 - Lithium-polymer
 - Capacitor augmentation?
 - Shorter wire run (power stored aft, closest to motor, not within avionics bay)
 - Ignition would be triggered via Triac/MOSFET

Turnaround impact:

- None

Anomaly #4: Parachutes did not deploy

Evidence:

- High velocity impact with ground

Flight Impact:

- Loss of vehicle
 - Subsystems damaged:
 - Airframe, Payload, Recovery, avionics, staging

Probable cause:

- Backup computer did not trigger pyrotechnic charges
- Mechanical failure of spring systems
- Spring systems triggered electrically
 - Capacitors measured post-crash had 0.3volts remaining
- Nature of mechanical failure indeterminable due to impact damage

Analysis:

Despite redundant computers and separation mechanisms, the failure of the upper stage motor to ignite effectively took the backup string out of commission. This is because the backup computer is merely an event timer, programmed to trigger pyrotechnic charges a specified number of seconds after launch. These settings were based on predictions of time elapsed until apogee (drogue) and when the vehicle reached 400 feet (main).

In the actual flight profile, without the upper stage ignition, apogee was reached much sooner than anticipated. Since the apogee was only an estimated 700 feet, the 400 foot altitude was also reached quickly. In fact, the vehicle had already impacted the ground when the backup computer was to have triggered the pyrotechnic charge for the drogue chute.

Early analysis assumed that the primary flight computer had lost power in flight. This was based on the fact that the power connection was severed when the vehicle was recovered after impact, as well as the fact that the data from the flight computer was corrupted, preventing a successful download. This early analysis would later prove to be in error.

Once the vehicle was returned to the lab and disassembly began, the voltage on the capacitors were checked since, when charged, they pose a small but significant safety risk since a sudden discharge of 50v is not trivial. The aft/drogue capacitor read a voltage of 0.3volts, and was then assumed that the electrical system had shorted out at impact. The vehicle did, after all, fall from 700 feet and impacted at an estimated 150 miles per hour.

However, had the system been suddenly discharged at impact the capacitors should have been completely discharged. 0.3volts were still present after the crash. This is typical of Triac

discharge circuits since the circuit remains closed provided the current is above a certain threshold. Once the current drops below that threshold, the circuit is opened, preventing the capacitor from fully discharging.

The voltage remaining indicates the flight computer successfully triggered the recovery system. This leaves the only remaining failure mode to be mechanical in nature.

Unresolved issues:

- Specific mechanical failures of recovery systems
- Data from flight computer corrupted
 - Possibility of data recovery by manufacturer
 - Data could verify that systems were in fact triggered at appropriate time

Resolution

- Build recovery systems to better tolerances to improve mechanical reliability
- Backup computer needs to handle changes in flight profile

Turnaround impact:

- Reconstruction of damaged subsystems required

Anomaly #5: Booster nosecones sheared from shock cords

Evidence:

- Nosecones not recovered with boosters that separated

Flight impact:

- None

Probable cause:

- Ejection charges too powerful
 - Sized for full-scale rockets, not minimum volume boosters
 - Booster that remained with vehicle kept its nosecone since it had already separated from booster airframe at time of ejection charge

Analysis:

The Aerotech G64 motors used in the boosters are traditionally used in rockets of comparable diameter to WARRIORS, albeit only half a tall. As such, their ejection charge is designed to deploy a much larger recovery system. In order to do so, a significant internal volume of the rocket has to be pressurized. This volume can be two orders of magnitude greater than the volume within the boosters that needed to be pressurized. It is no surprise then that the nosecones separated from the Kevlar shock cords due to the excessive force generated by the ejection charges.

Future use of these boosters will require a substantially smaller ejection charge. Future boosters should be designed with either a higher internal volume to be pressurized or otherwise require greater force to separate. Since probable booster redesign for the next academic year involves moving the staging electronics into the boosters, instead of the core of the vehicle as currently built, the boosters will probably be of a split body configuration that inherently requires higher forces than the current setup.

Unresolved issues:

- None

Resolution:

- Increase force required to separate nosecone
 - Better mechanical attachment
 - Additional mass forward of nosecone (staging electronics, et al)
- Decrease force exerted by ejection charges
 - Less black powder in charge

Turnaround impact:

- New nosecones required
- Shock cord mounts need to be repaired